

Technology Development for High Precision Micro/Nano-EDM

By

Deepak Kumar

Department of Mechanical Engineering
(Admission No.17DR000452)



THESIS SUBMITTED
TO

**INDIAN INSTITUTE OF TECHNOLOGY
(INDIAN SCHOOL OF MINES), DHANBAD**

For the award of the degree of
DOCTOR OF PHILOSOPHY

JANUARY 2023



Form No: PH13

INDIAN INSTITUTE OF TECHNOLOGY (INDIAN SCHOOL OF MINES) DHANBAD

CERTIFICATE FROM THE SUPERVISOR(S)
(To be submitted at the time of Thesis Submission)

This is to certify that the thesis entitled “**Technology development for high precision micro/nano-EDM**” being submitted to the Indian Institute of Technology (Indian School of Mines), Dhanbad by **Mr. DEEPAK KUMAR**, Admission No 17DR000452, for the award of Doctor of Philosophy (Ph.D.) Degree is a bonafide work carried out by him/her, in the Department of Mechanical Engineering, IIT (ISM), Dhanbad, under my/our supervision and guidance. The thesis has fulfilled all the requirements as per the regulations of this Institute and, in my/our opinion, has reached the standard needed for submission. The results embodied in this thesis have not been submitted to any other university or institute for the award of any degree or diploma.

Signature of Supervisor (s)

Name: Prof. Vivek Bajpai

Date: 18.01.2023

Signature of Co-Supervisor (s)

Name: Prof. Nirmal Kumar Singh

Date: 18.01.2023



INDIAN INSTITUTE OF TECHNOLOGY (INDIAN SCHOOL OF MINES) DHANBAD

CERTIFICATE FOR CLASSIFIED DATA

(To be submitted at the time of Thesis Submission)

This is to certify that the thesis entitled “**Technology development for high precision micro/nano-EDM**” being submitted to the Indian Institute of Technology (Indian School of Mines), Dhanbad by **Deepak Kumar** for the award of Doctor of Philosophy (Ph.D.) Degree in **Mechanical Engineering** does not contain any classified information. This work is original and has not been submitted to any institution or university for the award of any degree.

Signature of Supervisor (s)

Signature of Supervisor (s)

Signature of Scholar



Form No: PH12

INDIAN INSTITUTE OF TECHNOLOGY (INDIAN SCHOOL OF MINES) DHANBAD

CERTIFICATE REGARDING ENGLISH CHECKING

(To be submitted at the time of Thesis Submission)

This is to certify that the thesis entitled “**Technology development for high precision micro/nano-EDM**” being submitted to the Indian Institute of Technology (Indian School of Mines), Dhanbad by Mr. Deepak Kumar, Admission No 17DR000452 for the award of Doctor of Philosophy (Ph.D.) Degree has been thoroughly checked for the quality of English and logical sequencing of topics. It is hereby certified that the standard of English is good and that grammar and types have been thoroughly checked. It is now worthy for evaluation by the panel of examiners.

Signature of Supervisor (s)

Name: Prof. Vivek Bajpai

Date: 18.01.2023

Signature of Supervisor (s)

Name: Prof. Nirmal Kumar Singh

Date: 18.01.2023

Signature of Scholar

Name: Deepak Kumar

Date: 18.01.2023



INDIAN INSTITUTE OF TECHNOLOGY (INDIAN SCHOOL OF MINES) DHANBAD

COPYRIGHT AND CONSENT FORM

(To be submitted at the time of Thesis Submission)

To ensure uniformity of treatment among all contributors, other forms may not be substituted for this form, nor may any wording of the form be changed. This form is intended for original material submitted to the IIT (ISM), Dhanbad and must accompany any such material in order to be published by the ISM. Please read the form carefully and keep a copy for your files.

TITLE OF THESIS: Technology development for high precision micro/nano-EDM

AUTHOR'S NAME & ADDRESS: Deepak Kumar, Opal Hostel, Room No. 237, Indian Institute of Technology (ISM), Dhanbad-826004, Jharkhand.

COPYRIGHT TRANSFER

1. The undersigned hereby assigns to Indian Institute of Technology (Indian School of Mines), Dhanbad all rights under copyright that may exist in and to: (a) the above Work, including any revised or expanded derivative works submitted to the ISM by the undersigned based on the work; and (b) any associated written or multimedia components or other enhancements accompanying the work.

CONSENT AND RELEASE

2. In the event the undersigned makes a presentation based upon the work at a conference hosted or sponsored in whole or in part by the IIT (ISM) Dhanbad, the undersigned, in consideration for his/her participation in the conference, hereby grants the ISM the unlimited, worldwide, irrevocable permission to use, distribute, publish, license, exhibit, record, digitize, broadcast, reproduce and archive; in any format or medium, whether now known or hereafter developed: (a) his/her presentation and comments at the conference; (b) any written materials or multimedia files used in connection with his/her presentation; and (c) any recorded interviews of him/her (collectively, the "Presentation"). The permission granted includes the transcription and reproduction of the Presentation for inclusion in products sold or distributed by IIT(ISM) Dhanbad and live or recorded broadcast of the Presentation during or after the conference.
3. In connection with the permission granted in Section 2, the undersigned hereby grants IIT (ISM) Dhanbad the unlimited, worldwide, irrevocable right to use his/her name, picture, likeness, voice and biographical information as part of the advertisement, distribution and sale of products incorporating the Work or Presentation, and releases IIT (ISM) Dhanbad from any claim based on right of privacy or publicity.
4. The undersigned hereby warrants that the Work and Presentation (collectively, the "Materials") are original and that he/she is the author of the Materials. To the extent the Materials incorporate text passages, figures, data or other material from the works of others, the undersigned has obtained any necessary permissions. Where necessary, the undersigned has obtained all third-party permissions and consents to grant the license above and has provided copies of such permissions and consents to IIT (ISM) Dhanbad.

GENERAL TERMS

- * The undersigned represents that he/she has the power and authority to make and execute this assignment.
- * The undersigned agrees to indemnify and hold harmless the IIT (ISM) Dhanbad from any damage or expense that may arise in the event of a breach of any of the warranties set forth above.
- * In the event the above work is not accepted and published by the IIT (ISM) Dhanbad or is withdrawn by the author(s) before acceptance by the IIT(ISM) Dhanbad, the foregoing copyright transfer shall become null and void and all materials embodying the Work submitted to the IIT(ISM) Dhanbad will be destroyed.
- * For jointly authored Works, all joint authors should sign, or one of the authors should sign as authorized agent for the others.

Deepak Kumar

Signature of Scholar

ACKNOWLEDGEMENTS

I would like to thank, first and foremost, my parents (Lt. Ramchandra Pandit & Malti Devi) and my brother and sister (Santosh Kumar & Pinky Kumari) for the unconditional and continuous support, through thick and thin that they faced due to my prolonged research work. I would like to especially thank my research advisors and mentor, Prof. Vivek Bajpai (guide) and Prof. Nirmal Kumar Singh (Co-guide) for letting me work under his supervision and guiding me throughout my research and being extremely cool and calm support throughout. It has been an honor working under his guidance. For the last four years, he has been an excellent teacher not only in terms of the fundamentals of manufacturing engineering but also in guiding me to make my own decisions and providing a zeal and motivation towards learning. Without his guidance and persistent help, this dissertation would not have been possible.

I would also like to thank my research committee members- Prof. A. R. Dixit, Prof. A. K. Das, Prof. Abhishek Kumar Singh, Prof. Nirmal Kumar Singh, and Prof. Vivek Bajpai for the opportunity to work with them, the guidance and the valuable inputs towards my thesis document.

I would also like to thank Prof. Sachin Mastud who is always available for short intensive discussions, which are of great importance and for helping me in the initial part of the work, and for sharing his experience of micro-electrical discharge machining. I would also like to thank him for his unfailing inspiration, whole-hearted cooperation, and fruitful discussions which are embodied in this thesis. Special thanks are to Prof. A. K. Das for permitting me to carry out research work in the workshop. I owe many thanks to Mohan Kumar, Ravi Shankar Rai, Abhinav Kumar, Rajesh Sahoo, Harish Bishwakarma, Arnab Das, Nitesh Kumar, Shashank Shukla, Rachit Ranjan, and Ankit Jain, and for their invaluable help throughout the research process. I wish to express my gratitude to all the teaching faculties of IIT (ISM) Dhanbad for their direct and indirect help in my thesis.

I am also thankful to Prof. A. R. Dixit, Associate Professor and Head of the Department of Mechanical Engineering, Indian Institute of Technology, Dhanbad for providing all kinds of help throughout the completion of the thesis

Deepak Kumar

Deepak Kumar

Date: 18 / 01 /2023

Place: IIT (ISM) Dhanbad

ABSTRACT

Emerging trends towards miniaturization and growing demands have led to fabricating components having nanoscale features for electronics, robotics, aeronautics, biomedical, automobile, and bio-micro-electro-mechanical system (Bio-MEMS) sectors. This thesis covers an approach to downsize the resolution limits of electrical discharge machining (EDM) to a nanometric scale, bridging the gap between micro and nanoscale machining considering the thermal impact of electrical discharge. Nano-electrical discharge machining (Nano-EDM) technology may offer nanosized features, for instance, complex 3D nano-grooves, nanocavities, nanopores, nanotools, nano-painless needles for drug delivery, etc. Later on, the thesis identified the research issues and perspective solutions for the advancement of nano-EDM technology. The research gap, constraints, and opportunities are critically examined through state-of-the-art knowledge in the second chapter i.e., the literature review. The impact of advancements in pulse power technology upon the realization of nano-EDM is also briefly reviewed.

For developing any micro/nanoscale features, a stable machine tool is always required, hence the third chapter proposed a novel servo gap control mechanism for the micro-EDM process and tested its machining feasibility and performance on difficult-to-cut materials such as duplex stainless steel (DSS-2205). The interelectrode gap control mechanism is based on magnetic levitation using a unipolar linear motor. Here, the electromagnetic force (F_{em}) is made balanced to gravitational force (F_g) and spring restoring force (F_{rs}) to achieve a stable and uniform discharge. The equilibrium state of these forces provides the essential condition for better machine stability and fast positioning response. The system is empowered with a pure DC power source and triggered with innovative actuator arm technology. The swinging of the actuator arm facilitates the essential condition for dielectric straining within the small interelectrode gap. The machining feasibility and

performance were tested first by conducting preliminary experiments on duplex stainless steel (DSS-2205) in deionized water. It was found that the material removal rate (MRR), tool wear rate (TWR), and surface roughness (SR) is lies in the range of 117.6-223.8 $\mu\text{g}/\text{min}$, 10-29 $\mu\text{g}/\text{min}$, and average surface roughness (Ra) of 1.823-2.693 μm respectively. The system stability was tested in terms of the voltage-current (V-I) discharge characteristic curve. It was found that the system maintains the proper gap efficiently and stably for the occurrence of normal discharge. The proposed solution may be a good alternative for servo gap control strategy in EDM or micro-EDM. The same micro-EDM system was used further utilized for the nano-EDM machining work using a scale-down approach via ZnO nanorods as nanotools.

Fabrication and handing of the micro and nanotools are one of the great challenges for the commencement of nano-EDM. It is expected that the tool with a nanometric tip may deliver discharge energy at the nanoscale due to the size effect. Hence, the fourth chapter deals with the three different approaches for the fabrication of micro and nanotool for the commencement of nano-EDM. In the first approach, micro-tools of diameter 90-95 μm were fabricated first using an electrochemical micro-turning process. Here, due to the anodic dissociation and ion exchange phenomenon, the material was eroded from the job to develop the cylindrical microtools. The vicinity of the rotating tool applied voltage, concentration, gravitational, and mass diffusion impact is a substantial factor that defines the geometry of the fabricated microtools. In the second approach, 2D nanoplates like ZnO nanostructured tools were developed on the tip of the microelectrodes. Here, the combination of zinc nitrate hexahydrate $[\text{Zn}(\text{NO}_3)_2 \cdot 6\text{H}_2\text{O}]$ and hexamethylenetetramine (HMTA) is employed as a growth solution with a PH value of 6.0. The assembly of 2D nanostructures grown on microtip is accelerated by introducing the ultrafine discharge in the chemical growth solution. The synthesis, deposition, and growth time were limited to 20 seconds only. After

deposition and growth, annealing heat treatment was applied at 95⁰C for 45 minutes to eliminate any impurities or crystal defects. The structural/morphological characterization through field emission scanning electron microscopy (FESEM) confirms that the fabricated nanostructure is 2D nanosheet-like at a lower molar concentration. Nevertheless, at higher concentrations, the grown morphology changes to a marigold flower-like structure with porousness in its crystal structure. The chemical characterization through energy dispersive spectroscopy (EDS) confirms the dominance of the ZnO in the fabricated nanostructured tools. The X-ray diffraction (XRD) results confirm the phase pure hexagonal wurtzite structure of ZnO with an average crystalline thickness of 27 nm. The availability of functional group and molecular fingerprint corresponding to ZnO stretching is identified by Fourier transform infrared spectroscopy (FTIR) while the elemental composition and their chemical states were analyzed by X-ray photoelectron spectroscopy (XPS). The development of 2D ZnO nanoplate-like structure on the microprobe tip has not been used as nanotools and it is limited only to the optical and chemical characterization. It was the first attempt towards the fabrication of nanoplates/nanorods-like tools formation.

Literature on nano-EDM indicates that normally atomic force microscopy (AFM)/scanning tunneling microscopy (STM) nanoprobes/nanoindenter are used as nanotools for the nano-electro-machining process. These nanoprobes are quite expensive and handling these nanoprobes needs a special tool holder which is also very costly. ZnO nanorods which are lies in the same dimension as these nanoprobes may be tested as nanotools for nano-EDM experimentation. Hence, in the third approach, ZnO nanorods were fabricated on the microprobe tip through a low-temperature hydrothermal process and tested its machining feasibility towards nano-EDM. The basic mechanism of ZnO nanorods formation and the chemical reaction associated with active nuclei formation in seed solution and morphological transformation in growth solution has been elaborated briefly. The

fabricated ZnO nanorods were further used as nanotools for fabricating nano-patterned features on super-finished titanium alloy (Ti-6Al-4V) and Inconel-625 using the scale-down approach of micro-EDM.

The machining setup and nanotools are now available for testing the feasibility of nano-EDM. Hence, the fifth chapter deals with a scale-down approach for fabricating the nanopatterned features on super-finished titanium alloy (Ti-6Al-4V) using vertically aligned ZnO nanorods grown on the apex of the microtip. On the apex of the micro tools, the ZnO nanorods were grown by the low-temperature hydrothermal process by dipping the apex of the tip in seed and growth solution followed by essential heat treatment at 90⁰C. It was found that the grown nanorods were well-defined in shape and size and further utilized as nanotools during long-duration discharge (5ms) micro-EDM experiments. It was expected that by downsizing the tooltip, the discharge energy per unit pulse may be reduced due to the localization and size effect. Field emission scanning electron microscopy (FESEM) micrographs were utilized for the morphological characterization of formed nanopatterned cavities, microtools, and nanorods while the chemical characterization of the same is carried out by electron diffraction X-ray (EDX) spectroscopy. Additionally, the stability of the machining process was tested first for multiple discharge energy pulses then after a long duration discharge energy pulse has been characterized by voltage-current (V-I) waveforms. Finally, the supporting results of this experimental investigation show the feasibility of the approach toward nano-EDM.

The sixth chapter deals with a top-down approach that is applied to the novel maglev micro-electric discharge machining process to reduce the size of the feature down to the nanometric scale. ZnO nanorods, which are grown on the copper tooltip apex, were used as nanotools for this. The nanorods were fabricated by a low-temperature hydrothermal process that involved dipping the tooltip (Copper wire, $\varnothing 100\mu\text{m}$) in seed and growth solution

followed by critical heat treatment (95⁰C). The morphological characterization of the tooltip indicates that the nanorods on the top surface of the tip are well-grown in shape and size, with uniform distribution. Experiments with long-duration discharge (4.5 ms) were carried out in an open-air environment on the super-polished Inconel-625 work surface using ZnO nanorods as nanotools. The intensity of discharge energy per unit pulse is expected to decrease as a result of the nanotools' localization effect. The appearance of geometrically irregular nanopatterned cavities on the super-finished work surface supported this. The nanopatterned cavities are the negative impression of the bundles of nanorods that developed due to the thermal impact of electrical discharge, according to the field emission scanning electron microscopy (FESEM) micrograph. Voltage-current waveforms were used to characterize the discharge stability for long periods/multiple discharge energy pulses. The energy dispersive X-ray (EDX) spectroscopy technique was also used to characterize the tooltip and produce nanocavities on an elemental level. Finally, the results of this top-down approach reveal that nano-EDM is feasible and may pose a wide range of applications in micro/nanomanufacturing.

The seventh chapter deals with the conclusion and contribution and future work opportunities related to nano-EDM.

TABLE OF CONTENTS

Chapter-1: Introduction.....	1
1.0 Introduction.....	1
1.1 Nano-EM/EDM - An overview	3
1.2 Theories in micro/nano-EDM	4
Electro-mechanical theory:	4
Thermo-mechanical theory:	4
Thermo-electrical theory:.....	4
1.3 Mechanism of Nano-EM/EDM.....	5
1.4 Trends toward miniaturization in nanomachining	7
1.5 Need for Nano Electrical Discharge Machining Technology	9
Chapter 2: Literature Review	11
2.0 Introduction.....	11
2.1 Characterization of the features manufactured using nano-EDM.....	16
2.2 Nano-EDM system development issues and perspective solutions	21
2.2.1 Precise motion control for accurate positioning	22
2.2.2 Servo mechanism for gap monitoring	24
2.2.3 Dielectrics and flushing methods.....	29
2.2.4 Pulse discrimination and control.....	30
2.2.5 Measurement and characterization devices	32
2.3 Advancement in discharge power technology and their characterization to launch nano-EDM.....	34
2.3.1 Transistor-type iso-pulse generator.....	34
2.3.2 Capacity – coupled pulse generator	35
2.3.3 Electrostatic induction feeding (ESIF) pulse generator	37
2.3.4 Insulated gate bipolar transistor (IGBT) type pulse generator.....	39
2.4 Research statements and objectives	40

2.5 Innovation and originality in research	40
2.6 Structure of the thesis.....	41
Chapter- 3: Maglev micro-EDM experimental setup and its machining feasibility and performance analysis on DSS-2205	45
3.0 Introduction.....	45
3.1 Motivation and Research gap.....	47
3.2 Working principle of Maglev μ -EDM	53
3.3 Experimentation and methodology	54
3.3.1 Workpiece and tool material	54
3.3.2 Experimental Setup and its peripheral components.....	55
3.3.3 Experimental Procedure.....	63
3.4. Results and Discussions	65
3.4.1 Machine health monitoring through volt-ampere (V-I) characteristic curve.....	65
3.4.2 Material erosion rate (MER) and tool erosion rate (TER) analysis	68
3.4.3 Specific energy consumption (SEC)- A common performance index (CPI).....	71
3.4.4 Surface integrity (SI) analysis.....	73
3.4.5 Surface topography analysis through FESEM.....	76
3.4.6 Material migration and diffusion analysis through EDX.....	78
3.5 Conclusions.....	80
Chapter- 4: Development of micro- and nanotools for Nano-EDM	83
4.0 Introduction.....	83
4.1 Fabrication of microtool through the electrochemical micro-turning process.....	86
4.2 Fabrication of nanoplatelets like nanotool on microprobe tip and its chemical and optical characterization	88
4.2.1 Experimental setup.....	88
4.2.2 Materials and procedure.....	89
4.2.3 Heat treatment (annealing).....	91
4.2.4 Results and Discussion	91

4.2.5 Conclusions.....	99
4.3 Fabrication of ZnO nanorods as nanotools grown on microprobe tip through low-temperature hydrothermal process.....	100
4.3.1 Mechanism of nanorods growth.....	103
Chapter- 5: Achieving nano-patterned features through micro-EDM process using ZnO nanorods as nanotools on Ti-6Al-4V	105
5.0 Introduction.....	105
5.1 Research gap and motivation	106
5.2 Material and Methods	110
5.2.1 Experimental setup.....	110
5.2.2 Maglev micro-EDM principle.....	111
5.3 Materials and procedure.....	113
5.3.1 Fabrication of nanopatterned cavity through a long-duration discharge energy pulse	113
5.4 Results and Discussion	115
5.4.1 Morphological characterization	115
5.5 Reason for growing the nanorods on microtip.....	120
5.5 Voltage-current (V-I) characteristic curve of the machine	121
5.5 Chemical characterization through EDX	124
5.6 Conclusions.....	126
Chapter-6: Geometrically irregular nano-patterning using maglev-EDM via ZnO nanorods on Inconel-625: A feasibility study towards nano-EDM.....	129
6.0 Introduction.....	129
6.1 Motivation for research and technological gaps	130
6.2 Material and Methods	133
6.2.1 Experimental system.....	133
6.2.2 Materials and procedure.....	134
6.2.3 Growth mechanism of ZnO nanorods.....	136

6.2.4 Geometrically irregular nanocavity fabrication	138
6.3 Results and Discussion	139
6.3.1 Nanorods and machined surfaces morphological characterization.....	139
6.3.2 Discharge characteristic curve (V-I) of maglev μ -EDM	141
6.3.3 Elemental characterization through EDX	144
6.4 Conclusions.....	146
Chapter- 7: Conclusions, Contribution, and Future Scopes.....	149
7.1 Conclusion	149
7.1.1 Fabrication of maglev micro-EDM Setup and its machining feasibility and performance analysis on Duplex Stainless Steel (DSS-2205)	149
7.1.2 Development of micro/nanotools for nano-EDM process	150
7.1.3 Achieving nano-patterned features through a micro-EDM process using ZnO nanorods as nanotools on Ti-6Al-4V	151
7.1.4 Geometrically irregular nano-patterning using maglev-EDM using ZnO nanorods on Inconel-625: A feasibility study towards nano-EDM.....	152
7.2 Research Contribution	153
7.3 Future scope of the reported work	154
References.....	156
Appendix 1	193
List of publications	193
Journal Publications	193
International conferences	194

LIST OF FIGURES

Figure 1. 1 Industrial component where the need for nano-EDM technology is realized. Reproduced with permission [11–19].	3
Figure 1. 2 Mechanism of material erosion in nano electro-machining (nano-EM) process under (a) wet (b) dry conditions of the dielectric. Reproduced with modification [51].	6
Figure 1. 3 Avalanche motion of electrons and ions in nano-EDM for building plasma.	7
Figure 1. 4 Size comparison of several natural entities on a length scale to understand the concept of miniaturization. Reproduced with modification [41].	8
Figure 1. 5 Size comparison of manmade entities on a length scale to understand the concept of miniaturization.	9
Figure 1. 6 Need for miniaturization in machining technology.	9
Figure 2. 1 (a) Schematic for a two-temperature model (TTM) (b) simulated nano crater showing material ablation mechanism at varying pulse on time in MDS. Reproduced with permission [57].	14
Figure 2. 2 (a) Delta3 micro-EDM (b) resolution and repeatability measurement. Reproduced with permission [61].	16
Figure 2. 3 (a) Current displacement (I-Z) curve attained at the various tooltip quality (b) I-Z curve by Pt-Ir tooltip before machining (c) after machining. Reproduced with permission [23].	20
Figure 2. 4 (a) Nano-embossing through nanotip to create nanopattern (b) nanopositioning stage with their key elements (c) schematic of nano-EM setup for nano features fabrication. Reproduced with permission [24].	23
Figure 2. 5 Piezo-driving unit to control the gap width in micro-EDM. Reproduced with permission [83].	24

Figure 2. 6 Ignition delay criteria for the servo feed control mechanism. Reproduced with permission [9].	26
Figure 2. 7 Servo feed control criterion (a) resistance-capacitance (RC) (b) transistor iso-pulse generator. Reproduced with permission [80].	27
Figure 2. 8 Servo feed control mechanism applied by Kunieda for nano-EDM. Reproduced with permission [20].	29
Figure 2. 9 Variation in voltage and current pulse (V-I) at different stages of electrical discharge. Reproduced with modification [159,160].	31
Figure 2. 10 (a) Alicona (infinite focus) microscope (b) A Leica DCM 3D white light interferometer Reproduced with permission [161,162].	33
Figure 2. 11 Diagram of a transistor-based iso-pulse generator. Reproduced with permission [80].	35
Figure 2. 12 Electrostatic induction feeding principle in nano-EDM. Reproduced with permission [81].	38
Figure 2. 13 Flow chart of the research work on micro- to nano-EDM	43
Figure 3. 1 Maglev Micro-EDM machining experimental setup with their peripheral components.	56
Figure 3. 2 Multi-output programmable DC power source	57
Figure 3. 3 (a) Current clamp working mechanism (b) Current clamp with BNC type connector.	59
Figure 3. 4 Passive type voltage probe with BNC type connector	60
Figure 3. 5 Manual linear XYZ micro-positioning displacement platform	61
Figure 3. 6 Digital storage oscilloscope (DSO) with BNC type connector	63
Figure 3. 7 Dielectric circulation system (DCS) with its peripheral components	63

Figure 3. 8 Circuit diagram of the maglev micro-EDM system for servo gap control.....	67
Figure 3. 9 Real-time voltage and current waveform at (a) peak current setting of 450 mA and (b) 550 mA at the time scale of 5ms and (b) 1ms.....	68
Figure 3. 10 Effect of discharge power on material erosion rate (MER) and tool erosion rate (TER) in three repetitions of experiments.	71
Figure 3. 11 Comparison of the specific energy (SEC) of the current system with the existing literature.....	73
Figure 3. 12 (a-d) 3D geometry of the machined surface (a1-d1) variation in area surface roughness parameters.....	75
Figure 3. 13 variations in linear surface integrity parameters over six to eight slices (Ra, Rq, and Rz) at lower (450 mA) and higher current (550 mA) settings.....	76
Figure 3. 14 Surface topography analysis of machined workpiece parts through FESEM with constant voltage (30V) and at varying currents (a) 400mA, (b) 450mA, (c) 500mA, and (d) 550mA.....	78
Figure 3. 15 Chemical characterization of (a) parent material (DSS-2205), (b) tool material (tungsten rod), (c) material migration, and elemental diffusion analysis through EDX spectrum at (c) 400mA and (d) 550mA at the similar location of the machined workpiece. ..	80
Figure 4. 1 (a) Electrochemical etching method (b) sequence of nanotip tool fabrication in the electrochemical process (c) fabricated nano tipped tool. Reproduced with permission [220–222].	84
Figure 4. 2 Tipped tool fabricated through various methods by the various researcher for micro and nano-EDM. Reproduced with modification [236–242]......	85
Figure 4. 3 Schematic for fabricating the microelectrode in the electrochemical micro-turning process.....	87

Figure 4. 4 Fabricated microelectrode (micro rods) for growing ZnO nanorods on the apex of the microprobe tip at 2.5M @ 15V and 3.0 M@ 18V.	88
Figure 4. 5 (a) Schematic of the experimental setup for 2D fabrication of ZnO nanostructure along with key components, (b) Actual representation of the experimental setup.	89
Figure 4. 6 Stepwise by flowchart for the fabrication of 2D nanoplates of zinc oxide (ZnO)	90
Figure 4. 7 Morphology evolution from 2D nanostructure to 3D nanoporous cluster (flower-like structure) under varying molar concentrations at different scale bars.	93
Figure 4. 8 Deposition and growth mechanism for the 2D assembly of ZnO nanostructure. .	94
Figure 4. 9 Chemical composition of fabricated nanostructure with their elemental color mapping via EDX spectroscopy.	96
Figure 4. 10 (a) X-ray diffraction pattern of the fabricated 2D nanostructure (b) size distribution of nanosheets.	97
Figure 4. 11 (a) Infrared spectrum (FTIR) (b) XPS survey spectra (c) high-resolution XPS - Zn2p3 and -Zn2p1 (d) -O1s of the grown nanosheet at 50V and concentration 0.10 M.	99
Figure 4. 12 Method of seeding on tooltip and growth of ZnO nanorods through the low-temperature hydrothermal process.	102
Figure 4. 13 (a) Morphology of the fabricated microelectrode (tungsten) (b) grown ZnO nanorods on the top surface of the microprobe tip.	103
Figure 5. 1 Actual experimental setup of maglev micro-EDM with their peripheral components.	111
Figure 5. 2 Schematic for maglev micro-EDM with discharge circuit and actual representation.	113
Figure 5. 3 (a) Micro tool electrode fabricated through the electrochemical micro-turning process (inset: morphology of the microelectrode), (b) grown nanorods (ZnO) on the apex of	

the tooltip (inset: nanorods act as nanotool).	116
Figure 5. 4 (a-d) Morphology (wurtzite structure) of the grown nanorods on the apex of the microprobe tip at four varying locations.....	117
Figure 5. 5 (a, b) geometrically irregular series of nanocavity (c) overlapping trenches of nanocavity (d) broken nanorods on the machined surface.....	119
Figure 5. 6 (a) 3D- profile of a nanocavity (b) depth of the corresponding nanocavity formed at a high peak current setting (400mA).....	120
Figure 5. 7 (a) Stable discharge energy pulses (b) Uniformity in the pulse width (5ms) during multiple discharges on the maglev micro-EDM system.	123
Figure 5. 8 Time transient voltage-current waveform at time scales of (a) 100ns and (b) 1.00 μ s.....	124
Figure 5. 9 Chemical characterization of the (a) fabricated microelectrode (b) grown nanorods on the apex of the microelectrode tooltip.	125
Figure 5. 10 (a & b) Compositional analysis of the machined surface (nanopatterned cavity) through EDX spectroscopy at two varying locations.	126
Figure 6. 1 Experimental setup of maglev micro-EDM with their peripheral components. .	134
Figure 6. 2 (a) Active nucleation sites are seeded on the tooltip (b) the seeded tooltip is dipped in the growing solution for nanorod formation.....	136
Figure 6. 3 Growth mechanism of ZnO nanorods in the low-temperature hydrothermal process.....	137
Figure 6. 4 (a) 100 μ m copper wire as tool electrode (inset: the top surface of copper wire), (b) morphology of grown ZnO nanorods on the top surface.	139
Figure 6. 5 Morphology of the grown nanorods on the tip-top surface at two varying locations.	140

Figure 6. 6 Morphology of the fabricated geometrically irregular nanocavities in long-
duration discharge experiments through ZnO nanorods at (a)300mA, (b) 350mA, (c)400mA.
..... 141

Figure 6. 7 (a) Stable discharge energy pulse (b) uniform pulse width (4.5 ms) (c) long-
duration discharge energy pulse during nanofeatures fabrication. 144

Figure 6. 8 Chemical characterization of the fabricated ZnO nanorods on the apex of the
microtip 145

Figure 6. 9 Chemical characterization of the machined surface fabricated by grown nanorods.
..... 146

LIST OF TABLES

Table 1. 1 Highlighted comparison between macro-EDM, micro-EDM, and nano-EDM. Reproduced with modification [20–25].	3
Table 1. 2 Potential application of nano-EDM in industrial components. Reproduced with permission [53].	10
Table 2. 1 Comparative characteristic of various nano-machining processes. Reproduced with permission [53].	16
Table 2. 2 Features created by the various researcher through nano-EDM. (Reproduced with permission) [8,23,62,73,74].	17
Table 2. 3 Major structural challenges and perspective solutions for the development of nano-EDM technology.	21
Table 2. 4 Review of gap control strategies and servomechanism criteria in micro/nano-EDM. Reproduced with modification.	24
Table 3. 1 Elemental constituent (% weight) of duplex stainless steel (grade 2205) workpiece.	54
Table 3. 2 Thermomechanical property of tool electrode (Tungsten)	55
Table 3. 3 Technical features and specifications of the multi-output programmable DC power source	56
Table 3. 4 Technical features and specifications of the current clamp	58
Table 3. 5 Technical features and specifications of the voltage probe	59
Table 3. 6 Technical specifications of XYZ linear micro-positioning stage	60
Table 3. 7 Technical features and specifications of digital storage oscilloscope (DSO) (Tektronix: TDS2012C).	62

Table 3. 8 The measured gap voltage, gap current, and duty factor in four iterations during the processing of duplex stainless steel (DSS-2205).....	64
Table 4. 1 Selected process parameters for fabrication of 2D nanostructure (ZnO)	91
Table 4. 2 List of chemicals that have been used for fabricating the ZnO nanorods on the tooltip.....	101
Table 5. 1 Material and applied experimental condition for fabrication of nanopatterned features.....	115
Table 6. 1 Fabrication of nano features: materials and working environment	138

TABLE OF ABBREVIATION AND SYMBOLS

μ -EDM	Micro electrical discharge machining
R_a	Average surface roughness
R_q	Root mean square roughness
R_z	Peak-to-valley roughness
S_a	Average area surface roughness
S_q	Root mean square area surface roughness
S_z	Peak-to-valley area surface roughness
mA	Milliampere
nm	Nanometer
ns	Nanosecond
μ j	Microjoule
R	Resistance
C	Capacitance
V	Pulse voltage
A	Ampere
T_{ON}	Pulse on time
T_{OFF}	Pulse off time
GND	Ground
OC	Overcut
SiC	Silicon carbide
T_{r1}	Transistor 1
C1	Capacitance of capacitor 1
C2	Capacitance of capacitor 2

ZnO	Zinc Oxide
NEMS	Nano-electro-mechanical systems
MEMS	Micro-electromechanical systems
Nano-EM	Nano electro machining
CAM	Computer-aided manufacturing
A/D	Analog to digital converter
MOSFET	Metal oxide semiconductor field-effect transistor
CNT	Carbon nanotubes
WEDM	Wire electric discharge machining
WEDG	Wire electric discharge grinding
CFD	Computational fluid dynamics
FET	Field-effect transistor
RC	Resistance capacitance
SE	Scanning electron
ESIF	Electrostatic induction feeding
STM	Scanning tunneling microscopy
AFM	Atomic force microscopy
SPM	Scanning probe microscopy
PWM	Pulse-width modulation
PZT	Piezoelectric actuator
FESEM	Field emission scanning electron microscope
EDS	Energy dispersive x-ray spectroscopy
TEM	Transmission electron microscopy
MRR	Material removal rate
TWR	Tool wear rate

SR	Surface roughness
IGBT	Insulated gate bipolar transistor
DAQ	Data acquisition system
PID	Proportional integral derivative
FIM	Fused ion machining
TBNS	Tip-based nanomanufacturing systems
XRD	X-ray diffraction
FTIR	Fourier Transform Infrared Microscopy
XPS	X-ray photoelectron spectroscopy
Maglev	Magnetic levitation
SPM	Scanning probe microscopy
AFM	Atomic force microscopy
STM	Scanning tunneling microscopy
PSO-SVM	Particle swarm optimization-support vector machine
DNA	Deoxyribonucleic acid
DPN	Dip pen nanolithography
EBL	Electron beam lithography
CNT	Carbon nanotubes
KOH	Potassium hydroxide
NaOH	Sodium hydroxide
F_{em}	Electromagnetic force
F_g	Gravitational force
V-I	Voltage current
L-R	Inductance and resistance
DSO	Digital storage oscilloscope

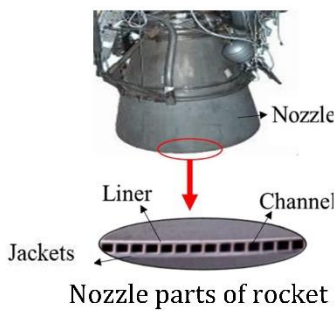


Chapter-1: Introduction

1.0 Introduction

Micromachined and nanomachined components are widely used in the electronic, aviation, biomedical, optics, and communications industries [1,2]. In recent years, nanomachining through non-conventional processes has become the key technology for the processing of exotic materials [3]. Electrical discharge machining (EDM) is one of the non-traditional machining processes in which material is removed due to the thermal impact of electrical discharge. Here, the material is removed in the form of microscale debris due to the controlled erosion of the tool and workpiece material under the dielectric media in a micro-confined gap (spark gap) via discharge energy. The machining process is unaffected by material properties like hardness and toughness, and it can handle a wide range of complex structures and features. The major advantage of this technology is that the machining process is of the non-contact type which means there is a complete elimination of mechanical disturbance, stress, chatter, etc. Recently, nano-EDM has gained traction as an important technology for nanomachining applications. Miniaturized products with features having nanoscale size can be easily formed through this process [4,5], which is one reason for increased interest in the use of EDM at the nanoscale [6]. The process is suitable for the fabrication of geometrically complex 3D nanostructures on any electrically conducting exotic materials that pose poor machinability. Burr-free and crack-free surfaces with close tolerances can be easily formed through this process at the nanoscale [6]. Also, the contactless-type process mechanism makes this process free from any mechanical vibration, chatter, and independent of tool rigidity [7]. Fabrication of nanopores for DNA detection,

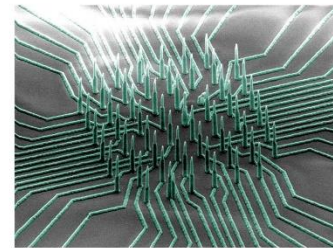
nanovias, nanojets for controlled drug delivery, nano-fluidics channel, interconnects for electronic devices, nanowires, nanorods, nanosieves for molecular sorting and future atomizers for nozzles, etc. are some noted application of nano-EDM [8,9]. Fig. 1.1 shows the varieties of industrial component features where the nano-EDM application is realized. To bring the machining technology to the nanoscale, Liu et al. [10] studied the impact of scaling for macro and micro-EDM systems in terms of influencing factors, dimensional tolerance (thermally), material microstructure, etc. They identified grain size, pulse duration, discharge frequency, and material microstructure as critical parameters in the scaling effect. Additionally, to feel the scaling effect, the fundamental differences among macro, micro, and nano-EDM are highlighted in Table 1.1.



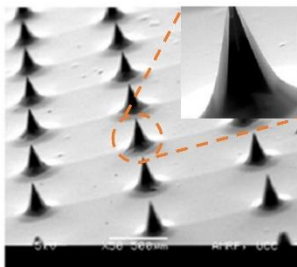
Nozzle parts of rocket



Dental-implant finished product



Neuron reading nanowire



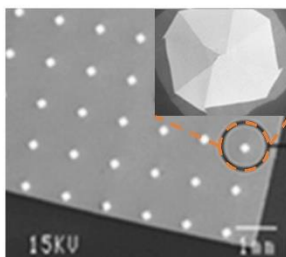
Micropattern array



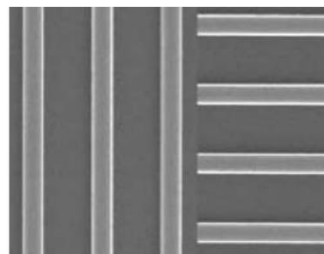
Accelerometer parts features



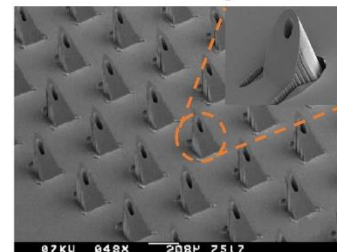
Surface integrity of biomedical implants



Nano features parts and texture



Microfluidic channels



Microneedle for controlled drug release.

Figure 1. 1 Industrial component where the need for nano-EDM technology is realized. Reproduced with permission [11–19].

Table 1. 1 Highlighted comparison between macro-EDM, micro-EDM, and nano-EDM. Reproduced with modification [20–25].

Points of distinction	Macro-EDM	Micro-EDM	Nano-EDM
Machine	Industrially available	Modifications of industrially available	STM/AFM machining platform or high-resolution positioning stage
Electrode material	Copper, tungsten, graphite	Tungsten, tungsten carbide	Pt-Ir, Tungsten, AFM, STM probes
Dielectric medium	EDM oil	De-ionized water and mineral oil	High dielectric constant medium and EDM oil (optional)
Operating voltage	40-400 V	40-200 V	300 mV-30 V
Current density	10^3 - 10^4 A/mm ²	10^3 - 10^4 A/mm ²	10^3 - 10^5 A/mm ²
Electrode diameter	~few mms	~5 μ m	15-25 nm
Discharge gap	0.0127-0.0508 mm	1-10 μ m	2-10 nm
Electric field strength	10^7 - 10^8 V/m	10^7 - 10^8 V/m	10^8 - 10^9 V/m
Flushing	Yes	Yes	Optional
Electrode polarity	+/-	+/-	+/-
Pulse duration	0.5 μ s-8 ms	ns-ms	ns-ms
Total cycle time	μ s-ms	ns-ms	ns-ms

1.1 Nano-EM/EDM - An overview

Nano-machining is recently identified as an emerging technology for machining difficult-to-cut or exotics material with undeformed chip thickness on the nanometric scale [26]. This technology can achieve ductile mode cutting with crack-free and smooth surfaces

in brittle materials. Nano-electrical discharge machining (nano-EDM) is an emerging processing tool for nano-level device and component fabrication. Its processing mechanism of material erosion is analogous to traditional EDM. However, the dimensions of the tool utilized, the character of pulse discharge, and the resolution of the movement within the subsequent direction signify the elemental difference in nano-EDM, micro-EDM, and EDM [27–29].

1.2 Theories in micro/nano-EDM

The material ablation theory in nano-EDM is quite complex due to the dynamic behavior of electrical discharge in nanoconfined space. Moreover, the discharge phenomenon in nanoconfined space covers multiple disciplines such as thermodynamics, electrodynamics, fluid dynamics, electromagnetics, etc. [30]. It is very challenging to understand the nature of the process considering a single stream. Hence, only the theoretical and mathematical modeling approach may help to understand the material erosion mechanism approximately in nano-EDM. Three theories are generally opted by the various researcher to understand the theory behind the discharge.

Electro-mechanical theory: This theory explains that the concentric electric fluid is responsible for material particle abrasion. The theory suggests that the forces of cohesion bind the material particle in lattice space and as the electric fields exceed the cohesive force of the lattice, the material gets eroded. The thermal impact is ignored in this theory [31,32]. Moreover, there is a lack of experimental evidence to judge this theory.

Thermo-mechanical theory: In this theory, a thermal flame jet causes material erosion, and these flame jets are formed due to the electrical impact of discharge. The evidence of experimental data does not support this theory efficiently. Moreover, the theory fails to provide a reasonable cause of spark erosion.

Thermo-electrical theory: The theory is well supported by theoretical as well as experimental

evidence. As per this theory, the material is eroded by the thermal impact of electrical discharge in highly ionized plasma [33].

1.3 Mechanism of Nano-EM/EDM

The fundamental of material processing and erosion in nano-EDM is much like that of micro-EDM. However, gap motoring via servo control with a nanotip size tool, discharge energy (nJ) in nano-confined space through nanosecond pulse power supply, and types of dielectrics with a flushing mode decides the condition for dimensional accuracy in the tolerance zone. In nano-EDM, the discharge is happening in similar phases to micro-EDM. The major portion of the supplied energy is consumed by the plasma channel in the build-up phase, discharge phase, and interval phase [34]. The build-up phase is nothing but the pre-breakdown phase of nano-EDM in which the foundation of the plasma channel occurs. In this phase, the breakdown of the insulating property of dielectric leads to bubble nucleation. Bubble nucleation takes place by bubble formation mechanism while its propagation occurs due to the electron impact mechanism. Later on, the impact mechanism leads to local ionization as an electron avalanche in the channel. The second phase denotes the plasma expansion phase where the vapor bubble is continuously expanding due to the pressure gradient between the vapor bubble and dielectric fluid. This further leads to a mass flow of liquid due to vaporization in the dielectric medium. Thermo-physical properties of the water vapor drastically change in this phase at high temperatures. This is due to the dissociation of molecules and ionization into charged particles. These charged particles are important because it plays a significant role in heat transfer between the anode and cathode. In the last phase, temperature increases abruptly and heat transfer takes place by radiation. Radiation heat transfer is overseen by Stefan- Boltzmann law while ion and electron bombardment is governed by the kinetic theory of ions [35]. Jahan et al. [23] bifurcated the material removal mechanism in dry and wet conditions of the dielectric medium through the nano electro-

machining process. The basic mechanics of material ablation in wet and dry nano-EM is represented in Fig. 1.2. As the nano pulse bias voltage is applied in the nanoconfined gap (2 nm) in dielectric medium (n-decane), the electrons and ions start to migrate towards each other. This movement of field-emitted electrons and ions causes ionization in the gap and provides a path to flow the current at minimum resistance. This avalanche motion of current (flow of electrons) causes local heating, melting, and evaporation of the tool and work part, which seems like a material erosion process in nano-EM.

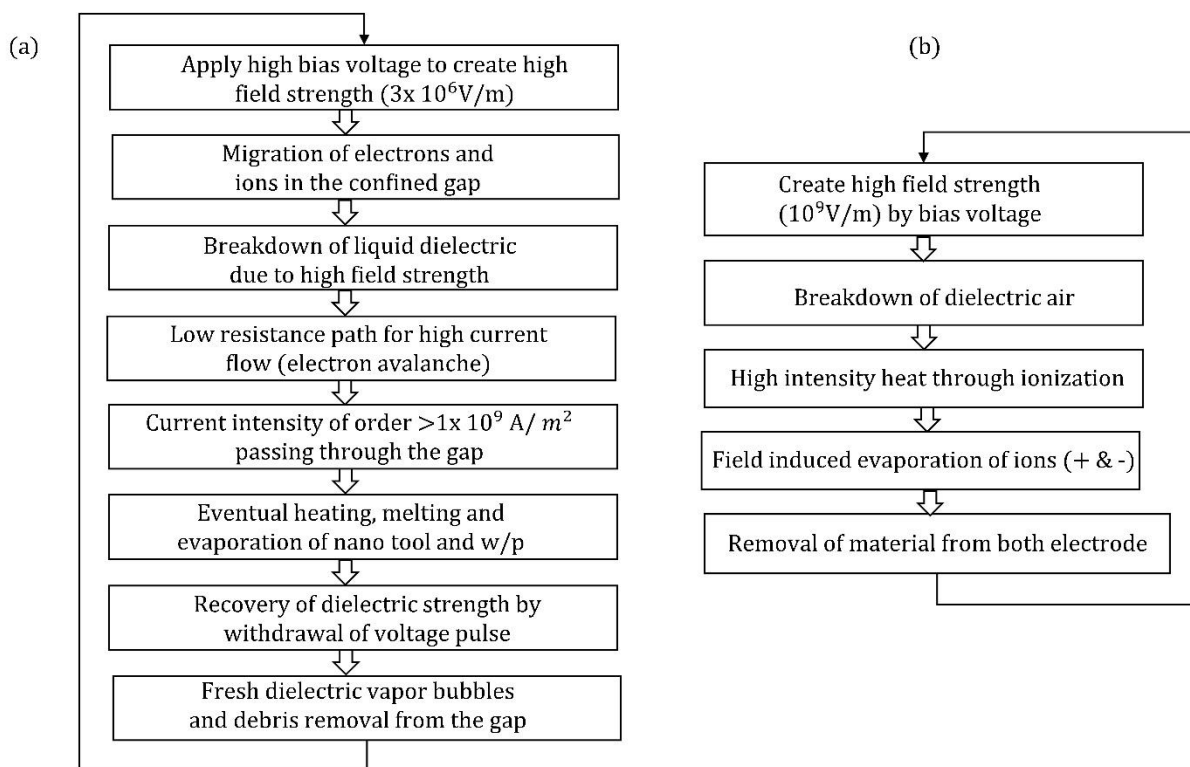


Figure 1. 2 Mechanism of material erosion in nano electro-machining (nano-EM) process under (a) wet (b) dry conditions of the dielectric. Reproduced with modification [36].

In dry nano electro machining, as the bias voltage is applied, the current starts to increase, which ends up in field-induced evaporation of electrode materials within the nanoconfined gap. Further, this field-induced evaporation reconditions the tooltip to build a new tool for creating sharper and more consistent nano features during machining. Hence, dry nano-EM material processing is directly related to field-induced evaporation, which

comes into the picture due to the breakdown of dielectric air. The dry nano-EM performance efficiency and stability were found much better compared to wet nano-EM due to the resharping ability of the tool under dry conditions. The avalanche motion of electrons and ions employing plasma characteristics and breakdown mechanisms in dry/wet nano-EM is demonstrated in Fig. 1.3.

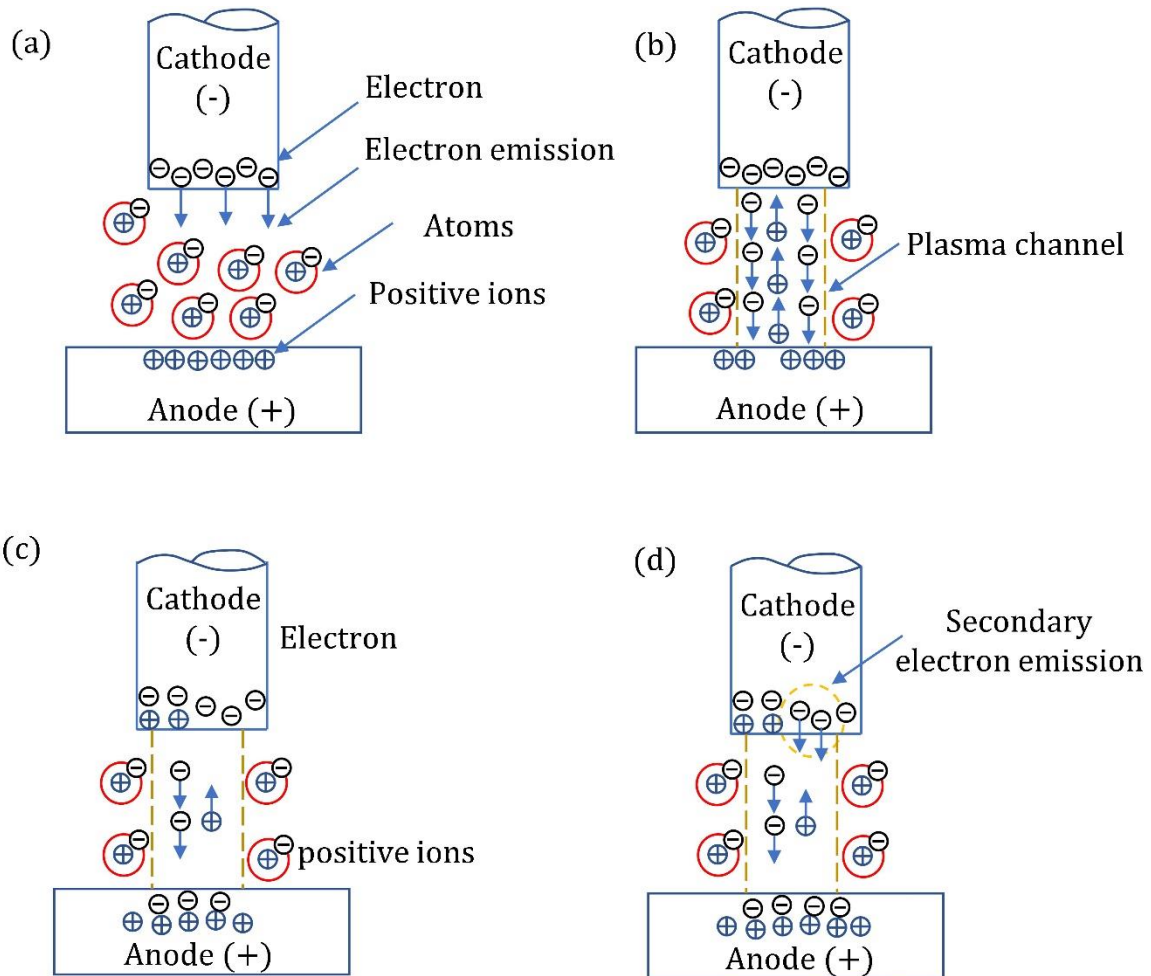


Figure 1. 3 Avalanche motion of electrons and ions in nano-EDM for building plasma.

1.4 Trends toward miniaturization in nanomachining

As scaling down in size of components, there is a need for improvement in technology. Miniaturization in the device is the fastest-growing technology in micro and nano machining industries [26]. To understand the concept of miniaturization, the size comparison of natural and manmade entities on a length scale is illustrated in Fig. 1.4 and Fig. 1.5. The

component such as micro nozzles [37–40], micro moulds [41–44], microsurgical instruments in biomedical applications [45–48], bio-implants [49,50], various automotive and avionic parts [1] lie in the category of micro-electro-mechanical system (MEMS) and nano-electro-mechanical system (NEMS). These all are being increasingly designed with features that are of micro to nanometer scale. Developments in these nanoscale features consume low power and material which causes improvement in functionality without space constraints. Moreover, a reduction in the mass of any components significantly enhances the performance efficiency of the device. Hence, it is very essential to bring microscale machining technology to the nanoscale. The need for miniaturization in technology for the industrial revolution is illustrated in Fig. 1.6.

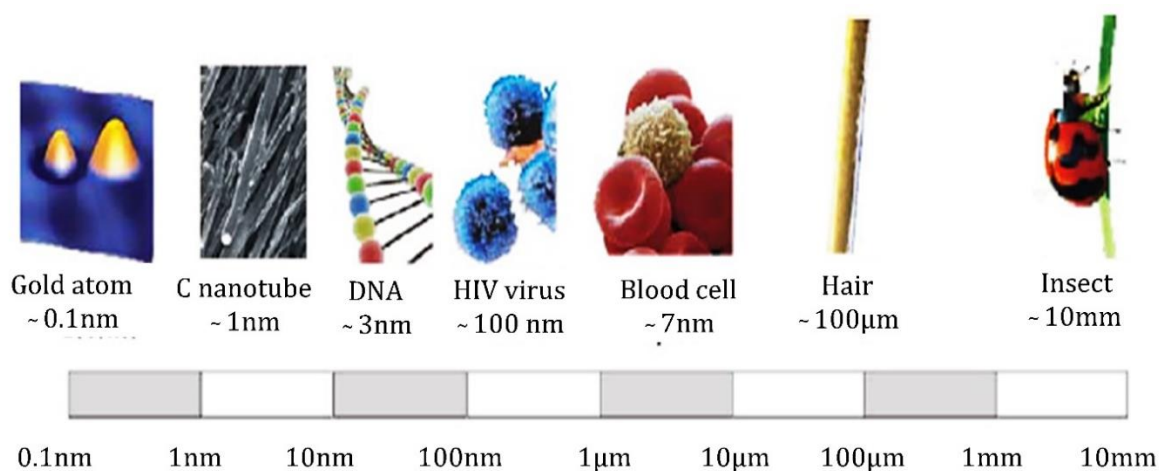


Figure 1. 4 Figure 1. 4 Size comparison of several natural entities on a length scale to understand the concept of miniaturization. Reproduced with modification [51].

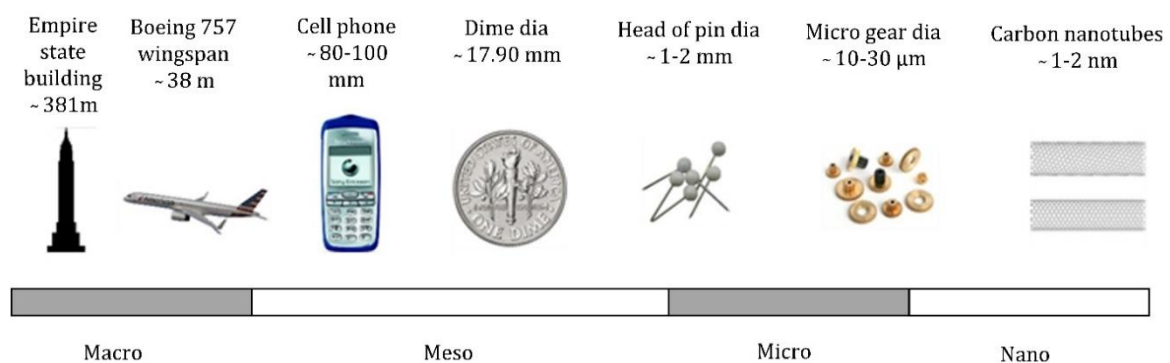


Figure 1. 5 Size comparison of manmade entities on a length scale to understand the concept of miniaturization.

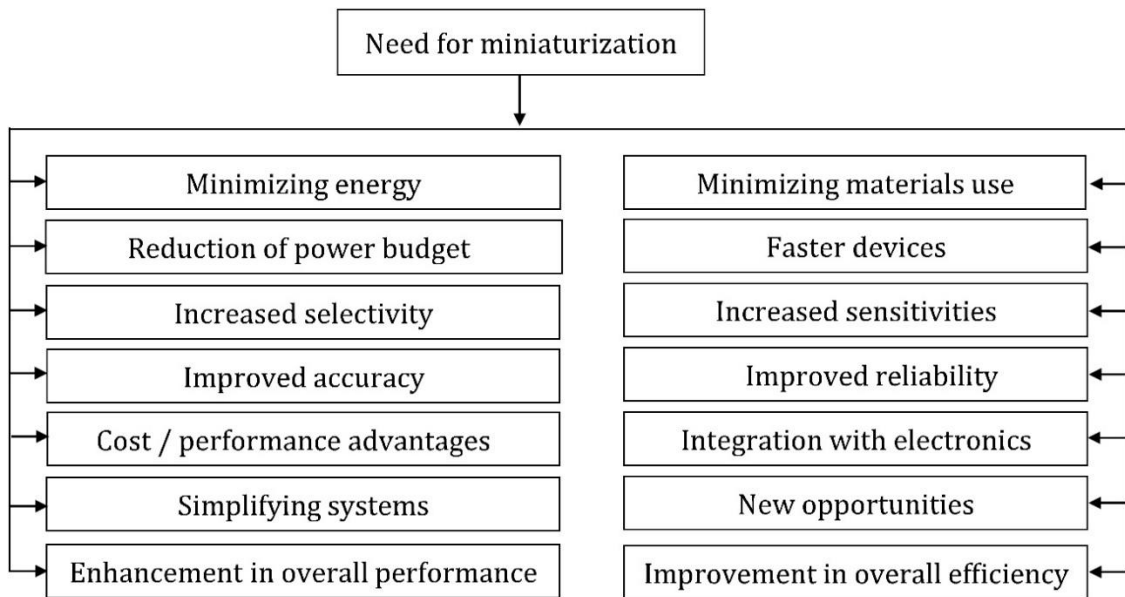


Figure 1. 6 Need for miniaturization in machining technology.

1.5 Need for Nano Electrical Discharge Machining Technology

Micro and nano-manufacturing industries are facing lots of challenges with the processing of exotic materials such as superalloys, composites, and non-conductive ceramics. Components made of these materials usually require high precision and excellent surface finish to perform the tasks for which they are designed. However, the manufacturing cost must still be maintained at an economic level. Nano-EDM is one technology that is suitable for the processing of such materials at the nanometric scale. This technology can be used to create nano-features such as nano-texturing on bio-implants, nanoindentation, nanocavity, nanoparticle synthesis, nanotools, nanoholes, nano-3D geometries, etc. Benilov et al. [52] used an electrochemically etched Pt-Ir tool to create micro and nano features by EDM in microfluidics. They reported that the balancing between open and short circuit modes (spark gap monitoring) creates favorable conditions for the uniform and stable spark in the gap width. Rajurkar et al. [53] presented a state-of-the-art knowledge of micro and nano

machining processes via electrophysical and chemical methods. In this study, they examined the impact of material behavior, residual stresses, environmental condition, and dielectric properties on machining performance. They further suggested that before processing any material through electro-physical-chemical machining, the material properties (grain size, crystallographic straining, and defects), thermal effect, residual stress, and machining condition must be checked. They also presented a table (Table 1.2) to display nano-EDM applications at the industrial level.

Table 1. 2 Potential application of nano-EDM in industrial components. Reproduced with permission [53].

Industry	Application samples
Aerospace	Transducers, gyroscopes
Automotive	Pressure sensors, nanojets nozzle, accelerometers
Electronics	Nanowires, nanogroove, flexible (paper-like) displays
Biomedical	Protein sorting molecular sieves, nano-dimples, DNA detection/separation devices
Healthcare	Catheters, intrauterine products, Nano therapeutic devices, infusion pumps

Nano-EDM technology has terrific potential to bring significant changes in nanomanufacturing. Nano-EDM technology is an open area of research, having little work available in the literature. Development in piezo driving technology with the advanced motion controller, development in an iso-pulse generator, and advancement in nanoprobes have almost solved the major issues of nano-EDM. Improvement in the servo control system (self-retraction) has solved the problem of gap monitoring. It is expected that the nano EDM technology will fulfill all the machining requirements at the nanoscale in the nearby future.

2

Chapter 2: Literature Review

2.0 Introduction

With trends towards miniaturization and growing demands for high-precision micro/nano components, advancements in technology are always required. The improvement in machining accuracy and precision must be there. High positioning accuracy and precision enhance the device's performance and make the product more reliable and exchangeable for human comfort [54]. In the past few decades, amazing development has been noted in ultraprecision machining where form accuracy and surface roughness are achieved at the nanometric scale or atomic scale. Currently, optical and nearby optical surface finish in micro/nanostructure components in geometrically irregular cavities can be easily achieved in multi-axis high-precision machining techniques. Applications for ultra-precise machining have included astronomy, light vehicles, biomedical devices, and a variety of other fields. The progress in ultraprecision machining technologies significantly affects the economy and construction of a nation. Ultra-precision diamond turning, ultra-precision milling, ultraprecision form finishing, ultraprecision polishing, and diamond stretching are coming in the category of ultraprecision machining techniques [55]. These ultraprecision machining techniques normally utilized the single crystal diamond tool for machining the difficult-to-cut material. In ultra-precision technology, the form accuracy and surface roughness can be achieved in the order of 0.1 μm and 1 nm. Although, ultraprecision machining techniques offer a very promising solution for micro-structured functional surfaces however fast tool servo response, burr dynamics, and depth of cut dynamics need to be studied more

comprehensively for intrinsic knowledge. High aspect ratio micro/nanofabrication, 3D features fabrication, and surface measurement and its characterization remain the challenge in ultraprecision machining techniques.

Product miniaturization and industrial realization significantly advance conventional micromachining techniques such as turning, milling, drilling, and grinding. Improvement in non-conventional techniques such as electrical discharge machining (EDM), electrochemical machining, laser beam machining (LBM), and ion beam machining (IBM) is also noted in current trends. Energy beam-based micromachining techniques pose the limitation of poor 3D features control, poor surface finish, low aspect ratio, and low material removal. In mechanical micromachining techniques, the material removal rate (MRR) is quite high and is capable of fabricating the 2D and 3D microfeatures in a broad range of stimulating materials. However, high tool wear, force transmissibility (vibration and chatter), instability at high temperatures, and high heat generation at the tool-workpiece interface region limit the process capability. The above issues in the conventional micromachining techniques are not involved in non-conventional micromachining techniques such as electrical discharge machining techniques. It is free from force transmissibility (vibration, chatter), mechanical instability at high temperatures, etc., however, its capability has been limited to the microscale level and not tested yet at the nanoscale level.

The technology capable of machining on the nanometric scale is still in a nascent stage. There is limited published literature available. The primary area covered in this section is a recent development in nano-EDM technology. It offers nanoscale machining with reasonable accuracy and precision.

Zhang et al. [56] applied a hybrid simulation technique, i.e., molecular dynamic simulation (MDS) combined with a two-temperature model to identify the processing mechanism in a single discharge nano-EDM system. This hybrid model was useful in the

thermal aspect because it comprehended the underlying machining mechanism in nano-EDM. The paper reported a tensile type of stress ($>3\text{GPa}$) during the cooling of the molten material, which further resulted in the breakdown of the material. The heterogeneous solidification was initiated at 1100 K followed by homogeneous solidification at 700 K. The white layer (re-solidified layer) and residual stress were also identified during the homogeneous solidification. The formation of white layer thickness was indicated as the result of quenching media however, the cooling effect was completely ignored for the model.

Yue and Yang [57] studied the material erosion mechanism by simulating a nano crater through molecular dynamic simulation and a two-temperature model. In this model, the concept of lattice vibration and free-electron movement was applied along with the heat conduction equation. Fig. 2.1 indicates the schematic of the two-temperature model and material ablation mechanism at varying pulse on time. The simulation results indicate that the inside pressure of the molten pool due to bubble formation is responsible for material erosion. As the inside pressure of the molten pool exceeds the binding force of the atoms, it explodes and the material gets eroded. Additionally, it was also observed that smaller grain sizes cause more denatured layers and structural defects. Xiao et al. [58] proposed a scaling approach to minimize the tungsten electrode tip size in the nanoscale patterning of carbon nanotubes (CNT) forests. This downsizing in the electrode tip (radius $3\mu\text{m}$) helps to reduce the discharge energy on the tip, which supports nano-EDM. The experimental results on CNT forests with various electrode tip sizes show that the minimum discharge energy can be easily attained on the tip to remove the material at the submicron level.

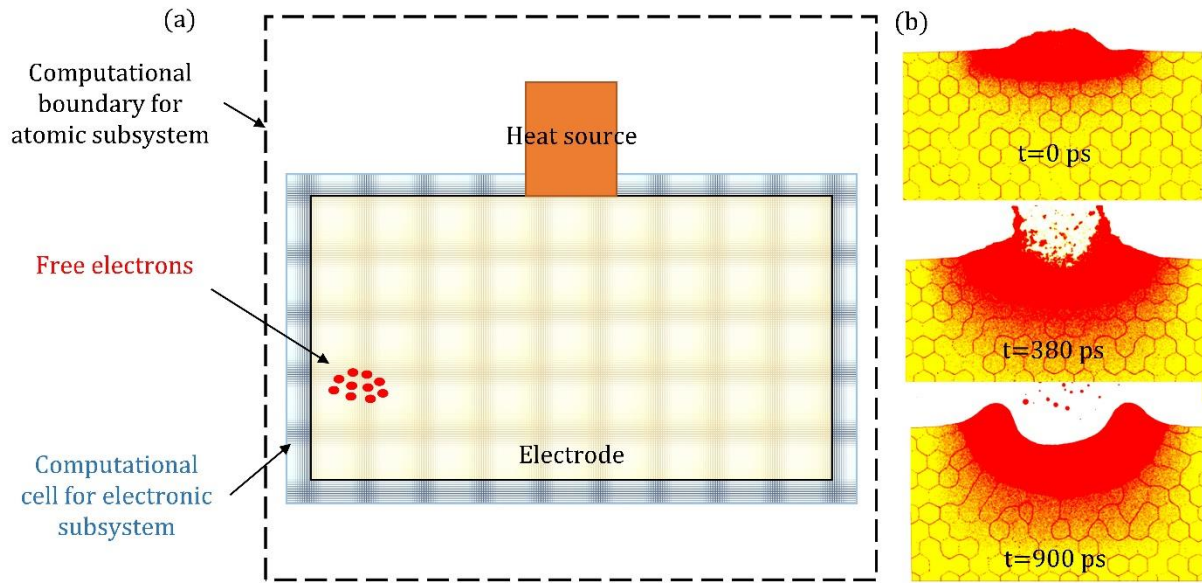


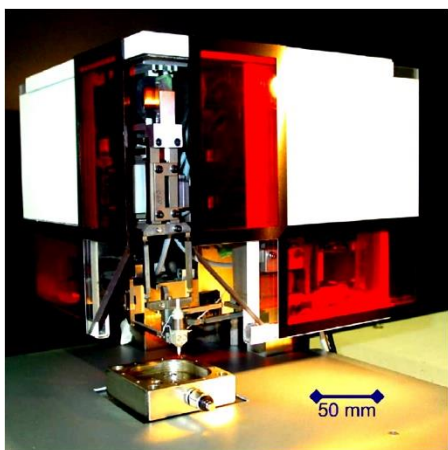
Figure 2. 1 (a) Schematic for a two-temperature model (TTM) (b) simulated nano crater showing material ablation mechanism at varying pulse on time in MDS. Reproduced with permission [57].

A multifunction miniature machine had been designed and developed at the National University of Singapore (NUS) for fabricating the nano features parts and devices. The micromachining setup was energized by a metal oxide semiconductor field-effect transistor (MOSFET) as well as resistance-capacitance (RC-type) pulse generators. The setup was supported by a feedback (close loop) control mechanism that gives dimensional accuracy within the sub-micron level. A resistance capacitance (RC-type) pulse power supply was utilized during the operation to get the desired level of nano finishing. It was capable of producing nano-discharge pulses for a long-duration [59]. These low discharge energy pulses fabricate the high aspect ratio microstructures like microelectrodes, micro slots, microgrooves, etc. It was concluded that the low discharge energy pulses may be beneficial for micro/nano features in micro-EDM.

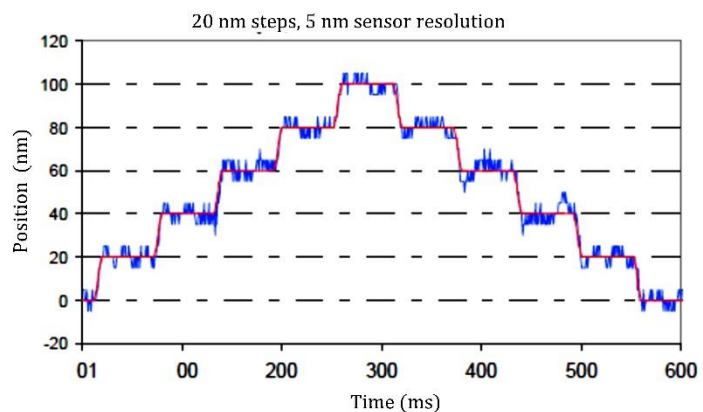
A capacity-coupled pulse generator was proposed by Kunieda et al. [20] for nano-EDM machining work. Using this pulse generator, they achieved a nanometric crater of

diameter $0.43\mu\text{m}$ by coupling the tool electrode via a capacitor. In this setup, they used a servo control mechanism to regulate the motion of the piezo table, the Z-axis tool, and the combined motion of the Z-axis and piezo table. The difference between gap voltage and reference servo voltage was used as the input to drive the Piezo table. The movable range of the Z-axis was $18\ \mu\text{m}$. Jung et al. [60] studied the modeling-based condition monitoring of pulse power supply via a discharge pulse counting approach. They reported the interaction between workpiece erosion and discharge pulses. It established the relationship between pulse frequency and spark gap via real-time gap monitoring control.

A highly precise micro-nano-EDM set-up had been developed by Beltrami et al. [61] for micro as well as nano-machining work at EPFL, named as Delta³ (Prototype III) (Fig. 2.2 (a)). The system was made using parallel kinematics with flexible joints. Mechanical disturbance such as friction, wear, and the backlash were eliminated to acquire the high resolution ($5\ \text{nm}$) (Fig. 2.2 (b)). Three linear electromagnetic motors were provided for mechanical actuation in three different axes. Moreover, the inclusion of a high-frequency AGIE pulse generator facilitates the essential energy for discharge in the nanometric gap. The setup was capable of eroding material as debris up to $100\ \text{nm}$ through ultra-short discharge energy pulses. Moreover, the high dynamic stability of the machine offers better flushing efficiency and accurate motion control over the gap.



(a)



(b)

Figure 2. 2 (a) Delta3 micro-EDM (b) resolution and repeatability measurement. Reproduced with permission [61].

2.1 Characterization of the features manufactured using nano-EDM

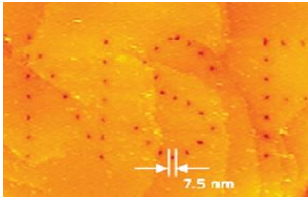
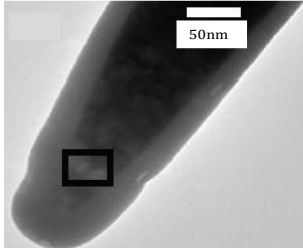
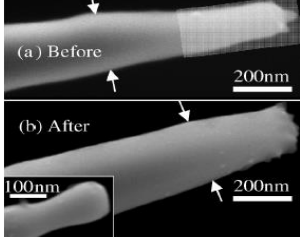
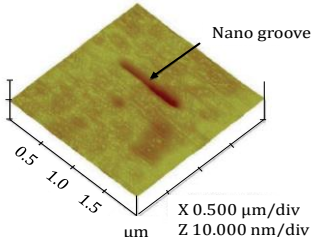
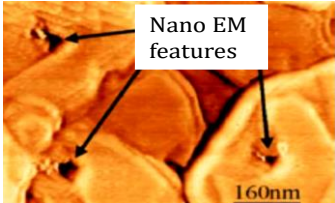
Nano electrical discharge machining enables the potential to construct nano features at the nanoscale level. This section shows the emerging report on nano electro-discharge machining techniques. The basic characterization of nano-EDM with the other nano machining technique has been demonstrated in Table 2.1. Moreover, the important features that had been created either through nano electro-machining or nano electro-discharge machining have been also included in Table 2.2. Malshe et al. [8] generated 10 nm nanofeatures over flat gold by platinum-iridium scanning probe (radius 15-20 nm). They noted resonant tunneling current as a significant factor that decides the material erosion rate under the dielectric medium of oil. K. R. Virwani et al. [62] examined the behavior of dielectric breakdown and tool erosion characteristics in nanoscale confinement via electrical discharge. Due to very high electric field intensity within the nanoconfinement gap, tungsten nanoparticles move towards the workpiece material (gold), which caused re-sharpening of the tooltip and consequently increases the material removal efficiency and durability of the process.

Table 2. 1 Comparative characteristic of various nano-machining processes. Reproduced with permission [53].

Process	Speed	Scalability	Work material	Minimum 3D feature	Contamination/Redeposition	Cost
Nano electro machining	Fast	Yes	All conducting	~ 20-80 nm	Redeposition	Low

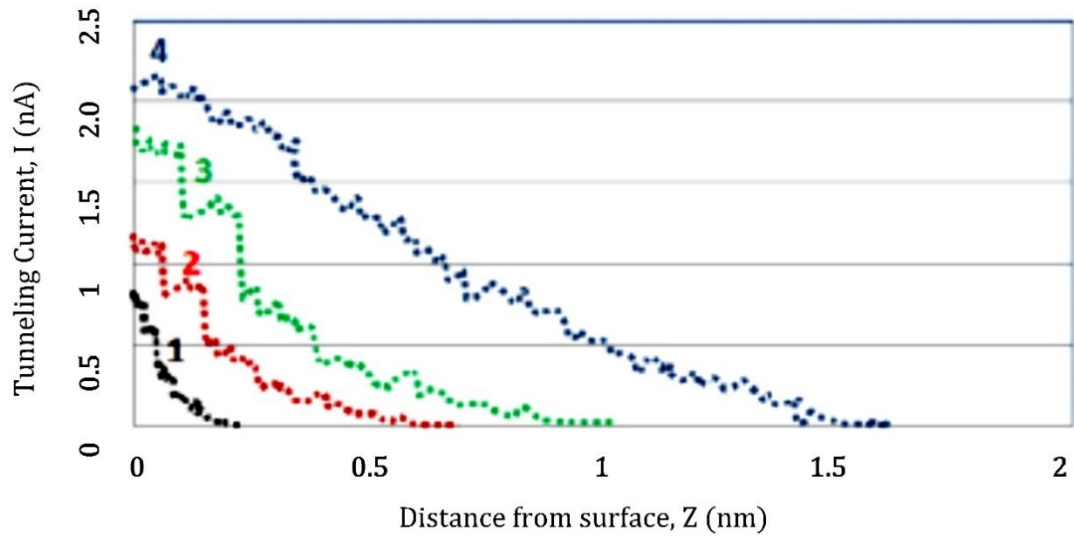
materials						
Nanoimprinting [63,64]	Fast	Yes	Polymers and silicon	10 nm	Residue buildup/contamination	Low
SPM based indentation and mechanical machining [65]	Fast	Yes	All	> 20 nm	Pileup	Low
X-ray lithography	Slow	No	All	1 nm	No	High
UV lithography [66,67]	Slow	Yes		90 nm		High
Electron beam lithography [66,68]	Slow	No	All	5 nm	No	High
Focused ion beam [69,70]	Slow	No	All	30 nm	Ga ⁺ ion implantation/redeposition	High
Femtosecond laser [71,72]	Fast	Yes	All	100 nm	-	High

Table 2. 2 Features created by the various researcher through nano-EDM. (Reproduced with permission) [8,23,62,73,74].

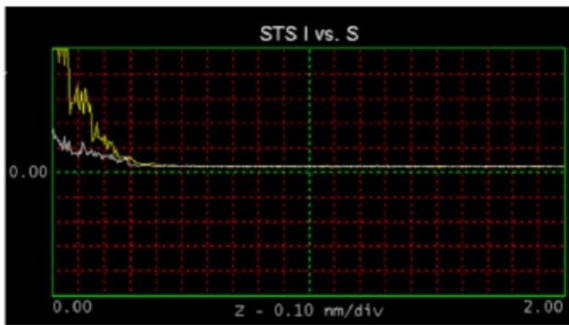
Author's	Features created	Images
Jahan et al., 2012	Nanoholes of an average diameter of 7.5 nm created using dry and wet nano electro-machining (EM). STM probes are used to remove the material at the nano-level via tunneling current.	
Virwani et al., 2007	TEM image of etched nano tool (after the breakdown of field strength on 0.8V/nm) fabricated through nano EM. The square box represents the scanning area at high resolution.	
Virwani et al., 2007b	SEM image of tungsten cathode (a) before (flat end) and (b) after breakdown increased shank diameter). The end radius of the cathode increased 35 nm before breakdown.	
Alkhaleel et al., 2006	Nano-groove formed through atomic force microscopy in copper of dimension 1000 x 150 x 2.4 nm. The nano features created through tunneling current rather than discharge current.	
Malshe et al., 2005	Nano features created by applying 10V with 60, 90, 120 seconds on atomically flat gold grown on mica using nano EM.	

Jahan et al. [23] applied dry nano-electro-machining to generate nanofeatures on the

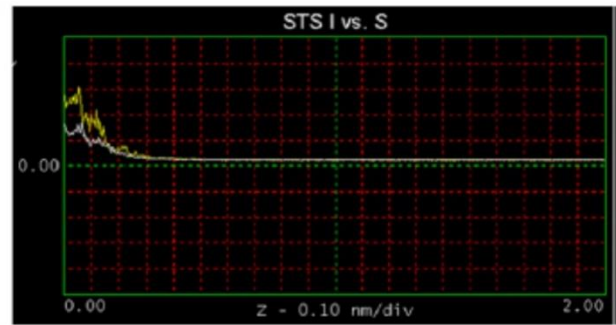
atomically flat gold substrate. STM was used as the nanomachining platform, while platinum-iridium was used as the tool electrode. The spark gap of 1-2 nm was maintained in the dielectric medium of air. The wear and tool quality were analyzed and explained through current-displacement (I-Z) characteristic curves after machining (Fig. 2.3). The confirmation test (nano-holes of 3-4 nm features size) was conducted on graphene to check the feasibility of the dry nano-EDM. Further on, comparative studies were conducted between dry and wet nano-EM to evaluate the erosion mechanism, dimensional repeatability, machining efficiency, and consistency of nanoholes. The dry nano-EM processing mechanism is allied with field-induced evaporation, where improvement in tool life was noted due to the re-sharpening ability of the tool. The wet nano-EM mechanism is based on the field-induced emission of the electron, which creates the low resistance path to the flow of high current within the nanogap. This low resistance path exhibits due to the dielectric breakdown and avalanche motion of ions and electrons within the confined gap. In wet nano-EM, there is a re-sharpening of the tool; hence machining efficiency is less compared to dry nano-EM [36].



(a)



(b)



(c)

Figure 2. 3 (a) Current displacement (I-Z) curve attained at the various tooltip quality (b) I-Z curve by Pt-Ir tooltip before machining (c) after machining. Reproduced with permission [23].

Cheng et al. [75] achieved an average surface roughness lower than 10 nm by fabricated nano-tool in nano-EDM. A nanogroove was created using atomic force microscopy on copper [73]. Kalyanasundaram et al. [76] examined the interaction of the machining interface and dielectric breakdown in the nano electro-machining process within a nanoconfined space of 3 nm. They explored the quasi-solid behavior of fluid dielectric (n-decane) through the molecular dynamics simulation (MDS) method with a boundary condition. They reported that the dielectric in nanoconfined space results quasi-solid dense medium, which significantly

influences the work function of the sample material.

2.2 Nano-EDM system development issues and perspective solutions

Achieving accurate control within the tiny interelectrode gap in EDM is a challenging task. In this section special attention is paid to those sources which are directly associated with motion control (piezo actuation technology), power supply (discharge energy control), dielectric flushing, tool category, and their material, servo mechanism (discharge gap control), debris and fumes management, in-process fabrication and measurement tools. Advancement in precision technology has almost solved the major structural issues related to nano-EDM (Table 2.3). Moreover, the major system development issues and the perspective solution has been identified and discussed briefly in the ahead section.

Table 2. 3 Major structural challenges and perspective solutions for the development of nano-EDM technology.

Major structural challenges	Perspective solutions
Precise motion control	Piezo driving nanopositioning stage or piezo actuators [77–79]
Discharge energy (pulse power supply)	High-frequency iso-pulse generator [80], capacity coupled [20], induction feeding power supply [81]
Servo control mechanism/ gap monitoring	LabVIEW, DAQ and advanced motion controller, and software [82], Arduino-based programming for adaptive control [83]
Dielectrics /flushing media	Diffused air (dry machining) [53], n-decane [76], bio-sustainable dielectrics [84]
Pulse characterization and control	Digital storage oscilloscope (DSO) [85]

Plasma characterization	High-speed imaging camera and spectrometer [86]
Current or voltage measurement	Highly sensitive voltage and current sensors (probes) [85]
Tool and workpiece wear monitoring and control	Online and off-line wear measurement and compensation techniques [87], cryogenic treatment [88]

2.2.1 Precise motion control for accurate positioning

The dimensional accuracy of any fabricated nano product significantly depends on precise motion control [89]. The piezo-driving nanopositioner and microactuator can offer control over the motion up to the nanometric scale [77]. This is essential for the accurate positioning of the tool electrode within the gap for nanomachining [90–92]. The highly precise positioning stage controls the effective number of discharge pulses within the smaller interelectrode gap by avoiding short-circuiting, arcing phenomena, etc. Fig. 2.4 showed the schematic of nano-EM fabricated by Malshe et al. [24] where a highly precise nanopositioning stage and the nano-tipped tool are used for precise motion control and nanofeatures fabrication. A maglev (Magnetic-levitation) microactuator arm is another option through which high positioning accuracy can be easily gained for micro and nano-EDM in 5 degrees of freedom [93–97]. He et al. [98] used the maglev micro-actuator arm for sub-micron positioning accuracy in a 5-DOF direction. Similarly, Fujiki et al. [99] used the high-speed piezo-driving microactuator to regulate the gap distance in real-time. Moreover, the fast retraction of the tool electrode in the axial direction was attained to enlarge the gap for fast recovery of average voltage which further causes improvement in machining efficiency and stability.

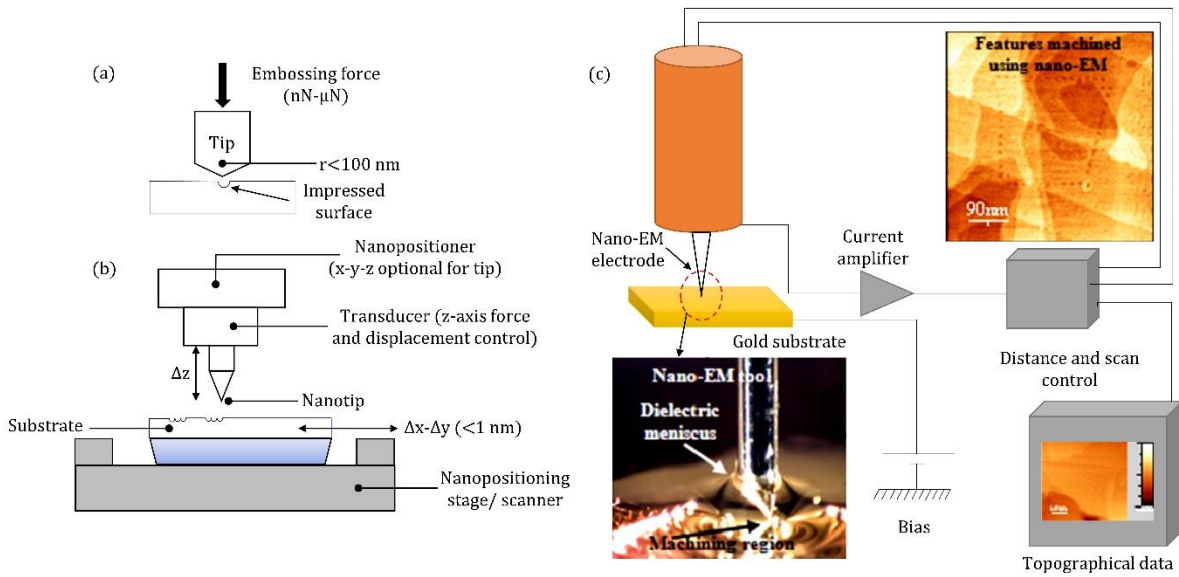


Figure 2. 4 (a) Nano-embossing through nanotip to create nanopattern (b) nanopositioning stage with their key elements (c) schematic of nano-EM setup for nano features fabrication. Reproduced with permission [24].

Perfilov et al. [83] used the piezo driving actuator (P-843.20, PI) to get a high dynamic response in the small interelectrode gap during EDM milling (Fig. 2.5). Especially designed kinematic pairs (flexure hinges) were used to get the free movement in work axes enabling with linear encoder for the stepper motor. Recently available nanopositioner, piezo driving micro-actuators may solve the issues related to positioning control. The discharge energy monitoring and control can be easily attainable in these stages within the specified gap. Furthermore, nanopositioning stages take less space for installation which reduces the overall size of the equipment and hence solves the problem associated with space constraints.

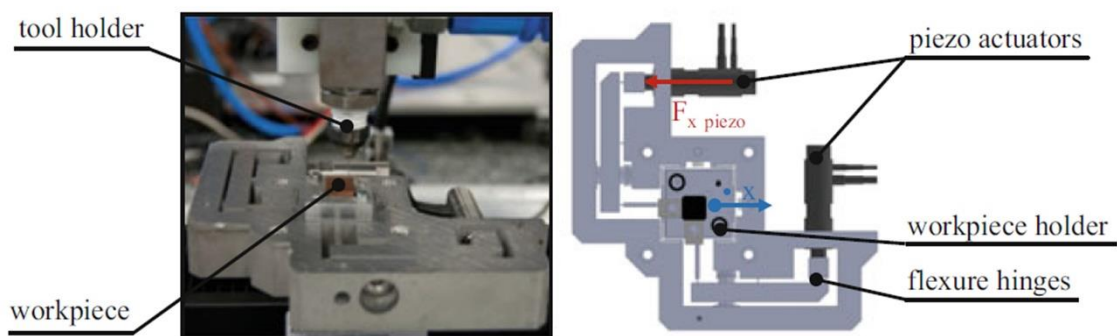


Figure 2. 5 Piezo-driving unit to control the gap width in micro-EDM. Reproduced with permission [83].

2.2.2 Servo mechanism for gap monitoring

Achieving high positional accuracy within the small gap is a challenging task for nano EDM. The servo mechanism plays an important role in the nano-EDM system since it predetermined the interelectrode gap for executing the electrical spark within the constant gap and thus, preventing short-circuiting, arcing, and contact. Moreover, a brief list of gap control strategies adopted by various researchers for servo control is represented in Table 2.4.

Table 2. 4 Review of gap control strategies and servomechanism criteria in micro/nano-EDM. Reproduced with modification.

Gap control strategy	Key remark	References
Adaptive control system	The error signal has been measured by comparing the reference signal with actual signal and fed the servo drive.	[100]
Real-time self-tuning regulator	Real-time gap states have been detected for self-tuning.	[101]
Adaptive control optimization (online)	Detect machining trends that lead to unnecessary conditions and to take appropriate action before the condition actually occurred.	[102]
Fuzzy control system	Self-adjusting the fuzzy inferences by reducing the temporal unstable conditions.	[103]
Fuzzy logic control	Irregular and short circuit discharge has been suspended to offer stable EDM machining	[104]

Self-adjusting fuzzy control	Self-adjusting the fuzzy inferences by reducing the temporal unstable conditions.	[105]
Tunable fuzzy logic	Dealing with the nonlinear and time-varying nature of electrical discharge through pulse discrimination	[106]
Fuzzy PI/PID	Linear feedback control theory in order to construct an asymptotically stable position feedback loop.	[107], [108], [109], [110]
Voltage threshold method	Pulse discrimination via microcomputer-based instrumentation	[111], [112]
Radiofrequency signal detection method	Gap monitoring via radio frequency signal	[113]
Waveform transform detection	Discharge waveform monitoring via wavelet transforms.	[114]
Fuzzy identification	Pulse discrimination by fuzzy control	[115]
Neural network identification	Online monitoring of discharge condition through neural network identification	[116], [117]
Ignition delay-based servo control	The average breakdown delay time is used for monitoring the gap in transistor iso-pulse power supply.	[118]
Voltage threshold method	Gap status has been recognized by comparing gap voltage with preset voltage.	[119]

The servo-controlled feed mechanism ensures the right spark gap [120] and consequently offers efficient machining in nano-EDM. Ignition delay is one of the important criteria to develop the servo control mechanism. Generally, a longer ignition delay time

indicates the larger gap condition between the two electrodes, and where the required gap voltage is a little bit high. In this situation, feed increases if the applied gap voltage is found more than the preset servo voltage. Similarly, feed decreases or electrodes retracted if the gap voltage is found less compared to servo voltage. Moreover, a short gap distance results in lower ignition delay which may further results in short-circuiting. Sometimes, the average delay time is used instead of gap voltage to control the gap state and discharge characteristics [121]. The ignition delay-based servo feed control strategy for gap monitoring and control is represented in Fig. 2.6. The stability and efficiency of the process significantly depend on the discharge state and servo control criteria. A stable gap monitoring system ensures a higher dimensional tolerance for the machined parts [122]. During the discharge phenomenon between two electrodes, it is highly recommended to control the spark gap distance [53]. Ideally, the servo system responds well to every effective pulse with the same frequency of discharge to avoid non-effective or bad pulses.

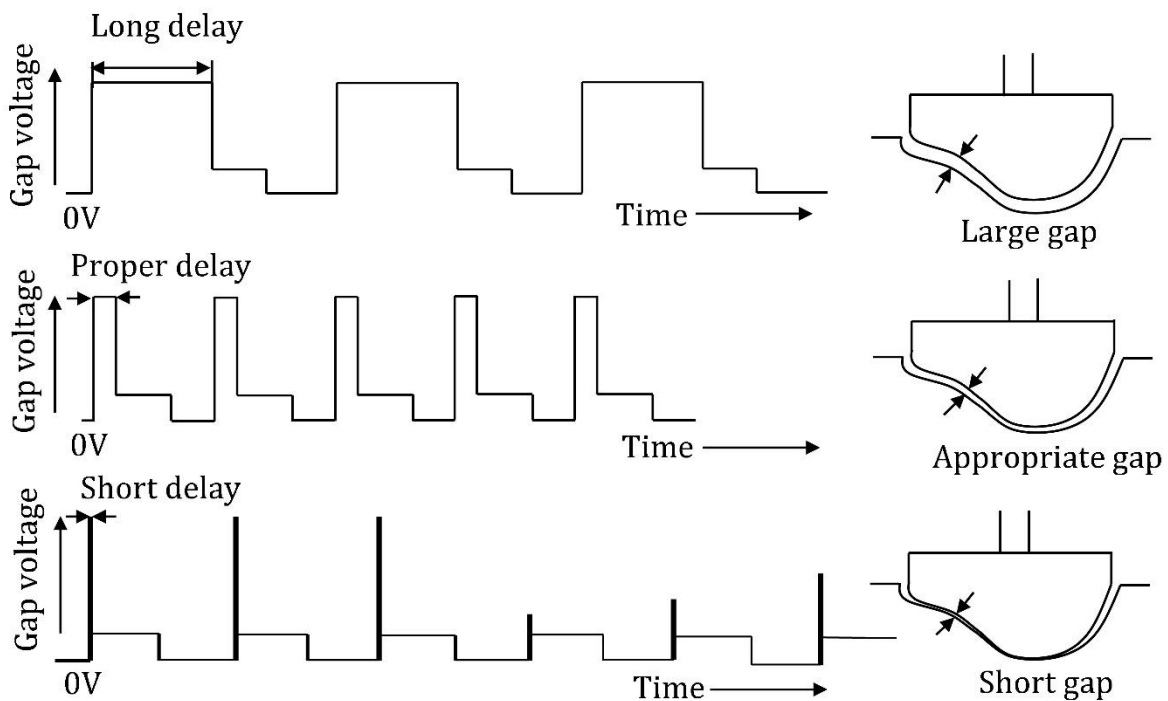


Figure 2. 6 Ignition delay criteria for the servo feed control mechanism. Reproduced with permission [9].

Han et al. [80] introduced the servo-control feedback system for resistance-capacitance (RC) and transistor-type iso-pulse type generators to study the machining characteristic of micro EDM (Fig. 2.7). The ignition delay time was taken as a critical factor to control the gap width and servo mechanism. The transistor-type iso-pulse generator was found more efficient in finishing due to its ultra-short discharge duration (30 ns). A piezo-driving electric actuator is generally preferred for shorter strokes while the motorized linear stage is utilized for longer strokes in a servo system. These actuators responded very fast with greater accuracy and stability in a few microseconds. Bani Melhem et al. [78] use a piezo driving actuator with a linear encoder motor to develop a dual-stage servo mechanism. They further applied a fuzzy control algorithm to control the gap width. Similarly, Wang et al. [123] introduced an equivalent circuit model to control the active gap during the processing of polycrystalline diamonds. Ten times better material erosion rate was noted compared to normal EDM with improved tool life. Xin et al. [124] studied the interaction between discharge energy and interelectrode gap through mathematical modeling. Also, the inter-electrode gap was controlled through self-tuning. They also suggested that the gap current, gap voltage, and plasma properties are key factors that decide the energy level for material erosion in the interelectrode gap. Similarly, Yang et al. [125] used the microcontroller to control the servo feed mechanism (based on voltage measurement) in micro-EDM.

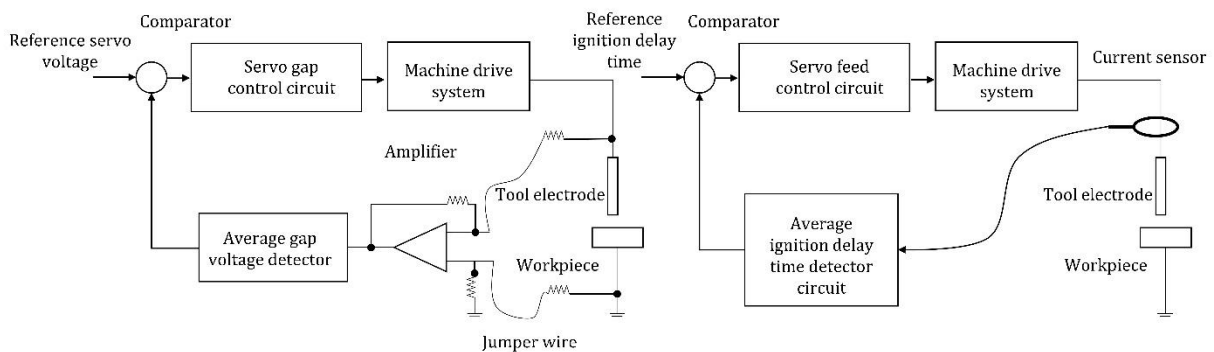


Figure 2. 7 Servo feed control criterion (a) resistance-capacitance (RC) (b) transistor iso-pulse generator. Reproduced with permission [80].

In contrast, the A/D module was used for conditioning the signal sent by the servo control system. A PWM module was used to drive the servo motor while the metal oxide semiconductor field-effect transistor (MOSFET) type generator was used as the power source unit to facilitate the essential energy for the discharge in the working gap. Mahendran et al. [126] developed micro-EDM by using the APA400MML actuator as a tool feed mechanism. A piezoelectric microactuator driver (PZT actuator) was used as a self-retraction system, while a rectifier was used to switch the signal from AC to DC obtained from the sensor. Metal oxide semiconductor field-effect transistor (MOSFET) type pulse generator was used for machining work. In this paper, they studied the impact of peak current, discharge voltage; pulse period, etc. on MRR, TWR, and SR. They further developed the tool wear compensation technique through the tool feed mechanism.

Three servo feed control mechanisms were used by Kunieda et al. [20] to regulate the movement of the Piezo table, machine Z-axis and cooperative movement of the Z-axis and Piezo table (Fig. 2.8). The difference between the open-circuit voltage and reference servo voltage was used as the input to drive the Piezo table. The movable range of the Z-axis was found to be 18 μm . Its fast response was noted in the Piezo table compared to the Z-stage during the operation. By applying this overall approach, they were ready to bring the EDM technology down to the nanoscale. In recent, a LabVIEW written control program with DAQ (I/P & O/P modules), and advanced Arduino-based programming may also resolve the problems related to gap monitoring and servo control for nano EDM.

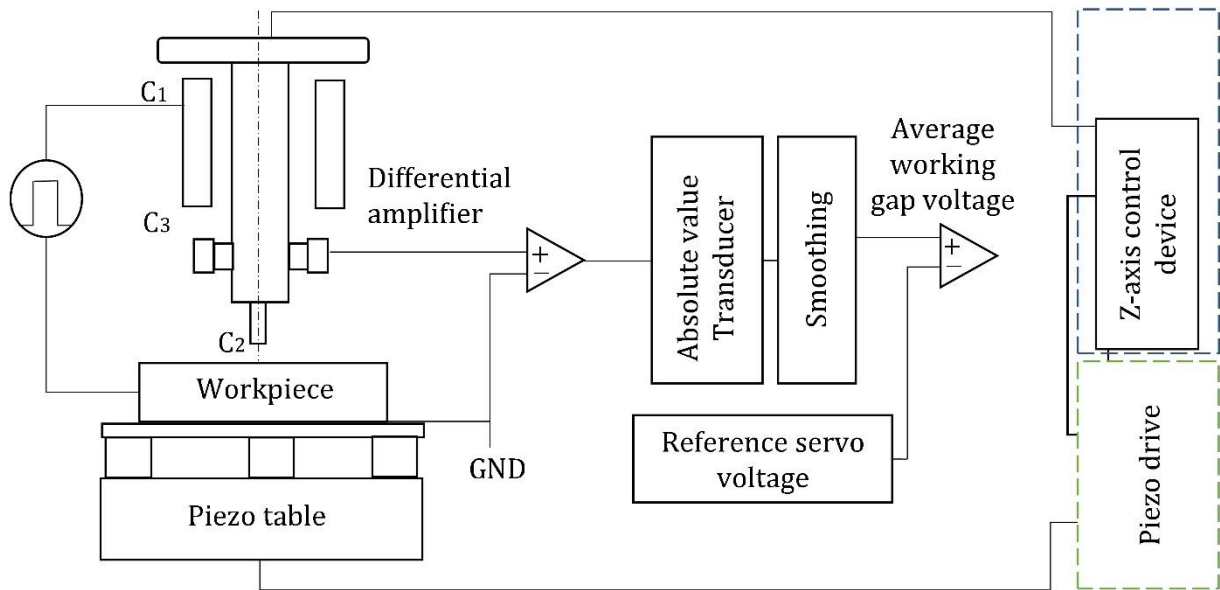


Figure 2. 8 Servo feed control mechanism applied by Kunieda for nano-EDM. Reproduced with permission [20].

2.2.3 Dielectrics and flushing methods

The dielectric in the interelectrode gap works as the insulator for a defined range of voltage potential. However, in further stages, it becomes a conductor to offer the low resistance path to flow the current. This further causes erosion in the material due to local heating, melting, and evaporation. After machining, it cools the discharge gap and provides the path to drive away the debris particle for creating the next spark in a cycle [127]. Roy et al. [128] segregated the discharge energy pulses based on debris nature via current and voltage characteristics. The gathering of nano debris may create problems like arcing, short-circuiting, micro-welding, etc. Hence, proper dielectric fluids with proper flushing systems are essential in these stages [129]. Usually, hydrocarbon-based dielectric fluids are mostly preferred due to their low conductivity, better flushing ability in small discharge gaps, etc. [130]. The decomposition of dielectric fluid due to high-temperature plasma increases the debris concentration in the gap, which causes unstable sparking. Deionized water may be preferred over there as a dielectric medium compared to mineral oil due to its higher MRR

[131–133]. However, due to the contaminated nature of this liquid, short-circuiting and arcing may be expected in further stages. Meanwhile, the adoption of wet dielectric fluid within the working gap creates environment and operator health safety questions [134,135]. Replacing the wet dielectric with a gaseous medium (diffused air/inert gas) may be beneficial as it is hazardous-free and environmentally friendly [136–138]. Near dry condition is another option through which bio-sustainability and green manufacturing issues can be solved for nano-EDM [139–141]. In near-dry conditions, the mixture of liquid dielectric and air (gas) is used as a dielectric medium. This approach facilitates stable machining with better flushing ability. Further, developing a bio-sustainable dielectric fluid for nano-EDM technology is a major issue. Neem oil [142,143], jatropha oil [144], water-oil emulsion [145–147], mixed air vapor (mist) [148], soybean oil, canola oil, sunflower oil [149], glycol [150], glycerin [151], compressed air, and are some bio-sustainable fluid [84,142,152–155] which may be tested for nano-EDM operation where sustainability issues are concerned.

2.2.4 Pulse discrimination and control

The nature of electrical discharge decides machining performance and stability. Generally, the occurrence of discharge is measured by connecting current and voltage probes (Hall Effect sensor) through a digital storage oscilloscope. The digital oscilloscope displays the different nature of waveforms for instance open circuits, regular discharge, arcing and short circuits during machining [9,156,157]. The electrical information and effectiveness of the waveform can be easily analyzed through this technique. The electrical information in terms of the current-voltage characteristic curve for different stages of discharge is shown in Fig. 2.9. This electrical information is essential to study the process capability and its effectiveness in the discharge system. Sometimes, a variation of the waveform is found in both directions from ground level which indicates the discharge of bipolar type [20]. Wu et al. [158] identified the various states of electrical discharge via the voltage-current (VI)

characteristic curve developed through the particle swarm optimization-support vector machine (PSO-SVM) algorithm in wire EDM. Moreover, the nature of electrical discharge in the interelectrode gap decides the cutting speed and process efficiency of the machining. Hence, it is very essential to monitor the current and voltage curve during discharge. Self-sustaining conditions of electrical discharge, power required, plasma formation voltage, machining voltage, discharge frequency, and amplitude variation can be easily understood by the voltage-current curve [85]. The study of the current-voltage characteristic curve reveals the actual mechanism of EDM and provides the guidelines for the design and development of pulse power supply and servo mechanism.

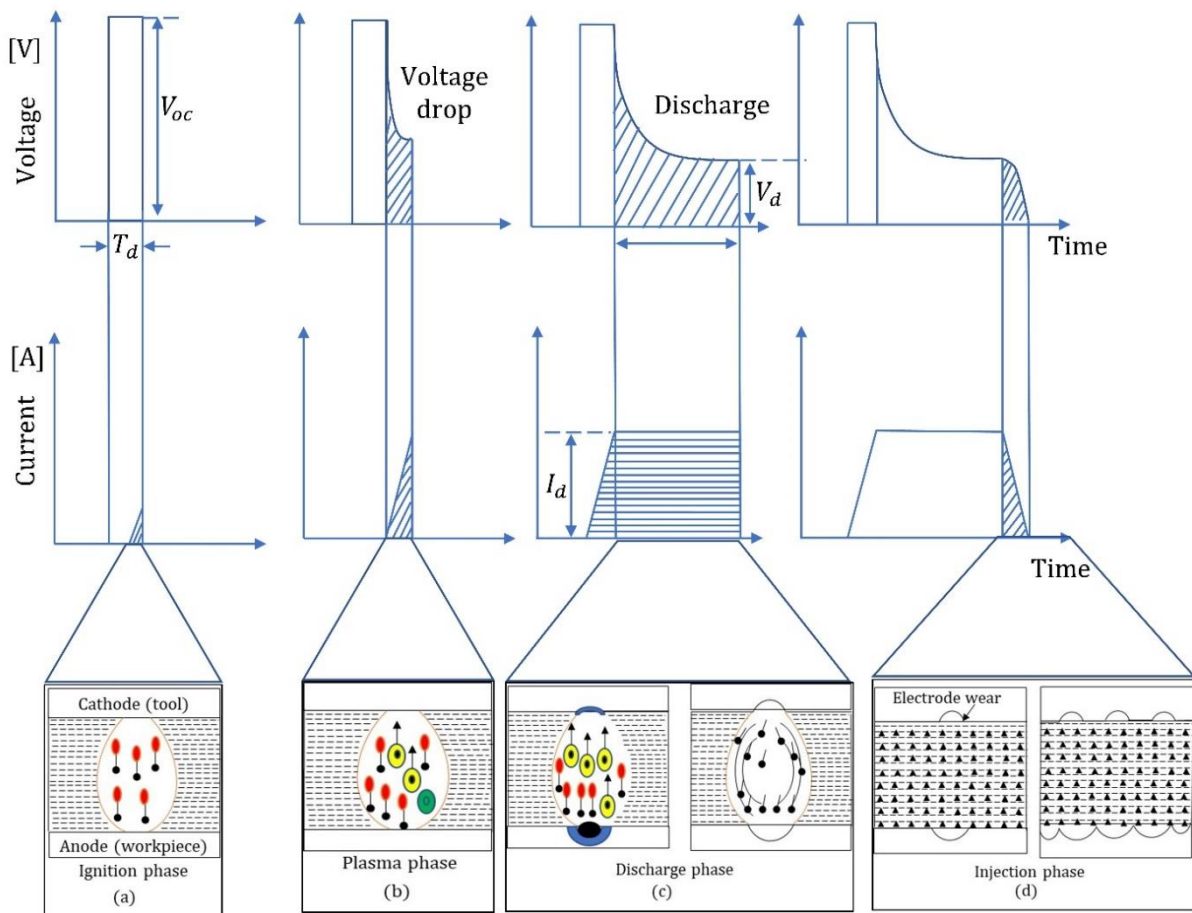


Figure 2. 9 Variation in voltage and current pulse (V-I) at different stages of electrical discharge. Reproduced with modification [159,160].

2.2.5 Measurement and characterization devices

Measurement is the key technique to ensure the product features at the nanoscale. In this section, the focus was made on the measurement of surface integrity (surface texture, roughness, and forms). The various types of nanoscale measurement tools (profilometers) and their working capabilities were analyzed and discussed.

Measurement device - The Alicona make microscope (Fig. 2.10(a)) is a device that is widely used to measure the surface texture using the focus variation principle. This machine has high repeatability and high resolution (vertical) to 10 nm. The data is acquired through vertical scanning within the objects, which is further converted into 3-D information via internal algorithms. Similarly, the Leica make DCM 3D (Fig. 2.10(b)) is one type of 3D profilometer which uses the principle of white light interferometry and confocal microscopy. The machine can measure to a resolution up to 0.1 nm. Similarly, the FE-SEM Supra 55 model microscope (Carl Zeiss make) uses the field effect scanning electron microscopy (FESEM) principle to acquire high-resolution images. Atomic force microscope (AFM), scanning tunneling microscope (STM), and transmission electron microscope (TEM) are some other sophisticated microscopy techniques that are extensively used to examine the nano-features and their characteristics at the nanoscale.

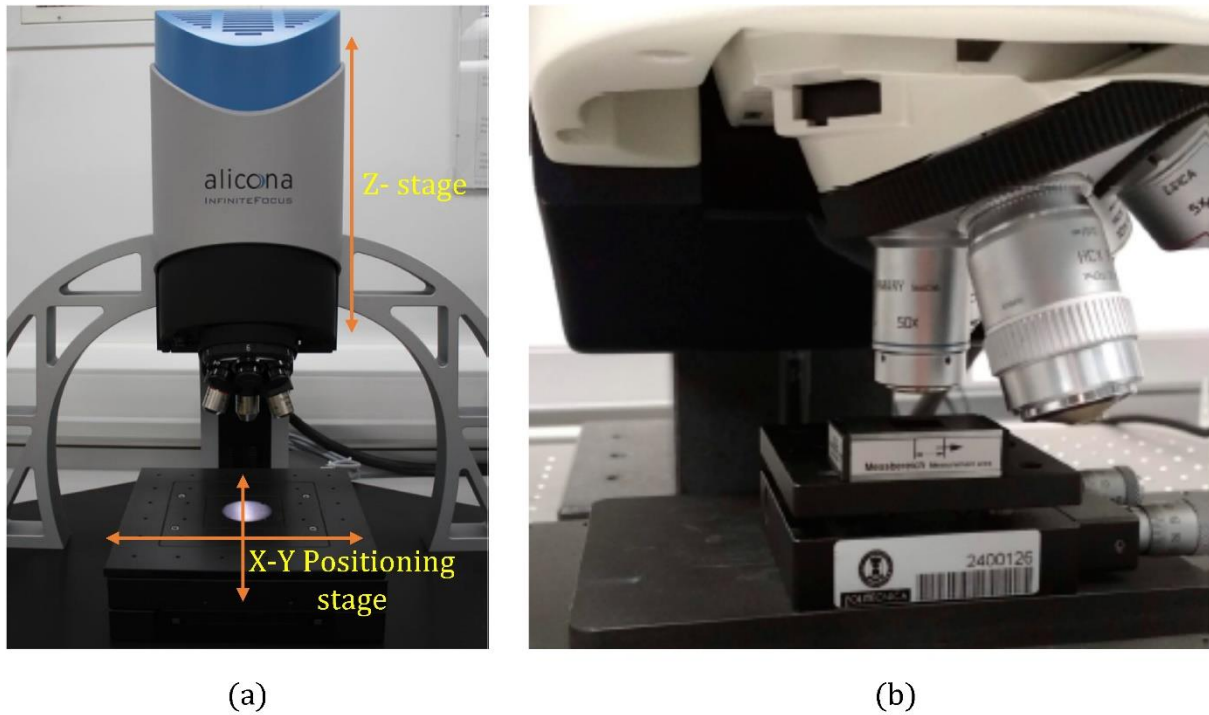


Figure 2. 10 (a) Alicona (infinite focus) microscope (b) A Leica DCM 3D white light interferometer Reproduced with permission [161,162].

High-speed imaging camera – The discharge that occurs in a small interelectrode gap is a complex phenomenon that involves cavitation, adhesion, and short-circuiting as key factors [163,164]. Moreover, understanding the breakdown behavior within the small interelectrode gap is quite challenging. A high-speed camera is recently in trend for measuring and analyzing the discharge phenomenon in a small gap because it provides direct observation of the process [165,166]. Moreover, high-speed imaging cameras [167] and digital oscilloscopes [86] offer visual and electrical statistics for analyzing the spark location within the plasma region. A high-speed camera captures a large number of images in a few seconds depending on the memory and sampling rate. Analyzing each image manually is a tedious and time-consuming task. Hence, MATLAB programming may sort out this problem by identifying the good and bad discharge from the image video database. Kumar et al. [168] utilized the high-speed camera for analyzing the bubble size and interelectrode gap under varying conditions of the dielectric in powder-mixed EDM. The sparking behavior, bubble formation, and gap

condition were explicitly explained by the image database. Further, the complex phenomenon of plasma growth and the occurrence of electrical discharge location can be easily obtained by this image processing technique [169,170].

2.3 Advancement in discharge power technology and their characterization to launch nano-EDM

The nano-EDM processing mechanism of material erosion is founded on the thermal impact of ultra-fine pulse discharge in the nanoconfined interelectrode gap. Nano EDM offers a crater size of less than 100 nm due to improvements in pulse generator technology [22]. Tahmasebipour et al. [6] developed a finite-volume heat transfer model based on CFD. It helps to understand the effect of heat flux and temperature in the formation of nano-craters at the duration of the pulse. The model investigated the impact of process variables such as discharge power, effective pulse duration, and workpiece thickness on the temperature distribution in a workpiece. A higher pulse duration causes a reduction in the final temperature of the workpiece. Moreover, the heat flux is exponentially distributed within the specified duration of the pulse. The nanofilm thickness was another factor that decides the condition for volumetric material removal and nano crater formation.

2.3.1 Transistor-type iso-pulse generator

Transistor-based pulse power generators are getting popular in recent trends because of their high discharge frequency of material erosion [171]. Discharge current and pulse width can easily be managed according to the requirement of machining characteristics.

The main problem associated with transistor-type pulse power is its delay time. It affects the machining time due to its long detection time after transmission of the signal. The transistor-type isopulse generator can reduce this delay time [80]. Fig. 2.11 shows the developed setup of the transistor-type isopulse generator. Points P_1 and P_2 were representing the short-circuiting point for roughing and semi-finishing operations, respectively. Finishing is done by

attaching an auxiliary circuit. FET₁ was used to fix the cut-off discharge current during roughing and semi-finishing operations. Pulse current was used for the detection of discharge. The output provided by the current sensor (<5V) was directly used as input in the pulse control circuit. As a result of this, a short pulse duration of 80 ns was attained. Pulse duration was further reduced by switching off the discharge current from the pulse discharge circuit. Rapid switch off of discharge current was done by disintegrating the two short-circuit points P₁ and P₂ and adding a new channel between them. Transistors Tr₁, Tr₂ and Tr₄, were made turned on to make the discharge current flow for machining. FET₂ was made turned off to make the condition of no discharge current flow within the gap. Getting FET₂ turned on by switching off Tr₁, Tr₂, and Tr₄ will initialize the discharge circuit [80]. Using this technique, minimum discharge energy at minimum pulse duration can be obtained, which results in removing the material at the micron level.

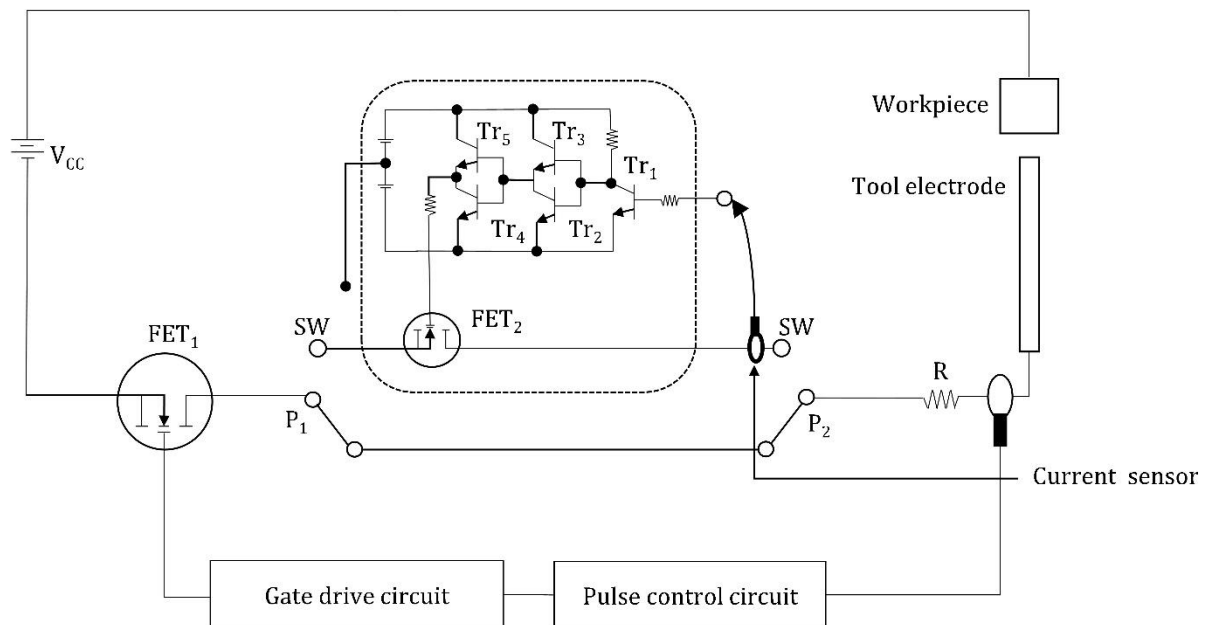


Figure 2. 11 Diagram of a transistor-based iso-pulse generator. Reproduced with permission [80].

2.3.2 Capacity – coupled pulse generator

The RC-type pulse power generator is still widely preferred for finishing and semi-

finishing operations. It has a constant pulse discharge energy capacity at a concise duration. The RC-type pulse generator is capable of producing a small discharge by reducing the capacitance of the circuit [172]. The capacity capacitance and wire inductance are two key factors that elect the intensity of discharge power in the relaxation-type pulse power supply [53]. The discharge frequency significantly lies in the charge storage capacity of the capacitor and resistance within the circuit. However, resistance cannot be brought up to zero because it may create more arcing rather than sparking [173]. The stray capacitance decides the availability of minimum discharge power per unit pulse within the gap. Sometimes, this stray capacitance is highly recommended for final finishing [53] in any EDM operation.

In the RC-type pulse generator, a low material erosion rate at a low discharge frequency is the major limitation. It takes time to store the charge for every sparking. Due to discharge variation, it is sometimes hard to achieve an excellent surface finish as it depends on the stored charge capacity. It creates thermal damage to the electrode surface because it cannot recover the dielectric strength without charging the capacitor [174]. Han et al. [175] reported that it is hard to reduce the crater diameter to less than $0.2\mu\text{m}$ in a traditional EDM power supply. The reason is that even after complete discharge, there is some residual capacitance available in the capacitor, which is known as stray capacitance which may affect the machining process. Kawakami and Kunieda [176] observed that stray capacitance is essential to regulate the intensity of discharge within a single pulse.

Further on, Egashira K [177] fabricated the microholes by lowering the gap voltage to smaller than 20 V. In this experiment, the electric feeder wire was shortened to avoid the effect of stray capacitance, and the desired level of accuracy of the machined part was maintained. Kunieda et al. [20] introduced a novel type of power generator for machining at the nanoscale level called a capacity-coupled pulse generator. They regulated the discharge energy by connecting a capacitor to the working electrode. The impact of stray capacitance

was eliminated through this technique. The required dimension was achieved within the nanoscale level to feel the execution of work through nano-EDM. A nanometric crater of diameter $0.43 \mu\text{m}$ was the achievement of this work.

2.3.3 Electrostatic induction feeding (ESIF) pulse generator

Yang et al. [81] proposed an induction-feeding type pulse generator. It could overcome some issues faced in the conventional pulse generator, such as the negative impact of stray capacitance. Fig. 2.12 displays the principle of the ESIF pulse generator in which C_1 indicates the capacitance of the tool electrode and the feeding electrode. Further, C_2 indicates the capacitance capacity lies in the tool electrode and work part. Additionally, C_1 was taken ten times more than that of C_2 . When the pulse voltage approaches V , then C_1 and C_2 get charged. This creates a negative polarity impact within the working gap, causing development of a strong electric field. Subsequently, discharge occurs, and electrons get delivered between two electrodes. After the discharge phase, the working voltage and discharge voltage become equal and no flow of current was noted within the circuit. The discharge was extinguished as the supply voltage approaches zero. Using this ESIF pulse generator, the stray capacitance impact was minimized within the discharge circuit due to the non-contact type feeding mechanism. This was helpful in constant discharge energy per unit voltage pulse, thereby realizing low discharge energy for nano craters formation.

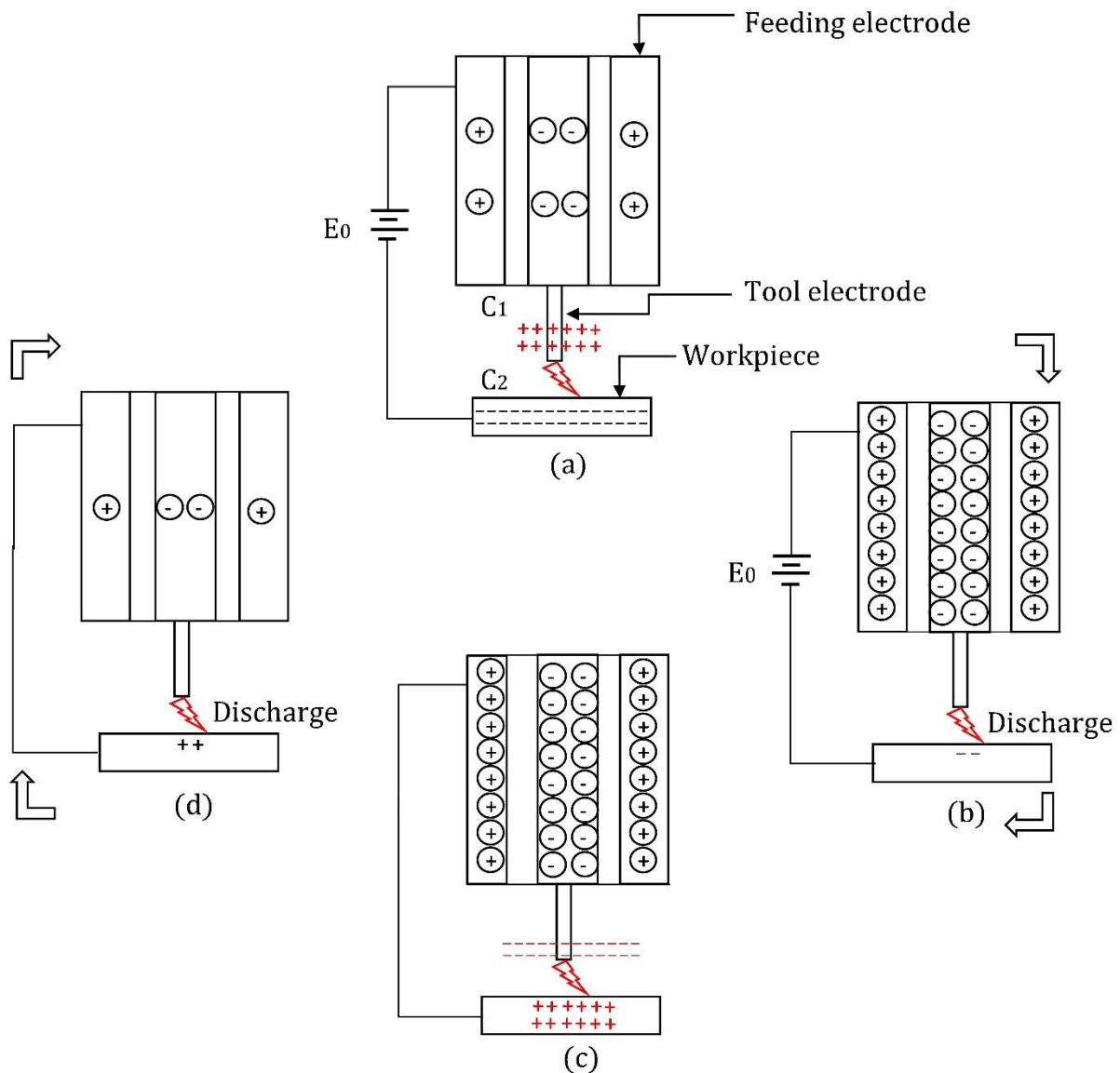


Figure 2. 12 Electrostatic induction feeding principle in nano-EDM. Reproduced with permission [81].

In addition to this, Yang et al. [178] used this ESIF method for obtaining microfeatures using wire electrical discharge machining (WEDM) with improved machining stability and lower consumption of discharge energy. The residual capacitance of the circuit was minimized to maintain the discharge energy at a low level within the gap. Through this strategy, they successfully attained micro slit of width $32.4 \mu\text{m}$ (narrow slot) and micro-beam of thickness $3.8 \mu\text{m}$ and a length of $100 \mu\text{m}$. Koyano and Kunieda [179] eliminated the

problem, such as low discharge energy pulse interval, localized sparking, and abnormal arcing by introducing the electrostatic induction feeding method during the fabrication of micro-beams. In this experimental work, they created a single discharge energy pulse at regular intervals of pulse voltage for each cycle in the working gap. This offers enough cooling and lower thermal damage to the machined surface, which results in an improvement in machining accuracy and speed. Zhao et al. [180] proposed EDM coring through an electrostatic induction feeding method on a silicon carbide (SiC) ingot. They studied the impact of multiple discharges on surface integrity and machining efficiency. They found significant improvement in material utilization and discharge frequency in induction-feeding pulse generators compared to conventional ones. The technique reports a substantial increase in surface integrity and the machining rate of the process.

2.3.4 Insulated gate bipolar transistor (IGBT) type pulse generator

The nano discharge energy pulses are essential to remove the material at the nanoscale. In recent years, the insulated gate bipolar transistor type pulse generator is getting popular. The main advantage of this pulse generator is that it provides ultra-short discharge pulses with very fast rise and fall time. It comes with a gate drive system of metal oxide semiconductor field-effect transistor (MOSFET) and a bipolar transistor which offers low saturation voltage with high current. The fast on-and-off switching mechanism prompts this pulse generator to use in EDM. Controlling voltage pulse in nanosecond width is a challenging task in the transistor-based power supply because resistance can't be made completely zero. Muthuramalingam and Mohan [181] used the insulated gate bipolar transistor-supported power supply to carry out the EDM work at the nanoscale. However, they were unable to bring the discharge frequency to more than 20 kHz. Modification in gate capacitance in these types of pulse generators may assist to bring the discharge frequency to the nanoscale. Moreover, proper design of the discharge drive circuit may control the frequent rise and fall

time of metal oxide semiconductor field-effect transistors (MOSFET). Further investigation is required to bring the discharge frequency at the nanoscale in the transistor-based pulse power supply.

2.4 Research statements and objectives

From the literature survey, it is clear that the technology developed for nanomachining through electrical discharge is limited. Based on the outcomes of the literature survey following techniques have been developed and implemented in the current study to achieve the nano features using the EDM principle which is novel in terms of gap control strategy, tools development, and nano-features fabrication: Hence, the present work research statement is “**technology development for high precision micro/nano-EDM**”.

To achieve the above research statement following are predefined objectives.

1. Maglev micro-EDM experimental setup (prototype) and testing its machining feasibility and performance analysis on difficult-to-cut materials (DSS-2205).
2. Development of micro- and nanotools through chemical growth and mechanical methods (ECM) for nano-EDM.
3. Achieving nano-patterned features through the maglev micro-EDM process using ZnO nanorods as nanotools on Ti-6Al-4V.
4. Geometrically irregular nanofeatures fabrication through maglev micro-EDM using ZnO nanorods as a tool on Inconel-625: A top-to-down approach.

2.5 Innovation and originality in research

The research carried out is new, Nano-EDM technology is in the developing stage and very limited resources are available in free literature. The research carried out shows the feasibility and the possibilities of electrical discharge machining at the nanoscale. The current state of art knowledge, key issues, and future research possibilities for nano EDM technology development are identified. The basic definition of nano EDM, related theories, and in-

process mechanisms are organized. The technological gap, the need for nano EDM technology development, and the characterization of the features that are made using nano EDM are covered explicitly. The technological challenges along with feasible solutions for accurate motion control, gap monitoring (servo system), discharge energy control, nanotools and fabrication techniques, metrology, and measurement, are covered briefly. The potential application of nano-EDM technology in various fields is identified and presented. Nevertheless, discharge energy has an immense impact on machining accuracy hence, advancement in discharge power technology upon realization of nano-EDM is covered separately. The development of a novel servo gap control mechanism, the development of nano tools, and the fabrication of the nano features using the electrical discharge energy principle is the major contribution of this research. A scaled-down approach has been used for achieving the nano-scale features using the electrical discharge machining principle. ZnO nanorods are used as nanotools which are grown on the microprobe tip. Due to the localization effect of the tool, it is expected to reduce the discharge energy level down to the nanometric scale. With the reduction in the discharge energy in the nanoconfined gap, nano features can be made.

2.6 Structure of the thesis

The complete thesis is divided into seven chapters. The flow chart of the research work carried out is separated into various chapters which are illustrated in fig. 2.13.

Chapter: 1 deal with the concept of miniaturization and its need for nanomachining. The classification of the human-made and nature-made entities are denoted on the length scale to clear the concept of miniaturization. The overview of micro nano-EDM along with the related theories are covered briefly in the initial part of the thesis. The mechanism related to dry and wet nano-EM/EDM is covered briefly in the introduction section.

Chapter: 2 covers the state-of-the-art review on micro as well as nano-EDM. The need for nano electrical discharge machining and its application area are denoted in the literature section. The characterization of the features that have been made previously through nano-EM and EDM has been presented. A comparative characteristic of nano-EM machining along with other nano-machining techniques has been denoted. The nano features that have been previously made by either nano EM or nano-EDM principle have been covered explicitly. The major development issues of nano EDM along with the perspective solution are identified. Moreover, the advancement in discharge power technology and their characterization to launch nano-EDM at the industrial level is also denoted briefly.

Chapter: 3 deals with the experimental setup of maglev micro-EDM and its peripheral components. The feasibility and performance of this machining setup were tested and compared to the existing literature in terms of specific energy. The material erosion rate, tool erosion rate, and surface roughness were also evaluated. The stability of the machining process was confirmed in terms of discharge characteristic curve i.e., voltage current waveforms.

Chapter: 4 deals with three different methods of micro and nanotools fabrication for nano-EDM. Nanoplatelets like tools on microprobe tips and fabrication of the microelectrode through the electrochemical discharge deposition process were demonstrated along with process physics. The fabrication of ZnO nanorods-like structure (nanotools) for nano-EDM operation and the growth mechanism is briefly explained.

Chapter: 5 deals with the fabrication of nanofeatures through a micro-EDM scale-down approach on Ti-6Al-4V. ZnO nanorods were used as nanotools for achieving the nanofeatures using the EDM principle. The stability of the machining process was tested for multiple discharge energy pulses in terms of the voltage-current curve.

Chapter: 6 deals with the fabrication of geometrically irregular type nanocavities on super-finished Inconel-625 surface. ZnO nanorods are used as nanotools electrodes. During nanomachining work, the machining stability was tested in terms of voltage current waveform. A top to down approach has been incorporated with the micro-EDM to achieve nano features

Chapter: 7 illustrated the conclusion, contribution, and future scope of the nano-EDM technology.

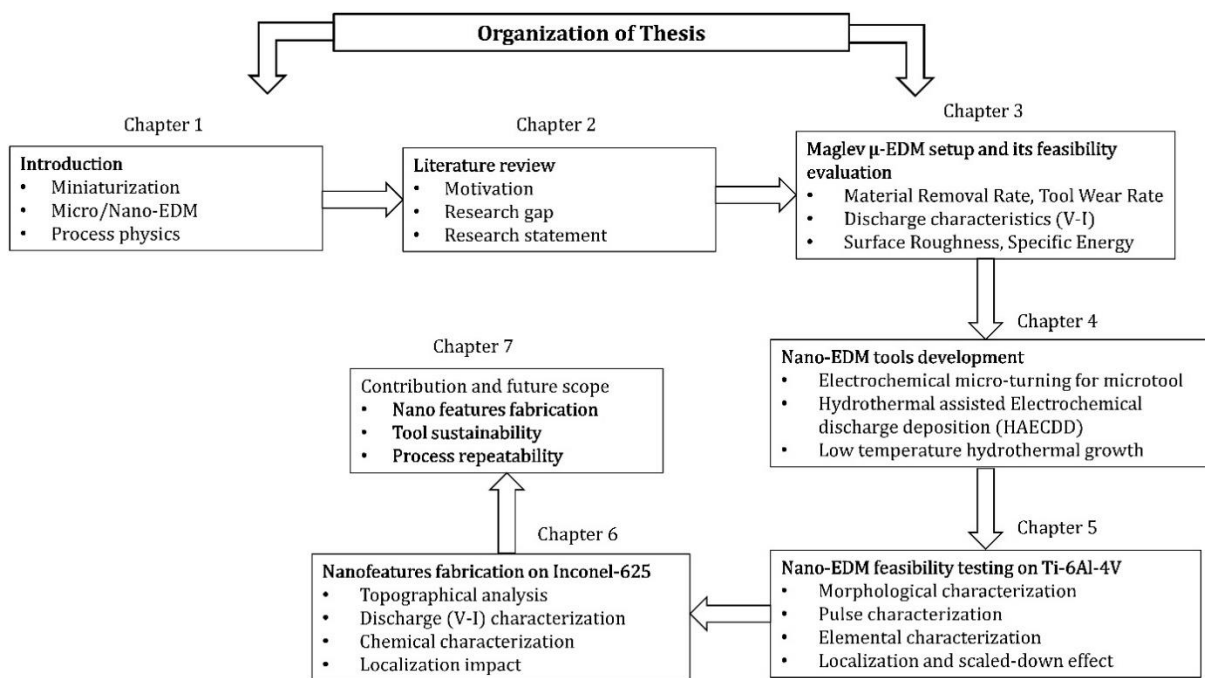


Figure 2. 13 Flow chart of the research work on micro- to nano-EDM

3

Chapter- 3: Maglev micro-EDM experimental setup and its machining feasibility and performance analysis on DSS-2205

3.0 Introduction

Micro-electrical discharge machining is a promising machining tool for electrically conducting materials, in which material is eroded in form of microscale debris by a succession of electrical discharges in a narrow-confined gap. Jahan et al. [182] discovered the numerous abilities of micro-EDM for processing complex shapes and features on electrically conductive materials. They identified the various aspect of tungsten carbide (WC) for processing composite materials by utilizing the EDM principle at micro- to nano-scale levels. In micro-EDM, the material removal process mechanism is based on the thermal impact of electrical discharge in a micro-confined called spark gap under a dielectric circulation medium. When the applied voltage potential crosses the threshold value (breakdown), there is the generation of ultrafine discharge in the gap. This discharge occurs due to the complete ionization of the dielectric fluid at the closest point [183]. The flow of discharge current in the gap developed a huge amount of heat and pressure which removes the material via melting and evaporation. By monitoring the flow of discharge energy (voltage, current, and duty factor) in the confined gap, various types of typical features and structures can be formed with better dimensional accuracy and stability [160].

In micro-EDM, as the discharge occurs in a very tiny interelectrode gap ($\leq 10 \mu\text{m}$), the gap condition is the most influential factor for machining stability [184]. Monitoring the gap condition under varying process variables is the hotspot for research in micro-EDM [185]. Generally, the average gap voltage reflects the gap condition in micro-EDM and is easily

accessible through pulse characterization (V-I curve) as quantified by Yeo et al. [186]. Wang et al. [187] studied the alternating behavior of discharge current through the real-time pulse counting method. In this method, they have taken the effective number of discharge pulses that are responsible for material erosion and tool wear. Wu et al. [158] developed an online discharge state monitoring system for high-speed wire-EDM processing. They proposed a particle swarm optimization - support vector machine (PSO-SVM) algorithm for detecting the different stages of discharge such as open circuit, normal discharge, short-circuiting and transient arcing. It was found that the proposed methodology has an accuracy rate of 98.917% for a running time of 0.84 seconds for identifying the discharge state. Identifying the real-time gap condition is essential to design the best servo feed control mechanism. The ideal servo mechanism helps to identify the good and bad discharge energy pulses during effective pulse on time [188]. Moreover, a well-defined servo control mechanism adjusts the process variables accurately for the occurrence of normal discharge which consequently increases the process efficiency and stability. Since the interelectrode gap in micro-EDM is very small ($\leq 10\mu\text{m}$) and continuously varying in nature with respect to time, monitoring spark behavior in real-time is quite challenging. Moreover, the machining process is complex and stochastic due to the time-transient behavior of discharge. A small deviation in design parameters may significantly differ the machining performance up to a great extent [189].

In micro-EDM, the servo control mechanism automatically adjusts the action of the mechanism by sensing the error in the feedback signal. Normally for positioning control (displacement), a linear in-built encoder with a position feedback sensor is used to get the desired output effect in terms of positioning accuracy, speed, and attitude [83]. Servo commonly utilized electric, pneumatic and hydraulic action to control the position of motion traditionally. Moreover, the error signals measured by the transducer at the output end are amplified to drive the system. However, this type of servo-controlled mechanism responded

slowly due to the inherent property of mass inertia, backlash, windup, hysteresis, etc., [190]. Moreover, governors are utilized in some cases to speed up the machining speed which further faces similar types of issues as mentioned above. But the recently developed servo motion controller is capable of adjusting the backlash in the lead screw drive system. The installation of a high-quality lead screw improves the machining accuracy while the finest nut design eliminates the backlash during the execution of the process [191]. In recent years, the typical type of gap controllers such as fuzzy logic controllers [192], PID controllers [193], self-tuning controllers [124], radio frequency (RF) signal-based controllers [194], neural network identification [195], wavelet transform detection [114], voltage thresholding [119] and machine learning (ML) and artificial intelligence (AI) [196] system, etc. are mostly in trends for interelectrode gap monitoring. This type of gap controller has certain limitations in terms of speed, feed, and positioning response. Moreover, these systems contain a complex type of drive and control unit which are designed considering nonlinear time-varying equations and complex algorithms.

3.1 Motivation and Research gap

In micro-EDM, the machining speed and the accuracy are critical issues that are limited by the probability of occurrence of normal discharge. Normal discharge is essential because it ensures good machining stability and the surface finish of the machined parts. A well-defined servo control mechanism responded well to ensure the occurrence of normal discharge because it restores the initial gap in the repeated cycle [197]. Additionally, the removal of debris particles from the machining gap should happen frequently to stabilize the machining process. During electrical discharge machining, the gap condition continuously changes to acquire a stable position [184]. Hence, Rapid retraction of the tool electrode promotes the effective removal of the debris particles in a small interelectrode gap in a low stroke length (mm) positioning system. Amouzegar et al. [198] proposed a centrifugal servo

control mechanism for the micro-EDM drilling process. Using this control mechanism, they successfully fabricated the micro holes, blind holes, and taper holes with a high aspect ratio. Moreover, the plunging action and the tool rotation improve the flushing condition by avoiding the occurrence of secondary discharge. This improves the machining speed, productivity, and machining quality.

In conventional micro-EDM technology, normally the lead screw-based/ball screw-based mechanism is used for the tool positioning. The positioning response of a such type of mechanism is slow due to mass inertia and the backlash problem. Due to the slow positioning response of the traditional servo head, this further causes arcing and short-circuiting. The phenomenon of arcing and short-circuiting is not good for the machine's health. It heavily affects the process efficiency, machining stability, performance, and surface integrity parts of the machined surface. Hence, there is a need for technology development for a high positioning response for the servo head. Magnetic levitation is one of the best alternatives through which a high-positioning servo response system can be attained. It is free from mass inertia and backlash problems and can facilitate quick response (fast retraction) in terms of positioning and gap control.

To improve the positioning response and machining accuracy, a high-speed actuator arm is required which can levitate stably and be positioned precisely during electrical discharge situations [199]. The frictionless pivot-bearing supported micro actuator arm may offer to accommodate the rapid retraction of tool electrodes for a millimeter stroke length positioning system. Moreover, the rapid retraction of the tool electrode during machining may help to strain the fresh dielectric by removing the debris particle by the action of jumping. The frequent jumping action improves the machining condition by avoiding the gathering of debris particles inside the spark gap. Imai et al [92] used the local actuator module for improving the micro EDM processing speed and accuracy in terms of micro-holes

drilling. Moreover, it was claimed that the use of a local actuator module in micro-EDM enables the system to do the microholes fabrication three times faster than the conventional one with 10-20% less electrode wear. Guo et al. [200] developed a magnetically levitated spindle for fabricating microholes through EDM. They achieved a fast axial response ($>150\text{Hz}$) of the spindle which was faster than the conventional ball screw servo head. The fast response frequency of the servo head improves the machining speed with better control over the accuracy of the machined part. He et al. [98] developed a 5-DOF-controlled local actuator arm for high-speed micro-EDM processing using a magnetic coupling mechanism. Using this technique, they attained the positional resolution of submicron level in the thrust direction (positioning stroke length 2mm), $180\mu\text{m}$ in radial, and 3.6 mrad in the tilt direction. The bandwidth frequency of the actuator arm was noted as greater than 200Hz . Moreover, the spindle shaft rotated at 2000min^{-1} with low vibrational amplitude ($1.5\ \mu\text{m}$ in radial and $30\mu\text{rad}$ in tilt direction). It was found that the precise movements of the actuator arm in three orthogonal directions offer a suitable interelectrode gap for the EDM contouring operation. The tilting direction motion was compensated by compensating the attitude error of the maglev actuator arm. The precise movements of the actuator arm in three orthogonal directions offer the suitable interelectrode gap for the EDM contouring operation while tilting direction motion-compensated the attitude error of the maglev actuator arm. Zhang et al. [93] developed a millimeter-stroke length local actuator and tested their potential for micro-EDM process using the magnetic levitation principle. The actuator arm achieved the positioning resolution of submicron (axial) and micro radian level (radial) for the stroke length of 2 mm in thrust direction with a positioning response frequency more than 100Hz . It was noted that the system offered better control over multi-directional microholes fabrication (stable and uniform). Additionally, rapid retraction of tool electrodes improved the machining condition by flushing out the debris particle from the discharge zone effectively. The reported

machining speed was enhanced by 21.8% compared to the conventional EDM system with better discharge stability. Later on, Tong et al. [201] developed a high-frequency micro dual-feed spindle for servo scanning 3D micro EDM process. The system was integrated with an ultrasonic linear motor (macro drive) and piezoelectric actuator (PZT) for servo feed control with real-time software such as LABVIEW and visual C++. The servo feed drive facilitates the proper discharge gap condition for EDM processing while the macro drive motor converts the motion into feed. The experimental results on this setup indicate that the machining process stability has been improved with a higher discharge ratio. The MRR, SR, and machining repeatability were observed around $1.58 \times 10^4 \mu\text{m}^3/\text{s}$, $0.37 \mu\text{m}$, and $<0.7\%$ respectively. Shafik et al. [202] utilized the piezoelectric servo feed drive (PZT) incorporated with a linear ultrasonic motor (USM) for developing the micro EDM servo system. The experimental results on this system indicate that the surface finish improves with the reduction in machining stability, processing time, MRR, arcing and short-circuiting phenomenon. Fujiki et al. [99] developed a novel gap control strategy for high-speed micro EDM milling operation. The developed gap controller facilitates the fast retraction of the tool electrode in the subsequent direction of orientation. An improvement of 30% is noted in MRR without losing the tool erosion and surface roughness. Melham et al. [78] designed a dual-stage servo feeding system using a fuzzy control algorithm via piezo driving actuator with linear motor (hybrid positioning). The linear motor facilitates the macro drive feeding while the piezoelectric actuator provides the micro feeding for positioning the gap control at high frequency. Using this fuzzy control algorithm, they improved the MRR 1.6 times better than the conventional EDM process.

In micro-EDM, machining characteristic is significantly affected by the process variable, dielectric fluid, and nature of discharge energy pulses. The nature of discharge energy is significantly reliant on the types of power supply. Normally two types of power

supply units are opted for discharging phenomenon in the micro-EDM system. One is resistance-capacitance (RC) type while the other is transistor type power supply [80]. Resistance-capacitance (RC-type) power faces the shortcoming in terms of a low material rate due to low discharge frequency. The frequent charging and discharging and variation in charge storing capacity of the capacitor is the major limitation of the RC-type power supply [203]. Transistor-type power supply overcomes the limitation of RC-type pulse power supply due to improved discharge frequency. Moreover, it facilitates fast triggering of the pulse (fast on-off) due to some delay in the circuit. The delay avoids abnormal discharge like arcing and short-circuiting by switching off the circuit for an ultrashort period which improves the material removal rate [85]. Nevertheless, the transistor type of power is also facing challenges in terms of resistance reduction. Ripple and attenuation (noise) in the deliberated signal due to internal resistance are the other issues that limit its potential for frequent use. The use of pure DC power may be a good option for facilitating the essential discharge energy in the spark gap because it is free from disturbance and attenuation (noise). Son et al. [204] explored the impact of pulsated DC power conditions (voltage, current, spark ratio) on machining performance (MRR, tool wear) in micro-EDM. They observed that voltage, current, and effective pulse on-time significantly influenced the machining performance. It was also noted that the shorter discharge energy pulses were more efficient in high material removal rates compared to longer discharge energy pulses. Yeo et al. [186] studied the behavior of pulse discharge in real-time through the pulse discrimination technique. This technique was further utilized for the development of a high-speed servo mechanism in micro-EDM. Similarly, Gostimirovic et al. [205] deliberated on the influence of discharge energy on machining characteristics via theoretical and experimental approaches. They further reported that the machining efficiency is predominantly affected by the thermal state of electrical discharge in the machining zone. Real-time power consumption efficiency for

efficient machining in micro-EDM milling is reported by Tristo et al. [206]. In this study, they employed open-access software, a data acquisition system, sensor, and microcontroller to record the data in the host computer. The analysis of data indicates that process efficiency significantly depends on machine input parameters. Proper adjustment of the interelectrode gap through fast servo control (self-retraction) mechanism is essential to overcome the issue in the micro-EDM system. Moreover, it directly affects the machining stability and performance efficiency hence, it must be the area of interest for upcoming advancing servo control technology [201]. Kumar et al. [207] demonstrated the various gap control strategies and servo control criteria for micro as well as nano EDM. In this paper, they briefly enclosed the recent advancement in piezo driving technology (positioning control), discharge power technology, gap monitoring technology, tooling system, and flushing system for achieving the nanoscale machining through electrical discharge phenomenon.

Hence, this chapter reports an innovative idea for controlling the interelectrode gap more precisely and accurately. The gap control mechanism is based on magnetic levitation where the electromagnetic force is made balanced with the restoring force and the gravitational force exhibited by the tool electrode. The equilibrium state of these forces facilitates a condition where the stability of the machining process has been achieved. The stability of the machining process during discharge is evaluated by the signal processing of the voltage-current discharge characteristic curve. The unavailability of the undesired signal such as arcing and short-circuiting signals indicates that most of the discharge energy pulses are highly stable. Most of the discharge energy pulses pose a uniform pulse width which means the energy delivered by each pulse is almost the same or const. Later on, the machining feasibility and performance were evaluated in terms of performance measures such as material removal rate, tool wear rate, and surface roughness on duplex stainless steel (DSS-2205). The morphological and chemical characterization was evaluated by field

emission scanning electron micrograph (FESEM) and electron diffraction spectroscopy (EDS) techniques respectively which is discussed in a further section.

3.2 Working principle of Maglev μ -EDM

The gap control mechanism of maglev μ -EDM is based on the concept of balancing three forces i.e., the electromagnetic force (F_{em}), gravitational force (F_g), and restoring force (F_s). The electromagnetic force acts in the upward direction while the other two forces are acting in the downward direction to levitate the tool by attaining the equilibrium state of these forces. The configuration of the setup is created using a unipolar linear motor (electromagnet) with an extended actuator arm. The actuator arm of the linear motor can move freely in the vertical direction as per the voltage and current applied. The tool electrode is thus connected to one end of the moving actuator arm. Now, as the power is applied through a DC power source, the tool electrode moves upward, and as the power is disconnected the tool electrode freely falls to touch the workpiece due to the loss in magnetization or due to the gravity effect. It was observed that when the tool electrode is moving upward, the spring attached to the actuator arm restores some force called spring restoring force (F_s). This restoring force aids in preserving the machining process's stability during discharge. Now, for EDM operation, unipolar linear motor one end is connected to the power source while another end is connected to the tool electrode. The positive terminal of the power source is connected to the work material. The complete configuration of the EDM circuit with the actual representation of the system is illustrated in fig. 3.1. As power is switched on, there is a current flow between the linear motor, tool electrode, and workpiece. This current retracted the tool electrode in an upward direction which means the tool electrode is getting separated from the workpiece. This separation facilitates the minimal optimal distance to induce a spark. This spark is known as an electrical discharge that erodes the material from both electrodes in the form of microscale debris via melting and evaporation under a dielectric

medium. The occurrence of a spark reduces the applied voltage potential of the power source. This reduction causes magnetic strength to be weak for the linear motor. In the presence of weak magnetic strength, the tool will try to fall to touch the work material. Nevertheless, when it falls it will again obtain an optimal discharge for the electrical spark to occur. The complete system is arranged in such a manner that the system automatically adjusts the interelectrode gap by balancing the three above-mentioned forces ($F_{em}=F_g+F_s$) for the occurrence of normal discharge. Based on this concept, the cycle repeats continuously and discharge occurs within the optimum electrode gap for maglev μ -EDM. The interelectrode gap was initially adjusted using XYZ linear micro-positioner (resolution 10 μ m) to control the discharge voltage.

3.3 Experimentation and methodology

3.3.1 Workpiece and tool material

A duplex stainless steel of grade 2205 (dimension: 30 mm x 30mm x 2mm) and tungsten rod of diameter (\varnothing 0.650 mm) and length (L) 10 mm were chosen as work and tool material respectively. The work material was preferably chosen as it falls in the category of exotic material and poses the research challenge in terms of machinability by the traditional methods. Furthermore, the material offers exceptional properties such as good corrosion and wear resistance at elevated temperatures and pressures, making it popular in industrial applications. The elemental composition of the work material along with the thermophysical properties of the tool electrode is presented in table 3.1 and table 3.2 respectively. The dielectric medium utilized in the experiment was commercial-grade deionized water.

Table 3. 1 Elemental constituent (% weight) of duplex stainless steel (grade 2205) workpiece.

Elemental composition	Ni	Cr	Mo	Ti	Fe	Mn	Nb	Si	C	V	W
% Weight	4.81	22.81	3.05	0.006	66.9	1.43	0.03	0.50	0.028	0.12	0.21
Mass density	7.8										
Melting point	g/cm ³										
	1440 ⁰										
	C										

Table 3. 2 Thermomechanical property of tool electrode (Tungsten)

Thermophysical properties	Value
Composition	99.95%
Density	19.3 g/cm ³
Melting point	3370 ⁰ C
Hardness (HB)	2570 MPa
Electrical resistivity	52.8 Ωm at 20 ⁰ C

3.3.2 Experimental Setup and its peripheral components

The newly developed maglev micro-EDM consists of a unipolar linear motor with a movable actuator arm and tool holding flair, linear power output DC source for facilitating essential discharge energy, XYZ manual micro-positioner for workpiece movement, dielectric flushing system, dielectric circulation tank with honeycomb features inside for workpiece tightening facility. The digital storage oscilloscope (Tektronix, TDS2012C, 2-channel, 100MHz bandwidth) is connected to the machining system for capturing the voltage-current (V-I) signal during the discharge. A differential-type voltage (TPP0201, Tektronix) and a current probe (65A-Hantek, BNC type) are connected to the circuit. The voltage probe is connected parallel to the load resistance i.e., across the tool and workpiece while the current probe is connected in series to the wire nearest to the workpiece. To

eliminates any residual magnetization or inductance, the degaussing button is pressed 4-5 times which shifted the current signal near the ground (GND) state.

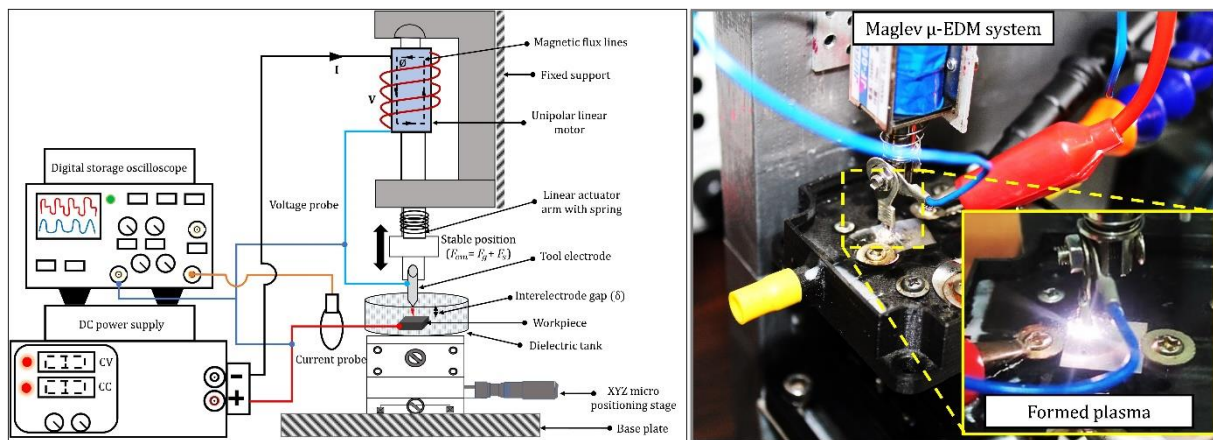


Figure 3. 1 Maglev Micro-EDM machining experimental setup with their peripheral components.

(a) Multi-output DC power supply (Model: APLAB-LQ6324P)

The essential energy for discharge is supplied through a multioutput pure DC power source as shown in fig. 3.2. It is an integral part of the maglev micro-EDM system. Its circuit is fully protected against overload and short-circuiting. This power source unit has an electrically floating voltage with respect to the ground is 500V DC. It facilitates precise regulation with low ripple and noise in constant voltage (CV) and constant current (CC) modes. The technical specification of the programmable multi-output DC power source is represented in table 3.3.

Table 3. 3 Technical features and specifications of the multi-output programmable DC power source

Features	Specification
Input voltage	220-240V AC, 50Hz, single phase (1- ϕ)
Output voltage (CV mode)	0-32 V

Output current (CC mode)	0-2A
Line Regulation CV *	$\pm 0.01\% \pm 2\text{mV}$
Line Regulation CC *	$\pm 0.1\% \pm 250\mu\text{A}$
Output Ripple CV	1mV rms
Operating environment temperature	0-50°C
Output Ripple CC	0.04% rms
Display Accuracy	± 3 counts
Indication (LED)	CV/CC
Protection	Overload (OV)/short circuit (SC)



Figure 3. 2 Multi-output programmable DC power source

(b) Current probe (Hantek 65A AC/DC, 20kHz bandwidth)

The current probe used in the present maglev EDM system is of a non-contact type with a BNC connector. It is a type of transducer that permit the measurement of the current data in form of waveforms. The current transducer is made of permalloy and hall sensing elements which linearly transform the AC/DC signal to the corresponding AC/DC voltage signal. It can measure the AC as well as DC signal in a digital manner without breaking the actual circuit. The current probe is allied in series with the circuit. When the current probe is

connected to the circuit it identifies the magnetic field by sensing the current flowing through the coil or conductor and converting it into a voltage signal which can be digitally seen in the digital storage oscilloscope. The technical features of the current probe are listed in table 3.4. The basic mechanism of the current clamp is indicated in fig. 3.3(a) while the actual figure of the current clamp is denoted in fig. 3.3(b).

Table 3. 4 Technical features and specifications of the current clamp

Features	Specification
Frequency measurement (AC/DC) range	up to 20kHz
Effective current measurement range	20mA to 65A DC
Accuracy (DCA range, 1mV/10mA)	$\pm(1.5\% \pm 5\text{mA})$ 10mA ~ 20A
Accuracy (ACA range, 1mV/10mA)	$\pm(6\% \pm 30\text{mA})$ 100mA ~ 10A (10KHz ~ 20KHz); $\pm(8\% \pm 30\text{mA})$ 10A ~ 15A (40Hz ~ 20KHz)
Battery	9V DC (6F22)
Connector	BNC type

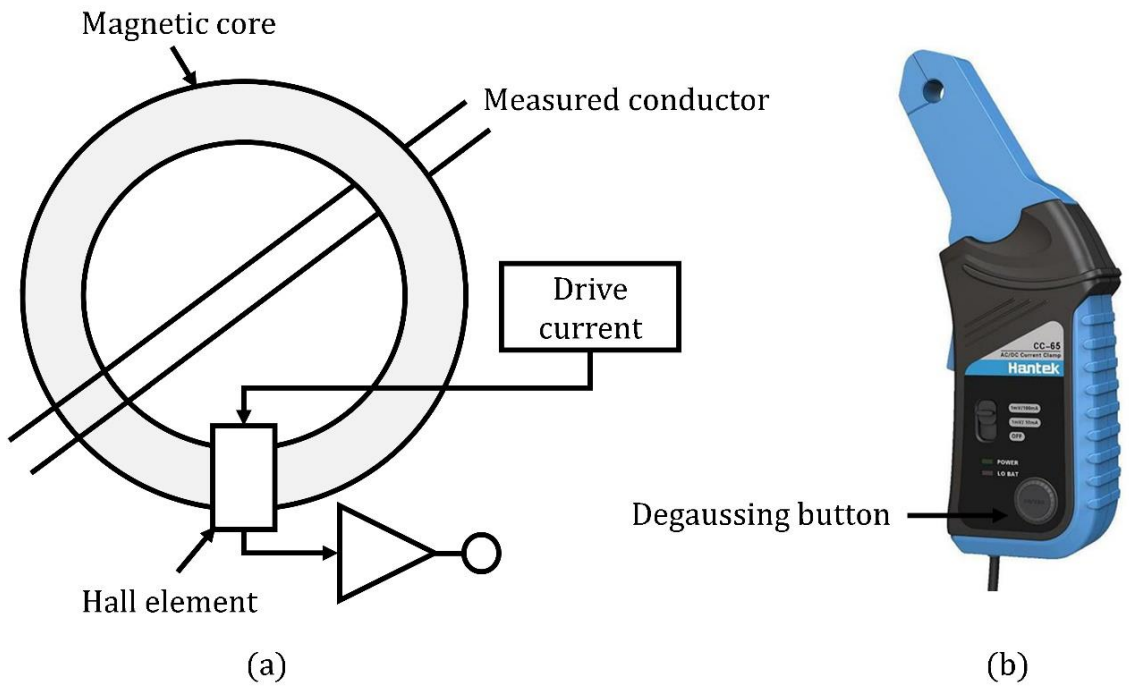


Figure 3. 3 (a) Current clamp working mechanism (b) Current clamp with BNC type connector.

(c) Voltage probe (Tektronix: TPP0201, Attenuation 10:1)

The voltage oscilloscope probe measures the high voltage by changing the input impedance of the circuit via attenuation of the signal by either 1X, 10X, and 100X factors. It is a passive-type voltage probe with a BNC connector (see fig. 3.4). It measures the voltage signal by reducing its amplitude to a safe and measurable range via a voltage divider circuit within the probe body. The technical specification of the voltage probe is presented in table 3.5.

Table 3. 5 Technical features and specifications of the voltage probe

Features	Specification
Bandwidth	100MHz
Probe type	Passive voltage probe
Maximum input voltage	300Vrms

Probe attenuation	10:1
Input resistance	10M Ω /20pF \pm 1.5%
Rise time	<2.3 ns (typical)
Compensation range	15 pF to 25 pF
Propagation delay	~6.1 ns



Figure 3. 4 Passive type voltage probe with BNC type connector

(d) XYZ manual micro-positioning linear stage

It is the three degrees of freedom, linear micro-positioning displacement platform for the precise motion of the work material in subsequent XYZ direction. Fig. 3.5 indicates the actual image of the XYZ linear micro-positioning stage. The technical specifications of the XYZ linear micro-positioning stage are tabulated in table 3.6.

Table 3. 6 Technical specifications of XYZ linear micro-positioning stage

Features	Specification
Degree of freedom (XYZ)	3 (V-type rail)
Travel range (X-axis), YZ axis	25 mm; 10mm
Positioning accuracy	0.001mm

Minimum scale	0.001mm
Top size	90 x 90 mm
Load capacity	5Kg
Mounting hole	M6

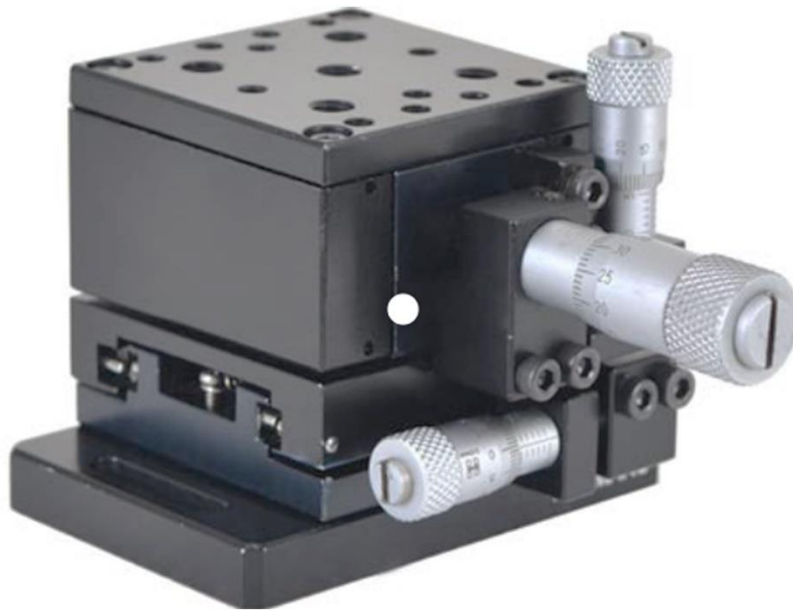


Figure 3. 5 Manual linear XYZ micro-positioning displacement platform

(e) Digital storage oscilloscope (DSO)

It is one type of oscilloscope that takes the input signal in form of an analog and processes it into digital output. It stores and analyzes the signal digitally. It has an advanced triggering, storage, display, and measurement option for accurate analysis. The technical specification of the digital storage oscilloscope (DSO) with its operating range is illustrated in table 3.7. The fig. 3.6 denotes the actual image of the digital storage oscilloscope.

Table 3. 7 Technical features and specifications of digital storage oscilloscope (DSO)
(Tektronix: TDS2012C)

Features	Specification
Number of channels	2
Bandwidth	100MHz
Sampling rate	2GS/s
Display monitor (LCD)	TFT
Input voltage	100-240VAC
Interface type	USB and GPIB type
Vertical resolution	8 bits
Vertical sensitivity	2 mV to 5 V/div
DC vertical accuracy	±3%
Input coupling	AC, DC, GND
Input impedance	1MΩ in parallel with 20 pF
Time base range	2.5ns to 50s/div
Rise time	3.5 ns

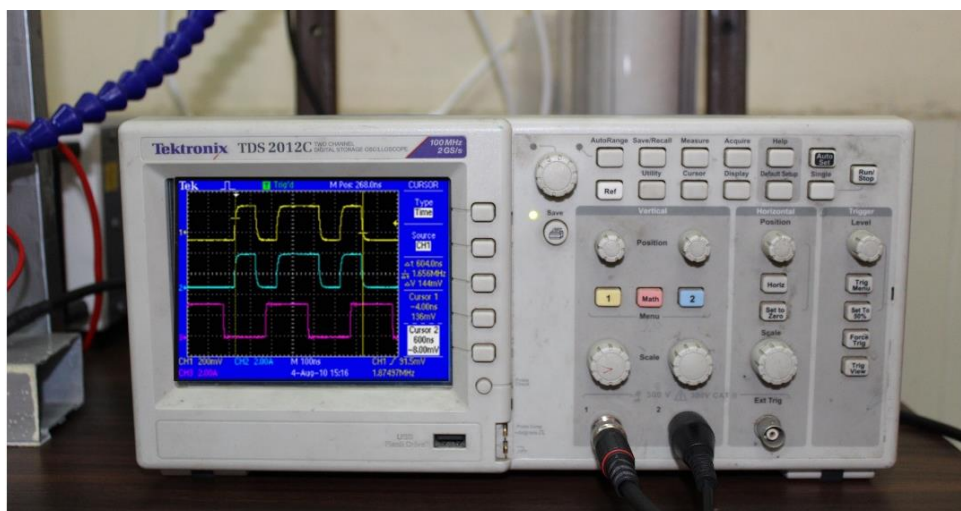


Figure 3. 6 Digital storage oscilloscope (DSO) with BNC type connector

(f) Dielectric circulation system (DCS)

The dielectric circulation system is an important part of the maglev micro-EDM system. It provides a favorable condition for the flow of dielectric during machining. The dielectric flow system flushes out the debris particles from the discharge zone and offers the ideal condition for the generation of the next stable discharge. It assists to avoid the arcing and short circuit phenomenon during discharge for stable and efficient machining. The current dielectric circulation system consists of a water booster pump (24V) with SMPS/adaptor (DC), a normal cartridge filter filled with deionizing sand, a glass filter with spun filter inside, a flow control valve, and flexible pipe hose with an adjustable nozzle. The dielectric circulation system with its peripheral components is illustrated in fig. 3.7.

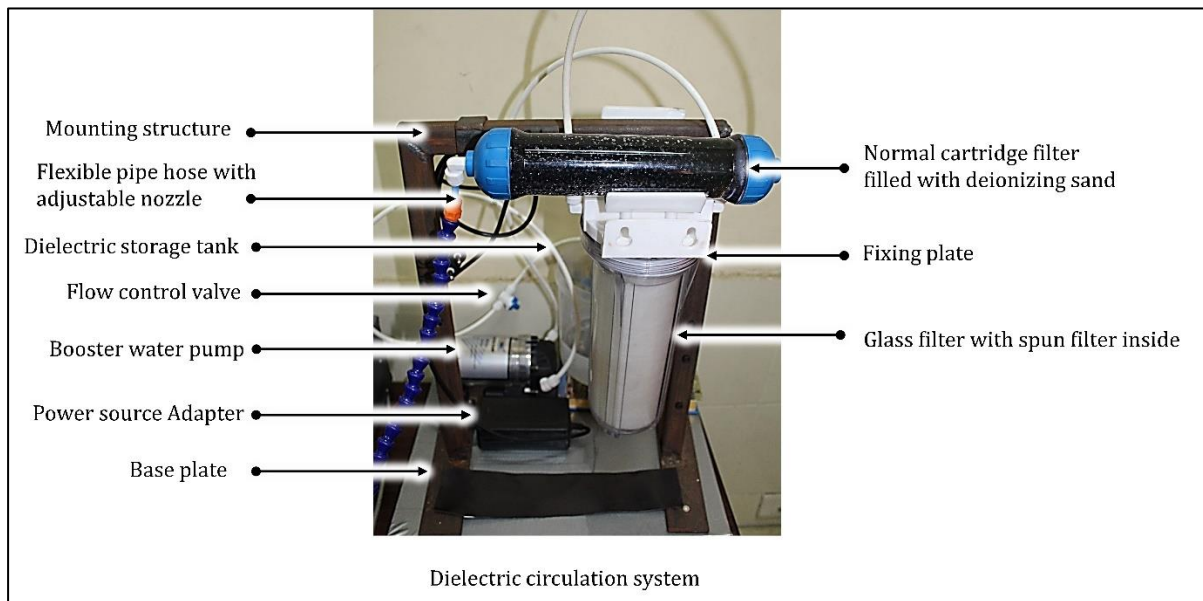


Figure 3. 7 Dielectric circulation system (DCS) with its peripheral components

3.3.3 Experimental Procedure

Prior to machining, the cross-section of the tool and workpiece were refined on a disc polishing machine (Chennai Metco) with emery polishing paper of grades 1800 and 2000. After that, a velvet cloth with diamond paste is used to create a mirror-like sheen. It's

necessary for a clear view of the crater generated on the machined surface.

Pilots' experiments were conducted initially to identify the level of the machining condition in terms of no-load voltage, discharge voltage, discharge current, machine on time, and duty factors. It was noted that the machine runs well in all voltage range between 20-32V (open circuit voltage) and a max peak current of 300mA-2A. Based on the pilot's experiments, the level of experimental conditions was determined which is registered in table 3.8.

Table 3. 8 The measured gap voltage, gap current, and duty factor in four iterations during the processing of duplex stainless steel (DSS-2205).

Open circuit voltage (V)	Applied current (A)	Discharge voltage (V)	Discharge current (A)	Duty factor	Machining time
	0.40	15.3	0.140	0.75	
	0.45	15.9	0.170	0.80	
30	0.50	15.6	0.130	0.75	10 minutes
	0.55	16.3	0.150	0.81	

The experiments were conducted in straight polarity i.e., the workpiece is connected to the positive terminal while the tool electrode is allied to the negative terminal of the power source. The workpiece is dipped in deionized water, and a 30 V open-circuit voltage is applied across the load, with a variable peak current setting (400mA-550mA). To maintain a constant interelectrode spacing, the tool begins to oscillate in the vertical direction. The machining begins with an electrical discharge voltage of 15.3-16.3 V and a discharge current of 140mA-180mA. During machining, the discharge characteristic in terms of voltage current waveform is captured in a digital storage oscilloscope (DSO) using a voltage and current

probe. This information is further utilized for calculating the discharge power and the specific energy of the system during machining. The material erosion rate (MER), and tool erosion rate (TER) is determined using the weight reduction method (Mettler Toledo, accuracy 1 μ g). Prior to characterization, the machined samples were ultrasonicated in distilled water to remove any adhering debris and dust particles.

3.4. Results and Discussions

3.4.1 Machine health monitoring through volt-ampere (V-I) characteristic curve

In micro-EDM, the nature of the electrical discharge and its machining stability significantly depends on the servo gap control mechanism and its positioning response. The essential energy for the discharge is supplied in the form voltage-current signal from the power source unit as electrical input. The supplied voltage current signals ionized the channel by breaking the dielectric strength of the medium and establishing a time-varying electric field between the electrodes. As plasma forms, the channel becomes conductive and poses the minimum resistance for the flow of discharge current. The thermal impact of electrical discharge current causes melting and evaporation of the electrode's material in the form of microscale debris. Additionally, gas bubbles that contain the ions and compounds of the molten metal are formed around the plasma channel. The voltage and current signals suddenly drop to zero at the end of the discharge which is referred to as pulse interval time or pulse off time. After discharge, the plasma channel and surrounding gas bubbles abruptly collapsed, creating a tremendous explosive pressure that forced the eroded material out of the discharge gap. Due to insufficient pressure and flushing, some of the molten material was reattached to the surface and formed the recast layer, a re-solidified layer.

The gap condition and type of discharge waveforms are considerably revealed by the examination of the current and voltage pulses. In order to start the ionization, the voltage must first increase to the dielectric's breakdown strength. The voltage pulses stabilize during

the ionization process for a certain period (known as the ignition delay), after which it begins to decline. Current starts to increase as voltage decreases. There comes a point where the voltage cannot be lowered any further. The generated plasma channel is now fully ionized and has the lowest possible impedance to flow discharge current. Discharge voltage, which is proven to be accountable for the actual erosion of the material, is the voltage at which the discharge occurs.

The most crucial factor determining the stability of the discharge phenomenon in the EDM process is the ignition delay since during this period that dielectric ionization occurs for short period. Discharge can sometimes occur immediately without any ignition delay, which can then result in the formation of a transient arc. These transient arcs should be avoided during machining since they are a bad signal for the surface finish and process efficiency. Another occurrence that frequently happens in traditional EDM is short-circuiting. This is brought on by the servo head's low response frequency and insufficient flushing of the debris from the discharge zone. Both electrodes make contact in this scenario. The massive amount of current can flow without discharging due to the direct connection between the electrodes.

The circuit diagram of the maglev micro-EDM system is illustrated in fig. 3.8. The maglev micro-EDM system is made with a unipolar linear motor (electromagnet) and spring-supported actuator arm technology. The linear motor consists of an inductor (L) circuit and due to the coil, it poses some internal resistance (R1). The second resistance (R2) is one type of variable resistance which referred to the resistance between the two electrodes due to the interelectrode gap. So, the complete arrangement of the maglev-EDM system is based on the inductance-resistance (L-R) circuit. The current maglev-EDM system is empowered with a pure DC power source having an electrically floating voltage with respect to ground up to 500V. It was observed that during the electrical discharge machining (EDM) operation, it varies between the 180-200V as voltage probe is connected across the gap resistance in

parallel and the current probe is connected to the circuit in a series nearby workpiece (case-1 in fig 3.8). For the DC power source, the inductor circuit acts as a short circuit, and the voltage drop across the L-R circuit is only due to the internal winding resistance. For the open circuit voltage of 30V, the short circuit voltage across the L-R1 circuit was varying between 8.5-10.6V according to the process parameter variation. This voltage is deducted from the discharge voltage (23.8-26.9V) to get the actual machining voltage across the interelectrode gap. The actual discharge voltage was found in the range of 15.3 V to 16.3 V. The observed duty factor was varying in the range of 0.75-0.81 during the machining process.

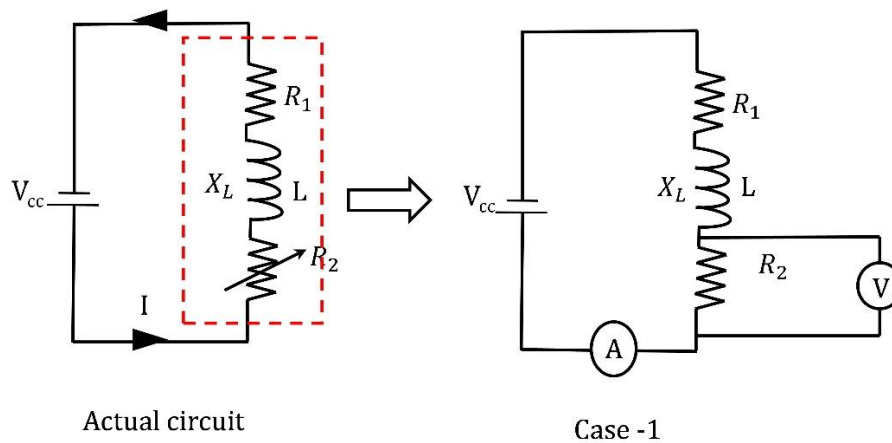


Figure 3. 8 Circuit diagram of the maglev micro-EDM system for servo gap control

The time transient discharge characteristic curve of the maglev micro-EDM is depicted in fig. 3.9 in the form of a voltage-current (V-I) waveform. The machining takes place when the open circuit voltage (30V) drops to the discharge voltage. As there is a voltage drop, there is a rise in the current during the pulse on time. A situation where voltage cannot be reduced and voltage and the current signal become stable. The presence of low ignition delay in the voltage-current curve indicates that the ionization is happening very fast indicating short ionization. The duty factor recorded in the digital storage oscilloscope (DSO) was found in the range of 0.75-0.81. Most of the discharge energy pulses are involved in removing the material during an effective pulse of time. Fig. 3.9 provided an illustration of

the real-time voltage current discharge energy pulse on maglev micro-EDM. The majority of the discharge energy pulses are stable and uniform, as seen in Fig. 3.9(a). The low ignition delay in the curve suggests that ionization is occurring quickly. The three discharge energy pulses at a time scale of 1ms are shown in Fig. 3.9(b). The majority of discharge energy pulses exhibit consistent pulse widths which are free from any undesirable signals like arcing and short-circuiting. The overall analysis of the voltage-current waveform indicates that the process is highly efficient and stable. This also suggests that the servo system discussed earlier effectively controls the gap condition during machining.

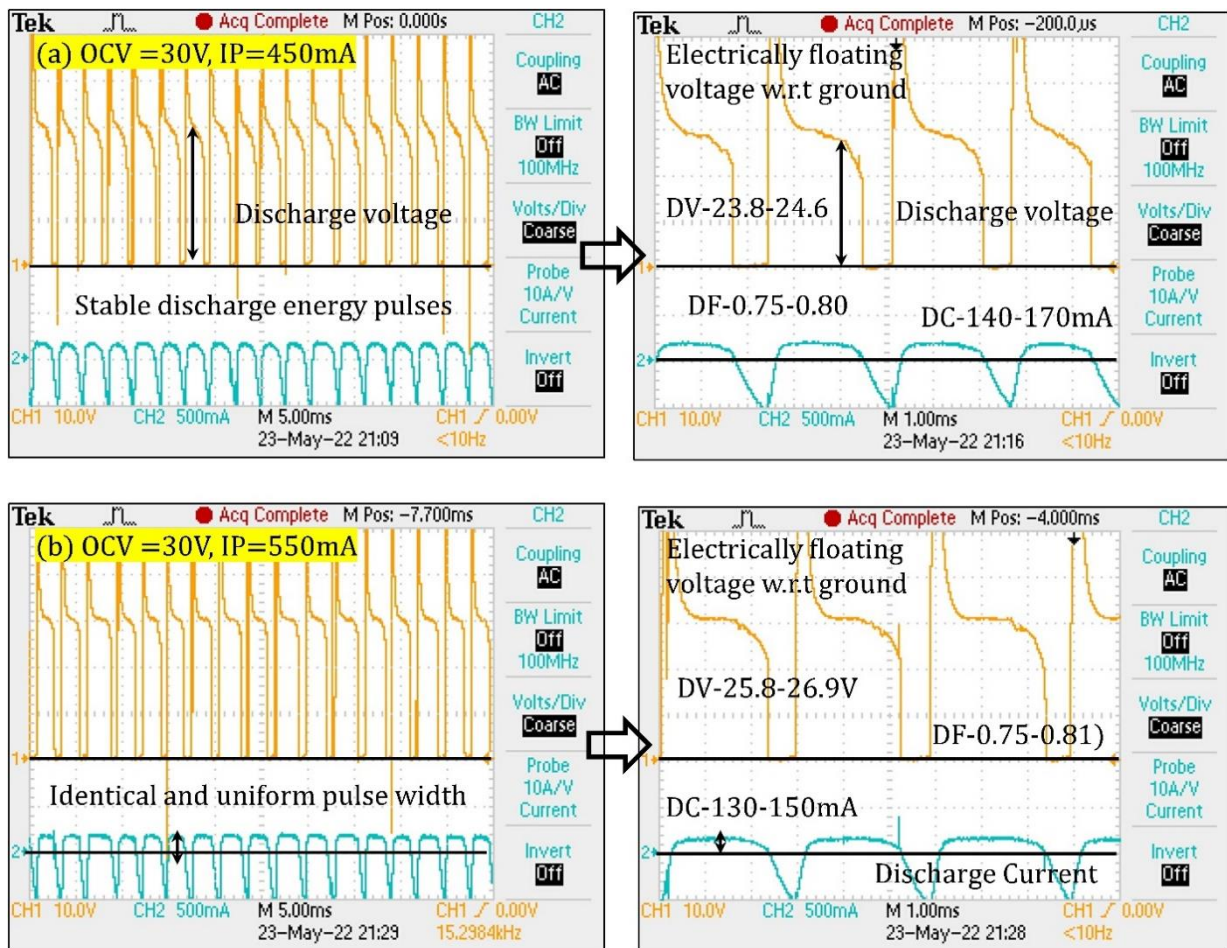


Figure 3. 9 Real-time voltage and current waveform at (a) peak current setting of 450 mA and (b) 550 mA at the time scale of 5ms and (b) 1ms.

3.4.2 Material erosion rate (MER) and tool erosion rate (TER) analysis

Material erosion rate (MER) is one of the prime output responses which significantly

depends on the availability of discharge energy in the spark gap. This discharge energy further relies on the discharge voltage, discharge current and effective pulse on time. During effective pulse on time, actual erosion occurs due to the thermal impact of electrical discharge. This electrical removes the material in the form of microscale particles called debris. Here, the material erosion rate is evaluated using the weight reduction method i.e., a difference between the initial weight and final weight of work material for a particular given time. The equation used for calculating MER using the weight loss method is illustrated below.

$$MER = \frac{(W_i - W_f)}{T_m} = \frac{(\Delta W_w)}{T_m} \dots\dots\dots (3.1)$$

Where, ΔW_w : weight reduced in given machining time (μg), T_m : machining time in seconds.

In the current maglev micro-EDM system, the maximum material erosion rate (MER) was found to be 223.8 $\mu\text{g}/\text{min}$ corresponding to a discharge power of 1.9344 j/sec while the minimum MER was 117.6 $\mu\text{g}/\text{min}$ corresponding to the discharge power of 1.8359 j/sec. It was noted as the discharge power increases the MER increases first but after achieving the maximum material erosion rate it starts decreasing despite increasing power output. At higher output power, the material erosion rate is decreasing, this may be due to the low plasma strength or may be due to insufficient flushing pressure. It was also noticed that once the discharge voltage and discharge current for an effective pulse on time are achieved, the further increase in power input does not influence much material erosion rate. Additionally, as the discharge voltage becomes higher, the interelectrode gap becomes wider. The wider interelectrode gap indicates a reduction in the intensity of the flow of current for a longer pulse. The reduction in the intensity of the discharge current consequently reduces the material removal rate to a great extent.

Tool wear is always exhibited with any machining process whether it is thermal

machining or any other machining process. It is an unavoidable phenomenon that significantly influences machining efficiency and accuracy. Moreover, frequent tool wear may affect the economics of the machining process. Literature indicates that tool wear decreases with increasing conductivity. The tool material density and the availability of discharge energy in the machining gap are the other two factors that significantly influence the tool wear rate. The experimental study on tool wear rate indicates that as the discharge power increases the tool wear rate increases up to a certain extent. Meanwhile, after achieving the maximum tool wear rate, it starts declining. The tool wear rate follows similar trends as the material erosion rate (MER). The reduction in tool wear rate may be due to improper flushing or may be due to the deposition of the electrode material on the tool surface which raised the issues of electrical conductivity. The maximum tool wear rate of 29 $\mu\text{g}/\text{min}$ was noted corresponding to the discharge power of 1.9334 while the minimum tool wear rate of 10 $\mu\text{g}/\text{min}$ was noted corresponding to the discharge power of 2.5469 j/sec. The impact of discharge power on the material erosion rate and tool erosion rate is represented in fig. 3.10. The tool erosion rate was calculated using the weight reduction method (WRM) which is represented in equation 3.2.

$$TWR = \frac{(T_{wi} - W_{wf})}{T_m} \dots\dots\dots (3.2)$$

Where, T_{wi} : initial tool weight before machining, T_{wf} : final tool weight after machining, T_m machining time in minutes.

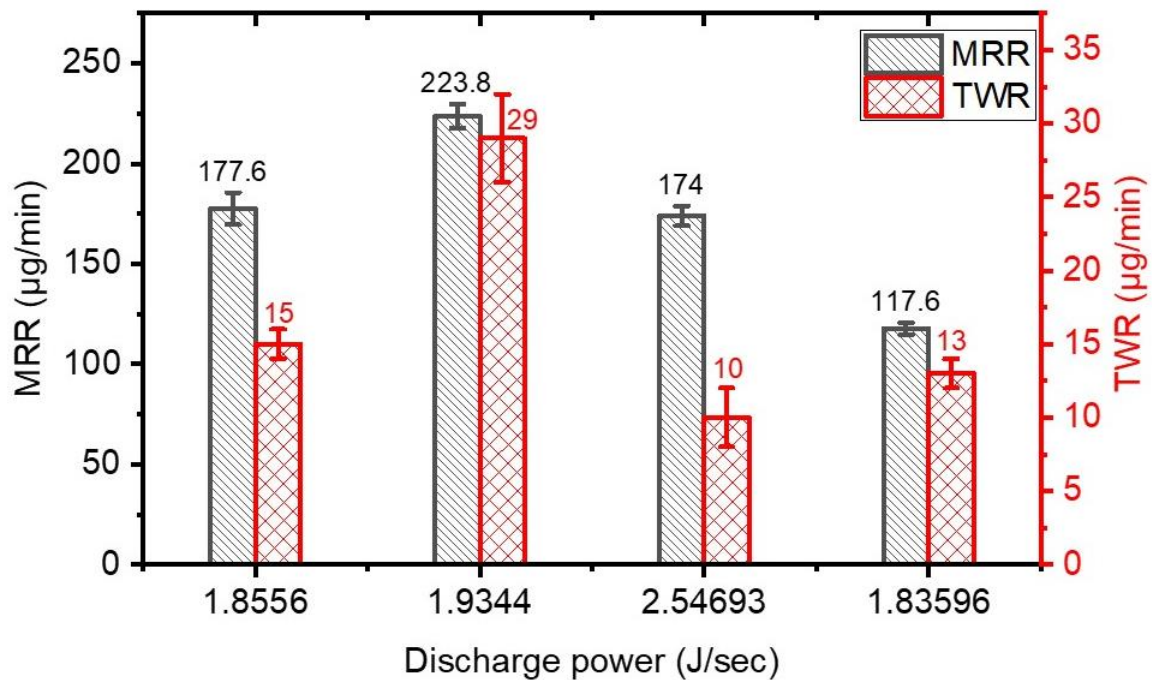


Figure 3. 10 Effect of discharge power on material erosion rate (MER) and tool erosion rate (TER) in three repetitions of experiments.

3.4.3 Specific energy consumption (SEC)- A common performance index (CPI)

The specific energy is the common performance index to evaluate the efficiency of any machine. It is defined as the amount of discharge energy required to remove a single unit of mass/volume. Here, the discharge power has been calculated using the captured voltage, current, and pulse on-time data (excel file) from the digital storage oscilloscope. Further, this discharge power has been divided by the material erosion rate which offers the specific energy of the system during machining. It was noticed that as the discharge power increases the specific energy increases. The maximum specific energy of the system was found to be 0.9367 J/µg corresponding to discharge power 1.83 J/sec while the minimum specific energy was 0.5173 J/µg corresponding to discharge power 2.54 J/sec. The equation used for calculating discharge power and specific energy is illustrated in equation 3.3 and equation 3.4. To compare the performance of the newly developed maglev micro-EDM system, its

common performance index i.e., specific energy is compared with the existing literature. According to Vishwanthvalet et al. [208], the specific energy of the micro-EDM system varying in between 0.133-0.647 J/μg for the varying discharge power range of 293.87-1145.45 J/s. The selected work material was super duplex grade 2507 while the working fluid was EDM oil. Bharat Singh, 2020 [209] reported that the specific energy of the EDM system ranges between 0.154-0.9656 J/μg for discharge powers of 12-270 J/sec. Similarly, Srinivas et al. [210] found that the specific energy lies in the range of 0.037-0.1107 J/μg for the discharge power range of 28-72 J/sec. The chosen workpiece was DSS-2205 while the working medium was air. Form the literature survey, it can be noted that the specific energy lies in between 0.037-0.9656 J/μg. The specific energy of the current maglev micro-EDM also lies in the same range as reported in previous literature. This indicates that the current maglev micro-EDM is as efficient as other available commercials micro-EDM systems. The comparative study of the specific energy of the current maglev micro-EDM system with the existing micro-EDM system is illustrated in fig. 3.11.

$$P_d = V_d \cdot I_{av} \cdot \tau \dots\dots\dots (3.3)$$

$$SEC = \frac{P_d}{MRR} \dots\dots\dots (3.4)$$

Where P_d represents the discharge power, V_d indicates the discharge voltage during machining, I_{av} is the average discharge current, τ represents the duty factor, SEC denotes the specific energy consumption.

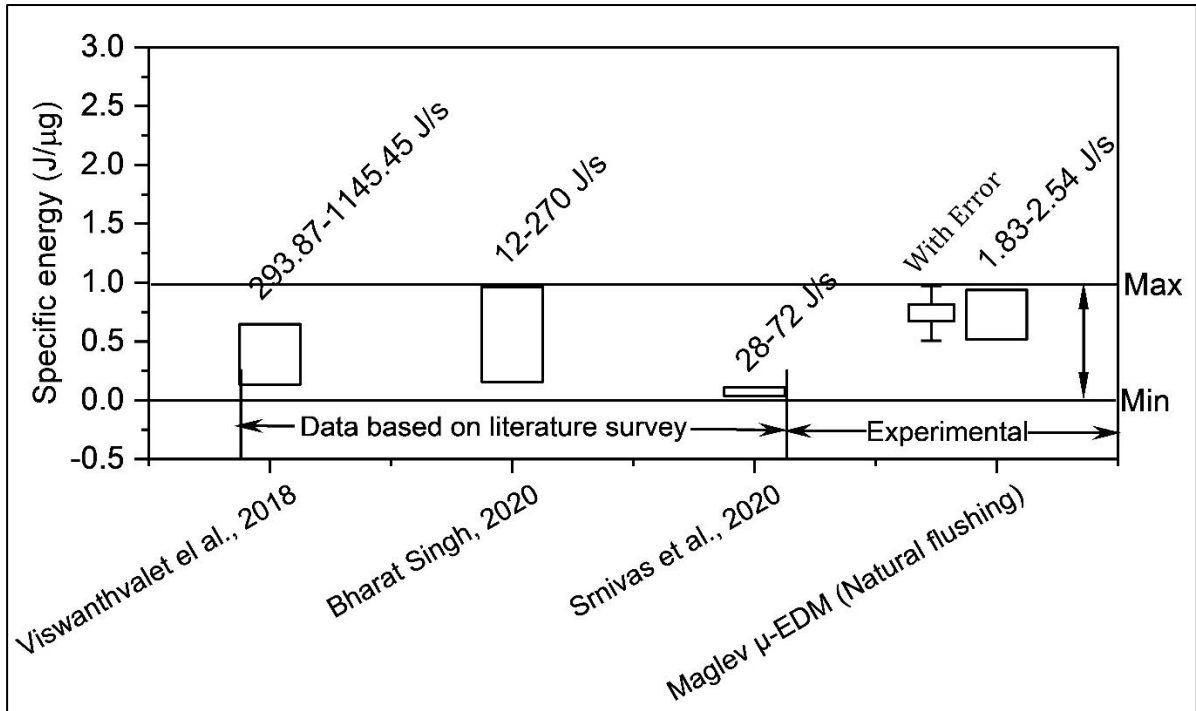
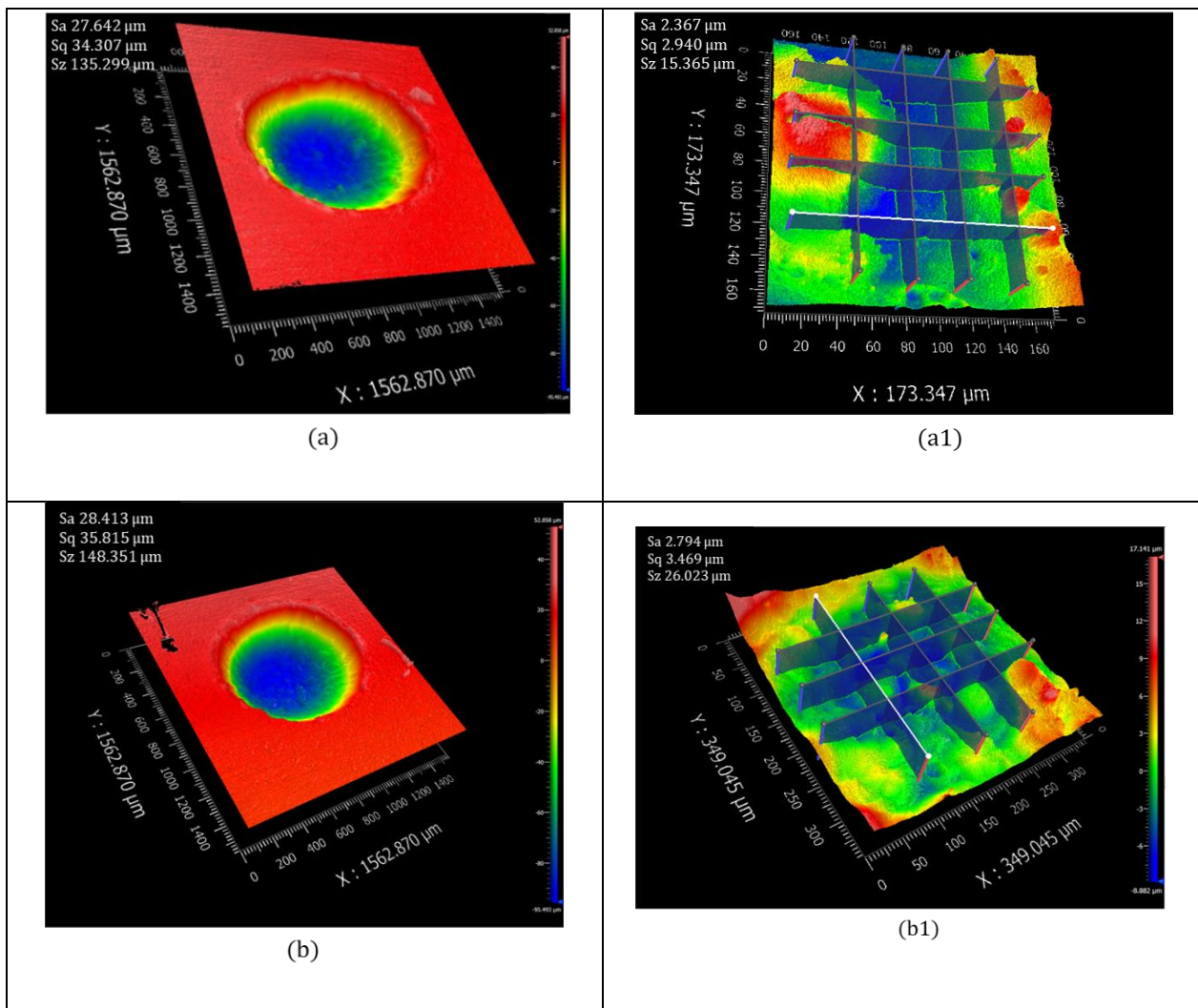


Figure 3. 11 Comparison of the specific energy (SEC) of the current system with the existing literature.

3.4.4 Surface integrity (SI) analysis

Surface roughness is one of the prime output responses in the micro-EDM process. This indicates the quality and finishing of the machining surface. The presence of micro craters, micropores, micro debris, and recast layers on the machining surface contributes to the formation of surface roughness. In the current work, the area surface parameters (S_a , S_q , and S_z) were measured using a non-contact type profilometer (Zygo, NewView 9k). Fig. 3.12 (a) indicates the geometry of the crater formed over the machined surface for the scanned area of $1562.870 \times 1562.870 \mu\text{m}^2$. Fig. 3.12 (b) represents the area surface roughness value over the machined surface. It was noted that the range of area surface roughness S_a , S_q , and S_z were $2.347\text{-}2.794 \mu\text{m}$, $2.875\text{-}3.469 \mu\text{m}$, and $15.365\text{-}26.379 \mu\text{m}$ respectively. Additionally, the variation in linear surface integrity parameters (R_a , R_q , R_z) was studied over six to eight different slices over the machined surface (see fig. 3.13). It was found that the R_a , R_q , and R_z , were varying in the range of $1.829\text{-}2.693 \mu\text{m}$, $2.386\text{-}3.042 \mu\text{m}$, and $5.678\text{-}7.493 \mu\text{m}$

respectively. The overall evaluation of the surface integrity parameters indicates that the average roughness value is low. The lower surface roughness indicates a better surface finish. The low surface roughness value may be due to the availability of low discharge energy in the machining gap. As the discharge energy increases, it forms a bigger surface crater over the machining surface which increases the surface roughness value. The discharge current was found to be the most influencing parameter compared to discharge voltage and discharge on time. Another essential criterion that enhances the surface roughness rating is proper flushing. The action of the tool electrode hopping enhances the flushing condition, resulting in a decreased surface roughness value.



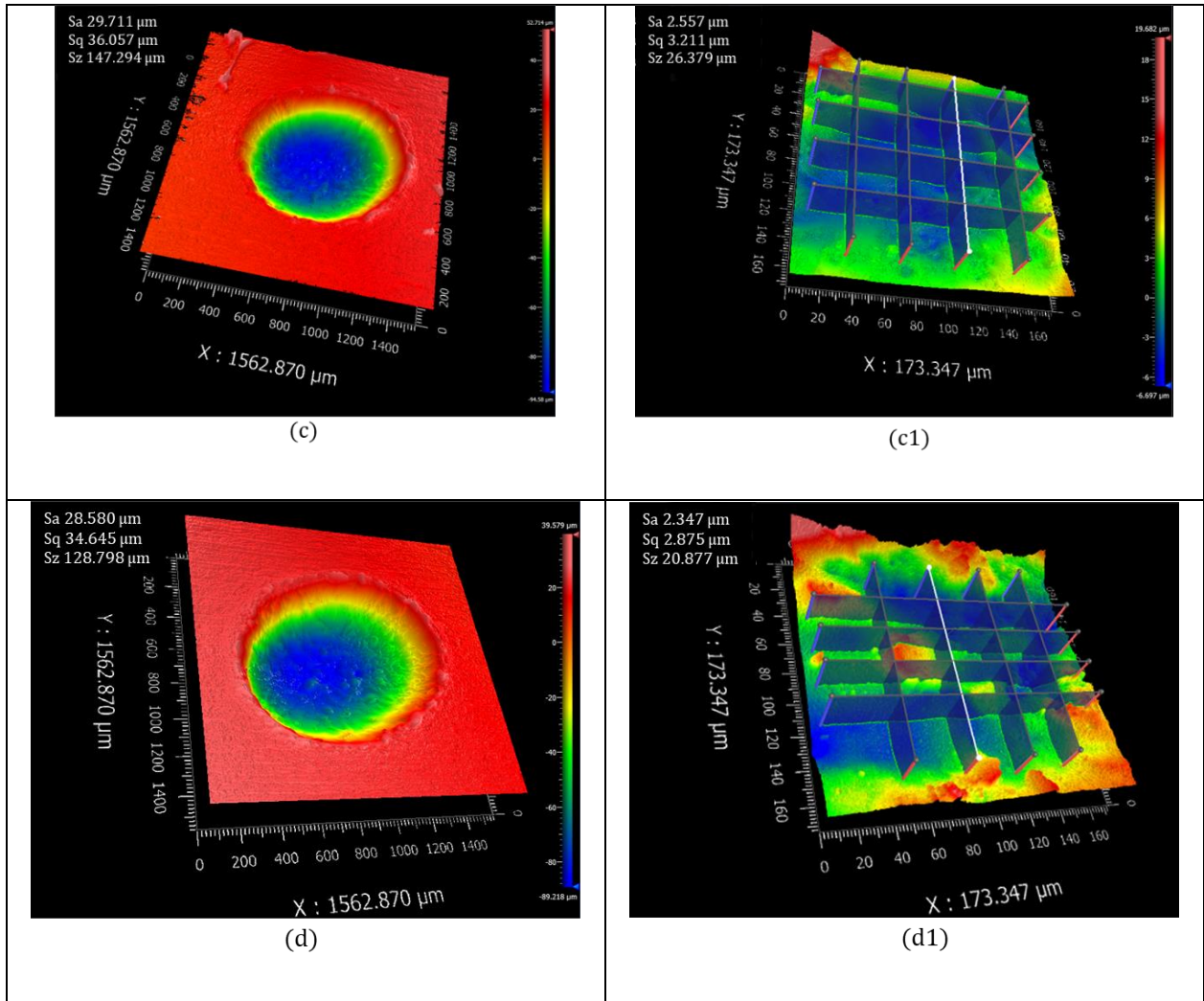


Figure 3. 12 (a-d) 3D geometry of the machined surface (a1-d1) variation in area surface roughness parameters.

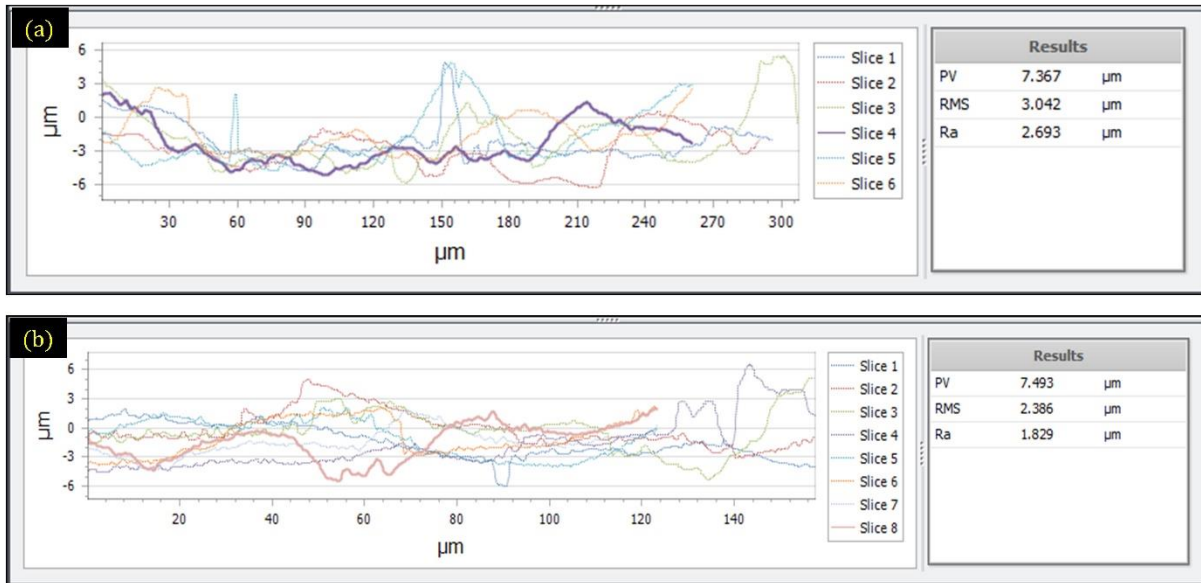
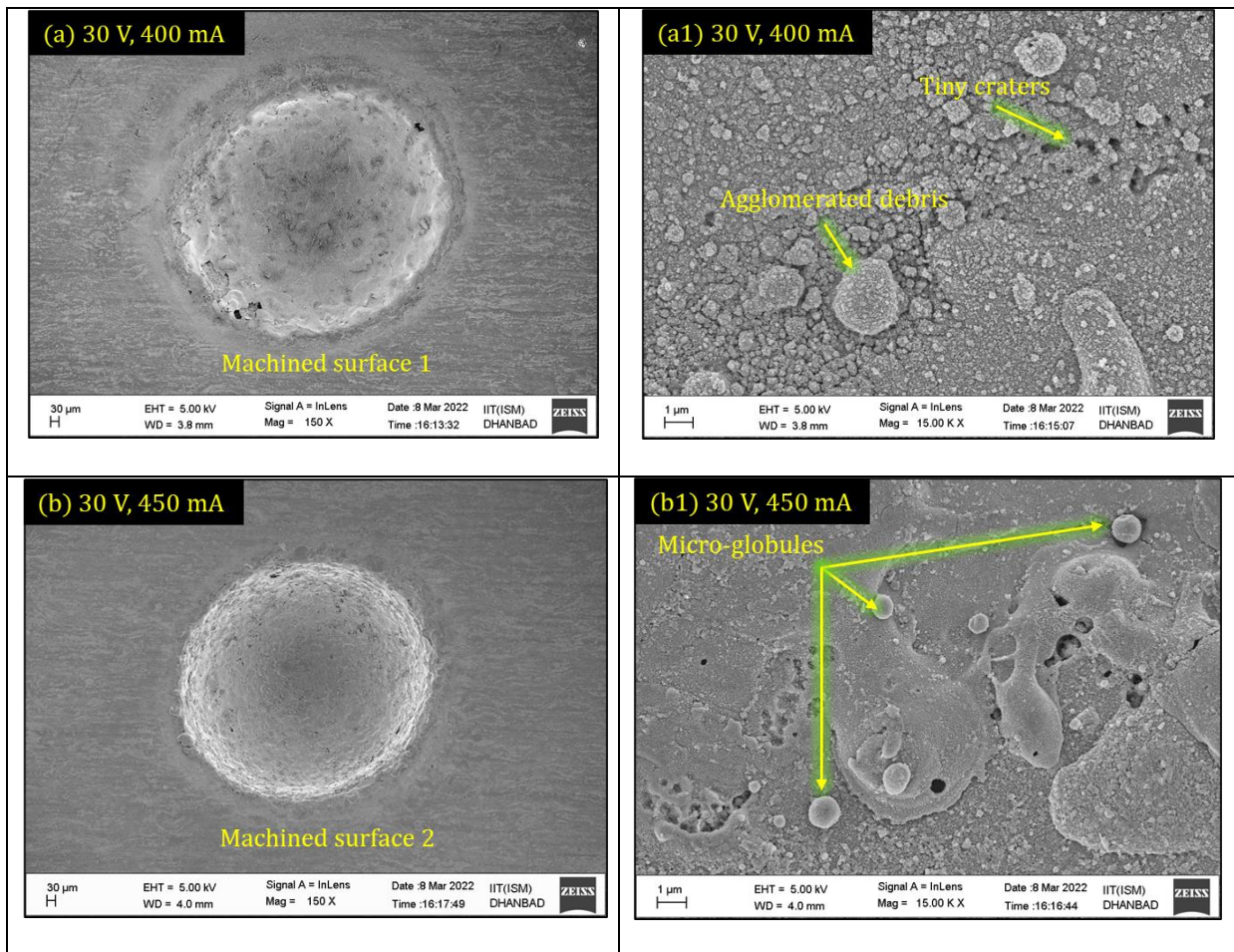


Figure 3. 13 variations in linear surface integrity parameters over six to eight slices (Ra, Rq, and Rz) at lower (450 mA) and higher current (550 mA) settings.

3.4.5 Surface topography analysis through FESEM

The surface topography of the machined surface was examined through the high-resolution field emission scanning electron microscopy technique. The surface morphology under different peak current settings is indicated in fig. 3.14. The morphology indicates there is the presence of microholes, micropores, microcavity, lumps of reattached debris particles, and micro globules on the machined surface. The pinholes and micropores were formed due to the trapping of the vapors and bubbles during solidification. The lumps of debris particles were formed to the reattachment of three or more three debris particles at a time during pulse interval time. The micro-globules were formed due to the complete evaporation of the working materteral into vapor clouds. These micro globules were attached to the machined surface due to the improper flushing pressure or may be due to mass density inertia property. The enrichment of microcavity, micro-globules, micropores, and pinholes was noted at a higher discharge current setting. The shape and size of the micro globules were found a little bit bigger at a higher current setting. Higher discharge current results in deeper crater formation which may deteriorate the surface finish of the machining surface. additionally, the

formation of some recast layer thickness was found near the edge of the machined surface as well as the interface region. This recast layer was formed due to insufficient flushing pressure or due to the inappropriate splashing of the molten material during the pulse interval state. This resolidified layer was found hard and contain a fine-grain structure of carbon due to the cracked dielectric. The resolidified layer was white in appearance and unaffected by the etching process. The recast layer thickness was mainly affected by the presence of carbon composition in the work material, types of dielectrics (especially hydrocarbon), and magnitude of discharge current and pulse on time.



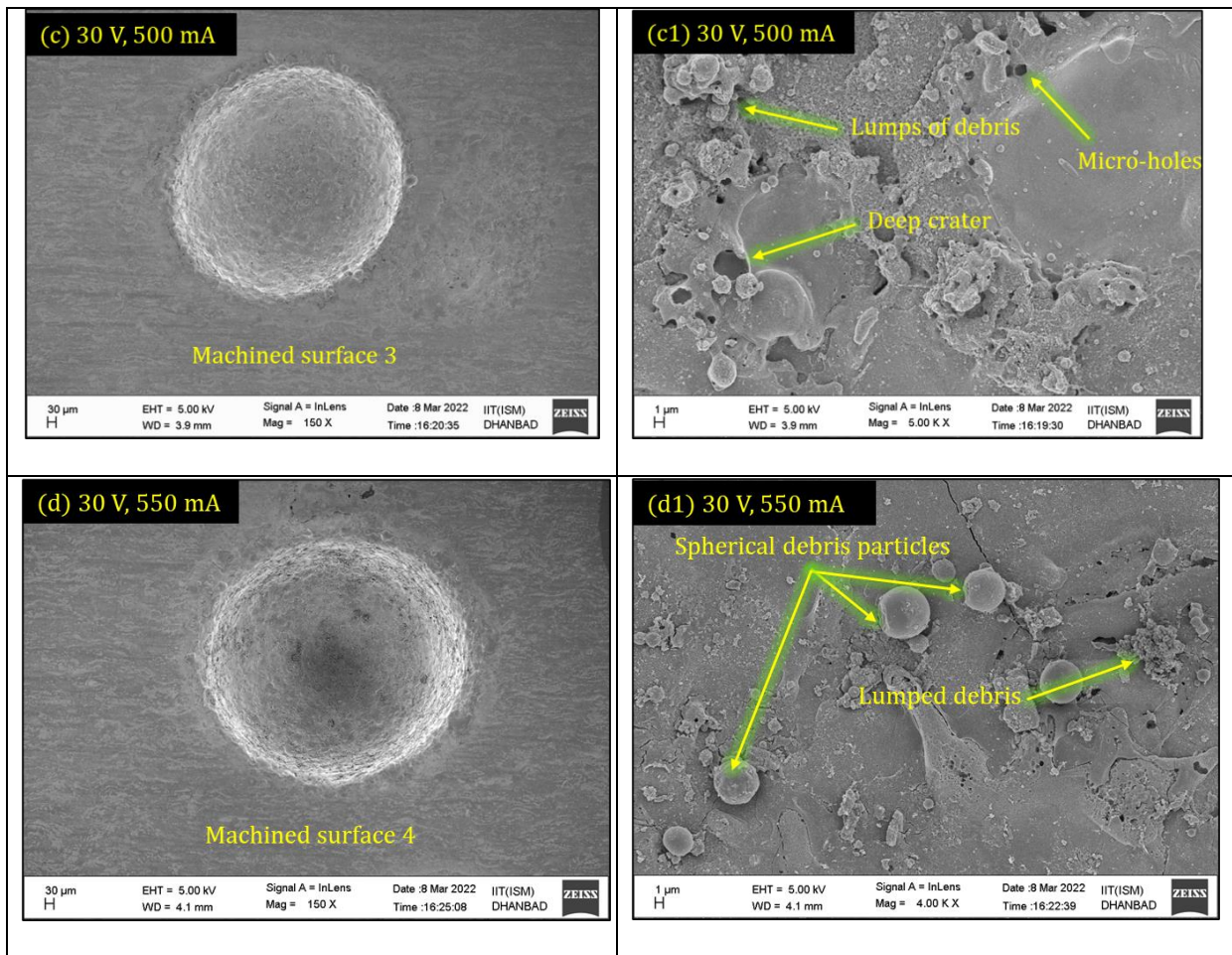


Figure 3. 14 Surface topography analysis of machined workpiece parts through FESEM with constant voltage (30V) and at varying currents (a) 400mA, (b) 450mA, (c) 500mA, and (d) 550mA.

3.4.6 Material migration and diffusion analysis through EDX

The compositional analysis of the machined surface was carried out using the energy-dispersive X-ray spectroscopy (EDS) technique. It is a quantitative method for evaluating the elements present on the machined surface. It facilitates the information about the availability of the elements in a particular material at a particular location in terms of either weight percentage or in terms of atomic percentage. In EDS, secondary and backscattered electrons are utilized in image formation for morphological analysis, as well as X-rays used for the identification and quantification of compounds present at measurable amounts. The detection

limit of EDS is determined by the smoothness of the sample surface; the smoother the surface, the lower the detection limit. It can detect major and minor elements with concentrations higher than 10 wt% (major) and minor concentrations (concentrations between 1 and 10 wt%). Fig. 15 (a & b) illustrate the elemental composition of the parent workpiece material (DSS-2205) and tool material (tungsten). In Fig. 15(a), it was found that terbium (24.14 wt%) is available in higher quantities which came as impurities during handling or due to oxide formation in an open environment. In Fig. 15(b), the presence of tungsten (84.88, wt%) EDS spectra indicates that the tool is made of pure tungsten. Fig. 3.15 (c & d) indicates the EDX spectrum of the various elements available on the work machined surface cross-sectional area. The exitance of ferrous (38.05-41.18 wt.%), chromium (18.37-18.95 wt.%), nickel (2.56-3.29 wt.%), manganese (2.63-2.92, wt.%), nitrogen (0.74, wt.%), Si (0.51-0.78, wt.%) on the work machined surface comes from the compositional part of the parent material. The availability of tungsten (2.34-2.67, wt.%) on the work machined surface indicates the bidirectional material migration and diffusion phenomenon. This also indicates that there is a surface alloying phenomenon that happens under the high temperature and high-pressure plasma region and due to insufficient flushing, they are deposited over the machined surface. Surface alloying causes the creation of various compounds in various phases, which may be investigated via X-ray diffraction (XRD) analysis. Furthermore, this surface alloying process enhances the machined part's surface quality and wear resistance. This occurs due to the mixing of two distinct elements in a high-temperature plasma region, resulting in the formation of an intermetallic compound that is dispersed as a metallic powder in the dielectric media. Due to the high-density mass inertia, this dispersed metallic powder settled on the machined surface. The settlement of the dispersed particles on the machined surface forms an intermetallic connection that improves the surface's wear resistance. The deep and shallow craters were filled with these particles, resulting in improved surface

roughness. The presence of carbon in a slightly larger quantity shows that the carbon is derived both from the carbon stub (sample linked to it) and from the decomposition of hydrocarbon oil in high-temperature plasma. The presence of oxygen implies that the surface has been oxidized, which could be due to ambient air contact.

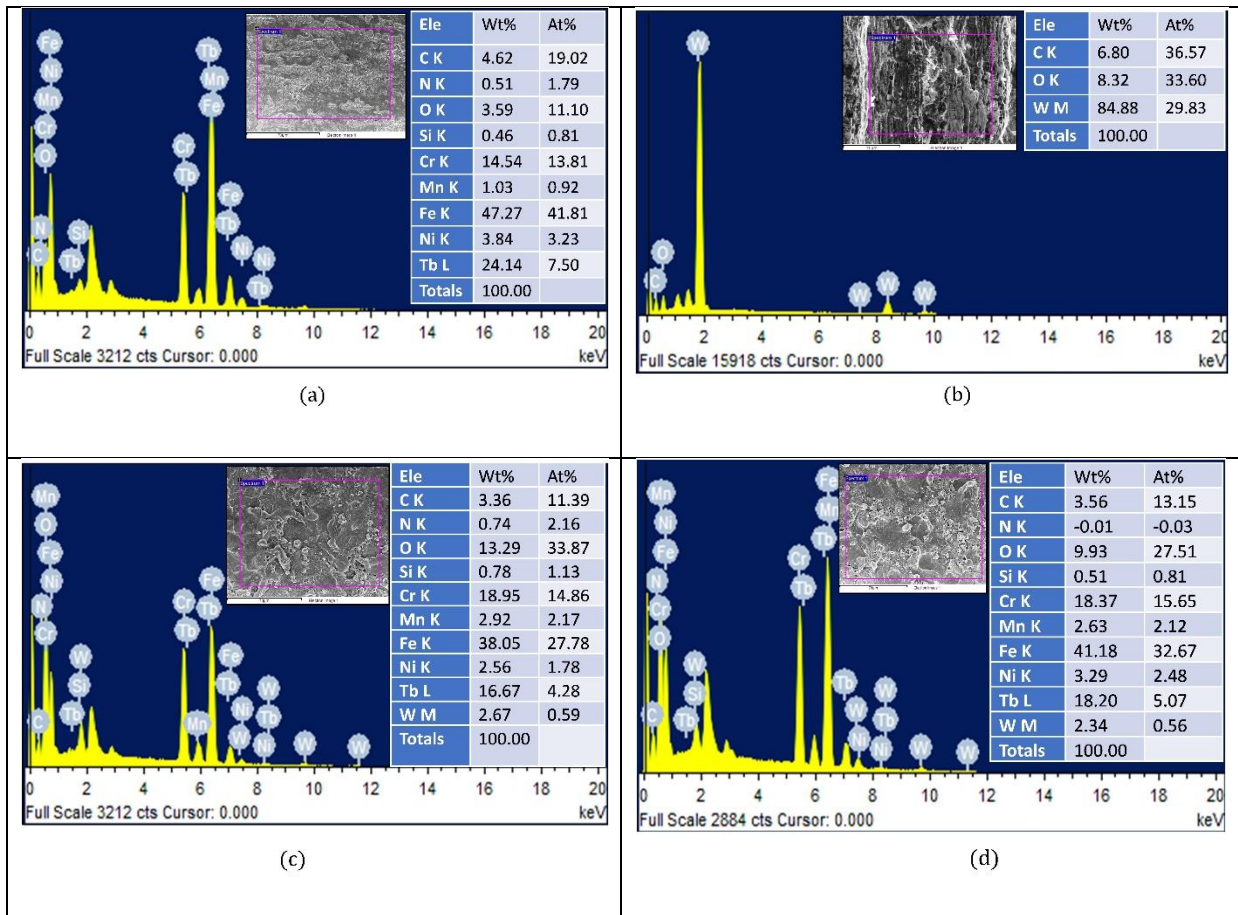


Figure 3. 15 Chemical characterization of (a) parent material (DSS-2205), (b) tool material (tungsten rod), (c) material migration, and elemental diffusion analysis through EDX spectrum at 400mA and (d) 550mA at the similar location of the machined workpiece.

3.5 Conclusions

This chapter provided a quick overview of the magnetic levitation-based servo stabilized gap control mechanism for micro-EDM and tested its feasibility for micro-machining. An actuator arm added to the system considerably enhances the flushing condition by action of

quick jumping or oscillating. The results of the current study and experimental examination are as follows.

- The innovative actuator arm technology and magnetic levitation have solved the slow positioning response of the traditional servo head caused by mass inertia and backlash.
- According to the time transient voltage-current (V-I) waveform, most discharge energy pulses are stable and uniform with low ignition delay. The short ignition delay indicates that the ionization is happening very fast.
- The maglev micro-EDM system's specific energy ranged from 0.5396-0.9356 J/ μg , which is consistent with earlier literature (0.037-0.9656 J/ μg). This indicates that the proposed system is just as effective as other available commercial EDM systems.
- According to the feasibility study, performance indicators like material erosion rate (MER), tool erosion rate (TER), and surface roughness (SR) change between 117.6-223.8 $\mu\text{g}/\text{min}$, 10-29 $\mu\text{g}/\text{min}$, and 1.829-2.693 μm , respectively, throughout three iterations.
- Examining the surface topography and morphology using FESEM images reveals that there are small amounts of melted debris, micropores, pinholes, micro craters, and micro-globules. This indicates that the surface is sufficiently smooth due to low discharge energy. Although re-solidification (white layer/recast layer) of melted debris was discovered close to the interface region, no microcracks were discovered across the machined surface. This can be the result of insufficient flushing pressure.
- According to chemical characterization by EDX analysis, there is material diffusion and there is bidirectional material transfer. Due to the phenomena of surface alloying, this further causes the formation of various compounds in various stages.

- The proposed technology might be a substitute for micro-servo EDM's gap control. The system is entirely autonomous and doesn't need a complicated drive or motion controller.

4

Chapter- 4: Development of micro- and nanotools for Nano-EDM

4.0 Introduction

Fabricating the nanotip size tool may be a challenging task for the commencement of nano-EDM. It is expected that the nanotip size tool may deliver the discharge energy at the nanoscale due to size effect. STM/FIM probes are coming with nanometric tip diameter and high aspect ratio apex length which increases their durability and uniformity for ions emission [211–213]. Tungsten is mostly preferred in STM tip fabrication because it poses high mechanical strength, low electrical resistivity, and high thermal stability and durability [214–218]. These nanotips may be tested as tools to find the possibilities of nano-EDM. Electrochemical etching is the most preferred method for fabricating nanosized tips. The method of applying electrochemical etching and a sequence of fabricating nanotips is illustrated in Fig. 4.1. Cheng et al. [219] developed an ultraprecise machine tool to fabricate the micro-nanotools via EDM. The fabricated nanotools offer a surface roughness of less than 10 nm. Alkhaleel et al. [73] generated nanocavities of varying depth 17 to 53 nm using single tip AFM probes via nano-electro machining principle. Multimode AFM machine was used as the machining platform while, copper and gold were the sample materials. In this experimental work, they studied the effect of the hammering act of electrostatic forces within the machining region. The created nanocavities from this hammering action were found stable within a time range of 48h. The gap distance in terms of gap voltage and scanning motion of the stage was identified as an important factor that decides the condition for the

fabrication of nano features at the nanoscale. The role of the electrostatic force was found less compared to the factor mentioned above.

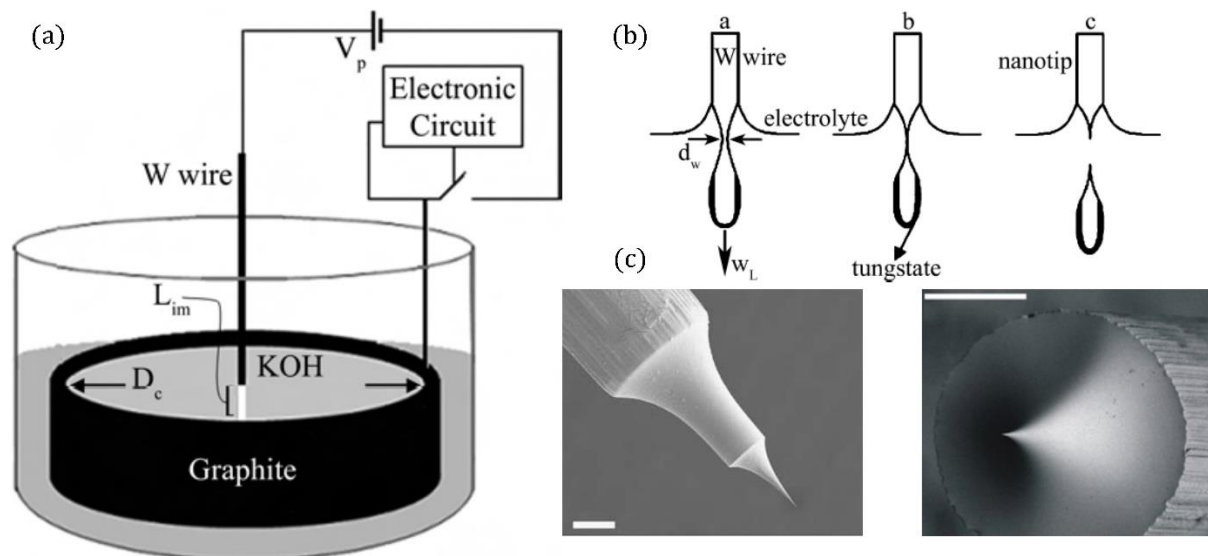


Figure 4. 1 (a) Electrochemical etching method (b) sequence of nanotip tool fabrication in the electrochemical process (c) fabricated nano tipped tool. Reproduced with permission [220–222].

Benilov et al. [223] used the Pt-Ir etched tool in scanning tunneling microscopy to create the nano features via the nano-EM principle. The measured tip dia was approx. 300 nm while the conic dia of the necking part was 1-10 μm . It is expected that development in nanotools like nanoprobes, nano-indenter, and nanotips may support the advancement of nano EDM technology [224]. Electrochemical etching [225–227], Chemical vapor deposition [228,229], molecular self-assembly [230], electrochemical deposition [231], nano growth techniques [232], and reverse micro-EDM [233,234] are some suggested techniques through which nano-tip-sized tools may be fabricated for nano-EDM. Normally, gold, silver, tungsten, Pt-Ir, and platinum are favorable materials for the fabrication of nano-size tipped tools [235]. Fig. 4.2 shows the various types of micro/nanotips fabricated by various methods by different researchers. However, before machining, the feasibility of these kinds of fabricated tools must be checked.

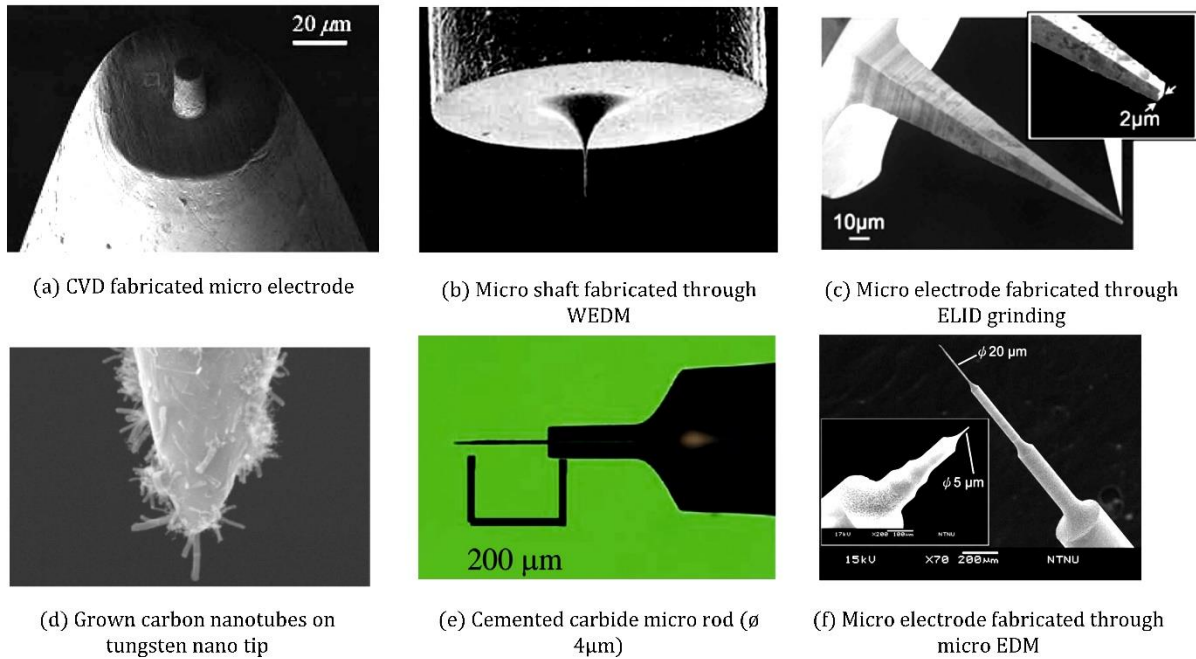


Figure 4. 2 Tipped tool fabricated through various methods by the various researcher for micro and nano-EDM. Reproduced with modification [236–242].

For achieving nano features through the nano-EDM principle, fabricating the nano tips is one of the important tasks. Literature indicates that in past years normally tip-induced lithography techniques are used for achieving the nano features on typical materials. Moreover, AFM/STM and SPM probes are used for fabricating the nanofeatures using the nano-electro machining (nano-EMM) process. Generally, these probe tip diameter lies in the range of 2-10nm and needed special attention during operation. These nano-tipped tools and its holder are very costly and not favorable from the economic point of view for nano machining.

Hence, in this chapter, three different techniques have been described for fabricating the micro and nanotools.

- I. Fabrication of microelectrode (microtool) through the electrochemical micro-turning process for growing nanorods and nanoplates like a tool on its micro tip.

- II. Fabrication of nanoplatelets like nanotools and their optical and chemical characterization.
- III. Fabrication of ZnO nanorods as nanotools grown on microprobe tip.

4.1 Fabrication of microtool through the electrochemical micro-turning process

The tungsten micro-electrodes of diameter 90-95 μm were fabricated by the electrochemical micro-turning process as mentioned in [243]. For this, the tungsten rod of diameter 0.65mm and truncated graphite rod ($\phi 5\text{ mm}$) was used as electrode materials. The tungsten rod is coated with non-conducting paraffin wax to make the job chemically inert. It also ensures the uniform distribution of current density in the working gap. The experiments were carried out in KOH electrolytic solution at a concentration of 2.5 M and 3.0 M with an applied voltage potential of 15 V and 18V respectively. The tool feed towards the job and uniform inter-electrodes distance was maintained through a manually operated X-Y stage (precision 5 μm). The machining time was limited to 5 minutes only. Due to the anodic dissociation and mass transfer phenomenon in the interelectrode gap, the materials get eroded from the rotating tool [244]. Close vicinity and tool feed motion towards the job plays a significant role in initiating the ionic dissociation or transfer of ions in the inter-electrode gap at the applied potential. Here, the uniform electric field is maintained by controlling the uniform gap. The tool is fed uniformly and material is removed due to chemical reaction. Due to the ion transfer phenomenon, this process ensures a better surface finish without any residual stress, cracks, and burr. Moreover, the cylindricity was monitored by controlling the interelectrode through a manually operated XY micro-positioning stage. The diameter of the job is reduced gradually at a uniform rate due to the electrochemical reaction. The fabricated microrods were initially dumbbell in shape due to mass diffusion layer effect and gravity effect. The neck formation (conical shape) can also be observed in some images which indicates the vicinity of the rotating tool, gravitational and mass diffusion impact on the

geometry of the tool electrode. Mass diffusion is nothing but the dissolving of ions (movement) within the electrolytic solution due to an applied potential difference and concentration difference. While gravity impact is the settling of suspended heavy particles due to gravity pull.

The schematic for fabricating the cylindrical microelectrodes through the electrochemical micro-turning process is shown in fig. 4.3 while the morphological image of the fabricated microtools at varying concentrations of 2.5 M and 3.0 M were represented in fig. 4.4.

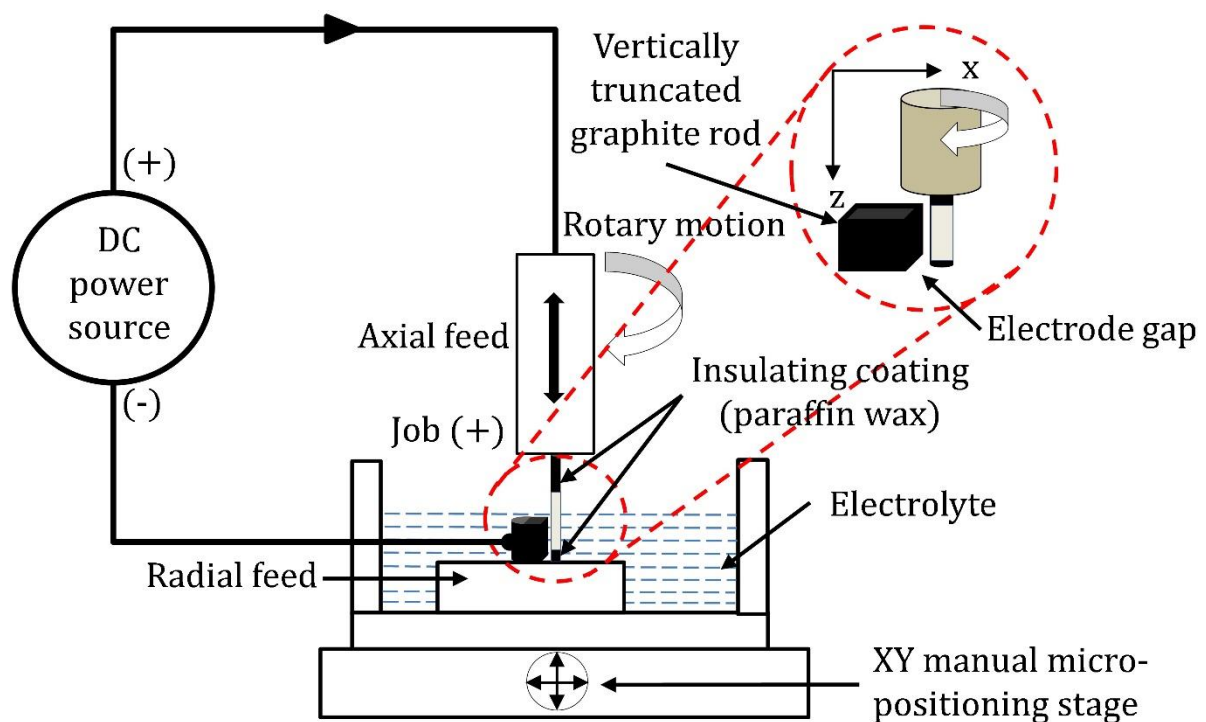


Figure 4. 3 Schematic for fabricating the microelectrode in the electrochemical micro-turning process.

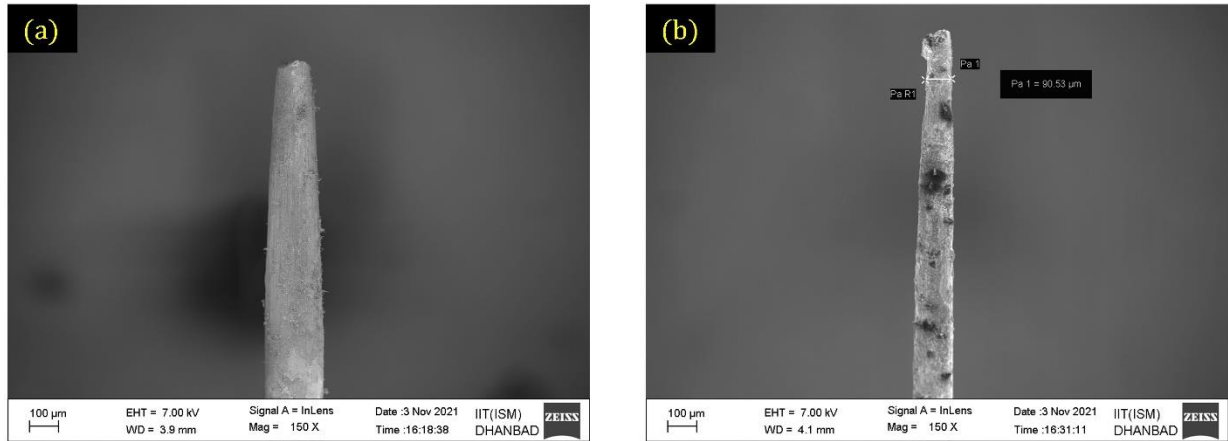


Figure 4. 4 Fabricated microelectrode (micro rods) for growing ZnO nanorods on the apex of the microprobe tip at 2.5M @ 15V and 3.0 M@ 18V.

4.2 Fabrication of nanoplatelets like nanotool on microprobe tip and its chemical and optical characterization

4.2.1 Experimental setup

The schematic and actual image of an indigenously developed micro-electrochemical discharge machining setup was utilized for the fabrication of 2D assembly of ZnO nanostructures as shown in fig. 4.5 (a & b). The setup contains a columnar angular structure, CNC motorized Z-stage, XY micro-positioning platform, pulsated DC power source, glass bowl, and host computer. The Z-stage motion was controlled using a motion control card, data acquisition system (NI), and LabVIEW software. The Z-stage (resolution 5 μm) regulates the motion of the tool in micro-stepping rates in a lateral (vertical) direction. A manual displacement positioning platform controls the motion of the workpiece and maintains the proper gap width via axial feed.

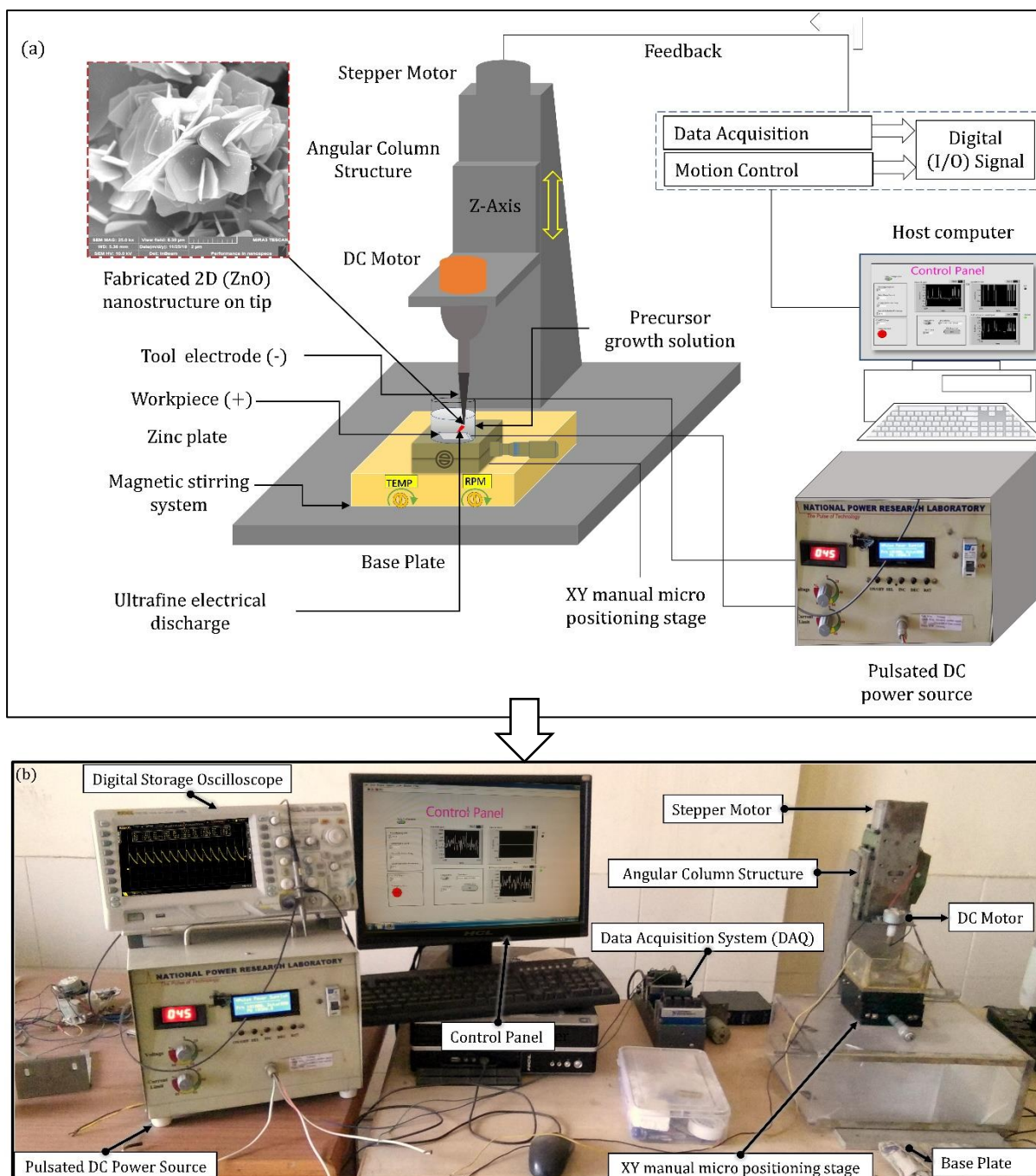


Figure 4. 5 (a) Schematic of the experimental setup for 2D fabrication of ZnO nanostructure along with key components, (b) Actual representation of the experimental setup.

4.2.2 Materials and procedure

The analytical grade chemicals reagents (zinc nitrate hexahydrate, hexamine (HMTA), acetone, ethanol, 99.0% pure) were utilized for the experimentation. Initially, a growth solution of zinc nitrate hexahydrate and hexamine (HMTA) was prepared at varying molar

concentrations (0.10M, 0.15M, 0.20M) by mixing them on a magnetic stirrer (500 rpm) at 60°C for 30 minutes. The flowchart of nanoplates fabrication is illustrated in fig. 4.6.

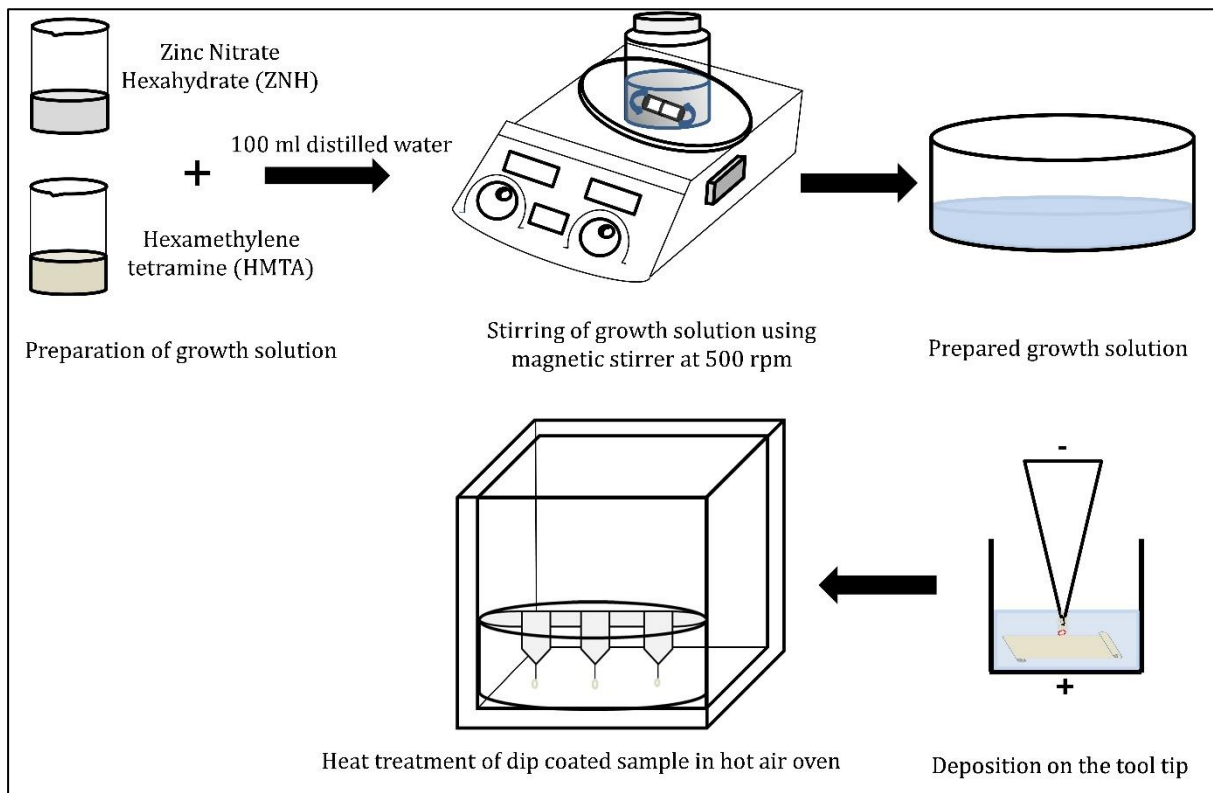


Figure 4. 6 Stepwise by flowchart for the fabrication of 2D nanoplates of zinc oxide (ZnO)

The experiments were conducted according to the condition listed in Table 4.1. A mechanically prepared conical tipped electrode ($\phi 150\text{-}200\mu\text{m}$) and counter electrode (zinc sheet) of dimension 30mm x 10mm x 0.5mm were utilized as cathode and anode materials in straight polarity. Prior to the experiments, these materials were ultra-sonicated in acetone (15 min), cleaned with ultrapure distilled water, and dehydrated in a hot air furnace. A motion-controlled program developed in LabVIEW software regulates the tool motion through Z-stage in the vertical direction. The proper interelectrode gap and axial feed were controlled by XYZ micro-positioning displacement platform (resolution 5 μm). A constant voltage potential of 50 V is applied through a transistor-based DC pulse power supply while growth solution concentration is varying from 0.10 M to 0.20 M. A well-defined nanocluster was deposited over the tip with porousness in its crystal structure.

Table 4. 1 Selected process parameters for fabrication of 2D nanostructure (ZnO)

In-process variables	Values
Selected molar concentration (M)	0.10, 0.15, 0.20
Deposition and growth time (seconds)	20
Precursor solution (growth)	Zinc nitrate hexahydrate + Methenamine (HMTA)
Applied voltage potential (DC)	50V
Conical microtip electrode diameter (μm)	150-200
Pulse period (μs)	50
Duty factor (%)	50
Pulse frequency (kHz)	10 (constant)
Counter electrode (dimension)	Zinc sheet (30 x10 x 0.5 mm ³)

4.2.3 Heat treatment (annealing)

Immediately after the deposition and growth, the deposited nanosheet cluster was rinsed in ultrapure distilled water and ethanol 3-4 times. After washing, the sample was kept inside the muffle furnace (hot air furnace) for heat treatment (annealing) at 95⁰ C for 45 minutes. Annealing heat treatment is essential because it eliminates moisture and crystal impurities. After heat treatment, the morphological/structural characterization of the deposited nanomaterials was assessed through various microscopic and optical methods.

4.2.4 Results and Discussion

4.2.4.1 Structural and morphological characterization

The structural and morphological characterization of synthesized ZnO nanostructure (2D)

was evaluated via the high-resolution field emission scanning electron microscopy technique (TESCAN, MIRA-3 LMH Model). At lower concentration (0.10M) the 2D nanosheet-like morphology was observed while at higher concentration (0.20M) 2D morphology changes to a marigold flower-like structure with porousness in its crystal structure. The morphology changes from 2D to flower-like nanostructure are not fully understood in the open literature. But here, the involvement of discharge energy within the interface region may be the one factor that accelerates the deposition and growth mechanics of nanocrystal sites. At lower concentrations, a few hydroxyl ions (OH^-) react with Zn^{2+} to generate zinc hydroxyl ions ($\text{Zn}(\text{OH})_4^{2-}$) that are finally dehydrated into the ZnO nanosheet. The individual nanosheet poses high surface energy with their exposed plane. Hence, they tried to aggregate to reduce surface energy by dropping the exposed surface areas. This drop in surface energy caused agglomeration of the nanosheets [245]. This agglomeration of nanosheets decreased the vacancies and interconnected at the edge to form the nanoflower (marigold) like structure. The complete morphological evolution/transformation from the 2D nanosheet to the nanoflower-like structure is illustrated in fig. 4.7.

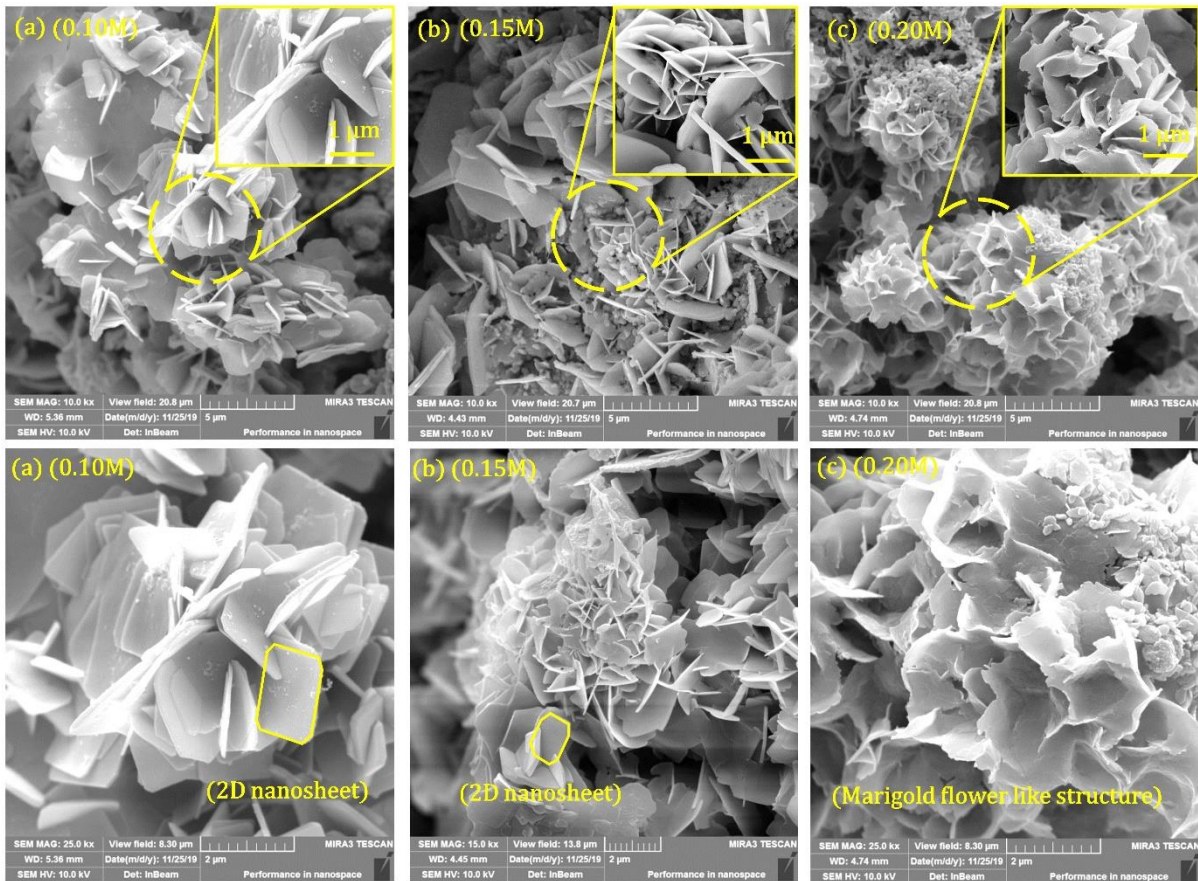


Figure 4. 7 Morphology evolution from 2D nanostructure to 3D nanoporous cluster (flower-like structure) under varying molar concentrations at different scale bars.

4.2.4.2 Role of microtip in nanostructure growth control

The tip-substrate interface plays a vital role in nanocluster fabrication. The high voltage potential within the tip-substrate interface sometimes led to mechanical contact which retards the formation of the nanocluster. Hence, a proper gap condition must be maintained to exhibit the condition for better jump-to-contact transfer of atoms or molecules within the interface [246]. The introduction of a microtip in the chemical growth solution promotes the localized deposition and controlled growth of active nuclei in 2D forms. The dissociation reaction will be more prominent at the microtip due to the high polarization effect. Moreover, the apex of the tip exhibits high capillary pressure within the interface region which increases the correct alignment, positioning, and assembly of grown nanosheets. Hu et al. [247] demonstrated the

role of a tip in tip-based nanomanufacturing systems (TBNS). They reported that when the tip and substrate are kept at a specific distance under the influence of polarization, it endorses certain events such as the joule heating effect, local reactions, molecular diffusion, and localized deposition. The significance of introducing the microtip for controlling deposition and growth mechanics is shown in fig. 4.8.

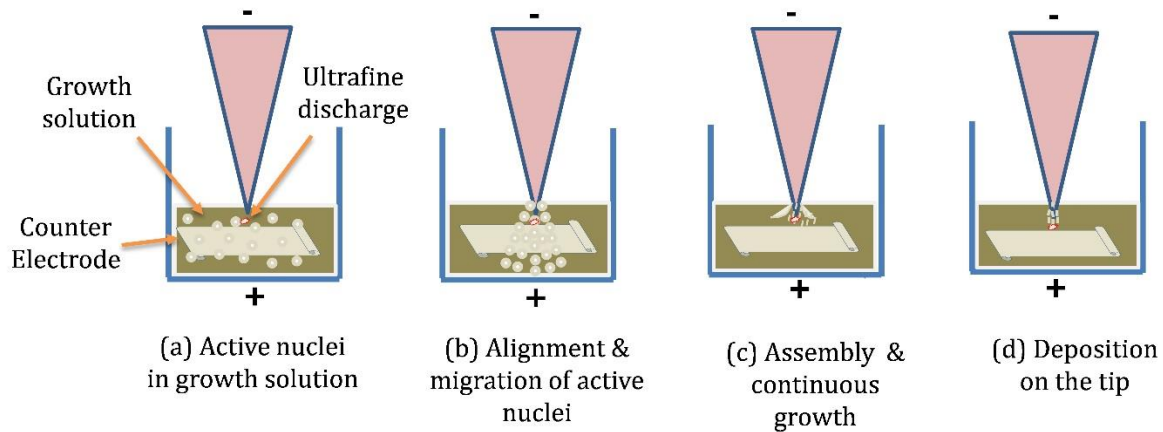


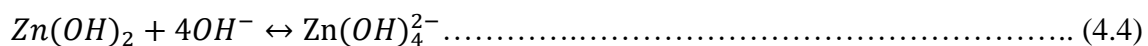
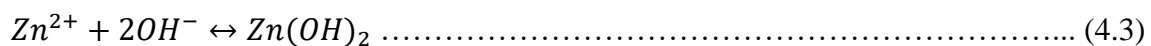
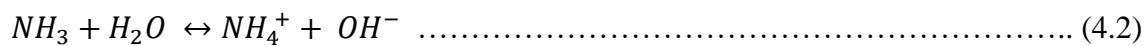
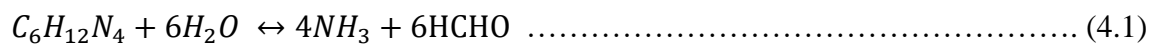
Figure 4. 8 Deposition and growth mechanism for the 2D assembly of ZnO nanostructure.

4.2.4.3 Mechanism of crystal growth

Under the influence of ultrafine discharge in chemical growth solution, the deposition and growth mechanics may be understood in two stages (a) nucleus (sites) forming stage and (b) growth stage [248]. In the nucleation stage, a large number of unstable active nuclei are formed due to prominent voltage potential. Here, the nucleation process occurs in three zones such as bulk solution zone, molecular transfer and diffusion zone, and compact layer zone. Moreover, the growth mechanics is determined by the solvent dipole moment which is prominently influenced by the molecular diffusion rate and electron transfer rate in the solution [249]. Ultimately, the oxidation and reduction state-run of the chemical reaction decides the growth morphology of active sites on the electrode surface.

In the current work, the deliberation of OH^- ions significantly influence the growth direction of the ZnO nanostructure. The tetrahedral coordination of Zn^{2+} and O^{2-} poses a

stacked layer along the c-axis during growth [250]. Here, Hexamine reacts with water molecules to develop formaldehyde (HCHO) and ammonia (NH₃) at retarded rate. The slow release of ammonia (NH₃) generates fewer numbers of OH⁻ ions which affect the nucleation rate of Zn²⁺ ions during hydrolysis [251]. Moreover, the existence of ammonia (NH₃) limited the growth of zinc hydroxide ions along the c-axis by absorbing the amine molecules on the surface [252]. The zincate ions combine with hydroxyl ions (OH⁻) to form the Zn(OH)₂ colloids and growth unit as tetrahedral zincate ions Zn(OH)₄²⁻ radicals. This tetrahedral zincate ion was finally dehydrated to form zinc oxide (ZnO) under heated conditions [253]. To understand the morphological evolution and growth mechanics, the spontaneous chemical reaction associated with the fabrication of 2D ZnO nanosheet is elaborated below.



4.2.4.4 Chemical characterization through EDX

The elemental composition of the fabricated nanomaterial is determined by energy-dispersive X-ray spectroscopy. The existence of zinc and oxygen in appreciable amount (100%) in the EDX spectrum indicates that the fabricated nanostructure is of zinc oxide. Fig. 4.9 shows the chemical composition of the fabricated nanostructure along with their elemental color mapping.

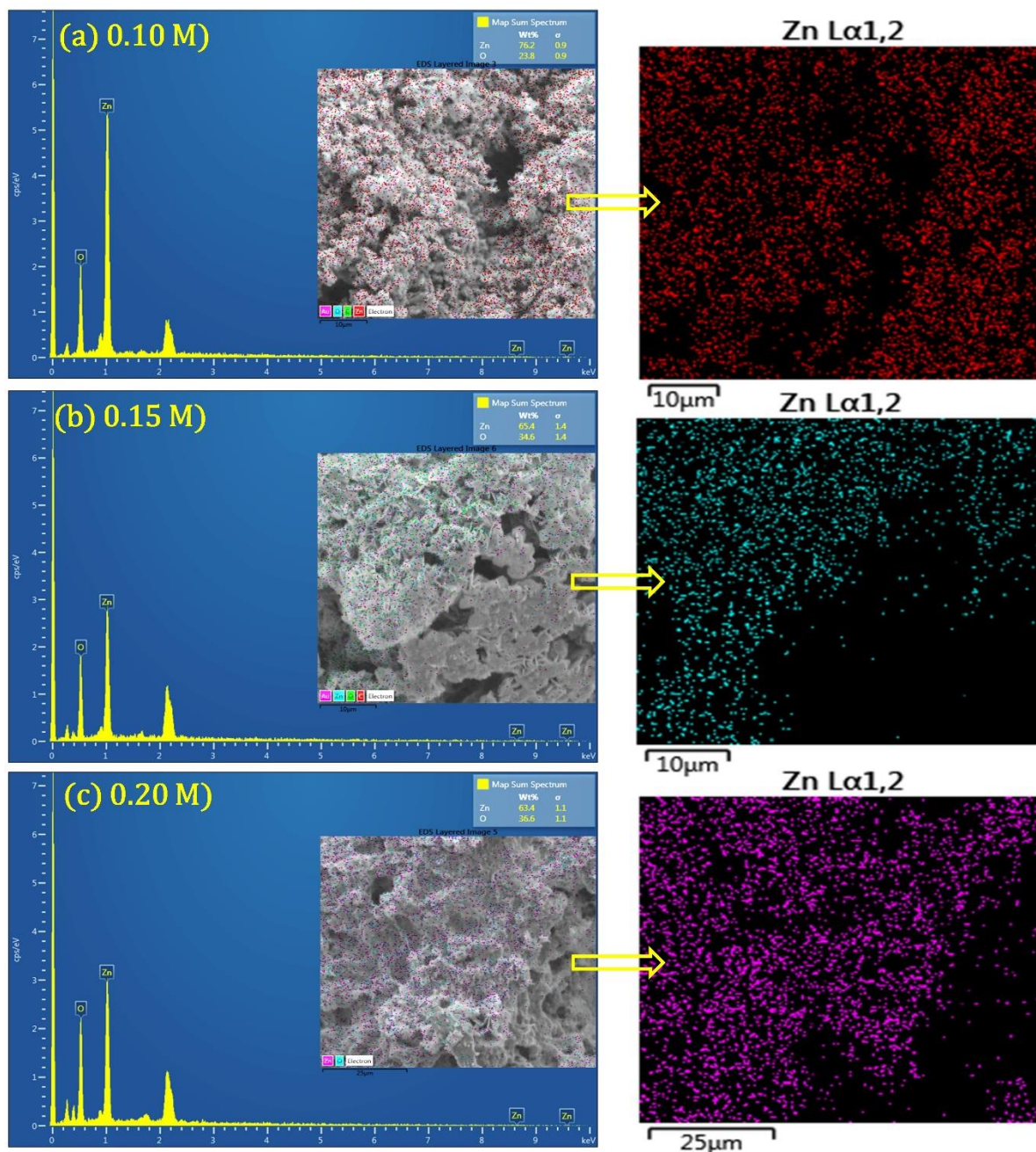


Figure 4. 9 Chemical composition of fabricated nanostructure with their elemental color mapping via EDX spectroscopy.

4.2.4.5 X-Ray diffraction (XRD) analysis

The diffraction pattern (fig. 4.10 (a)) was taken under copper source (Cu) radiation of wavelength K-Alpha1 (1.540598 Å) & K-Alpha2 (1.544426 Å), ratio K-Alpha2/K-Alpha1=0.5 in the scan range of 20 $^{\circ}$ to 80 $^{\circ}$ (2 θ) at accelerating voltage of 40kV. It was noted

that all the sample contains the same phase structure, which was indexed in the hexagonal wurtzite structure posing a lattice constant parameter ($a=0.32498$ nm and $c=0.52066$ nm (Reference code: 00-036-1451). The high-intensity peak for the plane (101) and (100) corresponds to $2\theta=36.1649$ and $2\theta=31.6506$ indicating 2D formation of ZnO nanostructure with crystallinity in phase purity. The low-intensity peak for the plane (002) indicates the retarded nature of growth in the vertical direction. The unavailability of any unwanted peak in the diffraction pattern confirms the phase pure crystalline structure of ZnO.

The crystallite size of the 2D nanosheet was estimated by X-ray line broadening (FWHM) using the Debye-Scherrer equation [254] i.e.

$$D_P = \frac{K\lambda}{\beta \cos\theta} \dots \dots \dots (4.6)$$

Where, D_P (average crystallite size), $K=0.94$ (shape factor constant), λ (X-ray wavelength, Cu $K\alpha$:0.15406 nm), β (line broadening or FWHM in radian), θ (Bragg's diffraction angle). The mean crystallite size (thickness) of the ZnO nanosheet was noted about 27 nm (fig. 4.10 (b)) while the width of the nanosheet was varying between 1400 nm to 1600 nm.

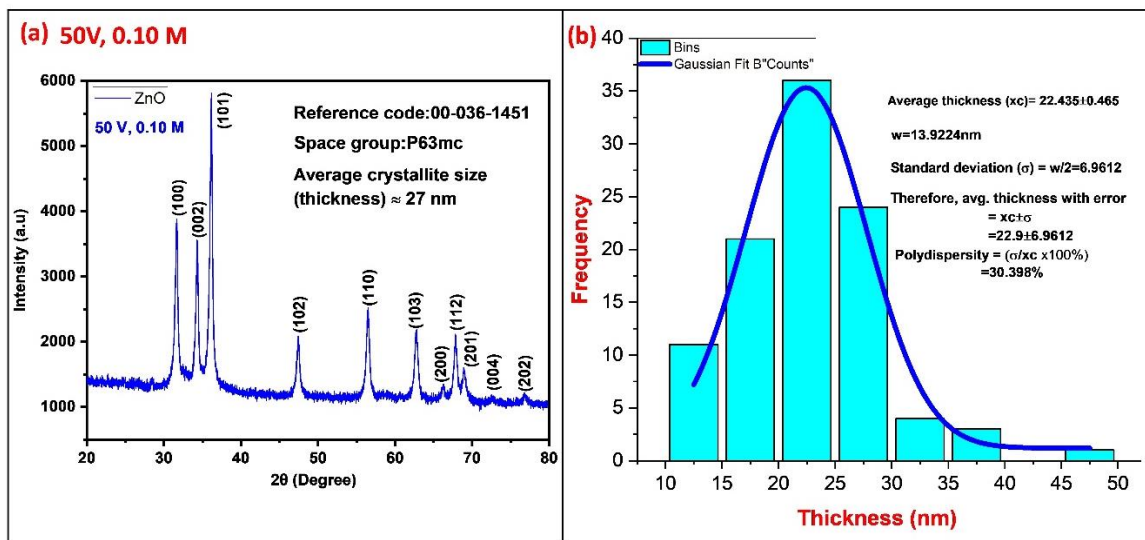


Figure 4. 10 (a) X-ray diffraction pattern of the fabricated 2D nanostructure (b) size distribution of nanosheets.

4.2.4.6 FTIR and XPS analysis

The availability of functional group and molecular fingerprint corresponding to ZnO stretching is identified by Fourier transforms infrared spectroscopy (FTIR) as shown in Fig. 4.11 (a). The availability of two strong absorption peaks (590.57 cm^{-1} & 645.02 cm^{-1}) in the fingerprint region might be associated with ZnO stretching. Ghosh et al. [255] noted the two strong absorption peaks corresponding to wavenumber 425 cm^{-1} & 570 cm^{-1} for 2D ZnO nanoflakes structure. The absorption peak of 1462.39 cm^{-1} may be associated with C-N stretching indicating the presence of the amide-I group. The O-H stretching may be raised due to the existence of alcohols/phenols corresponding to wavenumber 3350.90 cm^{-1} . The intensive peak of C-H (sp^2) might be associated with wavenumber 3137.90 cm^{-1} which indicates the presence of an alkenyl group. The H-O-H vibration corresponds to wavenumber 1666.91 cm^{-1} may indicate dehydration of water molecules under heated conditions.

The surface-sensitive quantification of fabricated ZnO nanosheets was analyzed through X-ray photoelectron spectroscopy (XPS) to identify the elemental composition and their oxidation states within the material. A broad survey scan was taken in a wide range of energy as shown in fig. 4.11 (b). Strong intensities of Zn, and O were detected in survey spectra of XPS. Fig. 4.11 (c) and Fig. 4.11 (d) indicate the -Zn2p and -O1s spectra at high resolution. The presence of a doublet pair peak of Zn2p corresponds to binding energy 1022.5 eV and 1045.5 eV indicating the Zn2p₃ and Zn2p₁. These two-core level also indicates the oxidation states (+2) for ZnO surface. The deviation in binding energy between these two core states (Zn2p₃ & Zn2p₁) was found approximately 23.0 eV for ZnO morphology which is consistent with as reported previously [256]. Moreover, the binding energy (532 eV) corresponding to peak -O1s might be associated with the absorption of water molecules (-OH).

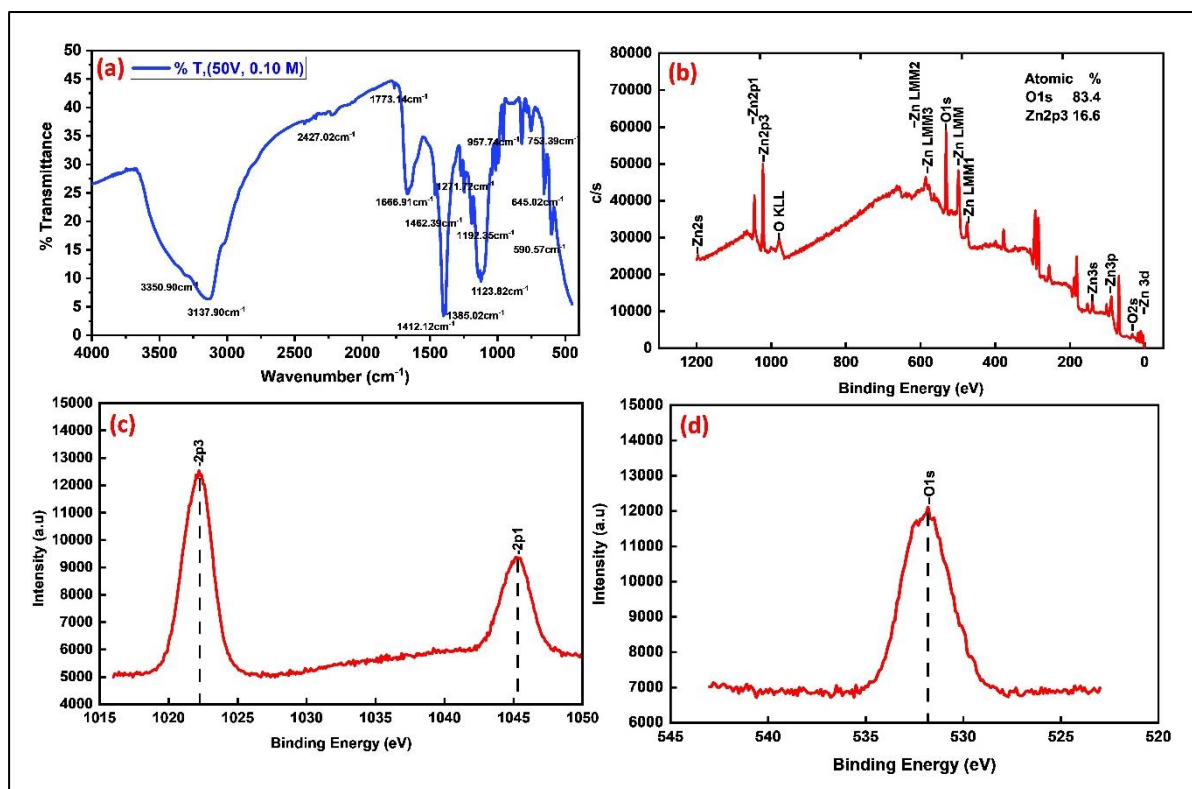


Figure 4. 11 (a) Infrared spectrum (FTIR) (b) XPS survey spectra (c) high-resolution XPS - Zn2p3 and -Zn2p1 (d) -O1s of the grown nanosheet at 50V and concentration 0.10 M

4.2.5 Conclusions

A systematic accelerated growth method for the fabrication of zinc oxide (ZnO) nanostructure especially 2D nanosheet is briefly covered on the microprobe tip. The introduction of ultrafine arc discharge accelerates the chemical reaction and promotes the rapid fabrication of the ZnO nanostructure. Different stages of nanostructure growth with their basic mechanism are elaborated briefly. A varying growth morphology from the nanosheet-like structure to the flower-like structure is found at concentrations of 0.15 M and 0.20M. The experimental results clearly show that the lower concentration is the best condition for 2D nanosheet formation. Moreover, the crystallinity and chemical characterization through XRD and EDX ensured that the varying concentration does not significantly influence the quality of the fabricated nanomaterial. Further, the availability of the functional group corresponding to ZnO stretching confirms the good transmittance

behavior of the fabricated nanosheets. The existence of doublet pairs in their core-shell in XPS spectra confirms the oxidation states of ZnO. With an excellent morphological structure and improved surface-to-volume ratio, its potential may be extended to energy harvesting devices, bio-sensing, optoelectronics, luminance industries, etc. However, this was the first attempt towards the fabrication of nanorods like a tool but this method provides 2D nanoplates-like tool on the microprobe tip.

4.3 Fabrication of ZnO nanorods as nanotools grown on microprobe tip through low-temperature hydrothermal process.

Developing the nanotools for the nano-EDM process is critical work. Moreover, holding the nanotools in the tool holder is very a very tedious task. Hence, here first of all micro-electrodes of diameter 90-95 μm were fabricated using the electrochemical micro-turning process as mentioned in previous section 4.1 and which can be held easily. On the tip of the microelectrodes, ZnO nanorods were developed using a low-temperature hydrothermal process. These nanorods were further used as nanotools for nano-EDM. For growing the nanorods, two solutions were prepared, one is a seed solution while the other is a growth solution. The seed solution was prepared by dissolving the zinc acetate dehydrate [62.5mg, $\text{Zn}(\text{CH}_3\text{COO})_2 \cdot 2\text{H}_2\text{O}$] in 100 ml of ethanol and stirring it on a magnetic stirrer (400rpm) at 60°C for 15 minutes. Another solution of sodium hydroxide (20mg, NaOH) was prepared in 20ml of ethanol and stirred at 400 rpm at 60°C for 15 minutes. This second solution was transferred to the seed solution and an additional 80ml of ethanol was added to complete the seed solution of 200 ml. This complete solution was stirred again under heated conditions (60°C) for another 20 minutes. This complete seed solution was further used for the formation of active nucleation sites. Now, the tip of the electrode is dipped into the seed solution for 15 minutes and then transferred to the hot air oven (90°C) for drying for another

15 minutes. This half an hour cycle was repeated 8 times continuously. A thin film of unstable nucleation sites is formed over the tip which further grows into nanorods after essential heat treatment. The list of chemicals used for preparing seed and growth solutions is presented in table 4.2.

Table 4. 2 List of chemicals that have been used for fabricating the ZnO nanorods on the tooltip

S. No.	Chemical used	Chemical formula	Utilization
1	Acetone	C_3H_6O	For washing/cleaning the samples
2	Water (distilled)	H_2O	For preparing the growth solution/rinsed the samples/substrate
3	Ethyl alcohol (ethanol)	CH_3-CH_2-OH	For preparing seed solution/cleaning samples
4	Sodium hydroxide	NaOH	pH controlling in seed solution
5	Zinc acetate dihydrate	$Zn(CH_3COO)_2 \cdot 2H_2O$	For seed solution preparation
6	Zinc nitrate hexahydrate	$Zn(NO_3)_2 \cdot 6H_2O$	Growth solution preparation
7	Hexamine	$C_6H_{12}N_4$	Growth solution preparation

After seeding the tooltip, a growth solution was prepared by mixing the 10mM of zinc nitrate hexahydrate and hexamine (HMTA) in 630ml of distilled water. This mixture was stirred on a magnetic stirrer for 15 minutes under normal environmental temperature (27⁰C). The pH of the growth solution was also maintained within 6.5-7. Now, for the hydrothermal

growth of ZnO nanorods, the seeded tip is dipped into the growth solution and kept inside the hot air furnace at 90°C for 8 hours. After 8 hours of heat treatment, the sample was taken out and rinsed with distilled water 6-8 times to hold any further growth. After washing, the sample was again kept inside the hot air furnace for another 24 hours for drying purposes at 30°C. The schematic for seeding on the tooltip and growing of nanorods through a low-temperature hydrothermal process is illustrated in fig. 4.12. Fig. 4. 13 (a) shows the morphology of the fabricated microelectrode (tungsten) while 4.13 (b) indicates the morphology of the grown ZnO nanorods on the top surface of the microprobe tip.

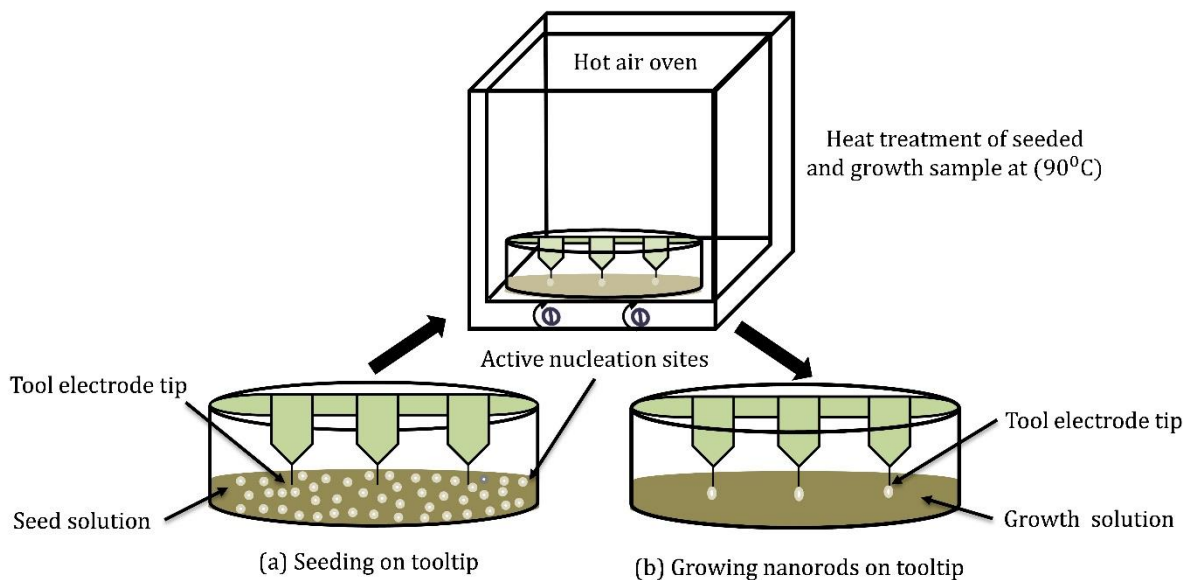


Figure 4. 12 Method of seeding on tooltip and growth of ZnO nanorods through the low-temperature hydrothermal process.

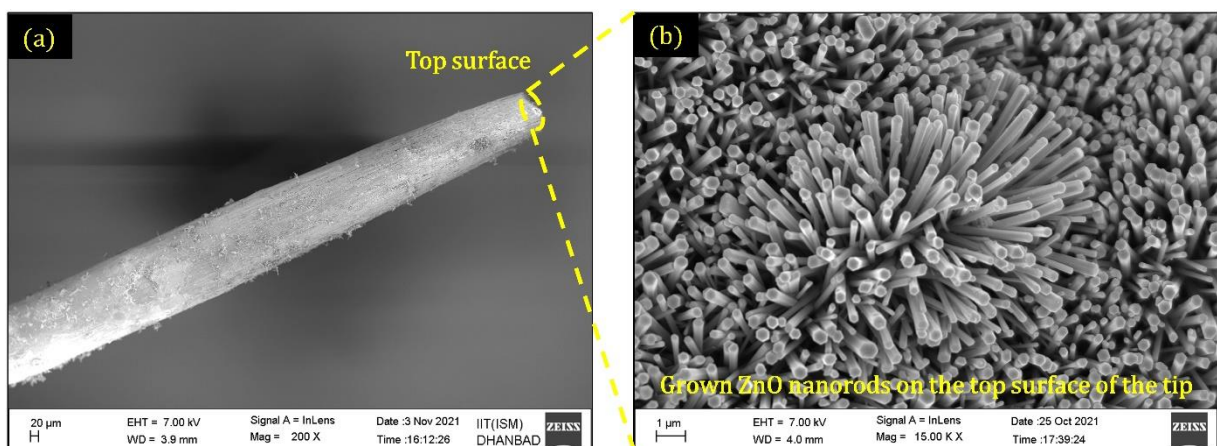
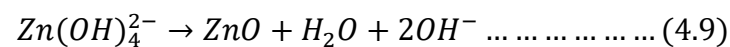
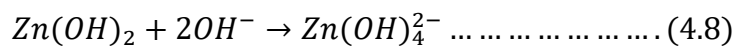
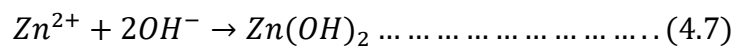


Figure 4. 13 (a) Morphology of the fabricated microelectrode (tungsten) (b) grown ZnO nanorods on the top surface of the microprobe tip.

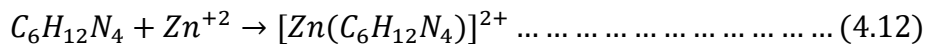
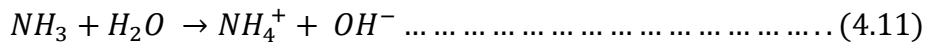
4.3.1 Mechanism of nanorods growth

The growth mechanism of nanorods can be described in two stages (a) active nucleation stage (growth site formation) and (b) growth stage. In the current work, the nucleation stage is activated by dipping the tooltip in the seed solution followed by essential heat treatment at 90⁰C. The seeding treatment forms a thin film over the tip with an enormous number of unstable active nuclei. This large number of active nuclei acts as growth sites in a further stage. Here, during seeding, the Zn²⁺ ions are formed due to zinc acetate while OH⁻ ions are liberated from sodium hydroxide [252]. This combined effect caused the formation of zinc hydroxyl ions. Likewise, the liberation of a large amount of OH⁻ ions significantly dominates the growth direction of ZnO nanorods. Due to the tetrahedral coordination of Zn²⁺ and O²⁻ ions, it poses a stacked layer along the c-axis about which it has more tendency to grow [257]. The chemical reaction involved during seeding on the tooltip can be represented by the following reactions (Eqn. 4.7-4.9).



Just after the seeding, the tooltip is dipped in growth solution for 8 hours at 90⁰C. This provides the essential environment for growing the active nucleation sites into nanorods. Here, hexamine (HMTA) reacts with water to form formaldehyde (H-CHO) and ammonia (NH₃). Later on, in an aqueous solution, ammonia hydrolyzed to create NH₄⁺ and OH⁻ which significantly affects the growth rate of Zn⁺ ions during hydrolysis. Zn²⁺ ions and ammonia (NH₃) ions combined to form Zn(NH₃)₄²⁺, a new complex ion. ZnO nanorods were formed when these complex ions were mixed with water molecules [258]. To understand the

morphological evolution and growth mechanics, the spontaneous chemical reaction associated with the fabrication of ZnO nanorods is elaborated below (Eqn. 4.10-4.13) [253].



Through the above growth mechanism i.e., low-temperature hydrothermal process bundles of well-defined ZnO nanorods were developed on the apex of the microprobe tip which is used as nanotools for the nano-EDM process. The fabrication of geometrically irregular nano-patterned features was developed on the super-finished titanium alloy (grade-5) which will be discussed in chapter -5. Here, chapter 4 deals only with the various methods for the fabrication of 2D nanoplates like tools or nanorods (ZnO) like tools for achieving nanofeatures using the EDM principle.

5

Chapter- 5: Achieving nano-patterned features through micro-EDM process using ZnO nanorods as nanotools on Ti-6Al-4V

5.0 Introduction

With advances in technology, there is a need for modification in the machining process [259]. Miniaturization in device parts, components, and systems has achieved tremendous attention in recent years due to its wide applicability of features in electronics, bi-medical, automotive, and avionics industries [58]. Nano-fabrication is the fastest-growing field for nano-electro-mechanical systems (NEMS) in manufacturing industries due to the emergence of the features at the nanoscale [207]. Replicating the nanopatterned features on any typical material through some specific machining process is one of the great challenges facing current micro-electro-mechanical system (MEMS)/ nano-electro-mechanical system (NEMS) industries [260]. The integrated circuit, memory chips, display elements, bio-chips, and bio-sensors have extensively identified the potential of these nano-features for improving the performance of the device [261]. Additionally, these nano features are also required in nanopores for Deoxyribonucleic acid (DNA) detection [262], nanovias for interconnects, nanojets for controlled drug release [263], fuel atomizer injectors, nozzle for nanofluidic devices, molecular sorting sieve [264], and nanowires templates [8], etc. The extensively recognized technique for fabricating these nano features are tip-induced lithography, scanning probe microscopy (SPM), laser nano-machining, etc. [24]. Probe-based nanomanufacturing techniques such as atomic force microscope (AFM)/scanning tunneling microscope (STM) tip based nano-electro-machining (nano-EM) [8], nano-electrochemical machining [265], dip-pen nanolithography (DPN) [266], etc. are very famous these days for producing

nanostructured features [76]. Some other techniques such as nano-imprinting [267], electron beam lithography (EBL)[68], X-ray lithography, UV-lithography [268], and scanning probe microscope (SPM) based indentation and scratching [269] are achieving much attention in recent times because these are capable to write the nanopatterned features by removing the material at the nanoscale. Most of the above-reported techniques for fabricating nanoscale features are primarily used for the removal of silicon and polymeric materials with certain limitations [270]. From the author's point of view, there is very less machining process that is eligible for writing precise nanoscale features and structures on exotic materials under non-vacuum conditions (open atmosphere) at low cost via electrical discharge. Most of the reported techniques such as AFM/STM/SPM based tip induced nano-electro machining (nano-EM) technique generally uses tunnelling current for removing the material at nanoscale rather than discharge current [8].

5.1 Research gap and motivation

Micro-electro-discharge machining (micro-EDM) is one of the prominent methods for fabricating the microscale features on any electrically conductive material irrespective of its mechanical properties such as strength and hardness. Here, the material is eroded in form of microscale debris due to the thermal effect of electrical sparks in the micro-confined gap (5-10 μ m). The typical gap phenomenon involves the formation of plasma channels, flow, and interaction of ions and electrons, melting, and evaporation due to heat transfer [53]. By controlling the rate of flow of discharge energy in the micro-confined gap, various typical micro-features such as microcavity, microholes, micro dimples, etc., can be easily fabricated. The gap voltage, gap current, and pulse on time are prime factors that decide the gap condition for the flow of discharge energy. For a confined gap, a certain level of voltage potential called threshold voltage is applied between the electrodes to overcome the insulating strength of the dielectric to induce an electrical spark. This spark has sufficient

energy to make vaporized the solid metal directly into vapor. The vaporization of the metal forms the micro/nano cavity as a negative imprint of the tool which is known as features.

It is well-known fact that the size of the nanocavity formed through controlled electric discharge is governed by the size of the tool and availability of discharge energy in the micro/nanoconfined gap. Hence, to develop the nanofeatures at the nano-regime, the tooltip size must bring out to be at the nanoscale. It was expected that the reduction in the tooltip size will reduce the flow of discharge energy per unit pulse due to the localization effect ($R=\rho.L/A$). Yeo and Yap [271] indicated that the discharge energy of a single spark is lying in the range of 100nJ to 10 μ J in the conventional micro-EDM process. In carbon nanotubes (CNT) machining via field emission technique in dry micro-EDM, the discharge energy can be brought into nanojoules [272]. Khalid et al. [273] lowered the discharge energy to microjoule through the scaling approach. They fabricated the long aspect ratio geometrically irregular micropatterns on carbon nanotubes forest using the micro-EDM principle. They achieved the smallest feature size of 5 μ m with an aspect ratio of 20 by using the high-frequency discharge energy pulses locally. The optimum voltage potential and peak currents were 30V and 60mA in a micro-confined discharge gap of \sim 10 μ m. A similar type of scaling approach was applied by Xiao et al. [58] for fabricating the nano grating-like structure through the micro-EDM process on carbon nanotubes (CNT) forest. They reported that the locality of the electrode tip significantly affects the breakdown potential of the fluid dielectric. Moreover, it was claimed that the reduction in the tooltip size is an effective method for reducing the discharge energy (1nJ) per unit pulse. Jahan et al. [36] tested the machining capability of STM-based tip-induced nano-electro-machining (nano-EM) process under dry (air) and wet conditions (n-decane) of dielectric in a nano-confined gap of 1-2 nm. It was reported that the wet nano-EM process erodes the material by field-induced emission while dry nano-EM erodes the material by field-induced evaporation via tunneling current.

Additionally, the machined nanoholes were found much more stable and consistent in dry conditions compared to the wet condition due to the self-tip-sharpening ability of the tooltip. They also recommended that the dry nano-EM may be scaled up for fabricating the mass number of nano features due to self-sharpening ability and enhanced tool life. In another investigation, Jahan et al. [23] fabricated the nanofeatures of dimension 7.5-10 nm on an atomically flat gold substrate using platinum-iridium (ratio:80:20, Pt-Ir) wire as tool electrode and STM as machining platform through nano-EM in an open environment. It was reported that the heat generated via local field-induced evaporation in the nano-confined gap is the major source of energy for eroding the work material under dry nano-EM conditions. They suggested that the process may be used for nanopatterning on the atomically flat conductive surface due to the self-conditioning ability (auto-sharpening) of the tooltip. Kunieda et al. [20] brought the discharge energy level down to the nanometric level by coupling a capacitor to the tool electrode via a pulse generator. They fabricated a nanocavity of diameter 0.43 μm by eliminating the effect of stray capacitance in the circuit. Likewise, they achieved the material removal rate 3.5 times much better in servo-controlled feed compared to manual feed. The obtained surface roughness (peak to valley, R_z) of the machined surface was 0.23 μm . Kalyanasundaram et al. [76] studied the dielectric behavior in a nanoconfined gap of less than 3nm during fabrication of 20nm features size in a nano-electro-machining (nano-EM) process performed on an STM platform. The quasi-solid behavior of normal decane was observed at a higher density under a nanometric interface of 20nm which enhances the charge transport facility between the nanometric tool tip and workpiece. Finally, it was concluded that the breakdown and recovery of the dielectric strength are highly associated with the confinement of the nanometric gap and the applied electric potential (field stress). From the above literature, it is clear that there is the almost negligible method where discharge current has been used for fabricating the nanopatterned features on any electrically conductive

materials under non-vacuum environment.

The current work reported a scale-down approach for fabricating the nanopatterned features through a tip-induced nanomachining technique. For this, first of all, a magnetic levitation-based gap control mechanism has been developed for the micro-EDM process. The working mechanism of maglev micro-EDM is briefly explained in the article. Later on, the stability of the machining process was tested first in terms of voltage-current discharge characteristic curve for long-duration discharge (5ms) and multiple discharge energy pulses. It was found that the machining process was very stable without any lags or abnormal discharge such as arcing and short-circuiting. Thereafter, microtools (tungsten) of diameter 90-95 μm were fabricated through the micro-electrochemical turning process. On the tip of the micro tools, ZnO nanorods were grown through a low-temperature hydrothermal process. The mechanism of nano-growth of ZnO nanorods is enclosed briefly in the article. The morphological characterization of micro tools and the apex of the tooltip indicates that the nanorod is well-grown on the tip and poses a wurtzite (hexagonal) structure as it naturally exists. These nanorods acted as nanotools in long-duration discharge (5ms) micro-EDM experiments. The analysis of the FESEM micrograph indicates that the nanotools are producing a negative imprint on the work surface. The formation of nanopatterned cavities over the super-finished work surface confirmed the fact that by downsizing the tooltip, the discharge energy can be lowered due to the localization effect. Finally, the auxiliary results of this experimental investigation show the possibility of the approach toward nano-EDM with widespread potential/applications in micro/nanofabrication devices. The geometrically irregular type nanopatterned features may identify its potential in high-density memory devices, bio-sensing, electronics chips, wettability control [274], improving the cell behavior of bioimplants and antibacterial activities [275], enhancing the tribological performance by dropping the specific contact area in the interpillar regions, improving the biocompatibility of

the interfaces [276], etc.

5.2 Material and Methods

5.2.1 Experimental setup

A newly developed maglev micro-EDM system was used for the experimentation. The setup is controlling the interelectrode gap by using the principle of electromagnetic levitation. The major elements of the setup are a unipolar linear electromagnetic motor, an actuator arm for holding tool electrodes, a programmable multioutput DC power supply, and a dielectric tank. A special honeycomb feature is made inside the dielectric tank to hold the workpiece tightly. The dielectric tank is fixed on the micro-positioning stages for the subsequent movement of the workpiece in XYZ direction. A 100MHz bandwidth and 2GS/s sampling rate digital storage oscilloscope (DSO, Tektronix, TDS2012C, 2-channel) with differential type voltage (TPP0201, Tektronix) and current probe (65A-Hantek, BNC type) is attached with the setup to capture the real-time voltage and current waveform. The current probe is clamped in one of the wires which are closer to the workpiece and degaussing button is pressed 3-4 times to eliminate any residual magnetization of the wire. The actual experimental setup of maglev micro-EDM with their peripheral components is illustrated in fig. 5.1.

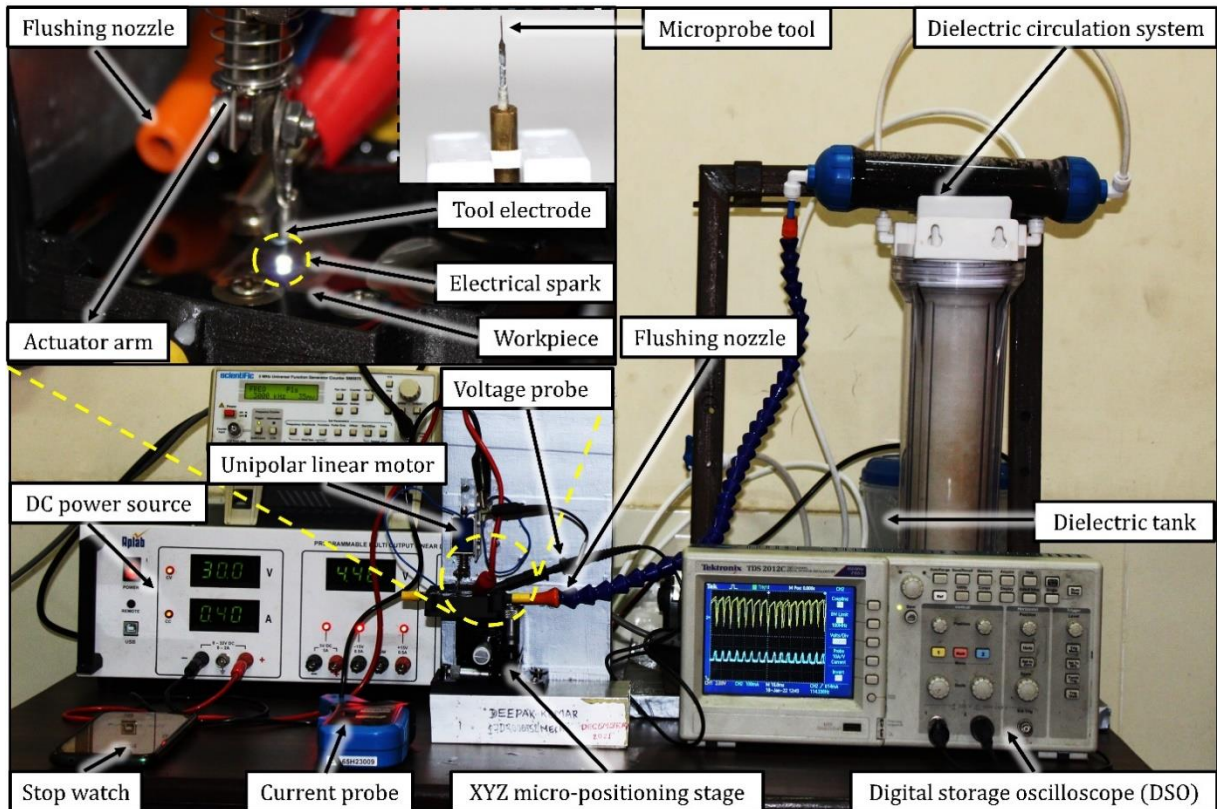


Figure 5. 1 Actual experimental setup of maglev micro-EDM with their peripheral components.

5.2.2 Maglev micro-EDM principle

The maglev micro-EDM works on the principle of magnetic levitation. Here, a precise gap control mechanism is developed by balancing the electromagnetic force (F_{em}) to the gravitational force (F_g) and spring force (F_s). A solenoid-based unipolar linear electromagnetic motor has been used with an extended actuator arm to develop the setup. The actuator arm can move freely up and down as per the applied current and voltage potential. Hence, the tool is attached to the movable actuator arm. When the voltage potential is applied through the DC power source, the actuator arm pulls the tool electrode upward and as power is switched off, the tool electrode freely falls to touch the workpiece due to mass gravity or loss of magnetic strength. It was also noted that during pulling, the spring restores some force called spring restoring force (F_s). This restoring force assists in maintaining the stability of

the machining process during discharge. Now, for the EDM process, the positive terminal of the DC power source is attached to the workpiece while the negative terminal is attached to the one terminal of the linear motor. The other terminal of the linear motor is attached to the tool electrode. The complete configuration of the circuit and attachment of the tool and workpiece electrode in maglev micro-EDM is illustrated in fig. 5.2. When the power is turned on, there is a flow of current through the linear motor, tool, and workpiece. The flow of current will energize the linear motor which retracts the tool electrode upward. As the tool electrode retracted upward it get separated from the workpiece. During separation, it will pose a minimum optimal distance (spark gap) to generate the spark. This spark is known as an electric discharge which removes the material via thermal evaporation. As a spark occurs, there is a reduction in the voltage potential of the power supply, the reduction in the voltage potential reduces the magnetic field strength of the linear motor and the tool will try to fall to touch the workpiece but again optimum distance will be maintained for the occurrence of electrical discharge. The whole arrangement is made in such a way that the system attained the equilibrium state where electromagnetic force is equal to the gravitational force and spring force i.e., ($F_{em}=F_g+F_s$). This equilibrium condition facilitates the optimum distance for the occurrence of normal electrical discharge. Based on this concept, the maglev micro-EDM is working. Later on, the linear micro-positioning stage (XYZ, resolution 5 μ m) is used for setting the initial gap condition. Moreover, this manual positioning stage controls the discharge voltage by setting the interelectrode gap (δ) precisely.

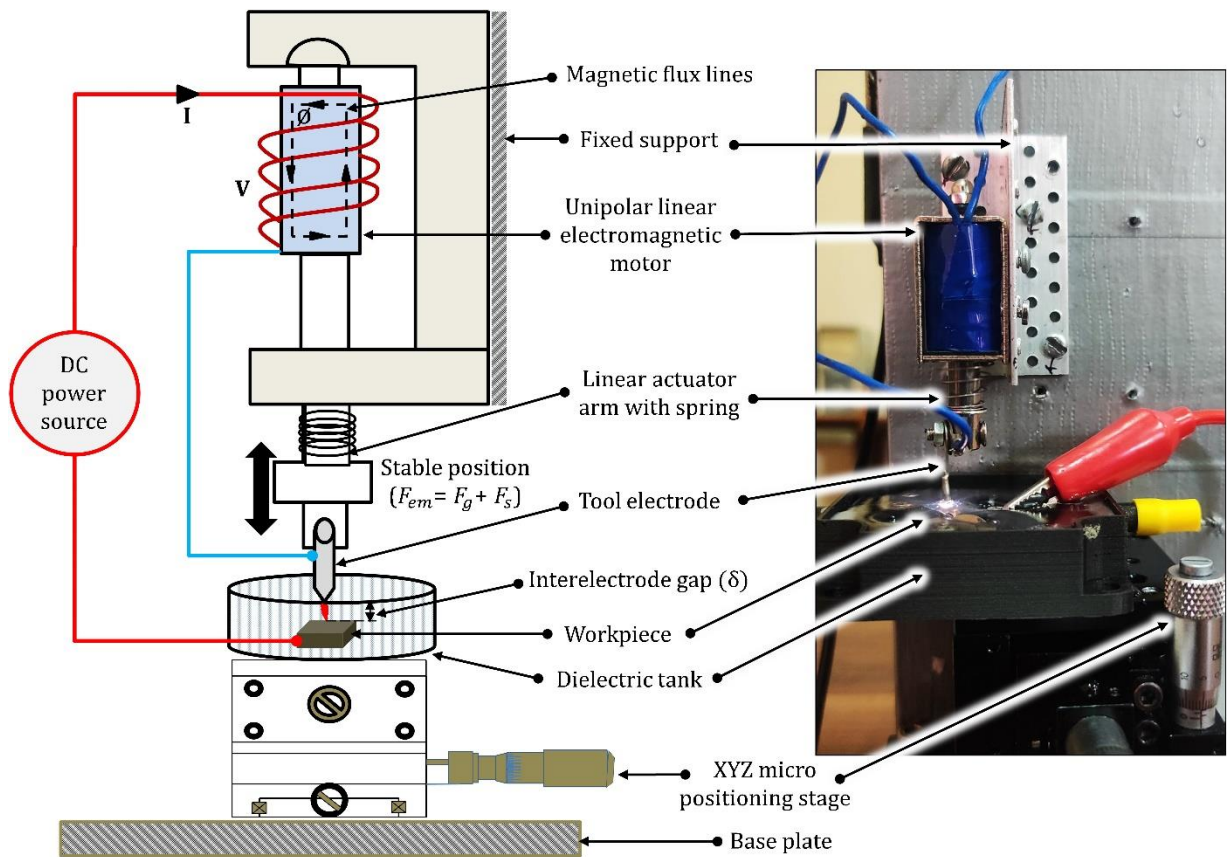


Figure 5. 2 Schematic for maglev micro-EDM with discharge circuit and actual representation.

5.3 Materials and procedure

The nanorods that are developed on the microprobe tip through a low-temperature hydrothermal process are used as nanotools for fabricating the geometrically irregular nanopatterned features. The fabrication of ZnO nanorods and their growth mechanism is already mentioned in previous section 4.3 in chapter 4.

5.3.1 Fabrication of nanopatterned cavity through a long-duration discharge energy pulse

Now, after fabricating the micro-electrodes and growing nanorods on the apex of the tooltip, these nanorods are acted as nanotools in long-duration discharge micro-EDM experiments. Nevertheless, before processing through the micro-EDM process, the work surface was polished with high-grade polishing paper (Grade:1500, 2000) on a disc polishing

machine (Chennai Metco). Additionally, the surface of the work material was made super-finished (mirror-like) using velvet cloth with diamond paste and aerosol. The sample was washed in acetone and distilled water using an ultra-sonicator to remove any impurities and dust particles from the work surface.

Pilot experiments were conducted first to check the stability of the machining process and for the identification of initial process parameters. It was found the machining process is stable enough with uniform pulse width. Moreover, servo-mechanism developed in maglev micro-EDM is controlling the interelectrode gap well to do the micromachining work without any lags.

After testing the stability of the machining process in multiple discharge energy pulses, now the actual long-duration discharge experiment was conducted using the nanorods-grown microprobe tip. The work material was cylindrical titanium alloy (Ti-6Al-4V) with a diameter of 10mm and a height of 5mm. The connection was made in straight polarity i.e., the workpiece was coupled to the positive terminal while the tipped tool electrode was connected to the negative side of the DC power supply. The experiment was conducted in dry conditions to avoid any contamination due to the dielectric breakdown because the ionization of dielectric may generate OH^- ions as free radicals due to chemical reactions. Also, the wet dielectric may absorb dirt as contamination which may affect the surface morphology [8]. The micro-positioning stages (XYZ) are used for setting the initial gap distance. An open gap voltage of 24 V was applied by setting the peak current at three different levels i.e., 300mA, 350mA, and 400mA. Later on, the long-duration discharge pulse characteristic was captured using a current and voltage probe (BNC type) in a digital storage oscilloscope (DSO) which is analyzed and discussed in a further section. The details of the experimental condition and material selected are arranged in table 5.1.

Table 5. 1 Material and applied experimental condition for fabrication of nanopatterned features.

a. Material selected for machining	
Workpiece	Superfinished Ti-6Al-4V (Grade-5)
Tool	≈100 μm tungsten rod with grown ZnO nanorods on the tip
Dielectric media	Open-air (dry micro-EDM)
Polarity	Straight
b. Machining condition	
Open circuit voltage (applied)	24V
Set peak current	300mA, 350 mA, 400mA
Duty factor	More than 90%
Pulse-type	Long-duration discharge (5ms) pure DC pulse

5.4 Results and Discussion

5.4.1 Morphological characterization

The surface morphology of the microtool with grown nanorods was tested first through a high-resolution field emission scanning electron microscope (FESEM, SUPRA-55, ZEISS). It was found that the microtool was almost cylindrical in length and ZnO nanorods were well-grown over the tip of the microtool in bulk amounts. The surface integrity of the upper cross-section of the tool electrode may affect the random distribution of the grown ZnO rods formation because, in the initial phase of formation of active nuclei on the surface, the better will be the surface finish, the better will be the distribution of the active nuclei and consequently, less will be disruption in the orientation of the ZnO nanorods. With less

randomization and less orientation distortion of ZnO nanorods, better will be the imprint quality of the nanocavities. Fig. 5.3 represents the morphology of the microtool with grown ZnO nanorods on the apex of the tip. It was noted that most of the nanorods are uniformly dispersed over the surface of the tooltip. However, some nanorods were coalited to each other and grown as a single unit while some are very close to each other. Later on, there is some variation noted in the diameter and length of nanorods which may be due to the varying calcination temperature and unstable growth of active nucleation sites. The majority of the ZnO nanorods posed a wurtzite structure that naturally exists in the environment. The diametral length was varying between 50nm-850 nm which was measured via Image J software. This diameter was enough to imprint the negative impression over the smooth surface through a long-duration discharge micro-EDM process. Fig. 5.4 represents the wurtzite morphology of the fabricated ZnO nanorods on the apex of the tip at four varying locations.

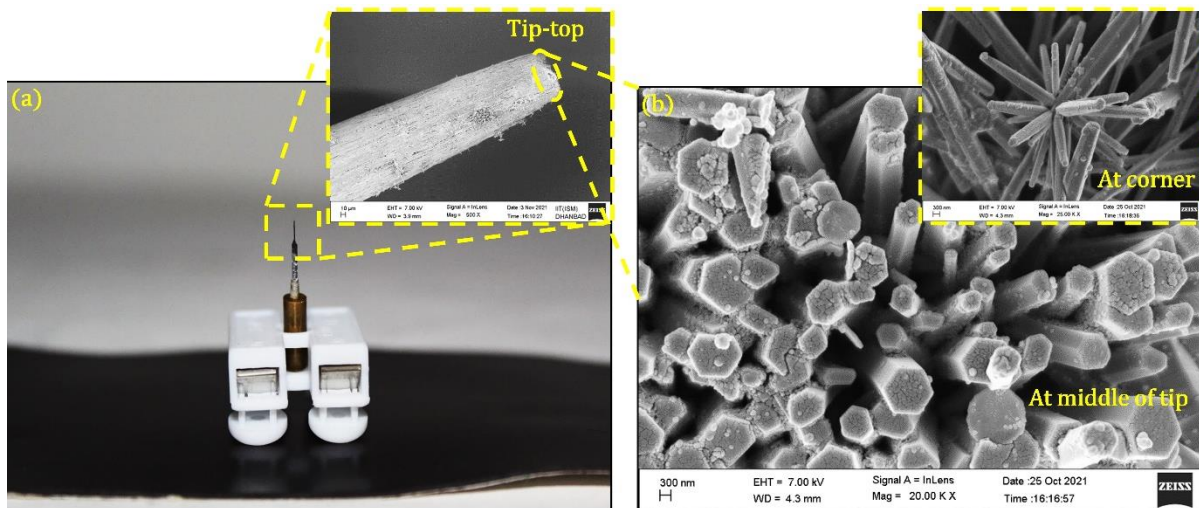


Figure 5. 3 (a) Micro tool electrode fabricated through the electrochemical micro-turning process (inset: morphology of the microelectrode), (b) grown nanorods (ZnO) on the apex of the tooltip (inset: nanorods act as nanotool).

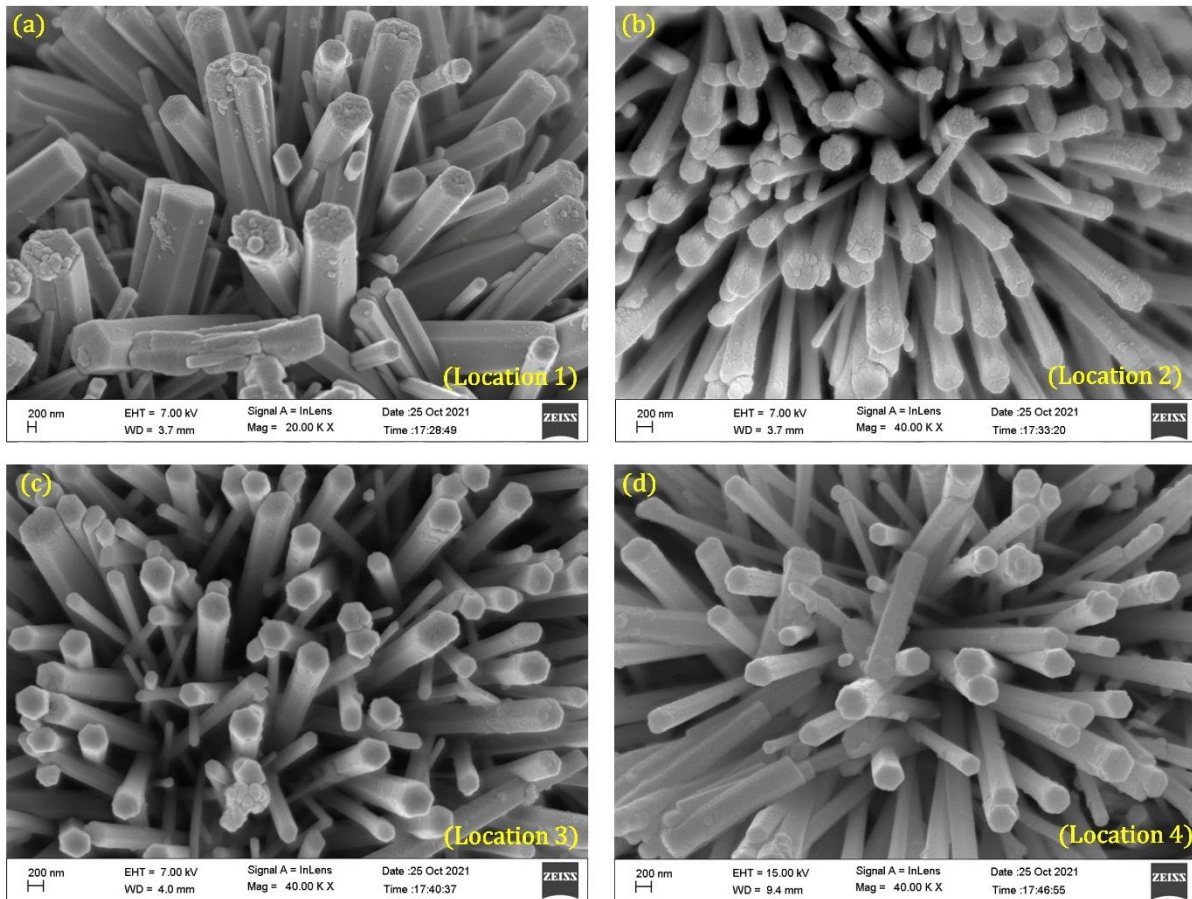


Figure 5. 4 (a-d) Morphology (wurtzite structure) of the grown nanorods on the apex of the microprobe tip at four varying locations.

The long-duration discharge experiments through ZnO nanorods were repeated 2-3 times at constant applied open-circuit voltage (24V) and varying peak current settings (0.30 A, 0.35 A, 0.40A) on a maglev micro-EDM setup. After long-duration discharge experiments, the formed nanopatterned cavities were examined through a FESEM micrograph. The surface morphology of the fabricated nanopatterned cavities at three different peak current settings (0.30 A, 0.35 A, 0.40A) is illustrated in fig. 5.5. It was found that most of the geometrically irregular nanocavities are a negative impression of the nanorods as it is dispersed over the apex of the tip surface (fig. 5.5(a)). As ZnO nanorods are randomly distributed with varying lengths and diameters. So, the features (nanocavities) fabricated are geometrically not uniform and there is randomness in the nanocavities. The

repeatability of the process has been tested with varying currents (0.30 A, 0.35 A, 0.40A) however in every result there is non-uniformity found in the shape and size of the nanocavities. Some trenches of the nanocavity overlapped with each other, this may be due to the coalited nanorods (fig. 5.5(b)). Additionally, the measured diameter of the formed nanocavities (50-850nm) almost lies in the same range as the diameter of the nanorods. However, some over-diameter nano-cavities are formed due to the overcut phenomenon. Fig. 5.5(c) indicates that touching two or more trenches at a time or may be formed due to the alliance of two or more two nanorods. Furthermore, it was also observed that after a certain number of repetitions of long-duration discharge experiments, the nanorods were losing their bonding and mechanical strength and fell on the machined surface as broken nanorods. Fig. 5.5(d) indicates the broken nanorods over the surface of formed nanocavities after a certain repetition of cycles. A series of formed nano-patterned cavities can also be seen in the same figure which indicates the imprint of nanorods under long-duration discharge conditions. Overall evaluation of all the morphology of the formed nanocavities, can be indicated that the higher flow of discharge energy (due to high current) forms deep trenches of nanocavity. By controlling the flow of discharge current at a lower state, much better nano-patterned cavities can be obtained.

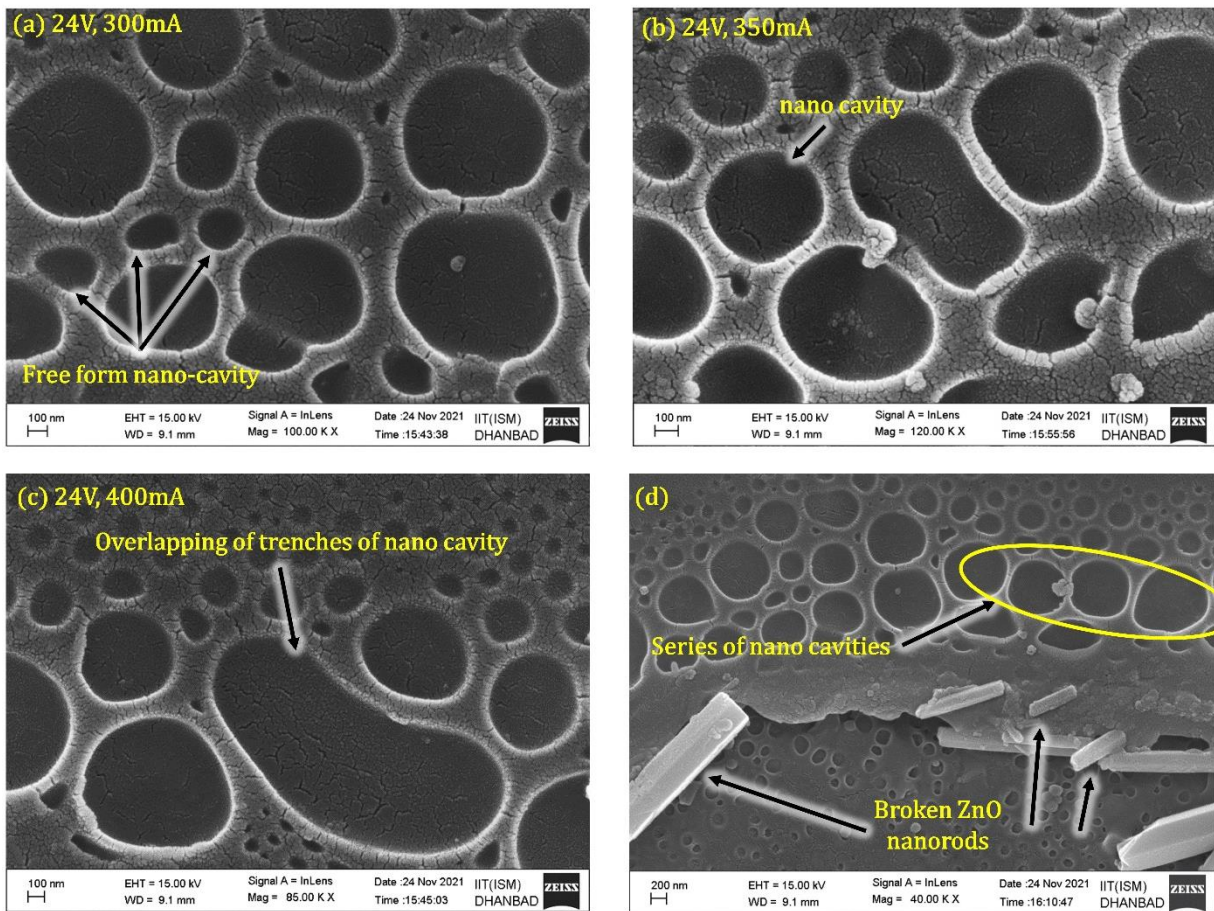


Figure 5. 5 (a, b) geometrically irregular series of nanocavity (c) overlapping trenches of nanocavity (d) broken nanorods on the machined surface.

After the morphological examination of the formed nanocavity, the depth of the nanocavities was measured using a white light interferometer (WLI) based profilometer (Zygo, NewView 9000). The positioning resolution of the profilometer is 80nm. Fig. 5.6 (a) indicates the 3D profile of a nanocavity while Fig. 5.6 (b) denotes the measured depth of the corresponding nanocavity formed during a long-duration discharge energy pulse at a high peak current setting (400mA). It came in observation that the average depth of the nanocavity was lying in the range of 340nm-440nm. The lower current setting contributes towards lower depth due to the availability of lower discharge energy while the higher current setting forms the deep trenches of nanocavity. By controlling the flow of discharge energy more precisely,

the shape, size, and depth can be controlled.

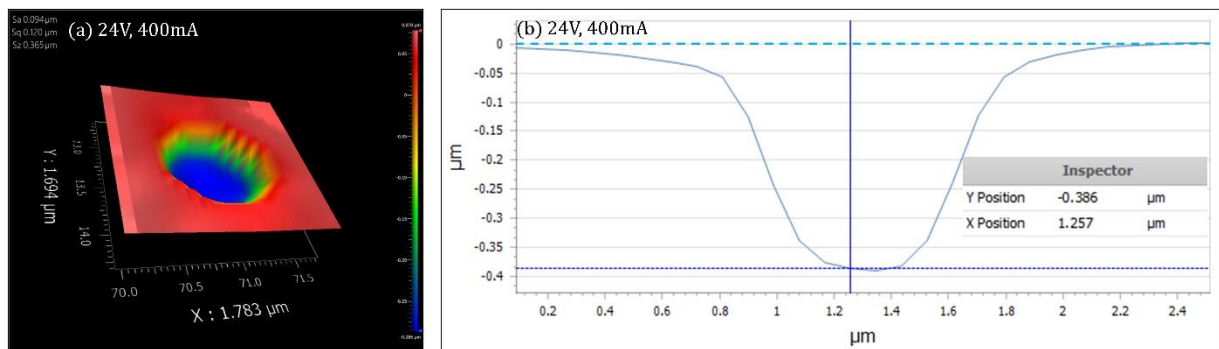


Figure 5. 6 (a) 3D- profile of a nanocavity (b) depth of the corresponding nanocavity formed at a high peak current setting (400mA).

5.5 Reason for growing the nanorods on microtip

Tip-based nanomachining is very popular these days for fabricating the nanostructured features on the substrate materials [24]. Most of the reported literature used sophisticated instruments for fabricating the nanopatterned features [277]. Here, a very simple scaling approach is implemented for replicating the nanopatterned features, although the fabricated nano features are geometrically irregular type and the process needs improvement. The reason for growing the nanorods on the microprobe tip is localizing the tip and surface interaction. It was expected that the reduction in the tooltip will reduce the discharge energy per unit pulse due to the localization effect. Reduction in the discharge energy can generate a nano feature as the negative impression of the tooltip during a long-duration discharge. To take the advantage of localization effect, the tool tip sizes reduce to nanometric level by growing the nanorods. A conductor with a reduced cross-sectional area has a higher resistance which results (for a constant voltage) in a reduced current, and therefore a reduced discharge energy. The effect of localization and reduction in the discharge energy can be understood by following equations.

$$R = \left(\rho \frac{L}{A} \right) \dots \dots \dots (5.1)$$

$$E = (V_d \cdot I_d \cdot T_{on}) \dots \dots \dots (5.2)$$

Where, ρ : resistivity of the tool material, L: length of the tool, A: cross-sectional area of the tool, R: resistance, I_d : discharge current, V_d : discharge voltage, T_{on} : effective pulse on time.

5.5 Voltage-current (V-I) characteristic curve of the machine

In micro-EDM, the essential energy for discharge is provided in the form of electrical input such as voltage, current, and effective pulse-on-time in the micro-confined gap. This discharge energy ionizes the medium (dielectric) to form the plasma channel in the interelectrode gap. The nature of the plasma channel is purely conductive which means the current can easily flow through the medium at minimum resistance. The flow of current appears as an electrical discharge which produces a thermal impact on the work surface and materials are eroded in the form of micro-scale debris. By controlling the flow of discharge energy in the micro-confined gap, various types of micro/nano features (dimples, texture, grooves) can be fabricated.

The analysis of voltage and current pulses is significantly important to understand the gap condition and flow of discharge energy because these are directly associated with the actual erosion mechanism of the process. The voltage-current waveform facilitates various electrical information such as ionization voltage, discharge voltage, transient arc voltage, short-circuiting condition, etc., [185]. Moreover, discharge frequency and pulse on-off time can be easily calculated through this voltage-current curve. Normally ionization voltage is known as breakdown voltage because at this voltage the dielectric strength of the dielectric breaks down. As breakdown happens there is a sudden drop in voltage potential. This drop-in voltage potential leads to the formation of the plasma channel due to ionization. The plasma channel offers the minimum resistance to the flow of the current and discharge occurs. The corresponding voltage and current are known as discharge voltage and discharge current which is responsible for the actual erosion of the material. Normally, ideal discharge happens

when there is an ignition delay. Ignition delay is important because during this time dielectric ionization happens. If the dielectric is not fully ionized, it may further cause the formation of a transient arc during discharge which reduces the stability and accuracy of the machining process. Short-circuiting is another condition that is harmful to the machined surface integrity and stability of the machine. Due to the mass inertia and backlash problem of the lead screw-based conventional servo head, the positioning response becomes slow. The slow positioning response and improper flushing in the machining gap sometimes result in direct contact between the two electrodes. This direct contact of electrodes causes a heavy amount of current to flow without any discharge. This type of condition is known as short-circuiting. This must be avoided during machining because it affects the surface integrity and formed surface features heavily. Fig. 5.7 illustrates the real-time time transient voltage-current (V-I) waveform of maglev micro-EDM during multiple discharge energy pulses. The presented voltage-current curve includes the voltage drop across the inductance-resistance (L-R) circuit as well as the voltage drop across the interelectrode gap resistance. By making the short circuit between the electrodes, it came into noticed that the voltage drop across the L-R circuit is approximately 6.5-7V. Hence, this voltage drop has been not included in the discharge power calculation. The only voltage drop across the interelectrode gap has been considered in the discharge power calculation. Later on, the extra signal suppressed by the ground line (GND) is neglected and not taken in the discharge power calculation. The current signal is bipolar type (varying in both directions) which may be due to the residual magnetization or due to the short-term swapping of the ions and electrons [20]. It was found that voltage-current signals are stable and the pulse widths are uniform (5ms) and identical. The voltage is dropping very fast which means ionization is happening quickly without any ignition delay. This also means that the process is continuous type micro-EDM. No arcing and short-circuiting are observed in the discharge curve, this means the process is stable and

efficient without any lags in servo control. Here, despite no ignition delay, the mechanism is balancing the open gap condition and short circuit condition very well for stable and efficient discharge.

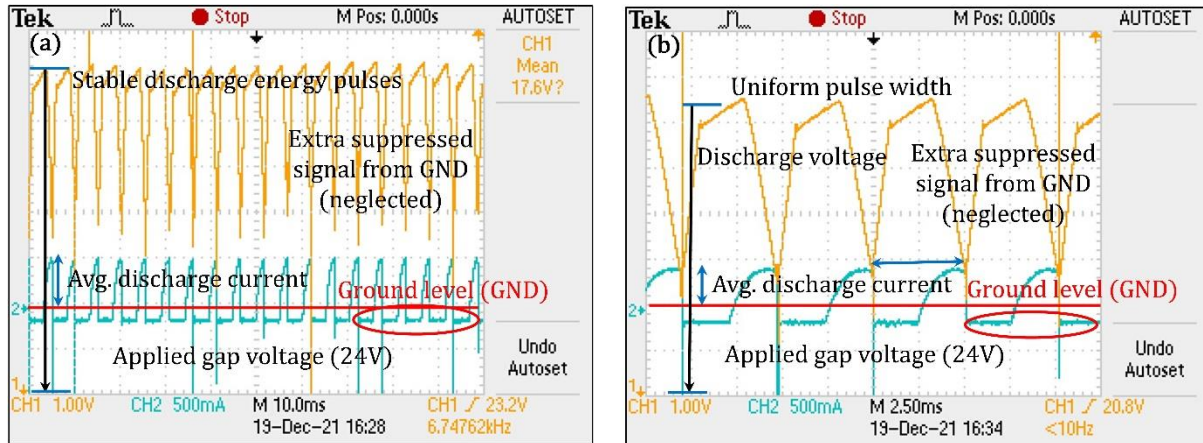


Figure 5. 7 (a) Stable discharge energy pulses (b) Uniformity in the pulse width (5ms) during multiple discharges on the maglev micro-EDM system.

Capturing the single energy pulse during a long-duration discharge (5ms) is very critical work because it instantly changes its nature within microseconds. Hence, an ultra-short discharge pulse was captured and a time scale was brought on nano/micro-scale (100ns, 1 μ s) to see the nature of a single energy pulse. Fig. 5.8 represents the voltage-current curve in real-time during the fabrication of nano features at the time scale of 100ns and 1 μ s. The open-circuit voltage was 24V while the set peak current was varying between 300-400mA at the interval of 50 mA. Fig. 5.8(a) indicates that there is a current rise corresponding to voltage rise, this reverse trend may be due to the fact that at some instant of time, the spark creates a cavity, and due to the cavity there is enlargement in the gap. The enlargement in the gap increases the voltage or there may exist a vacuum condition (in place of a cavity), to fill that vacuum, the flow of electrons may occur towards the vacuum, the flow of electrons indicating the presence of current rise at that situation. Fig. 5.8(b) indicates that there is a current rise corresponds to a voltage drop. This represents an ideal situation for the

occurrence of normal discharge. Later, the discharge power has been calculated with the help of the voltage-current curve. The observed average discharge voltage and current (excluding voltage drop across the L-R circuit) in the digital storage oscilloscope (DSO) were 6.5-7 V and 50-60mA with a duty factor of more than 90%. This means total discharge power was varied approximately 0.2925-0.378 joule/sec. This discharge power has been distributed among a large number of nanotips. The distribution of discharge power over a large number of nanotips reduces the intensity of discharge energy and reaches micro/nanojoules energy per unit tip due to the localization effect. The liberation of nanojoules energy from the nanotips produces the nanopatterned features on the substrate material as the negative impression in a long-duration discharge energy pulse. By reducing the tool size and lowering the discharge energy, it is possible to generate nanopatterned features via micro-EDM.

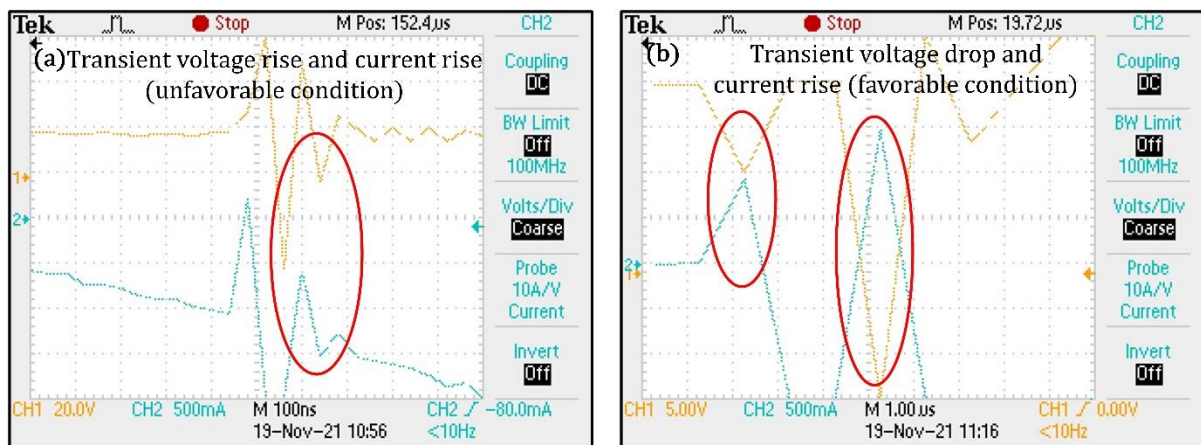


Figure 5. 8 Time transient voltage-current waveform at time scales of (a) 100ns and (b) 1.00µs.

5.5 Chemical characterization through EDX

First of all, the elemental characterization of the fabricated microelectrode having the grown nanorods on the apex of the tip is characterized by energy-dispersive X-ray spectroscopy. The presence of zinc (5.88, wt.%) and oxygen (11.40, wt.%) on the tip indicate that there is the formation of ZnO nanorods. The presence of tungsten (70.30, wt.%) in an

appreciable amount in the EDX spectrum referred that the parent material as tungsten. The EDX spectrum for elemental analysis of the fabricated microelectrode with grown nanorods is illustrated in Fig. 5.9 (a).

The elemental characterization of the grown nanorods was also carried out to verify the presence of zinc oxide. The EDX spectrum of the fabricated ZnO nanorods is represented in fig. 5.9(b). The spectrum indicates that zinc (57.97, wt.%) and oxygen (23.86, wt.%) is present in heavy amount. This means most of the nanorods are of zinc oxide (ZnO). The presence of carbon in the spectrum may be due to the carbon tape as the sample is pasted over it.

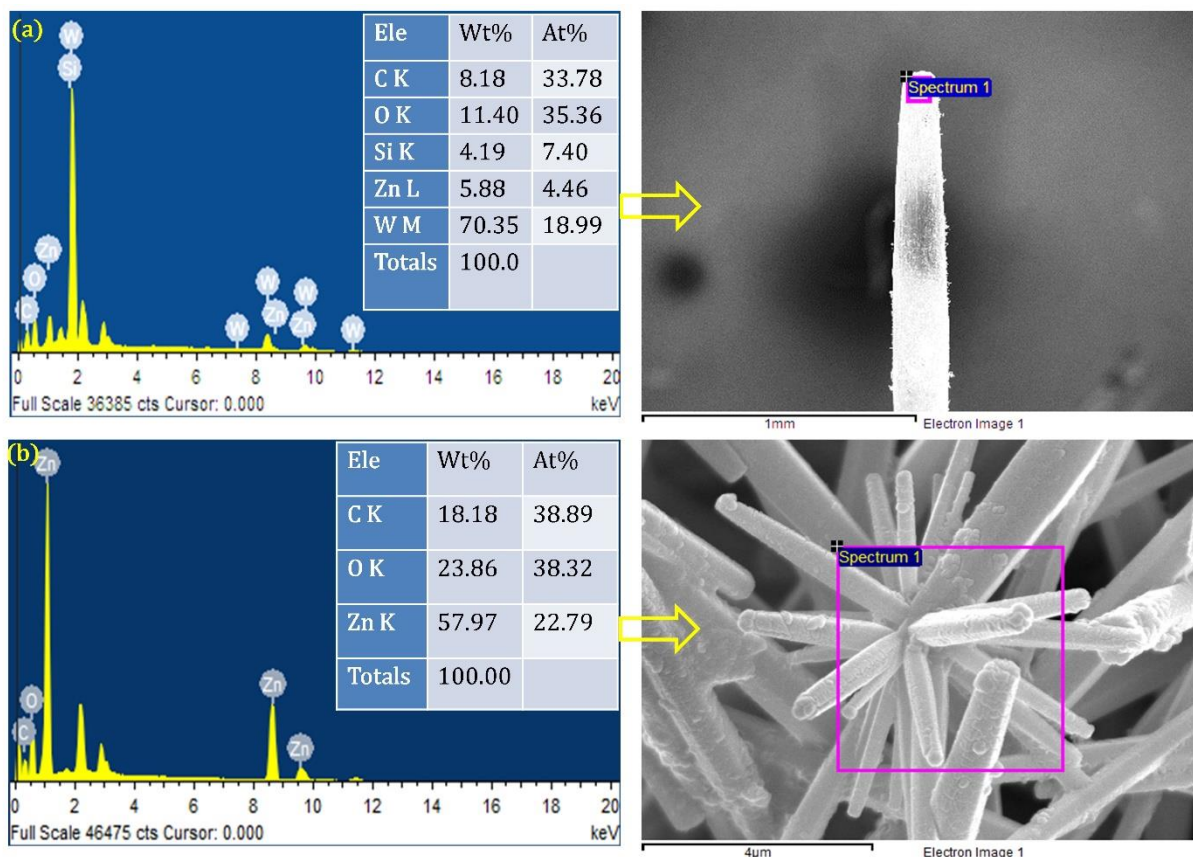


Figure 5. 9 Chemical characterization of the (a) fabricated microelectrode (b) grown nanorods on the apex of the microelectrode tooltip.

Fig. 5.10 (a & b) illustrate the chemical composition of the machined surface fabricated through ZnO nanorods at two different locations. It can be seen in the EDX

spectrum that titanium is the major element (44.95-47.56, wt. %) present on the machined surface which represents its compositional parts. The presence of aluminum (3.22-3.51, wt. %) and vanadium (0.13-0.43, wt. %) comes from the constituent of the base material. The availability of tungsten (5.65-6.36, wt. %) on the machined surface indicates that the material is transferred from the tool electrode as ZnO nanorods are grown on the apex of the tungsten tip. This material migration and molecular diffusion phenomenon come into the picture due to the plasma interaction within the small interelectrode gap.

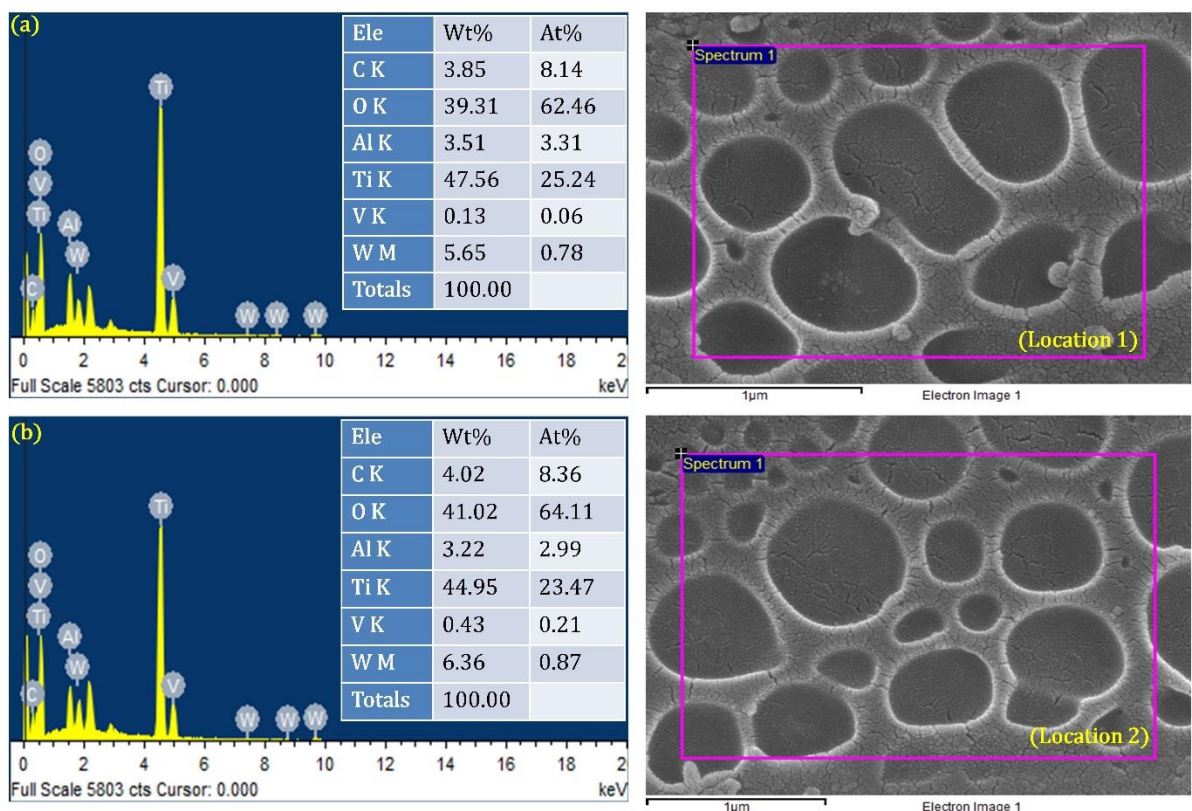


Figure 5. 10 (a & b) Compositional analysis of the machined surface (nanopatterned cavity) through EDX spectroscopy at two varying locations.

5.6 Conclusions

A scaling approach is successfully implemented in micro-EDM configuration for replicating the nanopatterned features on a super-finished work surface (Ti-6Al-4V). Here, the micro-EDM principle facilitates the essential discharge energy for tool electrodes while

tip-induced nanomachining helps in forming the nanopatterned cavities. The experimental results of this study indicate that the size of the tooltip significantly affects the breaking down the potential of the dielectric. Moreover, it was also noted that the reduction in the tooltip size is an effective method for decreasing the discharge energy. The reduction in the discharged energy forms the nanopatterned features due to the localization effect. The formation of geometrically irregular nanopatterned features on typical work material confirmed the same. The mechanism of novel maglev micro-EDM and the mechanism of the nano growth is explicitly covered in the manuscript. Additionally, the morphological characterization of micro tools and grown nanorods on the apex of the tip indicates that nanorods are well-defined in shape and acted as nanotools very well during the long-duration discharge (5ms) micro-EDM experiments. The availability of broken nanorods on the machined surface indicates that after certain repetitions of a long-duration discharge, the attached nanorods lose their mechanical and bonding strength. The characterization of single/multiple discharge energy pulses in terms of the voltage-current waveform indicates that magnetic levitation is controlling the interelectrode gap very well for stable and efficient discharge. Finally, the auxiliary outcomes of this experimental investigation show the feasibility of the approach toward nano-EDM with widespread potential/application in micro/nanodevices in nanofabrication industries.

6

Chapter-6: Geometrically irregular nano-patterning using maglev-EDM via ZnO nanorods on Inconel-625: A feasibility study towards nano-EDM

6.0 Introduction

To address the current need for cutting-edge technology, technological advancement is always required. Nanomachining, which deals with the size of features at the nanoscale, is the fastest-growing technology [207]. In recent years, the use of nano features size products/components has spread widely across the global market. Nano features are urgently required in biomedical, electronics, healthcare, automotive, aerospace, and telecommunications to improve device performance within a limited space [53]. Nanostructured features in electronics and medicinal applications are gaining popularity. Nano-vias for interconnects [5], nano-jets for controlled drug emission [263], nanopores DNA detection devices [262], fuel injectors for next-generation atomizers, nozzle for nanofluidic devices [8], and molecular sorting sieve [278], for example. Nanostructured features are typically fabricated on heterogeneous materials using a limited choice of machining processes. Major micro-electro-mechanical system (MEMS) and nano-electro-mechanical system (NEMS) firms are also exploring the vast potential of nano features in integrated circuits, memory devices, display units, biochips, and biosensors, among other applications [277], etc. Laser-based nanomachining [279], tip-induced lithography [280], and scanning probe microscopy technique [281] are commonly utilized to fabricate nano features on difficult-to-machine materials/substrates in the current environment. However, from a financial standpoint, these approaches are prohibitively expensive and demand a significant upfront investment.

6.1 Motivation for research and technological gaps

Micro-electro-discharge machining (micro-EDM) is a well-known and well-accepted technology for micromachining electrically conductive materials with limited precision down to the micrometer scale. By adjusting the discharge energy level, it can create a variety of microfeatures such as micro holes, microchannels, microcavities, micro patterns, micro dimples, and so on [282]. However, its potential for generating nanopatterned features using a regulated flow of discharge energy via a scale-down technique has yet to be fully explored. In general, the material removal mechanism in micro-EDM is based on the thermal impact of electrical discharge in a micro-confined gap. As the machining process is free from mechanical contact hence, no physical disturbances such as vibration, chatter, or stress have occurred throughout the machining process [7]. Here, the typical gap phenomenon completes in three stages (a) ignition stage (b) discharge stage, and (c) interval stage [160]. Due to dielectric breakdown, the plasma channel forms near the two nearest points of the electrodes during the ignition stage. The breakdown results in a drop in voltage potential and a sharp rise in current. During the discharge stage, the current remained constant due to the constant bombardment of electrons and ions on the electrode's surface. Rapid heating and evaporation of both materials occur as a result of the bombardment, resulting in material erosion. In the last stage i.e., the interval stage, the voltage, and current signals decline to near zero where heat generation stops and pressure is released due to collapsing vapor bubbles and debris ejected. For each discharge pulse, the entire cycle repeats [282]. The destructive tendency of electrical sparks can be employed for constructive activity by controlling the flow of discharge energy more precisely at the nanoscale.

The ability of the micro-EDM to fabricate microstructures larger than 5 μm is widely recognized. Efforts are being made to get micro-EDM downsizing technology down to the nanometric scale, but it is still a difficult task. The micro-EDM system's machining efficiency

is highly dependent on the energy level of a single discharge, which can range from 100nJ to 10J [271]. Although CNT machining with a discharge energy of up to 1nJ has been achieved using field emission scanning probe microscopy (SPM) [272]. For producing nanoscale features, the localization effect of the tooltip is explored to reduce the discharge energy down to the nanometric level. The advantages of using a tip in the nanomachining process were noted by Malshe et al. [24]. They claimed that the tip plays an important role in the atomic/molecular level interaction of two surfaces at a localized position. The nanoscale tip's localization effect is used in nanoindentation, nano electrical machining, and scanning probes microscopy techniques like SPM and AFM. On the STM machining platform, Jahan et al. [23,270] employed the tip-based nano-electro-machining (dry nano-EM) approach to fabricate nanoscale features of size 7.5-10 nm. They found that in the dry nano-EM process, the nanoconfined gap (1-2nm) and field-induced evaporation effect play a significant role in modulating heat liberation and, as a result, MRR. Khalid et al. [273] used a dry micro-EDM technique with a potential range of 20-35V and a peak current of 60mA to fabricate geometrically irregular micropatterned features on CNT forest with a discharge gap of 10 μm . They were able to create a 3D micropattern with an aspect ratio of 20 and the smallest feature size of 5 μm without disrupting the nanotube orientation. Finally, micro-EDM was recommended as a viable approach for generating 3D micropatterned on CNT forest to MEMS. Additionally, it is suggested that it can be used in other micromachined components such as a scanning probe microarray, a microprocessor heat sink, bio-sensor devices, and super-hydrophobic for micro/nanofluidic devices, optical antennas and lenses, and light-efficient energy devices, among others. For fabricating the micropatterned features on the CNT forest grown on the silicon wafer, Saleh et al. [272] used a reversed dry-EDM technique. To take advantage of the field emission phenomenon, they used a low voltage potential of 10V at a gap distance of 2.5 μm . The processed micropatterned features were

found to be free of crystalline defects and contamination, showing that the method is more stable and cleaner than traditional micro-EDM. Xiao et al. [58] applied a scaling approach to bring the micro-EDM resolution to a nanometric scale by fabricating the nanopatterned features on the CNT forest. The use of different sized pointed tool electrodes on a CNT forest indicated that the tool's scaling effect had a considerable impact on the working voltage and, as a result, the dielectric breakdown strength. Also, due to the localization effect, the reduction of the tooltip aids in minimizing the discharge energy. They were able to successfully manufacture a grating-like structure with a height of 200 nm and discharge energy of 1nJ, demonstrating the effectiveness of their approach towards nano-EDM. Kalyanasundaram et al. [76] used a nano electro machining technique (nano-EM) on an STM platform to investigate the breakdown behavior of n-decane in a nanoconfined gap of 3 nm. The effect of tunneling current (1nA) and bias voltage (100mV) on the device has been investigated. The dielectric breakdown and recovery were shown to be linked to the nanoconfined gap and applied electric potential. Later on, it was discovered that the density in the nanoconfined has a considerable impact on the dielectric's quasi-static behavior. According to the literature, there is a gap in bringing micro-EDM technology down to the nanometric scale. Almost negligible method for generating nanopatterned features on any electrically conductive materials using discharge current in a non-vacuum environment is disclosed. Hence,

This work reported a breakthrough approach for fabricating the nanoscale features through a long-duration discharge maglev micro-EDM process. The top-to-down approach has been applied by growing the nanorods on the microprobe tip. The growth mechanism of nanorods formation through the low-temperature hydrothermal process has been discussed in the article. During the long-duration discharge (4.5 ms) micro-EDM process, these nanorods serve as nanotools. The discharge energy per unit pulse has been lowered due to the tool's

localization effect. This decrease in discharge energy was found to be effective in the fabrication of nanopatterned structures. Later, field emission scanning electron micrographs were used to evaluate the morphological characterization of the tooltip, grown nanorods, and created nanopatterned cavities. The electron diffraction X-ray spectroscopy (EDX) technology is used to characterize the chemical composition of the machined surface. The machining stability was also examined using a voltage-current (V-I) discharge characteristic curve for long-duration discharge and multiple discharge energy pulses.

6.2 Material and Methods

6.2.1 Experimental system

Nanoscale features were created using a servo-stabilized electromagnetic levitation-based micro-EDM device. A unipolar linear motor, linear actuator arm (LAA) for holding the tipped tool electrode, programmable DC power source for long-duration discharge output power, XYZ micro-positioning displacement platform (resolution: 5 μ m) for positioning the workpiece in the subsequent direction, and a dielectric circulation tank are all part of the experimental setup. The workpiece is held tightly in the dielectric tank by unique honeycomb features. A digital storage oscilloscope (Tektronix, TDS2012C, 2-channel, 100MHz bandwidth) was also employed with a differential type voltage (TPP0201, Tektronix) and current probe (65A-Hantek, BNC type) to capture long-duration discharge/multiple discharge energy pulses. To get real-time current-voltage waveforms, the current probe and voltage probe is connected to the circuit. Before collecting the voltage and current waveform, the degaussing bottom (current clamp) is squeezed 4-5 times to remove any residual magnetism. Fig. 6.1 depicts the genuine image of the experimental setup, including peripheral components.

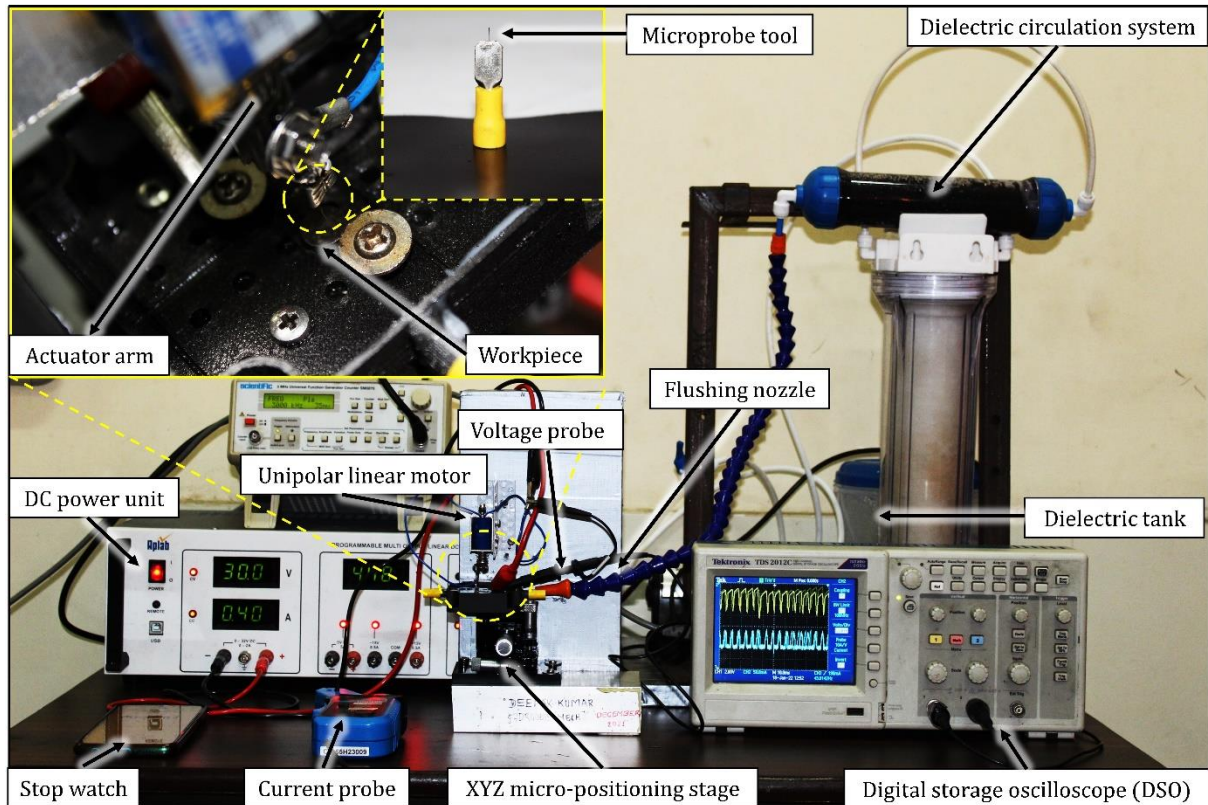


Figure 6. 1 Experimental setup of maglev micro-EDM with their peripheral components.

6.2.2 Materials and procedure

The work surface was polished with high-grade emery polishing paper (Grade 1800, 2000) on a disc polishing machine (Chennai Metco) prior to long-duration discharge machining through a nano-tipped tool electrode on Inconel-625. The velvet fabric with diamond paste is then used to finish the mirror-like surface (super finished). Before starting the experiment, the work sample was cleaned with acetone and distilled water to eliminate any dirt (impurities) and foreign particles in the ultra-sonicator.

Under dry conditions, trial experiments were carried out to determine the initial process parameters and the stability of the machining with multiple discharge energy pulses on maglev micro-EDM. The majority of the discharge energy pulses were determined to be steady, with uniform pulse width. The actual long-duration discharge experiments were then carried out in dry conditions with a nano-tipped tool.

All of the chemicals used to make nanorods on the tooltip were analytical grade and didn't need to be purified further. First and foremost, hydrothermally produced seed and growth solutions were prepared. 62.5mg zinc acetate dihydrate [$\text{Zn}(\text{CH}_3\text{COO})_2 \cdot 2\text{H}_2\text{O}$] was mixed in 100ml ethanol on a magnetic stirrer (500 rpm) at 60°C for 15 minutes to make the seed solution. A second solution was made by combining 20mg NaOH with 20 ml ethanol and rapidly agitating (500 rpm) for 15 minutes at 60°C . This second solution was added to the seed solution, along with an additional 80 ml of ethanol, to form a total solution volume of 200 ml. This entire solution was agitated for another 30 minutes under heating conditions. This seed solution was used for the formation of active nuclei on a micron-level tooltip. The tool's tip was dipped in seed solution for 15 minutes before being dried in a hot air oven at 95°C for 15 minutes. To finish the seeding procedure on the tooltip, this half-hour cycle was repeated eight times. The seeding of the tooltip allows active nuclei to form, which then act as growth sites for nanorod production [283].

A growth solution was made by dissolving 10mM zinc nitrate hexahydrate and hexamine (HMTA) in 630mL distilled water and stirring it for 15 minutes at room temperature (25°C) while maintaining a pH of 6-7.

The seeded tip of the tool is dipped in growth solution and heated for 8 hours in a hot air oven at 95°C for hydrothermal growth of nanorods. The sample was rinsed 5-8 times with distilled water after heat treatment to prevent any further growth. For drying reasons, the sample is placed back inside the hot air oven at room temperature (30°C). Fig. 6.2 shows the scheme for seeding on the tooltip and the development of nanorods through the hydrothermal process.

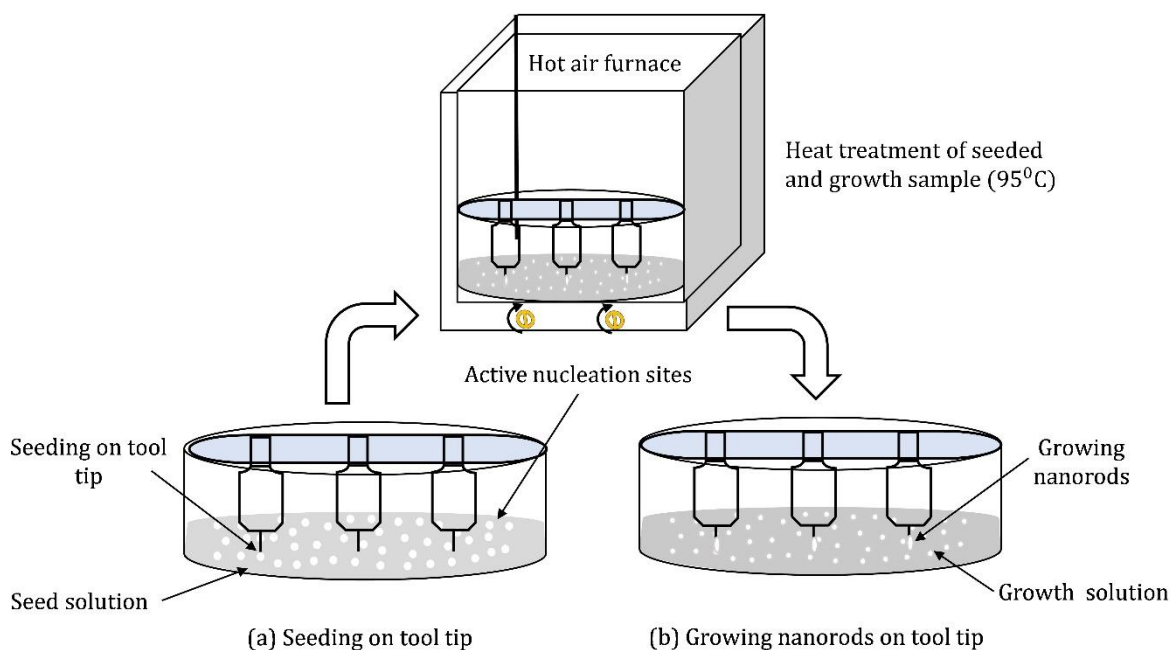


Figure 6. 2 (a) Active nucleation sites are seeded on the tooltip (b) the seeded tooltip is dipped in the growing solution for nanorod formation.

6.2.3 Growth mechanism of ZnO nanorods

One of the most widely used procedures for fabricating nanostructures on any substrate material is the hydrothermal process. The growth mechanism for the production of nanorods on the tooltip can be understood in two steps in the current study. The nucleation stage is the first, and the growth stage is the second [258]. The deposition and growth dynamics of ZnO nanorods formation on the tooltip are depicted in Fig. 6.3. The stable active nuclei are produced from the solution during the nucleation stage, when ions, atoms, and molecules begin to arrange themselves in a crystalline fashion. These nucleation sites are propagated outwards during the growth stage by absorbing free particles like ions and molecules under certain conditions to form a well-defined crystalline structure. The seed solution for the nucleation stage activation is prepared here. For the seeding and production of ZnO nuclei, the tooltip is dipped in the seed solution. The presence of zinc acetate dehydrate enhances the production of Zn^{2+} ions during seeding, whereas sodium hydroxide (NaOH) deduces free radicals as OH^- ions [284]. The development direction of ZnO nanorods

is mostly influenced by the liberation of OH^- ions. The combined impact resulted in the creation of zinc hydroxyl ions ($\text{Zn}(\text{OH})_4^{2-}$) which served as the nanorods' growth unit [285]. Due to the tetrahedral coordination of Zn^{2+} and O^{2-} ions, ZnO has a wurtzite structure and has a more tendency to grow along the c-axis (polar axis) [286]. The reactions involved in the production of active ZnO nuclei at an early stage are mentioned in the earlier section 4.3.1 (see equation 4.7-4.9).

After seeding, a thin film layer forms over the tip; now it's time to grow into nanorods. The seeded tooltip is dipped in growth solution and kept in the hot air furnace for 8 hours at 95°C to achieve this. The growth solution provides the necessary conditions for the active ZnO nuclei to propagate into nanorods [287]. The formaldehyde (H-CHO) group and ammonia (NH_3) were formed when HMTA ($\text{C}_6\text{H}_{12}\text{N}_4$) reacted with water (H_2O) molecules. Later, in an aqueous solution, ammonia hydrolyzed to create NH_4^+ and OH^- . Zn^{2+} ions and ammonia (NH_3) ions combined to form $\text{Zn}(\text{NH}_3)_4^{2+}$, a new complex ion. ZnO nanorods were formed when these complicated ions were mixed with water molecules. The reactions involved in the evolution and chemical events for the production of nanorods are mentioned in the earlier section 4.3.1 (see equation 4.10-4.13).

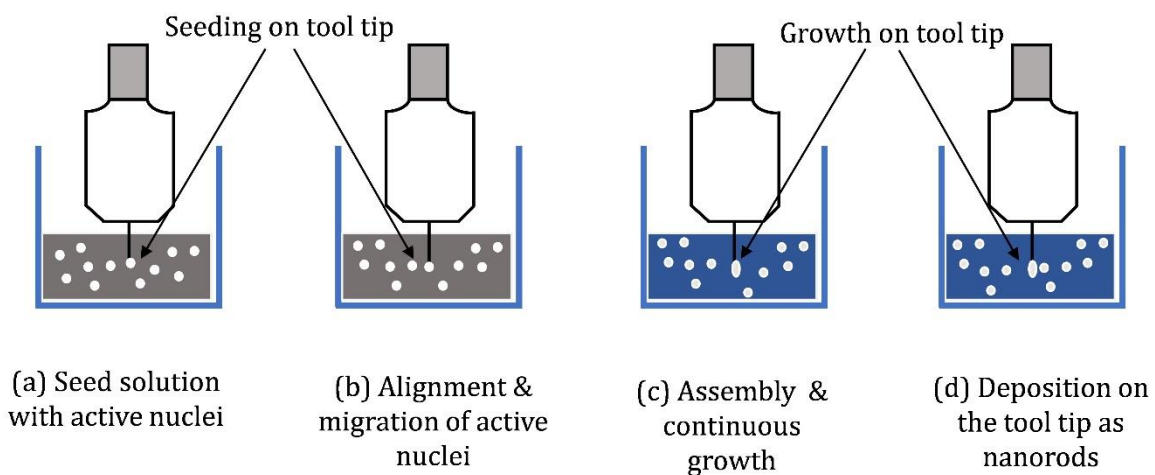


Figure 6. 3 Growth mechanism of ZnO nanorods in the low-temperature hydrothermal process.

6.2.4 Geometrically irregular nanocavity fabrication

On a maglev-EDM system, ZnO nanorods produced on microprobe-tipped electrodes were used in a long-duration discharge experiment. Straight polarity was employed for this, which means the pointed tool was connected to the power supply's negative terminal while the work material was linked to the positive terminal. No liquid dielectric was utilized since it could produce OH⁻ ions as oxidants during ionization, causing a chemical reaction. Furthermore, the dielectric can absorb dirt and free radicals as contamination, which can lead to alterations in the morphology of machined surfaces [8]. Later, using an XYZ micro-positioning displacement platform (resolution 5 μm), the work material and discharge gap were adjusted. By fixing the three peak current values (300mA, 350 mA, 400mA), a 30V open-circuit voltage was applied. Table 6.1 shows the actual experimental conditions used to fabricate nanopatterned features utilizing a long-duration discharge dry maglev micro-EDM technique.

Table 6. 1 Fabrication of nano features: materials and working environment

a. Material selected for machining	
Work material	Superfinished Inconel-625 surface
Tool	Grown ZnO nanorods on the 100-μm copper wire tip
Dielectric fluid	Open-air (dry condition)
Polarity	Straight
b. Machining environment	
No-load voltage (open)	30V
Set peak current	300mA, 350 mA, 400mA
Duty factor	Over 75%
Pulse-type	Long duration energy pulse (DC)

6.3 Results and Discussion

6.3.1 Nanorods and machined surfaces morphological characterization

High-resolution field emission scanning electron microscopy (FESEM, SUPRA-55, ZEISS) images were used to analyze the morphological characteristics of the produced nanorods. On the apex of the tip, the nanorods were found to be well-defined in shape and size. All of the nanorods are chemically stable, and their diameter and length vary somewhat. The top surface of the microtool and the generated nanorods on the top surface of the tooltip are shown in Fig. 6.4. The ZnO nanorods were found to be posing the wurtzite structure as it exists naturally in nature.

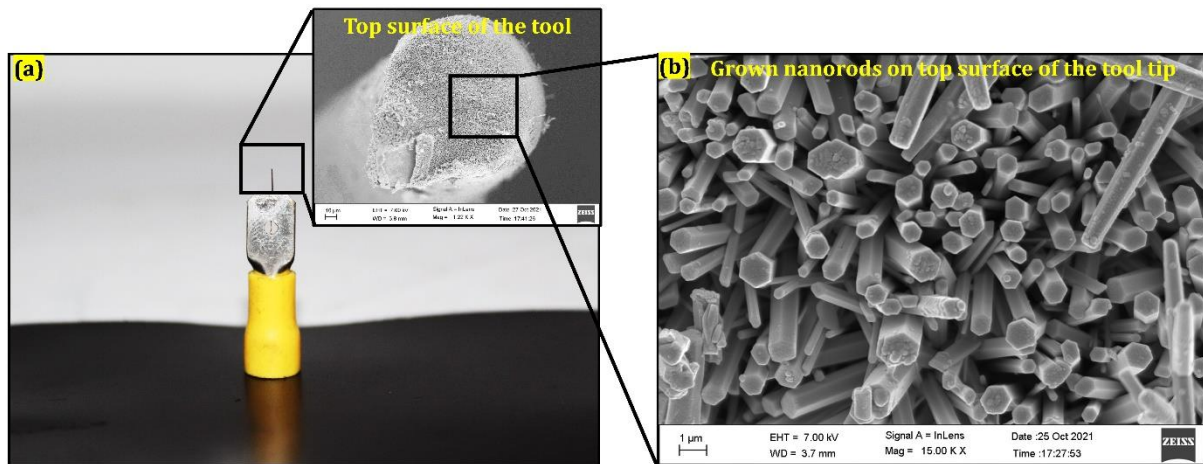


Figure 6. 4 (a) 100 μm copper wire as tool electrode (inset: the top surface of copper wire), (b) morphology of grown ZnO nanorods on the top surface.

The morphology of the ZnO nanorods and their distribution at two different positions on the apex of the tooltip is depicted in Fig. 6.5. The dimensions of all the nanorods are not equal, and their form and size vary, as shown in the images. This could be owing to the nucleation and crystal growth rates changing [288]. Some nanorods were also discovered to be branched, while others were formed with aggregated nucleus points. During the growth phase, the aggregated nucleus point developed anisotropically along the polar axis (c-axis) and formed a columnar-like structure [289]. The formation of branching-type nanorods is

caused by a change in the reaction rate of two complex ions, $Zn(NH_3)_4^{2+}$ and OH^- [258]. As a result of the negative imprint of the nanorods, variation in the morphology of the nanorods causes variation in the dimension of the nanopatterned cavities.

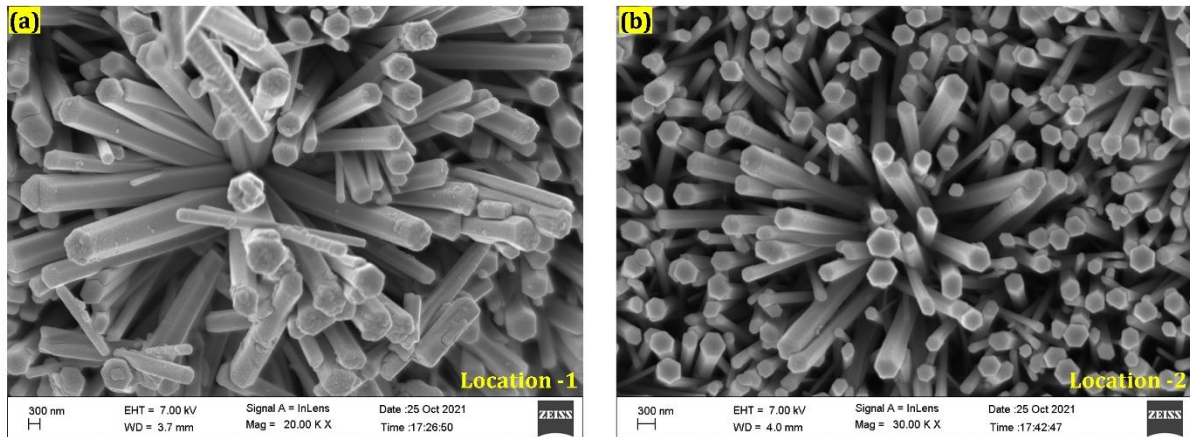


Figure 6. 5 Morphology of the grown nanorods on the tip-top surface at two varying locations.

FESEM micrographs are used to examine the morphology of the nanorod's negative impression on the Inconel-625 super-finished work surface. Fig. 6.6 shows the morphology of geometrically irregular nanocavities generated using a long-duration discharge micro-EDM technique with different peak current settings (300mA, 350mA, 400mA) and a constant voltage potential (30V). The nanocavities generated at the lower current setting (300mA) were found to be stable as noted in fig. 6.6(a). The dimensions of geometrically irregular nanocavities (20-750nm) vary in a similar range as the dimensions of nanorods (20-800nm). Some deep trenches of the cavity were found which may be formed due to the overlapping of certain nanocavities. Additionally, during the long-period discharge phenomena, nanocavities formed in the areas where the nearest gap is established. It was noted that the nanorods lose their mechanical and bonding strength after a few repetitions of the long-duration discharge phenomena at a higher current (400mA) setting, and they fall on the work surface as shattered nanorods. Fig. 6.6 (b) indicates the morphology of the nanocavities at a medium current

setting of 350mA. Fig. 6.6 (c) shows the shattered nanorods on the machined surface at a higher current setting. Overall, the morphology of the geometrically irregular nanocavities suggests that a lower current may be a good alternative for creating nanostructured features and may demonstrate the effectiveness of the approach toward nano-EDM. This could be owing to the nanoconfined gap and the availability of low-discharge energy.

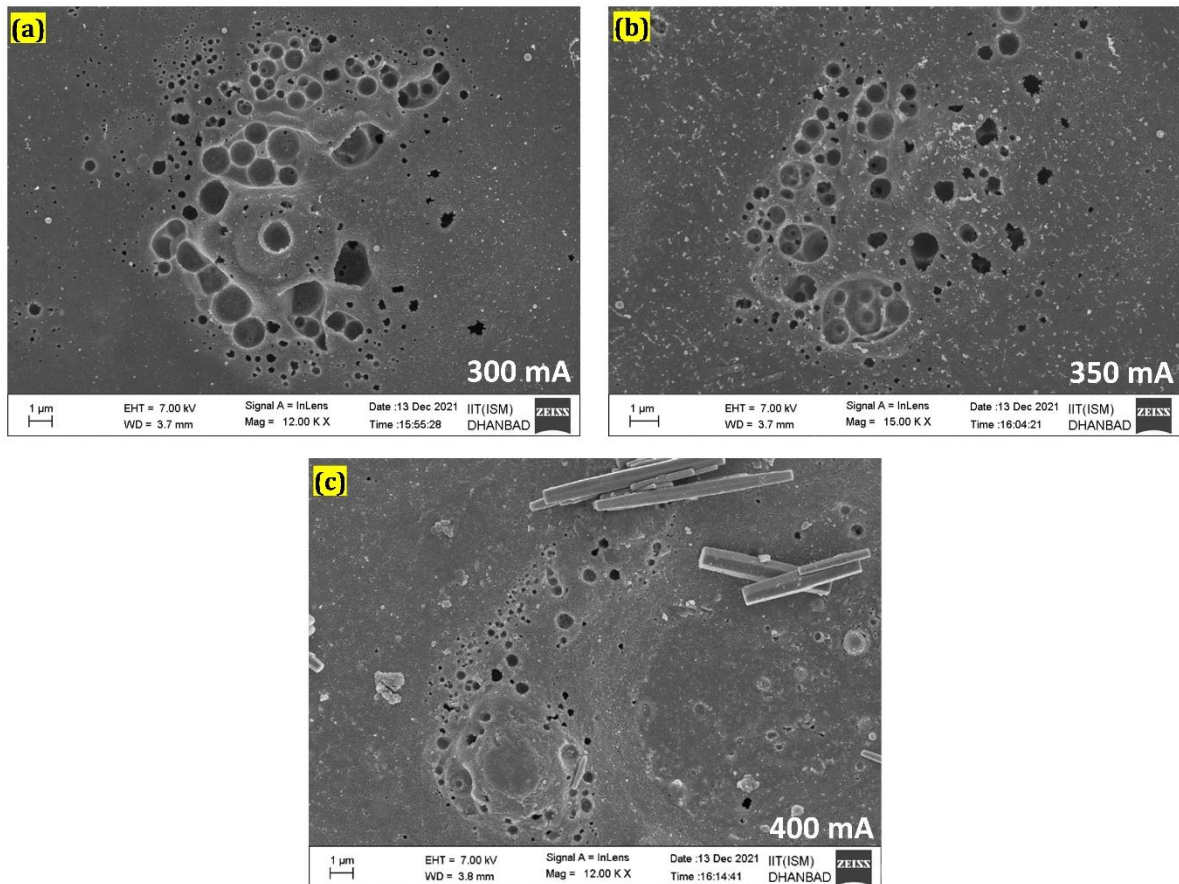


Figure 6. 6 Morphology of the fabricated geometrically irregular nanocavities in long-duration discharge experiments through ZnO nanorods at (a)300mA, (b) 350mA, (c)400mA.

6.3.2 Discharge characteristic curve (V-I) of maglev μ -EDM

The study of voltage-current characteristics is critical in micro-EDM because they are linked to the availability of discharge energy for the occurrence of electrical discharge in the micro-confined gap. The voltage-current curve makes it easier to perceive the important details like the open-circuit voltage, discharge voltage, transient arc voltage, short-circuiting

time, pulse on time, dielectric recovery time, voltage rise time, voltage fall time, pulse frequency, and so on [85]. The availability of discharge energy in the micro-confined gap may be simply computed using the above values. When the gap between the two electrodes is significant, the process usually starts with open-circuit voltage. There isn't any current flowing in this condition. When the applied voltage potential reaches the threshold value, the insulating strength of the dielectric between the electrodes begins to deteriorate. The corresponding voltage at which the dielectric loses its dielectric strength is known as the ionization voltage. The voltage drops suddenly as a result of the ionization, and a conducting plasma channel forms. For the flow of electric current, the plasma channel has the lowest resistance. The flow of current appears as an electrical discharge in the micro-confined gap. The corresponding voltage and current during discharge are called discharge voltage and discharge current. These two electrical quantities during effective pulse on time are responsible for the actual erosion of material in micro-EDM.

The normal discharge occurs in traditional micro-EDM with some ignition delay time and pulse interval time. Ionization requires an ignition delay, while fresh dielectric with full insulating strength requires a pulse interval time. During machining, lags in the recovery of actual dielectric strength might result in the production of a transient arc, affecting machining stability and performance [290]. Another condition is short-circuiting, which occurs when two electrodes come into contact without causing a discharge. Because significant current runs between the electrodes without any voltage drop, this sort of pulse is damaging to machining accuracy and surface integrity [291]. The three real-time voltage-current characteristic curves of the maglev micro-EDM are shown in Fig. 6.7. The voltage-current curves include the voltage drop across the inductor circuit (L-R circuit) as well as voltage drop due to the interelectrode gap resistance. The voltage drop across the inductive load (L-R circuit) was found approximately 12V. This fact was tested by making the short circuit

between the two electrodes. However, in the calculation of discharge power, the voltage drop across the inductive load (L-R circuit) was not considered. Only voltage drop across the interelectrode gap resistance was taken into account. The first V-I curve indicates the machining process is stable during multiple discharge energy pulses. Moreover, the absence of ignition delay in the curve represents the quick ionization of the dielectric fluid without any discharge stability issues. Due to fast ionization, the discharge happens quickly, indicating that the process is of continuous type micro-EDM. The second V-I curve indicates that there is no transient arc and short-circuiting. Most of the discharge energy pulses follow the uniform pulse width (10ms). The long-duration discharge energy pulse during the production of nanopatterned features is represented by the third V-I curve. The open-circuit voltage (30V) was observed to drop to the discharge voltage (7-11V) while the discharge current was 180-200 mA. The voltage drops across the inductive load (12V) ignored. The duty factor measured in the digital storage oscilloscope (DSO) was over 75 %. The discharge power was computed using the voltage-current curve excel file (.xls) and was determined to be between 1.575-3.465 joule/sec. This low discharge power has been attributed to nanotips, and it is on the nanoscale (nJ) level. The liberation of nanojoules energy from the locales (due to small size) of the nanotips assists in fabricating the geometrically irregular nanopatterned features on the substrate material.

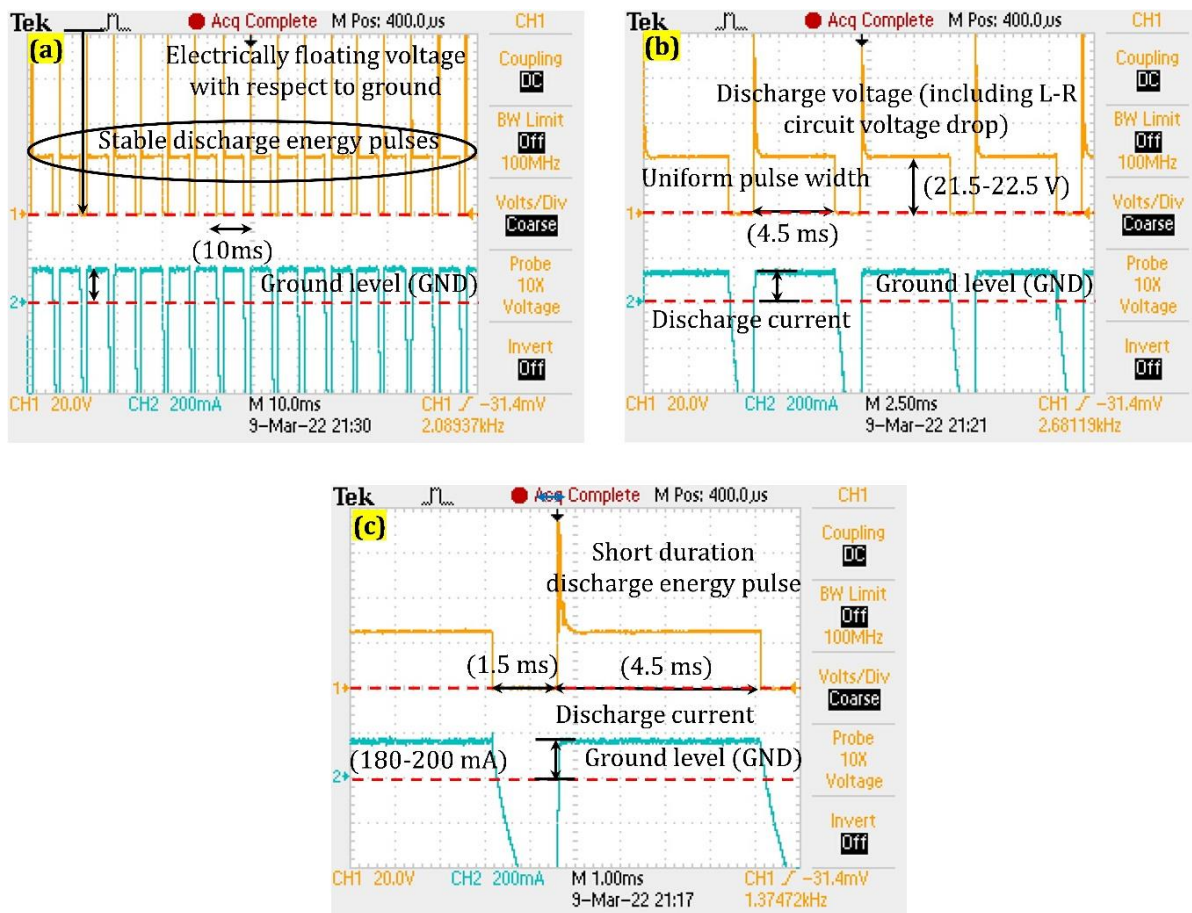


Figure 6. 7 (a) Stable discharge energy pulse (b) uniform pulse width (4.5 ms) (c) long duration discharge energy pulse during nanofeatures fabrication.

6.3.3 Elemental characterization through EDX

Energy-dispersive X-ray spectroscopy is used to analyze the elemental characterization of the manufactured ZnO nanorods on the microtip's apex, as shown in fig. 6.8. The presence of zinc and oxygen (in significant amounts) in the spectrum shows that zinc oxide makes up the majority of the component (ZnO). The presence of copper (3.36 wt.%) in the spectrum, on the other hand, suggests that the ZnO nanorods are developed on the copper micro-tip.

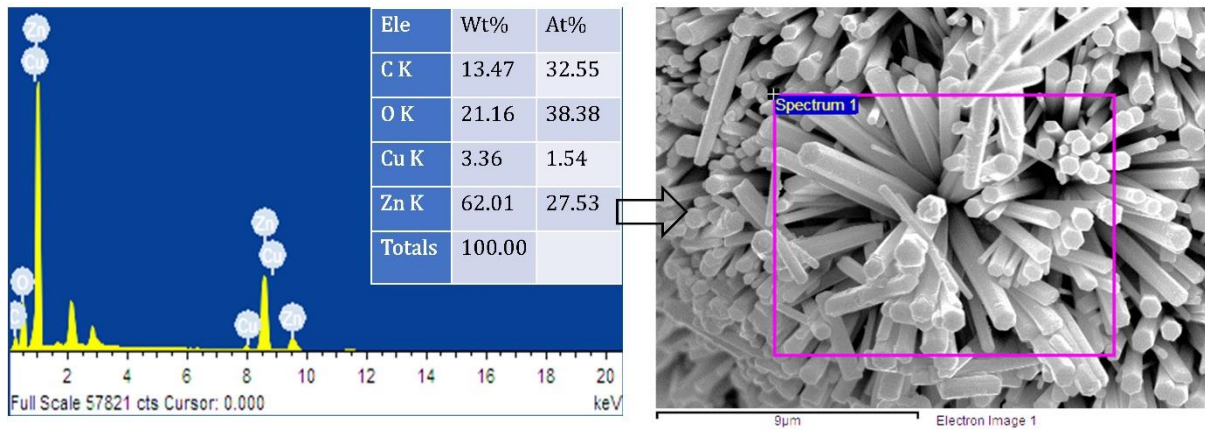


Figure 6. 8 Chemical characterization of the fabricated ZnO nanorods on the apex of the microtip.

The chemical characterization of the machined surface created using ZnO nanorods is shown in Fig. 6.9. The inclusion of components like ferrous (Fe), nickel (Ni), and chromium (Cr) originates from Inconel-625's compositional section. The existence of copper (57.33, wt. %) in the spectrum indicates that the material is transferred from the tool electrode (copper microtip). The material migration and diffusion may take place under the plasma region due to temperature gradient. The availability of carbon and oxygen may come from the carbon tape and the environment respectively.

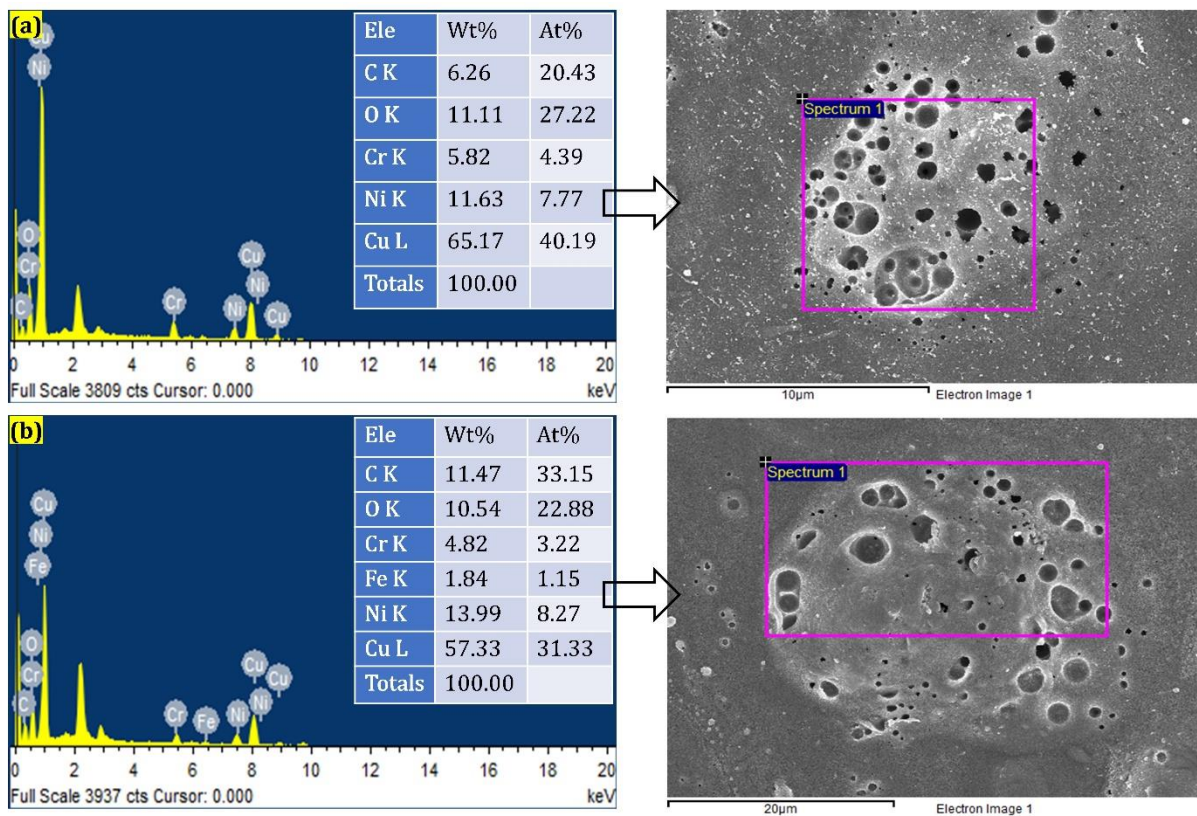


Figure 6. 9 Chemical characterization of the machined surface fabricated by grown nanorods.

6.4 Conclusions

For generating nanopatterned features with a long-duration discharge, a top-to-down technique has been successfully combined with a unique maglev micro-EDM technology. The servo gap control mechanism, as well as the process mechanics of nanostructure formation, are discussed in detail in the study. Even though the manufactured nano features are of the geometrically irregular type, the technique has to be improved. The creation of nanorods on the apex of tooltips demonstrates the efficacy of the nano-EDM technique. In the micro-confined gap, the nanotools localization effect was found to be effective in lowering the discharge power (1.575 J/sec) per unit pulse. Nanoscale morphological characterization of nanorods and manufactured cavities has been discovered. In the scaling technique using nanotools, a low current value was shown to be effective for generating nanopatterned features. Further, even at modest discharge energy power (1.575-3.465 J/sec), the EDX

spectrum of the machined surface shows material migration and diffusion. The absence of undesirable signals such as arcing and short-circuiting demonstrates the machining process's stability in long-period discharge and multiple discharge energy pulses. Finally, the findings of this study show that nano-EDM is feasible and may pose a wide range of potential applications in micro/nanodevices in the micro-electro-mechanical system (MEMS)/ nano-electro-mechanical system (NEMS) sectors.

7

Chapter- 7: Conclusions, Contribution, and Future Scopes

7.1 Conclusion

The presented research work focused on the fabrication of laboratory-scale maglev micro-EDM setup and testing its machining capabilities in the micro and nanodomains. The achievement of nano-patterned features (geometrically irregular type) through the scale-down approach of the micro-EDM system is the main target of this research. The consequences of the present study can be elaborated in the following sections:

- Fabrication of maglev micro-EDM Setup and its machining feasibility and performance analysis on Duplex Stainless Steel (DSS-2205)
- Development of micro/nanotools for the nano-EDM process
- Achieving nano-patterned features through a micro-EDM process using ZnO nanorods as nanotools on Ti-6Al-4V
- Geometrically irregular nano-patterning using maglev-EDM using ZnO nanorods on Inconel-625: A feasibility towards nano-EDM

7.1.1 Fabrication of maglev micro-EDM Setup and its machining feasibility and performance analysis on Duplex Stainless Steel (DSS-2205)

A novel servo gap control strategy for the micro-EDM process has been introduced for machining electrically conductive materials. The novel gap control strategy is based on magnetic levitation. Here, the electromagnetic force (F_{em}) is made balanced to gravitational force (F_g) and spring restoring force (F_{rs}) to achieve the equilibrium state. The equilibrium state of these forces provides the essential condition for the machine's stability and fast

positioning response. The system is empowered with a pure DC power source and triggered with innovative actuator arm technology. The swinging of the actuator arm facilitates the essential condition for dielectric straining within the small interelectrode gap. Later on, the machining feasibility and performance were tested by conducting preliminary experiments on duplex stainless steel (DSS-2205) in deionized water. It was found that the material removal rate (MRR), tool wear rate (TWR), and surface roughness (SR) is lies in the range of 117.6-223.8 $\mu\text{g}/\text{min}$, 10-29 $\mu\text{g}/\text{min}$, and average surface roughness of 1.823-2.2356 μm respectively. Finally, the system stability was tested in terms of the voltage-current (V-I) discharge characteristic curve through signal processing. It was found that the system maintains the proper gap efficiently and stably for the occurrence of normal discharge. The proposed solution may be a good alternative for servo gap control strategy in EDM or μ -EDM.

7.1.2 Development of micro/nanotools for nano-EDM process

In this section, 2D platelets (nanotools) like nanostructure have been developed on the microprobe tip, and investigation has been done for varying morphology under varying concentrations. The combination of zinc nitrate hexahydrate [$\text{Zn}(\text{NO}_3)_2 \cdot 6\text{H}_2\text{O}$] and hexamethylenetetramine (HMTA) is employed as a growth solution having a PH value of 6.0. The assembly of 2D nanostructures grown on microtip is accelerated by introducing the ultrafine discharge in the chemical growth solution. The synthesis, deposition, and growth time were limited to 20 seconds only. After deposition and growth, annealing heat treatment was applied at 95°C for 45 minutes to eliminate any impurities or crystal defects. The structural/morphological characterization through FESEM confirms that the fabricated nanostructure is 2D nanosheet-like at a lower molar concentration (0.10M). Nevertheless, at higher concentrations (0.20M), the grown morphology changes to a marigold flower-like structure with porousness in its crystal structure. The chemical characterization through EDX

confirms the dominance of the ZnO in the fabricated nanostructure. The XRD results confirm the phase pure hexagonal wurtzite structure of ZnO with an average crystalline thickness of ≈ 27 nm.

7.1.3 Achieving nano-patterned features through a micro-EDM process using ZnO nanorods as nanotools on Ti-6Al-4V

Fabricating the nanopatterned features through a cost-effective nanomachining technique is one of the great challenges in nano-electro-mechanical system (NEMS) industries. The micro-electrical-discharge machining process is one of the promising machining technologies which is capable to write the micro-scale features on any electrically conductive materials. However, its potential has not been tested yet for replicating the nanoscale features through the scaling approach. Hence, this article addresses a scaling approach for fabricating the nanopatterned features on super-finished titanium alloy (Ti-6Al-4V) using vertically aligned ZnO nanorods grown on the apex of the microtip. For achieving this, first of all, cylindrical micro-tools of diameter (\varnothing) 90-95 μm (tungsten) were fabricated through a micro-electrochemical turning process under KOH (2.5M) electrolyte medium. On the apex of the micro tools, the ZnO nanorods were grown by the low-temperature hydrothermal process by dipping the apex of the tip in seed and growth solution followed by essential heat treatment at 90°C . It was found that the grown nanorods were well-defined in shape and size and further utilized as nanotools during long-duration discharge (5ms) micro-EDM experiments. It was expected that by downsizing the tooltip, the discharge energy per unit pulse may be reduced due to the localization effect. Moreover, it is well-known fact that the discharge happens only in the nearest established gap in the micro-EDM process. The experimental results of this study confirmed the same. The FESEM micrographs were utilized for the morphological characterization of formed nanopatterned cavities, microtools, and nanorods while the chemical characterization of the same is carried out by EDX

spectroscopy. Additionally, the stability of the machining process was tested first for multiple discharge energy pulses then after a long-duration discharge energy pulse has been characterized by voltage-current (V-I) waveforms during nanocavity fabrication. Finally, the supporting results of this experimental investigation show the feasibility of the approach toward nano-EDM with extensive potential/applications in micro/nanofabrication devices.

7.1.4 Geometrically irregular nano-patterning using maglev-EDM using ZnO nanorods on Inconel-625: A feasibility study towards nano-EDM

Developing a cost-effective novel method for replicating nanoscale features on a wide range of stimulating materials is one of the great challenges. Hence, the present research used a unique maglev micro-electric discharge machining process to reduce the size of the feature towards the nanoscale. ZnO nanorods, which are grown on the tooltip apex, were used as nanotools for this. The nanorods were fabricated by a low-temperature hydrothermal process that involved dipping the tooltip (Copper wire, $\varnothing 100\mu\text{m}$) in seed and growth solution followed by critical heat treatment (95°C). The morphological characterization of the tooltip indicates that the nanorods on the top surface of the tip are well-grown in shape and size, with uniform distribution. Experiments with long-duration discharge (10ms) were carried out in an open-air environment on the super-polished Inconel-625 work surface using ZnO nanorods as nanotools. The intensity of discharge energy per unit pulse is expected to decrease as a result of the nanotools' localization effect. Furthermore, it is a well-known fact that the discharge occurs only where the nearest gap has been established. The appearance of geometrically irregular nanopatterned cavities on the super-finished work surface supported this. The nanopatterned cavities are the negative impression of the bundles of nanorods that developed due to the thermal impact of electrical discharge, according to the FESEM micrograph. Voltage-current waveforms were used to characterize the discharge stability of the machining process for long-period discharge/multiple discharge energy pulses. The EDX spectroscopy

technique was also used to characterize the tooltip and produce nanocavities on an elemental level. Finally, the results of this top-down approach reveal that nano-EDM is feasible and may pose a wide range of applications in micro/nano manufacturing industries such as micro-electro-mechanical system (MEMS)/ nano-electro-mechanical system (NEMS) in upcoming years.

7.2 Research Contribution

A novel servo gap control strategy based on magnetic levitation and electromagnetic induction feeding has been reported. The discharge energy pulses of the developed setup were identical and uniform. The absence of any arcing and short-circuiting signal in the discharge characteristic curve indicates that the process is highly stable and efficient. The specific energy of the current system also lies in the same as reported in the literature means its efficiency is almost similar to other available commercial EDM. The system is empowered with a pure DC power supply which reduces the complexity of the transistor and capacitive pulse power supply as utilized in commercially available micro-EDM. Further, the disclosed technology is anticipated to replace traditional servo mechanisms due to its ease of use, low cost, ease of maintenance, and availability of local components.

For the commencement of nano-EDM, fabricating a tool with a nanotip size could be challenging. The discharge energy at the nanoscale is expected to be delivered by a tool with a nanometric tip due to the size effect. Tungsten is mostly preferred in nano tip fabrication (nanoindenter) as it poses high mechanical strength, low electrical resistivity, and high thermal stability and durability. Three different approaches such as electrochemical micro turning (micro-ECM), electrochemical deposition for nanoplates like tools, and hydrothermal process for nanorods like nanotools are described briefly.

A scaled-down approach has been implemented to check the feasibility of the developed setup for the fabrication of nanoscale features using the principle of electrical

discharge machining (Nano-EDM). The preliminary results indicate that the nano-EDM is achievable and can be applied for a wide range of applications for nanofabrication work. The process capabilities and its repeatability has been tested with titanium and nickel-based superalloy which indicates that the process needs improvement in terms of process and features control. The fabricated geometrically irregular nanocavities may identify its potential in high-density memory devices, bio-sensing, electronics chips, wettability control, improving the cell behavior of bio-implant and antibacterial activities, enhancing the tribological performance by dropping the specific contact area in the interpillar regions, improving the biocompatibility of the interface, etc.

7.3 Future scope of the reported work

Nano electrical discharge machining is in the developing stage and very limited work has been carried out for achieving the nanofeatures using the discharge energy. Developing the nanotools for fabricating nanofeatures is a challenging task, a novel method may be introduced to develop the nanotool other than the growth or deposition technique. The nanotool's sustainability and the repeatability of the process for fabricating nanofeatures through electrical discharge on other conductive materials are open for future research work. The nanofabrication using the nano-EDM principle with other nanotools like nanotubes such as carbon nanotubes and titanium nanotubes needs to be investigated in upcoming work.

The prototype and the technologies now under development are still in their early phases. Testing under the different dielectric media (hydrocarbon and gases) and machining of hard and typical materials like Ti-6Al-4V, commercially pure titanium alloy (CPTI), Nimonic alloy, and nickel aluminum-based superalloy with various nanotool material (carbon nanotubes, titanium nanotubes, and other material nanorods) are being studied. The results are in line with the earlier studies. Improvements have been noted, and the results will be reported in the upcoming publication. Further, the disclosed technology is anticipated to

replace the traditional servo control mechanisms due to its simplicity, low cost, ease of maintenance, and component availability.

References

- [1] X. Luo, K. Cheng, D. Webb, F. Wardle, Design of ultraprecision machine tools with applications to manufacture of miniature and micro components, *J. Mater. Process. Technol.* 167 (2005) 515–528. <https://doi.org/10.1016/j.jmatprotec.2005.05.050>.
- [2] K.F. Ehmann, D. Bourell, M. Culpepper, R.E. DeVor, T. Hodgson, T. Kurfess, M. Madou, K. Rajurkar, An international assessment of micro-manufacturing research technology, in: *Process. Fabr. Adv. Mater. XIV With Front. Mater. Sci. 2005 Innov. Mater. Manuf. Techiques - Proc. a Symp.*, 2005: pp. 211–224.
- [3] X. Liu, R.E. DeVor, S.G. Kapoor, K.F. Ehmann, The Mechanics of Machining at the Microscale: Assessment of the Current State of the Science, *J. Manuf. Sci. Eng.* 126 (2004) 666. <https://doi.org/10.1115/1.1813469>.
- [4] J.-C. Huang, C.-M. Chen, The study on the atomic force microscopy base nanoscale electrical discharge machining, *Scanning.* 34 (2012) 191–199. <https://doi.org/10.1002/sca.20281>.
- [5] K.R. Virwani, A.P. Malshe, K.P. Rajurkar, Understanding sub-20 nm breakdown behavior of liquid dielectrics, *Phys. Rev. Lett.* 99 (2007). <https://doi.org/10.1103/PhysRevLett.99.017601>.
- [6] Y. Tahmasebipour, M. Ghoreishi, M. Tahmasebipour, Finite-Volume Heat Transfer Model of the Nano Electrical Discharge Machining Process, *J. Nanoelectron. Optoelectron.* 9 (2014) 601–607. <https://doi.org/10.1166/jno.2014.1641>.
- [7] K.H. Ho, S.T. Newman, State of the art electrical discharge machining (EDM), *Int. J. Mach. Tools Manuf.* 43 (2003) 1287–1300. [https://doi.org/10.1016/S0890-6955\(03\)00162-7](https://doi.org/10.1016/S0890-6955(03)00162-7).
- [8] A.P. Malshe, K. Virwani, K.P. Rajurkar, D. Deshpande, Investigation of nanoscale electro machining (nano-EM) in dielectric oil, *CIRP Ann. - Manuf. Technol.* 54 (2005)

- 175–178. [https://doi.org/10.1016/S0007-8506\(07\)60077-8](https://doi.org/10.1016/S0007-8506(07)60077-8).
- [9] M. Kunieda, B. Lauwers, K.P. Rajurkar, B.M. Schumacher, Advancing EDM through Fundamental Insight into the Process, *CIRP Ann. - Manuf. Technol.* 54 (2005) 64–87. [https://doi.org/10.1016/S0007-8506\(07\)60020-1](https://doi.org/10.1016/S0007-8506(07)60020-1).
- [10] Q. Liu, Q. Zhang, M. Zhang, J. Zhang, Review of size effects in micro electrical discharge machining, *Precis. Eng.* 44 (2016) 29–40. <https://doi.org/10.1016/j.precisioneng.2016.01.006>.
- [11] H.B. Liu, Y.Q. Wang, Z.Y. Jia, D.M. Guo, Integration strategy of on-machine measurement (OMM) and numerical control (NC) machining for the large thin-walled parts with surface correlative constraint, *Int. J. Adv. Manuf. Technol.* (2015). <https://doi.org/10.1007/s00170-015-7046-x>.
- [12] C.N. Elias, M.A. Meyers, R.Z. Valiev, S.N. Monteiro, Ultrafine grained titanium for biomedical applications: An overview of performance, *J. Mater. Res. Technol.* (2013). <https://doi.org/10.1016/j.jmrt.2013.07.003>.
- [13] R. Liu, R. Chen, A.T. Elthakeb, S.H. Lee, S. Hinckley, M.L. Khraiche, J. Scott, D. Pre, Y. Hwang, A. Tanaka, Y.G. Ro, A.K. Matsushita, X. Dai, C. Soci, S. Biesmans, A. James, J. Nogan, K.L. Jungjohann, D. V. Pete, D.B. Webb, Y. Zou, A.G. Bang, S.A. Dayeh, High Density Individually Addressable Nanowire Arrays Record Intracellular Activity from Primary Rodent and Human Stem Cell Derived Neurons, *Nano Lett.* (2017). <https://doi.org/10.1021/acs.nanolett.6b04752>.
- [14] E. Larrañeta, R.E.M. Lutton, A.D. Woolfson, R.F. Donnelly, Microneedle arrays as transdermal and intradermal drug delivery systems: Materials science, manufacture and commercial development, *Mater. Sci. Eng. R Reports.* (2016). <https://doi.org/10.1016/j.mser.2016.03.001>.
- [15] N. Gupta, S. Dutta, A. Panchal, I. Yadav, S. Kumar, Y. Parmar, S.R.K. Vanjari, K.K.

- Jain, D.K. Bhattacharya, Design and fabrication of SOI technology based MEMS differential capacitive accelerometer structure, *J. Mater. Sci. Mater. Electron.* (2019). <https://doi.org/10.1007/s10854-019-01955-0>.
- [16] A. Revathi, S. Magesh, V.K. Balla, M. Das, G. Manivasagam, Current advances in enhancement of wear and corrosion resistance of titanium alloys – a review, *Mater. Technol.* (2016). <https://doi.org/10.1080/10667857.2016.1212780>.
- [17] R.G. Willaert, K. Goossens, Microfluidic bioreactors for cellular microarrays, *Fermentation.* (2015). <https://doi.org/10.3390/fermentation1010038>.
- [18] K.W. Kwon, S.S. Choi, S.H. Lee, B. Kim, S.N. Lee, M.C. Park, P. Kim, S.Y. Hwang, K.Y. Suh, Label-free, microfluidic separation and enrichment of human breast cancer cells by adhesion difference, *Lab Chip.* (2007). <https://doi.org/10.1039/b710054j>.
- [19] M. Staples, K. Daniel, M.J. Cima, R. Langer, Application of micro- and nano-electromechanical devices to drug delivery, *Pharm. Res.* (2006). <https://doi.org/10.1007/s11095-006-9906-4>.
- [20] M. Kunieda, A. Hayasaka, X.D. Yang, S. Sano, I. Araie, Study on nano EDM using capacity coupled pulse generator, *CIRP Ann. - Manuf. Technol.* 56 (2007) 213–216. <https://doi.org/10.1016/j.cirp.2007.05.051>.
- [21] L. Raju, S.S. Hiremath, A State-of-the-art Review on Micro Electro-discharge Machining, *Procedia Technol.* 25 (2016) 1281–1288. <https://doi.org/10.1016/j.protcy.2016.08.222>.
- [22] S.P. (2018) Mehta K., Gupta M., Erratum to: Nano-Machining, Nano-Joining, and Nano-Welding, in: Gupta K. *Micro Precis. Manuf. Eng. Mater.* Springer, Cham, n.d. https://doi.org/10.1007/978-3-319-68801-5_9.
- [23] M.P. Jahan, A.P. Malshe, K.P. Rajurkar, Experimental investigation and characterization of nano-scale dry electro-machining, in: *J. Manuf. Process.*, 2012: pp.

- 443–451. <https://doi.org/10.1016/j.jmapro.2012.08.004>.
- [24] A.P. Malshe, K.P. Rajurkar, K.R. Virwani, C.R. Taylor, D.L. Bourell, G. Levy, M.M. Sundaram, J.A. McGeough, V. Kalyanasundaram, A.N. Samant, Tip-based nanomanufacturing by electrical, chemical, mechanical and thermal processes, *CIRP Ann. - Manuf. Technol.* (2010). <https://doi.org/10.1016/j.cirp.2010.05.006>.
- [25] K.P.R. Ajay P. Malshe, Kumar R. Virwani, Apparatus and method for nano-scale electric discharge machining, WO 2007/001347 A2, 2007. <https://patents.google.com/patent/WO2007001347A2/en>.
- [26] S. Gao, H. Huang, Recent advances in micro- and nano-machining technologies, *Front. Mech. Eng.* 12 (2017) 18–32. <https://doi.org/10.1007/s11465-017-0410-9>.
- [27] M. Rahman, A.B.M.A. Asad, T. Masaki, T. Saleh, Y.S. Wong, A. Senthil Kumar, A multiprocess machine tool for compound micromachining, *Int. J. Mach. Tools Manuf.* 50 (2010) 344–356. <https://doi.org/10.1016/j.ijmachtools.2009.10.007>.
- [28] T. Masuzawa, State of the Art of Micromachining, *CIRP Ann. - Manuf. Technol.* 49 (2000) 473–488. [https://doi.org/10.1016/S0007-8506\(07\)63451-9](https://doi.org/10.1016/S0007-8506(07)63451-9).
- [29] Y.S. Wong, M. Rahman, H.S. Lim, H. Han, N. Ravi, Investigation of micro-EDM material removal characteristics using single RC-pulse discharges, in: *J. Mater. Process. Technol.*, 2003: pp. 303–307. [https://doi.org/10.1016/S0924-0136\(03\)00771-4](https://doi.org/10.1016/S0924-0136(03)00771-4).
- [30] X. Chu, K. Zhu, C. Wang, Z. Hu, Y. Zhang, A Study on Plasma Channel Expansion in Micro-EDM, *Mater. Manuf. Process.* 31 (2016) 381–390. <https://doi.org/10.1080/10426914.2015.1059445>.
- [31] A. Singh, A. Ghosh, A thermo-electric model of material removal during electric discharge machining, *Int. J. Mach. Tools Manuf.* (1999). [https://doi.org/10.1016/S0890-6955\(98\)00047-9](https://doi.org/10.1016/S0890-6955(98)00047-9).

- [32] S. Dhanik, S.S. Joshi, N. Ramakrishnan, P.R. Apte, Evolution of EDM process modelling and development towards modelling of the micro-EDM process, *Int. J. Manuf. Technol. Manag.* (2005). <https://doi.org/10.1504/IJMTM.2005.006829>.
- [33] P.T. Eubank, M.R. Patel, M.A. Barrufet, B. Bozkurt, Theoretical models of the electrical discharge machining process. III. the variable mass, cylindrical plasma model, *J. Appl. Phys.* (1993). <https://doi.org/10.1063/1.353942>.
- [34] S. Hinduja, M. Kunieda, Modelling of ECM and EDM processes, *CIRP Ann. - Manuf. Technol.* (2013). <https://doi.org/10.1016/j.cirp.2013.05.011>.
- [35] S. Dhanik, S.S. Joshi, Modeling of a single resistance capacitance pulse discharge in micro-electro discharge machining, *J. Manuf. Sci. Eng. Trans. ASME.* (2005). <https://doi.org/10.1115/1.2034512>.
- [36] M.P. Jahan, K.R. Virwani, K.P. Rajurkar, A.P. Malshe, A comparative study of the dry and wet nano-scale electro-machining, in: *Procedia CIRP*, 2013: pp. 626–631. <https://doi.org/10.1016/j.procir.2013.03.081>.
- [37] Q. Liu, Q. Zhang, G. Zhu, K. Wang, J. Zhang, C. Dong, Effect of Electrode Size on the Performances of Micro-EDM, *Mater. Manuf. Process.* 31 (2016) 391–396. <https://doi.org/10.1080/10426914.2015.1059448>.
- [38] J.C. Pilligrin, P. Asokan, J. Jerald, G. Kanagaraj, Effects of electrode materials on performance measures of electrical discharge micro-machining, *Mater. Manuf. Process.* (2018). <https://doi.org/10.1080/10426914.2017.1364757>.
- [39] T. Masuzawa, C.L. Kuo, M. Fujino, A Combined Electrical Machining Process for Micronozzle Fabrication, *CIRP Ann. - Manuf. Technol.* (1994). [https://doi.org/10.1016/S0007-8506\(07\)62193-3](https://doi.org/10.1016/S0007-8506(07)62193-3).
- [40] V. Venkatesh, N. Swain, G. Srinivas, P. Kumar, H.C. Barshilia, Review on the machining characteristics and research prospects of conventional microscale

- machining operations, *Mater. Manuf. Process.* (2017).
<https://doi.org/10.1080/10426914.2016.1151045>.
- [41] Y. Lu, F. Chen, X. Wu, C. Zhou, H. Zhao, L. Li, Y. Tang, Precise WEDM of micro-textured mould for micro-injection molding of hydrophobic polymer surface, *Mater. Manuf. Process.* (2019). <https://doi.org/10.1080/10426914.2019.1660784>.
- [42] J. Giboz, T. Copponnex, P. Mélé, Microinjection molding of thermoplastic polymers: A review, *J. Micromechanics Microengineering.* (2007). <https://doi.org/10.1088/0960-1317/17/6/R02>.
- [43] M.P. Jahan, M.M. Anwar, Y.S. Wong, M. Rahman, Nanofinishing of hard materials using micro-electrodischarge machining, *Proc. Inst. Mech. Eng. Part B J. Eng. Manuf.* 223 (2009) 1127–1142. <https://doi.org/10.1243/09544054JEM1470>.
- [44] L. Alting, F. Kimura, H.N. Hansen, G. Bissacco, Micro engineering, *CIRP Ann. - Manuf. Technol.* 52 (2003) 635–657. [https://doi.org/10.1016/S0007-8506\(07\)60208-X](https://doi.org/10.1016/S0007-8506(07)60208-X).
- [45] S.P. Leo Kumar, D. Avinash, Review on effect of Ti-alloy processing techniques on surface-integrity for biomedical application, *Mater. Manuf. Process.* (2020). <https://doi.org/10.1080/10426914.2020.1748195>.
- [46] H. Bisaria, P. Shandilya, Experimental studies on electrical discharge wire cutting of Ni-rich NiTi shape memory alloy, *Mater. Manuf. Process.* (2018). <https://doi.org/10.1080/10426914.2017.1388518>.
- [47] M.L. Crichton, C. Archer-Jones, S. Meliga, G. Edwards, D. Martin, H. Huang, M.A.F. Kendall, Characterising the material properties at the interface between skin and a skin vaccination microprojection device, *Acta Biomater.* 36 (2016) 186–194. <https://doi.org/10.1016/j.actbio.2016.02.039>.
- [48] T.A. Fofonoff, S.M. Martel, N.G. Hatsopoulos, J.P. Donoghue, I.W. Hunter, Microelectrode array fabrication by electrical discharge machining and chemical

- etching, IEEE Trans. Biomed. Eng. (2004).
<https://doi.org/10.1109/TBME.2004.826679>.
- [49] S. kumar, M.A. Khan, B. Muralidharan, Processing of titanium-based human implant material using wire EDM, Mater. Manuf. Process. (2019).
<https://doi.org/10.1080/10426914.2019.1566609>.
- [50] V. Bajpai, P. Mahambare, R.K. Singh, Effect of Thermal and Material Anisotropy of Pyrolytic Carbon in Vibration-Assisted Micro-EDM Process, Mater. Manuf. Process. (2016). <https://doi.org/10.1080/10426914.2015.1127937>.
- [51] E. Serrano, G. Rus, J. García-Martínez, Nanotechnology for sustainable energy, Renew. Sustain. Energy Rev. 13 (2009) 2373–2384.
<https://doi.org/10.1016/j.rser.2009.06.003>.
- [52] A. Benilov, V. Skryshevsky, Y. Robach, M. Cabrera, Micro and nano electrical discharge machining in microfluidics and micro nanotechnology, Int. J. Mater. Form. 1 (2008) 1315–1318. <https://doi.org/10.1007/s12289-008-0145-6>.
- [53] K.P. Rajurkar, G. Levy, A. Malshe, M.M. Sundaram, J. McGeough, X. Hu, R. Resnick, A. DeSilva, Micro and nano machining by electro-physical and chemical processes, CIRP Ann. - Manuf. Technol. 55 (2006) 643–666.
<https://doi.org/10.1016/j.cirp.2006.10.002>.
- [54] Z. Zhang, J. Yan, T. Kuriyagawa, Manufacturing technologies toward extreme precision, Int. J. Extrem. Manuf. (2019). <https://doi.org/10.1088/2631-7990/ab1ff1>.
- [55] S. Zhang, Y. Zhou, H. Zhang, Z. Xiong, S. To, Advances in ultra-precision machining of micro-structured functional surfaces and their typical applications, Int. J. Mach. Tools Manuf. (2019). <https://doi.org/10.1016/j.ijmachtools.2019.04.009>.
- [56] G. Zhang, J. Guo, W. Ming, Y. Huang, X. Shao, Z. Zhang, Study of the machining process of nano-electrical discharge machining based on combined atomistic-

- continuum modeling method, *Appl. Surf. Sci.* 290 (2014) 359–367.
<https://doi.org/10.1016/j.apsusc.2013.11.084>.
- [57] X. Yue, X. Yang, Molecular dynamics simulation of material removal process and mechanism of EDM using a two-temperature model, *Appl. Surf. Sci.* 528 (2020) 147009. <https://doi.org/10.1016/j.apsusc.2020.147009>.
- [58] Z. Xiao, M. Dahmardeh, M.V. Moghaddam, A. Nojeh, K. Takahata, Scaling approach toward nano electro-discharge machining: Nanoscale patterning of carbon nanotube forests, *Microelectron. Eng.* 150 (2016) 64–70.
<https://doi.org/10.1016/j.mee.2015.11.008>.
- [59] H.S. Lim, Y.S. Wong, M. Rahman, M.K. Edwin Lee, A study on the machining of high-aspect ratio micro-structures using micro-EDM, in: *J. Mater. Process. Technol.*, 2003: pp. 318–325. [https://doi.org/10.1016/S0924-0136\(03\)00760-X](https://doi.org/10.1016/S0924-0136(03)00760-X).
- [60] J.W. Jung, Y.H. Jeong, B.-K. Min, S.J. Lee, Model-Based Pulse Frequency Control for Micro-EDM Milling Using Real-Time Discharge Pulse Monitoring, *J. Manuf. Sci. Eng.* 130 (2008) 031106. <https://doi.org/10.1115/1.2917305>.
- [61] I. Beltrami, C. Joseph, R. Clavel, J.P. Bacher, S. Bottinelli, Micro- and nanoelectric-discharge machining, in: *J. Mater. Process. Technol.*, 2004: pp. 263–265.
<https://doi.org/10.1016/j.jmatprotec.2004.03.002>.
- [62] K.R. Virwani, A.P. Malshe, K.P. Rajurkar, Understanding dielectric breakdown and related tool wear characteristics in nanoscale Electro-Machining process, *CIRP Ann. - Manuf. Technol.* 56 (2007) 217–220. <https://doi.org/10.1016/j.cirp.2007.05.098>.
- [63] J. Wang, X. Sun, L. Chen, S.Y. Chou, Direct nanoimprint of submicron organic light-emitting structures, *Appl. Phys. Lett.* (1999). <https://doi.org/10.1063/1.125143>.
- [64] M.D. Austin, H. Ge, W. Wu, M. Li, Z. Yu, D. Wasserman, S.A. Lyon, S.Y. Chou, Fabrication of 5 nm linewidth and 14 nm pitch features by nanoimprint lithography,

- Appl. Phys. Lett. (2004). <https://doi.org/10.1063/1.1766071>.
- [65] J. Song, Z. Liu, C. Li, H. Chen, H. He, SPM-based nanofabrication using a synchronization technique, Appl. Phys. A Mater. Sci. Process. (1998). <https://doi.org/10.1007/s003390051228>.
- [66] M.J. Madou, Fundamentals of Microfabrication, 2002. <https://doi.org/10.1201/9781482274004>.
- [67] P. Rai-Choudhury, Handbook of Microlithography, Micromachining, and Microfabrication. Volume 1: Microlithography, 1997. <https://doi.org/10.1117/3.2265070>.
- [68] Y.D. Park, K.B. Jung, M. Overberg, D. Temple, S.J. Pearton, P.H. Holloway, Comparative study of Ni nanowires patterned by electron-beam lithography and fabricated by lift-off and dry etching techniques, J. Vac. Sci. Technol. B Microelectron. Nanom. Struct. (2000). <https://doi.org/10.1116/1.591143>.
- [69] A. Olbrich, B. Ebersberger, C. Boit, P. Niedermann, W. Hänni, J. Vancea, H. Hoffmann, High aspect ratio all diamond tips formed by focused ion beam for conducting atomic force microscopy, J. Vac. Sci. Technol. B Microelectron. Nanom. Struct. (1999). <https://doi.org/10.1116/1.590842>.
- [70] S. Matsui, T. Kaito, J. Fujita, M. Komuro, K. Kanda, Y. Haruyama, Three-dimensional nanostructure fabrication by focused-ion-beam chemical vapor deposition, J. Vac. Sci. Technol. B Microelectron. Nanom. Struct. (2000). <https://doi.org/10.1116/1.1319689>.
- [71] G. Kamlage, T. Bauer, A. Ostendorf, B.N. Chichkov, Deep drilling of metals by femtosecond laser pulses, Appl. Phys. A Mater. Sci. Process. (2003). <https://doi.org/10.1007/s00339-003-2120-x>.
- [72] M. Meunier, B. Fiset, A. Houle, A. V. Kabashin, S. V. Broude, P. Miller, Processing of metals and semiconductors by a femtosecond laser-based microfabrication system,

- in: *Commer. Biomed. Appl. Ultrafast Lasers III*, 2003.
<https://doi.org/10.1117/12.478595>.
- [73] A.H. Alkhaleel, Z. Yu, M.M. Sundaram, K.P. Rajurkar, A.P. Malshe, Nanoscale features by electro- Machining using atomic force microscope, in: *Trans. North Am. Manuf. Res. Inst. SME*, 2006: pp. 437–444.
- [74] K.R. Virwani, A.P. Malshe, K.P. Rajurkar, Understanding sub-20 nm breakdown behavior of liquid dielectrics, *Phys. Rev. Lett.* 99 (2007) 1–4.
<https://doi.org/10.1103/PhysRevLett.99.017601>.
- [75] Y.K. Cheng X, Nakamoto K, Sugai M, Matsumoto S, Wang ZG, Development of ultra-precision machining system with unique wire EDM tool fabrication system for micro/nano-machining, *CIRP Ann Manuf Technol.* 57 (2008) 415–420.
- [76] V. Kalyanasundaram, K.R. Virwani, D.E. Spearot, A.P. Malshe, K.P. Rajurkar, Understanding behavior of machining interface and dielectric molecular medium in nanoscale electro-machining, *CIRP Ann. - Manuf. Technol.* 57 (2008) 199–202.
<https://doi.org/10.1016/j.cirp.2008.03.011>.
- [77] M. Rahman, A.B.M.A. Asad, Y.S. Wong, M.P. Jahan, T. Masaki, Compound and Hybrid Micromachining Processes, in: *Compr. Mater. Process.*, 2014.
<https://doi.org/10.1016/B978-0-08-096532-1.01105-5>.
- [78] M.K. Bani Melhem, M. Simic, C.Y. Lai, Y. Feng, S. Ding, Fuzzy control of the dual-stage feeding system consisting of a piezoelectric actuator and a linear motor for electrical discharge machining, *Proc. Inst. Mech. Eng. Part B J. Eng. Manuf.* (2020).
<https://doi.org/10.1177/0954405419889201>.
- [79] H.U. Danzebrink, L. Koenders, G. Wilkening, A. Yacoot, H. Kunzmann, Advances in scanning force microscopy for dimensional metrology, *CIRP Ann. - Manuf. Technol.* (2006). <https://doi.org/10.1016/j.cirp.2006.10.010>.

- [80] F. Han, S. Wachi, M. Kunieda, Improvement of machining characteristics of micro-EDM using transistor type isopulse generator and servo feed control, *Precis. Eng.* 28 (2004) 378–385. <https://doi.org/10.1016/j.precisioneng.2003.11.005>.
- [81] X.D. Yang, Y. Wan, F.Q. Hu, Study on Influence of Stray Inductance in Micro EDM Using Electrostatic Induction Feeding Method, *Key Eng. Mater.* 447–448 (2010) 263–267. <https://doi.org/10.4028/www.scientific.net/KEM.447-448.263>.
- [82] P. Kumar, P.K. Singh, D. Kumar, V. Prakash, M. Hussain, A.K. Das, A novel application of micro-EDM process for the generation of nickel nanoparticles with different shapes, *Mater. Manuf. Process.* (2017). <https://doi.org/10.1080/10426914.2016.1244832>.
- [83] I. Perfilov, J. Streckenbach, T.-M. Schimmelpfennig, E. Uhlmann, Module for Micro Electrical Discharge Machining with Gaseous Dielectrics, in: 2017. https://doi.org/10.1007/978-3-319-49269-8_3.
- [84] S. Das, S. Paul, B. Doloi, Feasibility assessment of some alternative dielectric mediums for sustainable electrical discharge machining: a review work, *J. Brazilian Soc. Mech. Sci. Eng.* (2020). <https://doi.org/10.1007/s40430-020-2238-1>.
- [85] Y.S. Fan, J.C. Bai, Study on volt-ampere characteristics of spark discharge for transistor resistor pulse power of EDM, *Int. J. Adv. Manuf. Technol.* (2018). <https://doi.org/10.1007/s00170-018-1702-x>.
- [86] Q. Li, X. Yang, Study on arc plasma movement and its effect on crater morphology during single-pulse discharge in EDM, *Int. J. Adv. Manuf. Technol.* (2020). <https://doi.org/10.1007/s00170-020-04964-0>.
- [87] S. Kar, P.K. Patowari, Electrode wear phenomenon and its compensation in micro electrical discharge milling: A review, *Mater. Manuf. Process.* (2018). <https://doi.org/10.1080/10426914.2018.1453144>.

- [88] S. Kumar, A. Batish, R. Singh, A. Bhattacharya, Effect of cryogenically treated copper-tungsten electrode on tool wear rate during electro-discharge machining of Ti-5Al-2.5Sn alloy, *Wear*. (2017). <https://doi.org/10.1016/j.wear.2017.01.067>.
- [89] X. Zhang, Y. Zhang, Q. Xu, Design and control of a novel piezo-driven XY parallel nanopositioning stage, *Microsyst. Technol.* (2017). <https://doi.org/10.1007/s00542-016-2854-y>.
- [90] M. Kunieda, T. Takaya, S. Nakano, Improvement of Dry EDM Characteristics Using Piezoelectric Actuator, *CIRP Ann. - Manuf. Technol.* 53 (2004) 183–186. [https://doi.org/10.1016/S0007-8506\(07\)60674-X](https://doi.org/10.1016/S0007-8506(07)60674-X).
- [91] I. Beltrami, C. Joseph, R. Clavel, J.P. Bacher, S. Bottinelli, Micro- and nanoelectric-discharge machining, in: *J. Mater. Process. Technol.*, 2004: pp. 263–265. <https://doi.org/10.1016/j.jmatprotec.2004.03.002>.
- [92] Y. Imai, T. Nakagawa, H. Miyake, H. Hidai, H. Tokura, Local actuator module for highly accurate micro-EDM, in: *J. Mater. Process. Technol.*, 2004. <https://doi.org/10.1016/j.jmatprotec.2004.01.060>.
- [93] X. Zhang, T. Shinshi, G. Kajiwara, A. Shimokohbe, Y. Imai, H. Miyake, T. Nakagawa, A 5-DOF controlled maglev local actuator and its application to electrical discharge machining, *Precis. Eng.* (2008). <https://doi.org/10.1016/j.precisioneng.2007.10.003>.
- [94] X. Zhang, T. Shinshi, H. Endo, A. Shimokohbe, Y. Imai, H. Miyake, T. Nakagawa, Development of a 5-DOF controlled, wide-bandwidth, high-precision maglev actuator for micro electrical discharge machining, in: *Proc. 2007 IEEE Int. Conf. Mechatronics Autom. ICMA 2007*, 2007. <https://doi.org/10.1109/ICMA.2007.4304016>.
- [95] X. ZHANG, T. SHINSHI, A. SHIMOKOHBE, T. SATO, H. MIYAKE, T. NAKAGAWA, High-Speed Electrical Discharge Machining By Using a 5-DOF

- Controlled Maglev Local Actuator, *J. Adv. Mech. Des. Syst. Manuf.* (2008).
<https://doi.org/10.1299/jamdsm.2.493>.
- [96] X. Zhang, Y. Ueyama, T. Shinshi, A. Shimokohbe, T. Sato, H. Miyake, T. Nakagawa, High-speed and high-accuracy EDM of micro holes by using a 5-DOF controlled maglev local actuator, in: *Mater. Sci. Forum*, 2009.
<https://doi.org/10.4028/www.scientific.net/MSF.626-627.255>.
- [97] Y. Ueyama, X. Zhang, T. Shinshi, A. Shimokhbe, T. Nakagawa, T. Sato, H. Miyake, Cooperative control system of a maglev local actuator and a conventional EDM machine, in: *Proc. 5th Int. Conf. Lead. Edge Manuf. 21st Century, LEM 2009*, 2009.
- [98] D. He, H. Morita, X. Zhang, T. Shinshi, T. Nakagawa, T. Sato, H. Miyake, Development of a novel 5-DOF controlled maglev local actuator for high-speed electrical discharge machining, *Precis. Eng.* (2010).
<https://doi.org/10.1016/j.precisioneng.2009.11.002>.
- [99] M. Fujiki, G.Y. Kim, J. Ni, A.J. Shih, Gap control for near-dry EDM milling with lead angle, *Int. J. Mach. Tools Manuf.* (2011).
<https://doi.org/10.1016/j.ijmachtools.2010.09.002>.
- [100] K.P. Rajurkar, W.M. Wang, R.P. Lindsay, A New Model Reference Adaptive Control of EDM, *CIRP Ann. - Manuf. Technol.* (1989). [https://doi.org/10.1016/S0007-8506\(07\)62680-8](https://doi.org/10.1016/S0007-8506(07)62680-8).
- [101] M. Zhou, F. Han, Adaptive control for EDM process with a self-tuning regulator, *Int. J. Mach. Tools Manuf.* (2009). <https://doi.org/10.1016/j.ijmachtools.2009.01.004>.
- [102] J.P. Kruth, R. Snoeys, H. Van Brussel, Adaptive control optimization of the EDM process using minicomputers, *Comput. Ind.* (1979). [https://doi.org/10.1016/0166-3615\(79\)90012-5](https://doi.org/10.1016/0166-3615(79)90012-5).
- [103] J.H. Zhang, H. Zhang, D.S. Su, Y. Qin, M.Y. Huo, Q.H. Zhang, L. Wang, Adaptive

- fuzzy control system of a servomechanism for electro-discharge machining combined with ultrasonic vibration, in: *J. Mater. Process. Technol.*, 2002. [https://doi.org/10.1016/S0924-0136\(02\)00573-3](https://doi.org/10.1016/S0924-0136(02)00573-3).
- [104] C.C. Kao, A.J. Shih, S.F. Miller, Fuzzy logic control of microhole electrical discharge machining, *J. Manuf. Sci. Eng. Trans. ASME.* (2008). <https://doi.org/10.1115/1.2977827>.
- [105] T. Kaneko, T. Onodera, Improvement in machining performance of die-sinking EDM by using self-adjusting fuzzy control, in: *J. Mater. Process. Technol.*, 2004. <https://doi.org/10.1016/j.jmatprotec.2004.02.006>.
- [106] J.B. Byiringiro, B.W. Ikua, G.N. Nyakoe, Fuzzy logic based controller for micro-electro discharge machining servo systems, in: *IEEE AFRICON Conf.*, 2009. <https://doi.org/10.1109/AFRCON.2009.5308293>.
- [107] V. Kumar, K.P.S. Rana, V. Gupta, Real-Time Performance Evaluation of a Fuzzy PI + Fuzzy PD Controller for Liquid-Level Process, *Int. J. Intell. Control. Syst.* (2008).
- [108] J.P. Segovia, D. Sbarbaro, E. Ceballos, An adaptive pattern based nonlinear PID controller, *ISA Trans.* (2004). [https://doi.org/10.1016/s0019-0578\(07\)60036-6](https://doi.org/10.1016/s0019-0578(07)60036-6).
- [109] G. Zhong, Z. Shao, H. Deng, J. Ren, Precise Position Synchronous Control for Multi-Axis Servo Systems, *IEEE Trans. Ind. Electron.* (2017). <https://doi.org/10.1109/TIE.2017.2652343>.
- [110] H.S. Lee, M. Tomizuka, Robust motion controller design for high-accuracy positioning systems, *IEEE Trans. Ind. Electron.* (1996). <https://doi.org/10.1109/41.481407>.
- [111] D.F. Dauw, R. Snoeys, W. Dekeyser, Advanced Pulse Discriminating System for EDM Process Analysis and Control, *CIRP Ann. - Manuf. Technol.* (1983). [https://doi.org/10.1016/S0007-8506\(07\)60181-4](https://doi.org/10.1016/S0007-8506(07)60181-4).

- [112] Y.S. Wong, M. Edkins, C.F. Noble, An investigation of the power output and gap voltage during electrical discharge machining using microcomputer-based instrumentation, *Int. J. Mach. Tools Manuf.* (1987). [https://doi.org/10.1016/S0890-6955\(87\)80050-0](https://doi.org/10.1016/S0890-6955(87)80050-0).
- [113] S.K. Bhattacharyya, M.F. El-Menshawy, Monitoring the e.d.m. process by radio signals, *Int. J. Prod. Res.* (1978). <https://doi.org/10.1080/00207547808930027>.
- [114] S.F. Yu, B.Y. Lee, W.S. Lin, Waveform monitoring of electric discharge machining by wavelet transform, *Int. J. Adv. Manuf. Technol.* (2001). <https://doi.org/10.1007/s001700170168>.
- [115] Y.S. Tarng, C.M. Tseng, L.K. Chung, A fuzzy pulse discriminating system for electrical discharge machining, *Int. J. Mach. Tools Manuf.* (1997). [https://doi.org/10.1016/S0890-6955\(96\)00033-8](https://doi.org/10.1016/S0890-6955(96)00033-8).
- [116] J.Y. Kao, Y.S. Tarng, A neural-network approach for the on-line monitoring of the electrical discharge machining process, *J. Mater. Process. Technol.* (1997). [https://doi.org/10.1016/S0924-0136\(97\)00004-6](https://doi.org/10.1016/S0924-0136(97)00004-6).
- [117] E. Pajak, K. Wiczorowski, Classification of Discharges in Electrocontact Discharge Machining (ECDM) by Means of Neural Networks, *VDI Berichte.* (1998).
- [118] F. Han, S. Wachi, M. Kunieda, Improvement of machining characteristics of micro-EDM using transistor type isopulse generator and servo feed control, *Precis. Eng.* 28 (2004) 378–385. <https://doi.org/10.1016/j.precisioneng.2003.11.005>.
- [119] A.W. Behrens, J. Ginzler, F.L. Bruhns, Threshold technology and its application for gap status detection, in: *J. Mater. Process. Technol.*, 2004. <https://doi.org/10.1016/j.jmatprotec.2003.10.041>.
- [120] M. Rahman, Y.S. Wong, M.D. Nguyen, Compound and Hybrid Micromachining: Part II - Hybrid Micro-EDM and Micro-ECM, in: *Compr. Mater. Process.*, 2014.

<https://doi.org/10.1016/B978-0-08-096532-1.01329-7>.

- [121] F. Altpeter, R. Perez, Relevant topics in wire electrical discharge machining control, in: *J. Mater. Process. Technol.*, 2004. <https://doi.org/10.1016/j.jmatprotec.2003.10.033>.
- [122] L. Zhang, Z. Jia, W. Liu, A. Li, A two-stage servo feed controller of micro-EDM based on interval type-2 fuzzy logic, *Int. J. Adv. Manuf. Technol.* 59 (2012) 633–645. <https://doi.org/10.1007/s00170-011-3535-8>.
- [123] X. Wang, S. Yi, M. Easton, S. Ding, Active gap capacitance electrical discharge machining of polycrystalline diamond, *J. Mater. Process. Technol.* (2020). <https://doi.org/10.1016/j.jmatprotec.2020.116598>.
- [124] B. Xin, M. Gao, S. Li, B. Feng, Modeling of Interelectrode Gap in Electric Discharge Machining and Minimum Variance Self-Tuning Control of Interelectrode Gap, *Math. Probl. Eng.* 2020 (2020) 20. <https://doi.org/10.1155/2020/5652197>.
- [125] H.B. Yang, G. H.; Liu, F.; Lin, Research on an Embedded Servo Control System of Micro-EDM, in: *Appl. Mech. Mater.* 2011,120, 2011: pp. 573–577.
- [126] S. Mahendran, I. Fazli, S. Thinesh Chander, Development of Micro EDM with Directly Mounted APA 400MML Actuator as Tool Feed Mechanism, *Adv. Mater. Res.* 314–316 (2011) 1811–1817. <https://doi.org/10.4028/www.scientific.net/AMR.314-316.1811>.
- [127] S.A. Mullya, G. Karthikeyan, Dielectric flow observation at inter-electrode gap in micro-electro-discharge-milling process, *Proc. Inst. Mech. Eng. Part B J. Eng. Manuf.* (2018). <https://doi.org/10.1177/0954405416662082>.
- [128] T. Roy, D. Datta, R. Balasubramaniam, Debris based discharge segregation in reverse micro EDM, *Meas. J. Int. Meas. Confed.* (2020). <https://doi.org/10.1016/j.measurement.2019.107433>.
- [129] Y.S. Wong, L.C. Lim, L.C. Lee, Effects of flushing on electro-discharge machined

- surfaces, *J. Mater. Process. Tech.* 48 (1995) 299–305. [https://doi.org/10.1016/0924-0136\(94\)01662-K](https://doi.org/10.1016/0924-0136(94)01662-K).
- [130] F. Klocke, D. Lung, D. Thomaidis, G. Antonoglou, Using ultra thin electrodes to produce micro-parts with wire-EDM, in: *J. Mater. Process. Technol.*, 2004. <https://doi.org/10.1016/j.jmatprotec.2003.10.061>.
- [131] Z.Y. Yu, K.P. Rajurkar, H. Shen, High aspect ratio and complex shaped blind micro holes by micro EDM, *CIRP Ann. - Manuf. Technol.* 51 (2002) 359–362. [https://doi.org/10.1016/S0007-8506\(07\)61536-4](https://doi.org/10.1016/S0007-8506(07)61536-4).
- [132] K.Y. Song, D.K. Chung, M.S. Park, C.N. Chu, Micro electrical discharge drilling of tungsten carbide using deionized water, *J. Micromechanics Microengineering*. (2009). <https://doi.org/10.1088/0960-1317/19/4/045006>.
- [133] K. Kagaya, Y. Oishi, K. Yada, Micro-electrodischarge machining using water as a working fluid-I: micro-hole drilling, *Precis. Eng.* (1986). [https://doi.org/10.1016/0141-6359\(86\)90034-6](https://doi.org/10.1016/0141-6359(86)90034-6).
- [134] G. Kibria, B.R. Sarkar, B.B. Pradhan, B. Bhattacharyya, Comparative study of different dielectrics for micro-EDM performance during microhole machining of Ti-6Al-4V alloy, *Int. J. Adv. Manuf. Technol.* (2010). <https://doi.org/10.1007/s00170-009-2298-y>.
- [135] S.P. Sivapirakasam, J. Mathew, M. Surianarayanan, Multi-attribute decision making for green electrical discharge machining, *Expert Syst. Appl.* (2011). <https://doi.org/10.1016/j.eswa.2011.01.026>.
- [136] N.K. Singh, P.M. Pandey, K.K. Singh, Experimental investigations into the performance of EDM using argon gas-assisted perforated electrodes, *Mater. Manuf. Process.* (2017). <https://doi.org/10.1080/10426914.2016.1221079>.
- [137] V.K. Yadav, P. Kumar, A. Dvivedi, Performance enhancement of rotary tool near-dry

- EDM of HSS by supplying oxygen gas in the dielectric medium, *Mater. Manuf. Process.* (2019). <https://doi.org/10.1080/10426914.2019.1675889>.
- [138] N.K. Singh, P.M. Pandey, K.K. Singh, M.K. Sharma, Steps towards green manufacturing through EDM process: A review, *Cogent Eng.* (2016). <https://doi.org/10.1080/23311916.2016.1272662>.
- [139] V.K. Yadav, P. Kumar, A. Dvivedi, Effect of tool rotation in near-dry EDM process on machining characteristics of HSS, *Mater. Manuf. Process.* (2019). <https://doi.org/10.1080/10426914.2019.1605171>.
- [140] K. Dhakar, A. Dvivedi, Parametric Evaluation on Near-Dry Electric Discharge Machining, *Mater. Manuf. Process.* 31 (2016) 413–421. <https://doi.org/10.1080/10426914.2015.1037905>.
- [141] K. Dhakar, K. Chaudhary, A. Dvivedi, O. Bembalge, An environment-friendly and sustainable machining method: near-dry EDM, *Mater. Manuf. Process.* (2019). <https://doi.org/10.1080/10426914.2019.1643471>.
- [142] R. Katna, K. Singh, N. Agrawal, S. Jain, Green manufacturing—performance of a biodegradable cutting fluid, *Mater. Manuf. Process.* (2017). <https://doi.org/10.1080/10426914.2017.1328119>.
- [143] S. Das, S. Paul, B. Doloi, Feasibility investigation of neem oil as a dielectric for electrical discharge machining, *Int. J. Adv. Manuf. Technol.* (2020). <https://doi.org/10.1007/s00170-019-04736-5>.
- [144] J.B. Valaki, P.P. Rathod, C.D. Sankhavara, Investigations on technical feasibility of *Jatropha curcas* oil based bio dielectric fluid for sustainable electric discharge machining (EDM), *J. Manuf. Process.* (2016). <https://doi.org/10.1016/j.jmapro.2016.03.004>.
- [145] Y. Liu, Y. Zhang, R. Ji, B. Cai, F. Wang, X. Tian, X. Dong, Experimental

- characterization of sinking electrical discharge machining using water in oil emulsion as dielectric, *Mater. Manuf. Process.* (2013). <https://doi.org/10.1080/10426914.2012.700162>.
- [146] J.B. Valaki, P.P. Rathod, Investigating Feasibility Through Performance Analysis of Green Dielectrics for Sustainable Electric Discharge Machining, *Mater. Manuf. Process.* (2016). <https://doi.org/10.1080/10426914.2015.1070430>.
- [147] H. Dong, Y. Liu, M. Li, Y. Zhou, T. Liu, D. Li, Q. Sun, Y. Zhang, R. Ji, Sustainable electrical discharge machining using water in oil nanoemulsion, *J. Manuf. Process.* (2019). <https://doi.org/10.1016/j.jmapro.2019.08.035>.
- [148] G. Li, W. Natsu, Realization of micro EDM drilling with high machining speed and accuracy by using mist deionized water jet, *Precis. Eng.* (2020). <https://doi.org/10.1016/j.precisioneng.2019.09.016>.
- [149] E. Kuram, B. Ozcelik, E. Demirbas, E. Şik, I.N. Tansel, Evaluation of new vegetable-based cutting fluids on thrust force and surface roughness in drilling of AISI 304 using Taguchi method, *Mater. Manuf. Process.* (2011). <https://doi.org/10.1080/10426914.2010.536933>.
- [150] F.N. Leão, I.R. Pashby, A review on the use of environmentally-friendly dielectric fluids in electrical discharge machining, in: *J. Mater. Process. Technol.*, 2004: pp. 341–346. <https://doi.org/10.1016/j.jmatprotec.2003.10.043>.
- [151] W. König, L. Jörres, Aqueous Solutions of Organic Compounds as Dielectrics for EDM Sinking, *CIRP Ann. - Manuf. Technol.* (1987). [https://doi.org/10.1016/S0007-8506\(07\)62564-5](https://doi.org/10.1016/S0007-8506(07)62564-5).
- [152] J.C. M’Peko, D.L.S. Reis, J.E. De Souza, A.R.L. Caires, Evaluation of the dielectric properties of biodiesel fuels produced from different vegetable oil feedstocks through electrochemical impedance spectroscopy, *Int. J. Hydrogen Energy.* (2013).

- <https://doi.org/10.1016/j.ijhydene.2013.05.086>.
- [153] C.D. Mandolesi De Araújo, C.C. De Andrade, E. De Souza E Silva, F.A. Dupas, Biodiesel production from used cooking oil: A review, *Renew. Sustain. Energy Rev.* (2013). <https://doi.org/10.1016/j.rser.2013.06.014>.
- [154] J.B. Valaki, P.P. Rathod, Assessment of operational feasibility of waste vegetable oil based bio-dielectric fluid for sustainable electric discharge machining (EDM), *Int. J. Adv. Manuf. Technol.* (2016). <https://doi.org/10.1007/s00170-015-7169-0>.
- [155] P.S. Ng, S.A. Kong, S.H. Yeo, Investigation of biodiesel dielectric in sustainable electrical discharge machining, *Int. J. Adv. Manuf. Technol.* (2017). <https://doi.org/10.1007/s00170-016-9572-6>.
- [156] K. Furutani, D. Hiraoka, Condition monitoring in concurrent micro-hole electrical discharge machining with electrode feeding devices employing AZARASHI (Seal) mechanism, in: *Procedia CIRP*, 2014. <https://doi.org/10.1016/j.procir.2014.03.079>.
- [157] R. Snoeys, D.F. Dauw, J.P. Kruth, Survey of adaptive control in electro discharge machining, *J. Manuf. Syst.* (1983). [https://doi.org/10.1016/S0278-6125\(83\)80028-4](https://doi.org/10.1016/S0278-6125(83)80028-4).
- [158] H. Wu, T. Wang, J. Wang, Research on discharge state detection of finishing in high-speed wire electrical discharge machine, *Int. J. Adv. Manuf. Technol.* (2019). <https://doi.org/10.1007/s00170-019-03708-z>.
- [159] F.L. Amorim, W.L. Weingaertner, The behavior of graphite and copper electrodes on the finish die-sinking electrical discharge machining (EDM) of AISI P20 tool steel, *J. Brazilian Soc. Mech. Sci. Eng.* (2007). <https://doi.org/10.1590/S1678-58782007000400004>.
- [160] D. Kumar, N.K. Singh, V. Bajpai, Recent trends, opportunities and other aspects of micro-EDM for advanced manufacturing: a comprehensive review, *J. Brazilian Soc. Mech. Sci. Eng.* (2020). <https://doi.org/10.1007/s40430-020-02296-4>.

- [161] P. Bowland, E. Ingham, J. Fisher, L.M. Jennings, Development of a preclinical natural porcine knee simulation model for the tribological assessment of osteochondral grafts in vitro, *J. Biomech.* (2018). <https://doi.org/10.1016/j.jbiomech.2018.06.014>.
- [162] C. Wang, J. Caja, E. Gómez, P. Maresca, Procedure for calibrating the Z-axis of a confocal microscope: Application for the evaluation of structured surfaces, *Sensors* (Switzerland). (2019). <https://doi.org/10.3390/s19030527>.
- [163] M. Mahardika, K. Mitsui, A new method for monitoring micro-electric discharge machining processes, *Int. J. Mach. Tools Manuf.* (2008). <https://doi.org/10.1016/j.ijmachtools.2007.08.023>.
- [164] M. Mahardika, T. Tsujimoto, K. Mitsui, A new approach on the determination of ease of machining by EDM processes, *Int. J. Mach. Tools Manuf.* (2008). <https://doi.org/10.1016/j.ijmachtools.2007.12.012>.
- [165] T. Shitara, K. Fujita, J. Yan, Direct observation of discharging phenomena in vibration-assisted micro-electrical discharge machining, *Int. J. Adv. Manuf. Technol.* (2020). <https://doi.org/10.1007/s00170-019-04877-7>.
- [166] T. Kitamura, M. Kunieda, K. Abe, High-speed imaging of EDM gap phenomena using transparent electrodes, in: *Procedia CIRP*, 2013. <https://doi.org/10.1016/j.procir.2013.03.082>.
- [167] A. Kojima, W. Natsu, M. Kunieda, Spectroscopic measurement of arc plasma diameter in EDM, *CIRP Ann. - Manuf. Technol.* (2008). <https://doi.org/10.1016/j.cirp.2008.03.097>.
- [168] A. Kumar, A. Mandal, A.R. Dixit, D.K. Mandal, Quantitative analysis of bubble size and electrodes gap at different dielectric conditions in powder mixed EDM process, *Int. J. Adv. Manuf. Technol.* (2020). <https://doi.org/10.1007/s00170-020-05189-x>.
- [169] A. Okada, Y. Uno, M. Nakazawa, T. Yamauchi, Evaluations of spark distribution and

- wire vibration in wire EDM by high-speed observation, *CIRP Ann. - Manuf. Technol.* (2010). <https://doi.org/10.1016/j.cirp.2010.03.073>.
- [170] M. Nakazawa, A. Okada, T. Yamauchi, Y. Uno, Evaluation of spark location distribution in wire EDM by high-speed observation, in: *Proc. 5th Int. Conf. Lead. Edge Manuf. 21st Century, LEM 2009*, 2009.
- [171] M.P. Jahan, Micro-electrical discharge machining, in: *Nontradit. Mach. Process. Res. Adv.*, 2013: pp. 111–151. https://doi.org/10.1007/978-1-4471-5179-1_4.
- [172] J. Qian, F. Yang, J. Wang, B. Lauwers, D. Reynaerts, Material removal mechanism in low-energy micro-EDM process, *CIRP Ann. - Manuf. Technol.* 64 (2015) 225–228. <https://doi.org/10.1016/j.cirp.2015.04.040>.
- [173] Y.S. Wong, M. Rahman, H.S. Lim, H. Han, N. Ravi, Investigation of micro-EDM material removal characteristics using single RC-pulse discharges, in: *J. Mater. Process. Technol.*, 2003: pp. 303–307. [https://doi.org/10.1016/S0924-0136\(03\)00771-4](https://doi.org/10.1016/S0924-0136(03)00771-4).
- [174] M.P. Jahan, Micro-electrical discharge machining, in: *Nontradit. Mach. Process. Res. Adv.*, 2013: pp. 111–151. https://doi.org/10.1007/978-1-4471-5179-1_4.
- [175] F. Han, Y. Yamada, T. Kawakami, M. Kunieda, Investigations on Feasibility of Sub-micrometer Order Manufacturing Using Micro-EDM, *ASPE 2003 Annu. Meet.* 22 (2003) 172–175.
- [176] T. Kawakami, M. Kunieda, Study on factors determining limits of minimum machinable size in micro EDM, *CIRP Ann. - Manuf. Technol.* 54 (2005) 167–170. [https://doi.org/10.1016/S0007-8506\(07\)60075-4](https://doi.org/10.1016/S0007-8506(07)60075-4).
- [177] M.K. Egashira K, EDM at low open-circuit voltage, *Int. J. Electromach.* 10 (2005) 21–26.
- [178] X. Yang, C. Xu, M. Kunieda, Miniaturization of WEDM using electrostatic induction

- feeding method, *Precis. Eng.* 34 (2010) 279–285.
<https://doi.org/10.1016/j.precisioneng.2009.07.002>.
- [179] T. Koyano, M. Kunieda, Achieving high accuracy and high removal rate in micro-EDM by electrostatic induction feeding method, *CIRP Ann. - Manuf. Technol.* 59 (2010) 219–222. <https://doi.org/10.1016/j.cirp.2010.03.068>.
- [180] Y. Zhao, M. Kunieda, K. Abe, Multi-discharge EDM coring of single crystal SiC ingot by electrostatic induction feeding method, *Precis. Eng.* (2015).
<https://doi.org/10.1016/j.precisioneng.2014.12.007>.
- [181] T. Muthuramalingam, B. Mohan, Design and fabrication of control system-based ISO pulse generator for electrical discharge machining, *Int. J. Mechatronics Manuf. Syst.* (2013). <https://doi.org/10.1504/IJMMS.2013.053823>.
- [182] M.P. Jahan, M. Rahman, Y.S. Wong, A review on the conventional and micro-electrodischarge machining of tungsten carbide, *Int. J. Mach. Tools Manuf.* 51 (2011) 837–858. <https://doi.org/10.1016/j.ijmachtools.2011.08.016>.
- [183] C.J. Luis, I. Puertas, G. Villa, Material removal rate and electrode wear study on the EDM of silicon carbide, *J. Mater. Process. Technol.* (2005).
<https://doi.org/10.1016/j.jmatprotec.2005.02.045>.
- [184] Y.C. Lin, H.S. Lee, Machining characteristics of magnetic force-assisted EDM, *Int. J. Mach. Tools Manuf.* 48 (2008) 1179–1186.
<https://doi.org/10.1016/j.ijmachtools.2008.04.004>.
- [185] Z. Li, J. Bai, Impulse discharge method to investigate the influence of gap width on discharge characteristics in micro-EDM, *Int. J. Adv. Manuf. Technol.* 90 (2017) 1769–1777. <https://doi.org/10.1007/s00170-016-9508-1>.
- [186] S.H. Yeo, E. Aligiri, P.C. Tan, H. Zarepour, A new pulse discriminating system for Micro-EDM, *Mater. Manuf. Process.* 24 (2009) 1297–1305.

<https://doi.org/10.1080/10426910903130164>.

- [187] J. Wang, F. Yang, J. Qian, D. Reynaerts, Study of alternating current flow in micro-EDM through real-time pulse counting, *J. Mater. Process. Technol.* (2016). <https://doi.org/10.1016/j.jmatprotec.2015.12.010>.
- [188] Y.S. Liao, T.Y. Chang, T.J. Chuang, An on-line monitoring system for a micro electrical discharge machining (micro-EDM) process, *J. Micromechanics Microengineering.* (2008). <https://doi.org/10.1088/0960-1317/18/3/035009>.
- [189] M. Niamat, S. Sarfraz, E. Shehab, S.O. Ismail, Q.S. Khalid, Experimental Characterization of Electrical Discharge Machining of Aluminum 6061 T6 Alloy using Different Dielectrics, *Arab. J. Sci. Eng.* (2019). <https://doi.org/10.1007/s13369-019-03987-4>.
- [190] N.L.S. Hashim, A. Yahya, M.R. Daud, S. Syahrullail, A. Baharom, N.H. Khamis, N. Mahmud, Review on an electrical discharge machining servomechanism system, *Sci. Iran.* (2015).
- [191] Q. Li, G. Zhu, J. Bai, Development and application of open CNC system for micro-EDM machine, *Harbin Gongcheng Daxue Xuebao/Journal Harbin Eng. Univ.* (2015). <https://doi.org/10.3969/jheu.201308003>.
- [192] R. Martínez-Alvarado, E.E. Granda-Gutiérrez, A. Hernández-Rodríguez, R.J. Praga-Alejo, Pulse Classification for an Electrochemical Discharge Machining Process Based on Fuzzy Logic Approach, *Int. J. Precis. Eng. Manuf.* (2020). <https://doi.org/10.1007/s12541-020-00385-x>.
- [193] K.H. Tseng, Y.S. Lin, C.Y. Chang, M.Y. Chung, A study of a PID controller used in a microelectrical discharge machining system to prepare TiO₂ nanocolloids, *Nanomaterials.* (2020). <https://doi.org/10.3390/nano10061044>.
- [194] J. Ahola, V. Särkimäki, A. Muetze, J. Tamminen, Radio-frequency-based detection of

- electrical discharge machining bearing currents, *IET Electr. Power Appl.* (2011).
<https://doi.org/10.1049/iet-epa.2010.0153>.
- [195] L. Vinet, A. Zhedanov, A neutral-network approach for the on-line monitoring of the electrical discharge machining process, *J. Phys. A Math. Theor.* (2011).
- [196] J. Wang, J.A. Sanchez, I. Ayesta, J.A. Iturrioz, Unsupervised machine learning for advanced tolerance monitoring of wire electrical discharge machining of disc turbine fir-tree slots, *Sensors (Switzerland)*. (2018). <https://doi.org/10.3390/s18103359>.
- [197] Q. Jing, J. Li, Y. Zhang, L. Kong, M. Xu, A Study of Influence of Servo-Control Strategy on Machining Efficiency in Micro-EDM, *Nanomanufacturing Metrol.* (2020).
<https://doi.org/10.1007/s41871-019-00054-2>.
- [198] E. Amouzegar, S.R. Ahmadi, A. Donyavi, State of the art micro-EDM drilling using centrifugal servo-mechanism for workpiece actuation, *Int. J. Adv. Manuf. Technol.* (2016). <https://doi.org/10.1007/s00170-015-7330-9>.
- [199] T. NAKAGAWA, H. MIYAKE, Y. IMAI, H. TOKURA, Development of Micro-EDM using Magnetic Levitation Actuator, *J. Japan Soc. Precis. Eng. Contrib. Pap.* (2006).
<https://doi.org/10.2493/jspe.72.730>.
- [200] Y. Guo, Z. Ling, X. Zhang, Y. Feng, A magnetic suspension spindle system for small and micro holes EDM, *Int. J. Adv. Manuf. Technol.* (2018).
<https://doi.org/10.1007/s00170-017-0990-x>.
- [201] H. Tong, Y. Li, Y. Wang, D. Yu, Servo scanning 3D micro-EDM based on macro/micro-dual-feed spindle, *Int. J. Mach. Tools Manuf.* (2008).
<https://doi.org/10.1016/j.ijmachtools.2007.11.008>.
- [202] M. Shafik, H.S. Abdalla, P. Fransson, A piezoelectric servo feed drive for electro discharge machining system industrial applications using linear ultrasonic motor, *J. Manuf. Sci. Eng. Trans. ASME*. (2013). <https://doi.org/10.1115/1.4023707>.

- [203] M.P. Jahan, Micro-electrical discharge machining, in: *Nontradit. Mach. Process. Res. Adv.*, 2013. https://doi.org/10.1007/978-1-4471-5179-1_4.
- [204] S.M. Son, H.S. Lim, A.S. Kumar, M. Rahman, Influences of pulsed power condition on the machining properties in micro EDM, *J. Mater. Process. Technol.* (2007). <https://doi.org/10.1016/j.jmatprotec.2007.03.108>.
- [205] M. Gostimirovic, P. Kovac, M. Sekulic, B. Skoric, Influence of discharge energy on machining characteristics in EDM, *J. Mech. Sci. Technol.* (2012). <https://doi.org/10.1007/s12206-011-0922-x>.
- [206] G. Tristo, G. Bissacco, A. Lebar, J. Valentinčič, Real time power consumption monitoring for energy efficiency analysis in micro EDM milling, *Int. J. Adv. Manuf. Technol.* 78 (2015) 1511–1521. <https://doi.org/10.1007/s00170-014-6725-3>.
- [207] D. Kumar, V. Bajpai, N.K. Singh, Nano electrical discharge machining—the outlook, challenges, and opportunities, *Mater. Manuf. Process.* (2021). <https://doi.org/10.1080/10426914.2021.1905832>.
- [208] S. Viswanthvaleti, R. Radhakrishnan, G. Rajyalakshmi, Multi-response optimization of process parameters of green electrical discharge machining on aisi 2507 super duplex stainless steel using grey relational analysis (Gra), *Int. J. Mech. Prod. Eng. Res. Dev.* (2018). <https://doi.org/10.24247/ijmperdjun201895>.
- [209] S. Bharat, Evaluation of EDM Characteristic of Duplex Stainless Steel (DSS) using Taguchi Method, *Int. J. Adv. Sci. Technol.* 29 (2020) 3503–3511. <http://sersc.org/journals/index.php/IJAST/article/view/22067>.
- [210] V. V. Srinivas, R. Ramanujam, G. Rajyalakshmi, Application of MQL for developing sustainable EDM and process parameter optimisation using ANN and GRA method, *Int. J. Bus. Excell.* (2020). <https://doi.org/10.1504/IJBEX.2020.111476>.
- [211] I.W. Rangelow, S. Biehl, High aspect ratio silicon tips field emitter array,

- Microelectron. Eng. (2001). [https://doi.org/10.1016/S0167-9317\(01\)00492-0](https://doi.org/10.1016/S0167-9317(01)00492-0).
- [212] A. Pasquini, G.B. Picotto, M. Pisani, STM carbon nanotube tips fabrication for critical dimension measurements, in: *Sensors Actuators, A Phys.*, 2005. <https://doi.org/10.1016/j.sna.2005.02.036>.
- [213] M.J. Vasile, D.A. Grigg, J.E. Griffith, E.A. Fitzgerald, P.E. Russell, Scanning probe tips formed by focused ion beams, *Rev. Sci. Instrum.* (1991). <https://doi.org/10.1063/1.1142334>.
- [214] S. Kerfriden, A.H. Nahlé, S.A. Campbell, F.C. Walsh, J.R. Smith, The electrochemical etching of tungsten STM tips, *Electrochim. Acta.* (1998). [https://doi.org/10.1016/s0013-4686\(97\)00316-2](https://doi.org/10.1016/s0013-4686(97)00316-2).
- [215] A.D. Müller, F. Müller, M. Hietschold, F. Demming, J. Jersch, K. Dickmann, Characterization of electrochemically etched tungsten tips for scanning tunneling microscopy, *Rev. Sci. Instrum.* (1999). <https://doi.org/10.1063/1.1150022>.
- [216] J. Méndez, M. Luna, A.M. Baró, Preparation of STM W tips and characterization by FEM, TEM and SEM, *Surf. Sci.* (1992). [https://doi.org/10.1016/0039-6028\(92\)91036-B](https://doi.org/10.1016/0039-6028(92)91036-B).
- [217] R. Zhang, Preparation of sharp polycrystalline tungsten tips for scanning tunneling microscopy imaging, *J. Vac. Sci. Technol. B Microelectron. Nanom. Struct.* (1996). <https://doi.org/10.1116/1.589029>.
- [218] L. Ottaviano, L. Lozzi, S. Santucci, Scanning Auger microscopy study of W tips for scanning tunneling microscopy, *Rev. Sci. Instrum.* (2003). <https://doi.org/10.1063/1.1581392>.
- [219] X. Cheng, K. Nakamoto, M. Sugai, S. Matsumoto, Z.G. Wang, K. Yamazaki, Development of ultra-precision machining system with unique wire EDM tool fabrication system for micro/nano-machining, *CIRP Ann. - Manuf. Technol.* 57 (2008)

- 415–420. <https://doi.org/10.1016/j.cirp.2008.03.137>.
- [220] G. Tahmasebipour, Y. Hojjat, V. Ahmadi, A. Abdullah, Optimization of STM/FIM nanotip aspect ratio based on the Taguchi method, *Int. J. Adv. Manuf. Technol.* (2009). <https://doi.org/10.1007/s00170-008-1799-4>.
- [221] G. Tahmasebipour, V. Ahmadi, A. Abdullah, Y. Hojjat, Fabrication of STM tungsten nanotip by electrochemical etching method, *Int. J. Nanosci.* (2009). <https://doi.org/10.1142/S0219581X09006110>.
- [222] G. Tahmasebipour, Y. Hojjat, V. Ahmadi, A. Abdullah, Effect of fabrication process parameters on the apex-radius of STM tungsten nanotip, *Scanning.* (2009). <https://doi.org/10.1002/sca.20142>.
- [223] A. Benilov, V. Skryshevsky, Y. Robach, M. Cabrera, Micro and nano electrical discharge machining in microfluidics and micro nanotechnology, *Int. J. Mater. Form.* (2008). <https://doi.org/10.1007/s12289-008-0145-6>.
- [224] A.A. Baski, Fabrication of Nanoscale Structures using STM and AFM, in: *Adv. Semicond. Org. Nano-Techniques*, 2003. <https://doi.org/10.1016/B978-012507060-7/50024-6>.
- [225] R. Kazinczi, E. Szocs, E. Kálmán, P. Nagy, Novel methods for preparing EC STM tips, *Appl. Phys. A Mater. Sci. Process.* (1998). <https://doi.org/10.1007/s003390051197>.
- [226] A.J. Melmed, The art and science and other aspects of making sharp tips, *J. Vac. Sci. Technol. B Microelectron. Nanom. Struct.* (1991). <https://doi.org/10.1116/1.585467>.
- [227] H.J. Lim, Y.M. Lim, S.H. Kim, Fabrication of arbitrarily shaped microelectrodes by electrochemical etching, *Japanese J. Appl. Physics, Part 1 Regul. Pap. Short Notes Rev. Pap.* (2003). <https://doi.org/10.1143/jjap.42.1479>.
- [228] S. Tang, Y. Zhang, Y. Tian, S. Jin, P. Zhao, F. Liu, R. Zhan, S. Deng, J. Chen, N. Xu, A two-dimensional structure graphene STM tips fabricated by microwave plasma

- enhanced chemical vapor deposition, *Carbon* N. Y. (2017).
<https://doi.org/10.1016/j.carbon.2017.06.014>.
- [229] J.P. Edgeworth, D.P. Burt, P.S. Dobson, J.M.R. Weaver, J. V. MacPherson, Growth and morphology control of carbon nanotubes at the apexes of pyramidal silicon tips, *Nanotechnology*. (2010). <https://doi.org/10.1088/0957-4484/21/10/105605>.
- [230] J.S. Lee, J. Song, S.O. Kim, S. Kim, W. Lee, J.A. Jackman, D. Kim, N.J. Cho, J. Lee, Multifunctional hydrogel nano-probes for atomic force microscopy, *Nat. Commun.* (2016). <https://doi.org/10.1038/ncomms11566>.
- [231] G. Amin, P.M. Willander, *ZnO and CuO Nanostructures: Low Temperature Growth, Characterization, their Optoelectronic and Sensing Applications*, 2012.
- [232] A.G. Macedo, D. Ananias, P.S. André, R.A. Sá Ferreira, A.L. Kholkin, L.D. Carlos, J. Rocha, Functionalization of atomic force microscope tips by dielectrophoretic assembly of Gd₂O₃:Eu³⁺ nanorods, *Nanotechnology*. (2008).
<https://doi.org/10.1088/0957-4484/19/29/295702>.
- [233] S. Kar, P.K. Patowari, Effect of non-electrical parameters in fabrication of micro rod using BEDG, *Mater. Manuf. Process.* (2019).
<https://doi.org/10.1080/10426914.2019.1643475>.
- [234] A.K. Singh, P.K. Patowari, N. V. Deshpande, Effect of tool wear on microrods fabrication using reverse μ EDM, *Mater. Manuf. Process.* (2017).
<https://doi.org/10.1080/10426914.2016.1198015>.
- [235] M.G. Boyle, L. Feng, P. Dawson, Safe fabrication of sharp gold tips for light emission in scanning tunnelling microscopy, *Ultramicroscopy*. (2008).
<https://doi.org/10.1016/j.ultramic.2007.08.012>.
- [236] C. Wang, W. He, Y. Xiao, Fabrication of Micro Structures by Ultrashort Voltage Pulse Electrical Discharge Machining, *J. Miner. Mater. Charact. Eng.* (2018).

- <https://doi.org/10.4236/jmmce.2018.62017>.
- [237] N. Kumar, N. Mandal, A.K. Das, Micro-machining through electrochemical discharge processes: a review, *Mater. Manuf. Process.* (2020). <https://doi.org/10.1080/10426914.2020.1711922>.
- [238] M.P. Jahan, M. Rahman, Y.S. Wong, Micro-Electrical Discharge Machining (Micro-EDM): Processes, Varieties, and Applications, in: *Compr. Mater. Process.*, 2014: pp. 333–371. <https://doi.org/10.1016/B978-0-08-096532-1.01107-9>.
- [239] H. Ohmori, Y. Uehara, K. Katahira, Fabrication of Ultrafine Tools Using a Desktop Microgrinder, *Int. J. Autom. Technol.* (2010). <https://doi.org/10.20965/ijat.2010.p0097>.
- [240] B. Xiao, S. Albin, Carbon nanotube probe for scanning tunneling microscopy, *Int. J. Nanosci.* (2005). <https://doi.org/10.1142/S0219581X05003279>.
- [241] M. Yamazaki, T. Suzuki, N. Mori, M. Kunieda, EDM of micro-rods by self-drilled holes, in: *J. Mater. Process. Technol.*, 2004. <https://doi.org/10.1016/j.jmatprotec.2004.03.006>.
- [242] S.T. Chen, H.Y. Yang, Study of micro-electro discharge machining (micro-EDM) with on-machine measurement-assisted techniques, in: *Meas. Sci. Technol.*, 2011. <https://doi.org/10.1088/0957-0233/22/6/065702>.
- [243] A.K. Das, P. Saha, Fabrication of cylindrical micro tools by micro electrochemical form turning operation, *Proc. Inst. Mech. Eng. Part B J. Eng. Manuf.* (2014). <https://doi.org/10.1177/0954405413497007>.
- [244] Z.W. Fan, L.W. Hourng, C.Y. Wang, Fabrication of tungsten microelectrodes using pulsed electrochemical machining, *Precis. Eng.* (2010). <https://doi.org/10.1016/j.precisioneng.2010.01.001>.
- [245] J. Huang, Y. Wu, C. Gu, M. Zhai, K. Yu, M. Yang, J. Liu, Large-scale synthesis of

- flowerlike ZnO nanostructure by a simple chemical solution route and its gas-sensing property, *Sensors Actuators, B Chem.* (2010).
<https://doi.org/10.1016/j.snb.2010.02.052>.
- [246] S. Maupai, A.S. Dakkouri, P. Schmuki, Tip-induced nanostructuring of alloy surfaces with an electrochemical scanning tunneling microscope, *Surf. Sci.* (2005).
<https://doi.org/10.1016/j.susc.2004.05.146>.
- [247] H. Hu, H.J. Kim, S. Somnath, Tip-based nanofabrication for scalable manufacturing, *Micromachines.* (2017). <https://doi.org/10.3390/mi8030090>.
- [248] J.T.D. Ty, H. Yanagi, Electrochemical deposition of zinc oxide nanorods for hybrid solar cells, in: *Jpn. J. Appl. Phys.*, 2015. <https://doi.org/10.7567/JJAP.54.04DK05>.
- [249] S. Sucharitakul, R. Panyathip, S. Choopun, Effect of annealing temperature on ECD grown hexagonal-plane zinc oxide, *Materials (Basel)*. 11 (2018) 1–14.
<https://doi.org/10.3390/ma11081360>.
- [250] B. Deka Boruah, A. Misra, Energy-Efficient Hydrogenated Zinc Oxide Nanoflakes for High-Performance Self-Powered Ultraviolet Photodetector, *ACS Appl. Mater. Interfaces.* (2016). <https://doi.org/10.1021/acsami.6b04954>.
- [251] A. Gupta, S.S. Pandey, M. Nayak, A. Maity, S.B. Majumder, S. Bhattacharya, Hydrogen sensing based on nanoporous silica-embedded ultra dense ZnO nanobundles, *RSC Adv.* (2014). <https://doi.org/10.1039/c3ra45316b>.
- [252] S. Harish, M. Navaneethan, J. Archana, A. Silambarasan, S. Ponnusamy, C. Muthamizhchelvan, Y. Hayakawa, Controlled synthesis of organic ligand passivated ZnO nanostructures and their photocatalytic activity under visible light irradiation, *Dalt. Trans.* (2015). <https://doi.org/10.1039/c5dt01572c>.
- [253] Y. Qiu, D. Yang, J. Lei, H. Zhang, J. Ji, B. Yin, J. Bian, Y. Zhao, L. Hu, Controlled growth of ZnO nanorods on common paper substrate and their application for flexible

- piezoelectric nanogenerators, *J. Mater. Sci. Mater. Electron.* (2014).
<https://doi.org/10.1007/s10854-014-1924-0>.
- [254] M. Goswami, N.C. Adhikary, S. Bhattacharjee, Effect of annealing temperatures on the structural and optical properties of zinc oxide nanoparticles prepared by chemical precipitation method, *Optik (Stuttg).* (2018).
<https://doi.org/10.1016/j.ijleo.2017.12.174>.
- [255] S. Ghosh, D. Majumder, A. Sen, S. Roy, Facile sonochemical synthesis of zinc oxide nanoflakes at room temperature, *Mater. Lett.* (2014).
<https://doi.org/10.1016/j.matlet.2014.05.112>.
- [256] V. Gaddam, R.R. Kumar, M. Parmar, M.M. Nayak, K. Rajanna, Synthesis of ZnO nanorods on a flexible Phynox alloy substrate: Influence of growth temperature on their properties, *RSC Adv.* (2015). <https://doi.org/10.1039/c5ra12773d>.
- [257] S.G. Leonardi, Two-dimensional zinc oxide nanostructures for gas sensor applications, *Chemosensors.* (2017). <https://doi.org/10.3390/chemosensors5020017>.
- [258] W. Zhang, P. Wang, X. Fei, Y. Xiu, G. Jia, Growth mechanism and morphologies tuning of ZnO nanostructures, *Int. J. Electrochem. Sci.* (2015).
- [259] K.P. Rajurkar, G. Levy, A. Malshe, M.M. Sundaram, J. McGeough, X. Hu, R. Resnick, A. DeSilva, Micro and nano machining by electro-physical and chemical processes, *CIRP Ann. - Manuf. Technol.* 55 (2006) 643–666.
<https://doi.org/10.1016/j.cirp.2006.10.002>.
- [260] Y. Xia, J.A. Rogers, K.E. Paul, G.M. Whitesides, ChemInform Abstract: Unconventional Methods for Fabricating and Patterning Nanostructures, *ChemInform.* (2010). <https://doi.org/10.1002/chin.199938264>.
- [261] G.Y.H. LEE, C.T. LIM, NANOTECHNOLOGY AND HUMAN DISEASES, *COSMOS.* (2007). <https://doi.org/10.1142/s0219607707000232>.

- [262] J. Li, M. Gershow, D. Stein, E. Brandin, J.A. Golovchenko, DNA molecules and configurations in a solid-state nanopore microscope, *Nat. Mater.* (2003). <https://doi.org/10.1038/nmat965>.
- [263] M. Moseler, U. Landman, Formation, stability, and breakup of nanojets, *Science* (80-). (2000). <https://doi.org/10.1126/science.289.5482.1165>.
- [264] C.T. Kresge, M.E. Leonowicz, W.J. Roth, J.C. Vartuli, J.S. Beck, Ordered mesoporous molecular sieves synthesized by a liquid-crystal template mechanism, *Nature*. (1992). <https://doi.org/10.1038/359710a0>.
- [265] A.H. Alkhaleel, M.M. Sundaram, K.P. Rajurkar, A.P. Malshe, Electro machining of nano grooves using the AFM, in: *Proc. 15th Int. Symp. Electromachining, ISEM 2007*, 2007.
- [266] G. Liu, M. Hirtz, H. Fuchs, Z. Zheng, Development of Dip-Pen Nanolithography (DPN) and Its Derivatives, *Small*. (2019). <https://doi.org/10.1002/smll.201900564>.
- [267] S. Takei, Direct Nanoimprint Lithography of Polyethersulfone Using Cellulose-Based Mold, *Macromol. Mater. Eng.* (2020). <https://doi.org/10.1002/mame.201900853>.
- [268] V.J. Gómez, M. Graczyk, R.J. Jam, S. Lehmann, I. Maximov, Wafer-scale nanofabrication of sub-100 nm arrays by deep-UV displacement Talbot lithography, *Nanotechnology*. (2020). <https://doi.org/10.1088/1361-6528/ab8764>.
- [269] D.A. Lucca, K. Herrmann, M.J. Klopstein, Nanoindentation: Measuring methods and applications, *CIRP Ann. - Manuf. Technol.* (2010). <https://doi.org/10.1016/j.cirp.2010.05.009>.
- [270] M.P. Jahan, K.P. Rajurkar, A.P. Malshe, A Comparative Study on Machining Capabilities of Wet and Dry Nano-scale Electro-machining, in: *Procedia CIRP*, 2016. <https://doi.org/10.1016/j.procir.2016.02.211>.
- [271] S.H. Yeo, G.G. Yap, A feasibility study on the micro electro-discharge machining

- process for photomask fabrication, *Int. J. Adv. Manuf. Technol.* 18 (2001) 7–11.
<https://doi.org/10.1007/PL00003950>.
- [272] T. Saleh, M. Dahmardeh, A. Bsoul, A. Nojeh, K. Takahata, Field-emission-assisted approach to dry micro-electro-discharge machining of carbon-nanotube forests, in: *J. Appl. Phys.*, 2011. <https://doi.org/10.1063/1.3663438>.
- [273] W. Khalid, M.S.M. Ali, M. Dahmardeh, Y. Choi, P. Yaghoobi, A. Nojeh, K. Takahata, High-aspect-ratio, free-form patterning of carbon nanotube forests using micro-electro-discharge machining, *Diam. Relat. Mater.* (2010).
<https://doi.org/10.1016/j.diamond.2010.08.007>.
- [274] X. Zhao, J. Wen, L. Li, Y. Wang, D. Wang, L. Chen, Y. Zhang, Y. Du, Architecture design and applications of nanopatterned arrays based on colloidal lithography, *J. Appl. Phys.* (2019). <https://doi.org/10.1063/1.5120601>.
- [275] Y. Yang, A. Keller, Ion beam nanopatterning of biomaterial surfaces, *Appl. Sci.* (2021). <https://doi.org/10.3390/app11146575>.
- [276] S. Portal, C. Corbella, Surface nanopatterning by colloidal lithography, in: *Funct. Nanostructured Interfaces Environ. Biomed. Appl.*, 2019.
<https://doi.org/10.1016/B978-0-12-814401-5.00004-9>.
- [277] X.N. Xie, H.J. Chung, A.T.S. Wee, Scanning probe microscopy based nanoscale patterning and fabrication, in: *Sel. Top. Nanosci. Nanotechnol.*, 2009.
https://doi.org/10.1142/9789812839565_0001.
- [278] Kresge CT, Leonowicz ME, Roth WJ, Vartuli JC, Beck JS, Ordered mesoporous molecular sieves synthesized by a liquid-crystal template mechanism, *Nature*. (1992).
- [279] Y. Wen, F. Wang, H. Yu, P. Li, L. Liu, W.J. Li, Laser-nanomachining by microsphere induced photonic nanojet, *Sensors Actuators, A Phys.* (2017).
<https://doi.org/10.1016/j.sna.2017.03.009>.

- [280] T. Gotszalk, G. Józwiak, J. Radojewski, T. Fröhlich, R. Füssl, E. Manske, M. Holz, T. Ivanov, A. Ahmad, I.W. Rangelow, Tip-based nano-manufacturing and -metrology, *J. Vac. Sci. Technol. B.* (2019). <https://doi.org/10.1116/1.5083044>.
- [281] X.N. XIE, H.J. CHUNG, A.T.S. WEE, SCANNING PROBE MICROSCOPY BASED NANOSCALE PATTERNING AND FABRICATION, *COSMOS.* (2007). <https://doi.org/10.1142/s0219607707000207>.
- [282] P.J. Liew, J. Yan, Micro-electrical Discharge Machining of Hard Brittle Materials, in: 2018. https://doi.org/10.1007/978-981-13-0098-1_25.
- [283] R.S. Rai, V. Bajpai, Recent advances in ZnO nanostructures and their future perspective, *Adv. Nano Res.* (2021). <https://doi.org/10.12989/anr.2021.11.1.037>.
- [284] N. Siriphongsapak, S. Denchitcharoen, P. Limsuwan, Hydrothermal growth of ZnO nanostructures using sodium hydroxide as a source of hydroxide ion, in: *Mater. Today Proc.*, 2020. <https://doi.org/10.1016/j.matpr.2019.12.263>.
- [285] R.S. Rai, V. Bajpai, Hydrothermally grown ZnO NSs on Bi-Directional woven carbon fiber and effect of synthesis parameters on morphology, *Ceram. Int.* (2021). <https://doi.org/10.1016/j.ceramint.2020.11.180>.
- [286] S. Baruah, J. Dutta, Hydrothermal growth of ZnO nanostructures, *Sci. Technol. Adv. Mater.* (2009). <https://doi.org/10.1088/1468-6996/10/1/013001>.
- [287] D. Kumar, R.S. Rai, N.K. Singh, An innovative approach to deposit ultrathin ZnO nanoflakes (2D) through hydrothermal assisted electrochemical discharge deposition and growth method, *Ceram. Int.* (2020). <https://doi.org/10.1016/j.ceramint.2020.07.009>.
- [288] H. Wang, J. Xie, K. Yan, M. Duan, Growth Mechanism of Different Morphologies of ZnO Crystals Prepared by Hydrothermal Method, *J. Mater. Sci. Technol.* (2011). [https://doi.org/10.1016/S1005-0302\(11\)60041-8](https://doi.org/10.1016/S1005-0302(11)60041-8).

- [289] A.M. El-Rafei, M.F. Zawrah, Effect of alkali concentration and reaction time on the morphology of ZnO nano-microparticles prepared by hydrothermal method, *J. Ceram. Sci. Technol.* (2014). <https://doi.org/10.4416/JCST2014-00002>.
- [290] K.H. Tseng, K.H. Chen, C.Y. Chang, Y. Cahyadi, M.Y. Chung, Implementation of a micro-electrical discharge machining system to fabricate TiO₂ nanocolloid, *Mechatronics*. (2021). <https://doi.org/10.1016/j.mechatronics.2021.102649>.
- [291] M.T. Yan, H.T. Chien, Monitoring and control of the micro wire-EDM process, *Int. J. Mach. Tools Manuf.* 47 (2007) 148–157. <https://doi.org/10.1016/j.ijmachtools.2006.02.006>.

Appendix 1

List of publications

Journal Publications

1. **Kumar, D.**, Bajpai, V., & Singh, N. K. (2021). Nano electrical discharge machining—the outlook, challenges, and opportunities. *Materials and Manufacturing Processes*, 1-35.
2. **Kumar, D.**, Singh, N. K., & Bajpai, V. (2020). Recent trends, opportunities and other aspects of micro-EDM for advanced manufacturing: a comprehensive review. *Journal of the Brazilian Society of Mechanical Sciences and Engineering*, 42(5), 1-26.
3. **Kumar, D.**, Singh, N. K., & Bajpai, V. (2022). Achieving nano-patterned features by micro-EDM process using vertically aligned ZnO nanorods grown on microprobe tip: A scaling approach. *Microelectronic Engineering*, 111792.
4. **Kumar, D.**, Rai, R. S., & Singh, N. K. (2020). An innovative approach to deposit ultrathin ZnO nanoflakes (2D) through hydrothermal assisted electrochemical discharge deposition and growth method. *Ceramics International*, 46(16), 26216-26220.
5. **Kumar, D.**, Rai, R. S., Bajpai, V., & Singh, N. K. (2021). Mass fabrication of 2D nanostructure (ZnO) in chemical growth solution using tip induced lithography. *Materials and Manufacturing Processes*, 1-9.
6. **Kumar, D.**, Sisodiya, M. S., & Bajpai, V. (2022). A novel servo-stabilized electromagnetic levitation for micro-EDM processing and its feasibility analysis. Proceedings of the Institution of Mechanical Engineers, **Part B: Journal of Engineering Manufacture**, 09544054221124473.
7. **Kumar, D.**, Sisodiya, M. S., Mandal, D. K., & Bajpai, V. (2023). Maglev micro-EDM: Feasibility and performance analysis on Inconel 625. *CIRP Journal of Manufacturing Science and Technology*, 40, 155-166.

International conferences

1. **Deepak Kumar**, Nirmal Kumar Singh, Vivek Bajpai “Fabrication of microcylinder using a tubular electrode in magnetic levitation based μ -EDM” (**WCMNM-2021**)”, IIT, Bombay, 21-23 September 2021.
2. **Deepak Kumar**, Harish Bishwakarma, Mohan Kumar, Nirmal Kumar Singh “Vivek Bajpai Tip induced growth of zinc oxide nanoflakes through electrochemical discharge deposition process and their optical characterization” **MSEC-2020**, University of Cincinnati, USA, June 21 – 25, 2020.
3. **Deepak Kumar**, Vivek Bajpai Nirmal Kumar Singh “Synthesis and Characterization of Zinc Oxide Nano Flakes through Electrochemical Discharge Deposition and Growth Method” (**COPEN 2019**), IIT, Indore, December 12-14, 2019,
4. **Deepak Kumar**, Shakti Kumar, Dheeraj Kumar, Nirmal Kumar Singh“ Effect of Two Different Dielectrics on the Machining Performance and Their Parametric Optimization Through Response Surface Methodology, (**ICAMME – 2019**), KIIT, Bhubaneswar, March 15-17, 2019.
5. Abhinav Kumar, **Deepak Kumar**, Nirmal Kumar Singh “Fabrication of microholes through micro-EDM and their circularity testing” International conference on innovative product design and intelligence manufacturing system (**IPDIMS-2021**), 30-31 December 2021, NIT Rourkela.